ADVANCES IN POLYMER SCIENCE

Volume Editor: M. Schmidt

150

New Developments in Polymer Analytics I

Springer

150
Advances in Polymer Science

Springer
Berlin
Heidelberg
New York
Barcelona
Hong Kong
London
Milan
Paris
Singapore
Tokyo

New Developments in Polymer Analytics I

Volume Editor: M. Schmidt

With contributions by
M. Antonietti, H. Cölfen, H. Engelhardt,
O. Grosche, H. Pasch

Springer

This series presents critical reviews of the present and future trends in polymer and biopolymer science including chemistry, physical chemistry, physics and materials science. It is addressed to all scientists at universities and in industry who wish to keep abreast of advances in the topics covered.

As a rule, contributions are specially commissioned. The editors and publishers will, however, always be pleased to receive suggestions and supplementary information. Papers are accepted for „Advances in Polymer Science" in English.

In references Advances in Polymer Science is abbreviated Adv. Polym. Sci. and is cited as a journal.

Springer APS home page: http://link.springer.de/series/aps/ or
http://link.springer-ny.com/series/aps
Springer-Verlag home page: http://www.springer.de

ISSN 0065-3195
ISBN 3-540-66077-1
Springer-Verlag Berlin Heidelberg New York

Library of Congress Catalog Card Number 61642

Printed in Germany

Typesetting: Data conversion by MEDIO, Berlin
Cover: E. Kirchner, Heidelberg
SPIN: 10706195 02/3020 - 5 4 3 2 1 0 - Printed on acid-free paper

Volume Editor

Prof. Manfred Schmidt
Institute of Physical Chemistry
University of Mainz
D- 55099 Mainz, FRG
E-mail: mschmidt@mzdmza.zdv.uni.mainz.de

Editorial Board

Preface

The two volumes "New Developments in Polymer Analytics" deal with recent progress in the characterization of polymers, mostly in solution but also at surfaces. Despite the fact that almost all of the described techniques are getting on in years, the contributions are expected to meet the readers interest because either the methods are newly applied to polymers or the instrumentation has achieved a major breakthrough leading to an enhanced utilization by polymer scientists.

The first volume concentrates on separation techniques. H. Pasch summarizes the recent successes of multi-dimensional chromatography in the characterization of copolymers. Both, chain length distribution and the compositional heterogeneity of copolymers are accessible. Capillary electrophoresis is widely and successfully utilized for the characterization of biopolymers, particular of DNA. It is only recently that the technique has been applied to the characterization of water soluble synthetic macromolecules. This contribution of Grosche and Engelhardt focuses on the analysis of polyelectrolytes by capillary electophoresis. The last contribution of the first volume by Coelfen and Antonietti summarizes the achievements and pitfalls of field flow fractionation techniques. The major drawbacks in the instrumentation have been overcome in recent years and the "triple F techniques" are currently advancing to a powerful competitor to size exclusion chromatography.

The second volume starts with the introduction of a fascinating new technique developed by Köhler and Schäfer to monitor different averages of the Brownian diffusion coefficient of polymers in solution exhibiting a broad molar mass distribution. The technique is based on a scattering experiment by thermal grating, thus simultaneously monitoring Brownian and thermal diffusion of macromolecules. The last contribution by Sheiko addresses recent advances in atomic force microscopy. Besides some theoretical and experimental background the visualization of single macromolecules is discussed and complemented by the characterization and the patterning of surfaces.

Mainz, April 1999 Manfred Schmidt

Contents

Contents of Volume 151

New Developments in Polymer Analytics II

Volume Editor: M. Schmidt

Hyphenated Techniques in Liquid Chromatography of Polymers

Harald Pasch

Deutsches Kunststoff-Institut, Schloßgartenstrasse 6, D-64289 Darmstadt, Germany
E-mail: hpasch@dki.tu-darmstadt.de

Complex polymers are distributed in more than one direction of molecular heterogeneity. In addition to the molar mass distribution, they are frequently distributed with respect to chemical composition, functionality, and molecular architecture. For the characterization of the different types of molecular heterogeneity it is necessary to use a wide range of analytical techniques. Preferably, these techniques should be selective towards a specific type of heterogeneity. The combination of two selective analytical techniques is assumed to yield two-dimensional information on the molecular heterogeneity.

The present review presents the principle ideas of combining different analytical techniques in two-dimensional analysis schemes. Most promising protocols for hyphenated techniques refer to the combination of two different chromatographic methods and the combination of chromatography and spectroscopy. This review will discuss the basic principles of two-dimensional chromatography and the hyphenation of liquid chromatography with selective detectors.

Keywords. Polymer analysis, Liquid chromatography, Hyphenated techniques, Multidimensional chromatography

Advances in Polymer Science, Vol. 150

List of Abbreviations

a	Mark–Houwink exponent
ACN	acetonitrile
AH	adipic acid-hexane diol polyester
c	concentration
CCD	chemical composition distribution
CE	capillary electrophoresis
D-RI	dual density-refractive index detection
ELSD	evaporative light scattering detector
EPDM	ethylene-propylene-diene rubber
ESI	electrospray ionization
f	response factor
FAE	fatty alcohol ethoxylate
FTD	functionality type distribution
FTIR	Fourier transform infrared spectroscopy
ΔG	Gibbs free energy
GC	gas chromatography
ΔH	interaction enthalpy
HPLC	high performance liquid chromatography
K	constant factor in the Mark–Houwink equation
$K^\star$	optical constant in light scattering
K_d	distribution coefficient
LAC	liquid adsorption chromatography
LALLS	low angle laser light scattering
LC-CC	liquid chromatography at critical conditions
M	molar mass
M_n	number-average molar mass
M_v	viscosity-average molar mass
M_w	weight-average molar mass
MAD	molecular architecture distribution

MALDI-MS	matrix-assisted laser desorption/ionization mass spectrometry
MALLS	multi-angle laser light scattering
MS	mass spectrometry
MMD	molar mass distribution
m_i	mass of species i
n_i	number of species i
NMR	nuclear magnetic resonance
NP	normal phase
P (Θ)	scattered light angular dependence
PB	polybutadiene
PEG	poly(ethylene glycol)
PEO	poly(ethylene oxide)
PnBMA	poly(*n*-butyl methacrylate)
PtBMA	poly(*t*-butyl methacrylate)
PDMA	poly(decyl methacrylate)
PDMS	poly(dimethyl siloxane)
PMMA	poly(methyl methacrylate)
PPO	poly(propylene oxide)
PS	polystyrene
R_g	radius of gyration
R (Θ)	intensity of scattered light
RI	refractive index
RP	reversed phase
ΔS	conformational entropy
S/N	signal-to-noise ratio
SAN	styrene-acrylonitrile copolymer
SEC	size exclusion chromatography
THF	tetrahydrofuran
UV	ultraviolet
V_e	elution volume
V_h	hydrodynamic volume
w	weight fraction
η	viscosity of a solution
$[\eta]$	intrinsic viscosity, Staudinger index
η_o	viscosity of a solvent
η_{rel}	relative viscosity
η_{sp}	specific viscosity
λ	wavelength

1 Introduction

Synthetic polymers are highly complex multicomponent materials. They are composed of macromolecules varying in chain length, chemical composition, and architecture. By definition, complex polymers are heterogeneous in more

than one distributed property (for example, linear copolymers are distributed in molar mass and chemical composition).

In general, the molecular structure of a macromolecule is described by its size, its chemical structure, and its architecture. The chemical structure characterizes the constitution of the macromolecule, its configuration and its conformation. For a complete description of the constitution the chemical composition of the polymer chain and the chain ends must be known. In addition to the type and quantity of the repeat units their sequence of incorporation must be described (alternating, random, or block in the case of copolymers). Macromolecules of the same chemical composition can still have different constitutions due to constitutional isomerism (1,2 vs. 1,4 coupling of butadiene, head-to-tail vs. head-to-head coupling, linear vs. branched molecules). Configurational isomers have the same constitution but different steric patterns (*cis*- vs. *trans*-configuration; isotactic, syndiotactic and atactic sequences in a polymer chain). Conformational heterogeneity is the result of the ability of fragments of the polymer chain to rotate around single bonds. Depending on the size of these fragments, interactions between different fragments, and a certain energy barrier, more or less stable conformations may be obtained for the same macromolecule (rod-like vs. coil conformation).

Depending on the composition of the monomer feed and the polymerization procedure, different types of heterogeneities may become important. For example, in the synthesis of tailor-made polymers telechelics or macromonomers are frequently used. These oligomers or polymers usually contain functional groups at the polymer chain end. Depending on the preparation procedure, they can have a different number of functional end groups, i.e. be mono-, bifunctional, etc. In addition, polymers can have different architectures, i.e. they can be branched (star- or comb-like), and they can be cyclic.

The structural complexity of synthetic polymers can be described using the concept of molecular heterogeneity (see Fig. 1) meaning the different aspects of molar mass distribution (MMD), distribution in chemical composition (CCD), functionality type distribution (FTD) and molecular architecture distribution (MAD). They can be superimposed one on another, i.e. bifunctional molecules can be linear or branched, linear molecules can be mono- or bifunctional, copolymers can be block or graft copolymers, etc. In order to characterize complex polymers it is necessary to know the molar mass distribution within each type of heterogeneity.

Using the traditional methods of polymer analysis, such as infrared or nuclear magnetic resonance spectroscopy, one can determine the type of monomers or functional groups present in the sample. However, the determination of functional end groups is complicated for long-chain molecules because of low concentration. On the other hand, these methods do not yield information on how different monomer units or functional groups are distributed in the polymer molecule. Finally, these methods do not in general provide molar mass information.

With respect to methods sensitive to the size of the macromolecule, one can encounter other difficulties. Size exclusion chromatography, which is most fre-

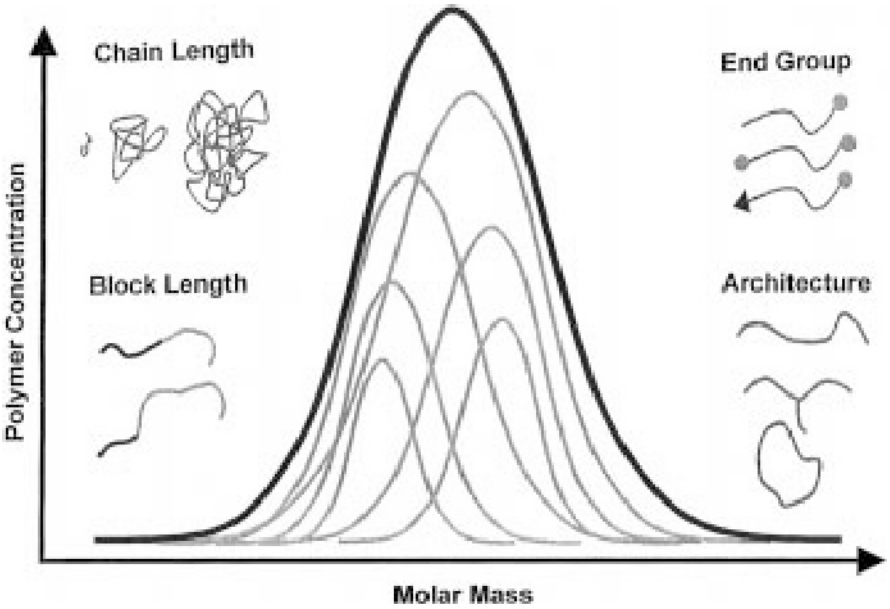

Fig. 1. Schematic representation of the molecular heterogeneity of complex polymers

quently used to separate polymer molecules from each other according to their molecular size in solution, must be used very carefully when analyzing complex polymers. The molecular size distribution of macromolecules can in general be unambiguously correlated with molar mass distribution only within one heterogeneity type. For samples consisting of a mixture of molecules of different functionality, the distribution obtained represents a sum of distributions of molecules having a different functionality and, therefore, cannot be attributed to a specific functionality type without additional assumptions. For the analysis of copolymers by SEC either the chemical composition along the molar mass axis must be known or detectors must be used which, instead of concentration information, can provide molar mass information. To this end, SEC has to be coupled to composition-sensitive or molar-mass-sensitive detectors.

Another option for the analysis of complex polymers is the separation with respect to chemical composition or functionality by means of interaction chromatography. In this case, functionally or chemically homogeneous fractions are obtained which can then be subjected to molar mass determination.

To summarize, for the complete analysis of complex polymers a minimum of two different characterization methods must be used. It is most desirable that each method is sensitive towards a specific type of heterogeneity. Maximum efficiency can be expected when, similar to the two-dimensional distribution in properties, two-dimensional analytical techniques are used. A possible approach in this respect is the coupling of different chromatographic modes in

two-dimensional chromatography or the coupling of a separation technique with selective detectors.

2 Hyphenation in Polymer Analysis

Hyphenated techniques are very frequently used in low molar mass organic chemistry. Using high-resolution chromatographic techniques, such as capillary gas chromatography (GC), gradient high performance liquid chromatography (HPLC) and capillary electrophoresis (CE), complex mixtures are separated into single components which are then identified by mass spectrometry (MS). By hyphenated GC-MS, HPLC-MS, and CE-MS up to several hundreds of different components can be separated and identified in one run with very high sensitivity. This is particularly important for environmental and biological samples, where frequently only very limited sample amounts are available.

Polymers are typically complex mixtures in which the composition depends on polymerization kinetics and mechanism and process conditions. To obtain polymeric materials of desired characteristics, polymer processing must be carefully controlled and monitored. Furthermore, one needs to understand the influence of molecular parameters on polymer properties and end-use performance. Molar mass distribution and average chemical composition may no longer provide sufficient information for process and quality control nor define structure-property relationships. Modern characterization methods now require multidimensional analytical approaches rather then average properties of the whole sample [1].

Different from low molar mass organic samples, where single molecules are to be determined, for complex synthetic polymers the analytical task is the determination of a distributed property. The molecular heterogeneity of a certain complex polymer can be presented either in a three-dimensional diagram or a

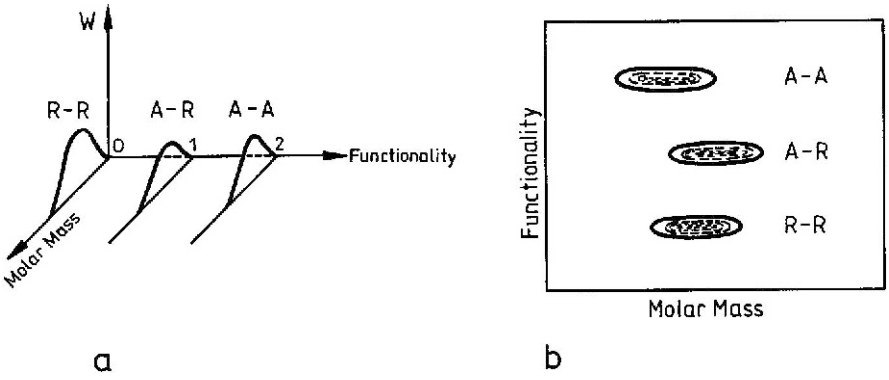

Fig. 2. Representation of the molecular heterogeneity of a telechelic polymer in a 3D diagram (**a**) and a contour plot (**b**)

so-called "contour plot". These presentations are given for a telechelic polymer in Fig. 2.

Using appropriate analytical methods, the type and concentration of the different functionality fractions must be determined and, within each functionality, the molar mass distribution has to be obtained. To do this, two different methods must be combined, each of which is preferably selective towards one type of heterogeneity. For example, a chromatographic method separating solely with respect to functionality could be combined with a molar-mass-selective method. Another approach would be the separation of the sample into different molar mass fractions which are then analyzed with respect to functionality.

For copolymers, in particular random copolymers, instead of discrete functionality fractions a continuous drift in composition is present (see Fig. 3). To determine this chemical composition drift in interrelation with the molar mass distribution, a number of classical methods have been used, including precipitation, partition, and cross-fractionation [2]. The aim of these very laborious techniques is to obtain fractions of narrow composition and/or molar mass distribution which are then analyzed by spectroscopy and SEC.

During the last 20 years, a number of techniques have been introduced in organic chemistry and applied to polymer analysis, combining chromatographic separation with spectroscopic detection [3]. GC-MS has been used in polymer analysis [4–11] but, due to the low volatility of high molar mass compounds, it is limited to the oligomer region. The combination of pyrolysis and GC-MS, however, is of great value for polymer characterization [12,13]. It provides for the analysis of complex polymers with respect to chemical composition. For a number of polymer systems characteristic low molar mass pyrolysis products are obtained, which yield information of the average composition and the "blockiness" of the polymer chain. Molar mass information, however, is not available from pyrolysis-GC-MS.

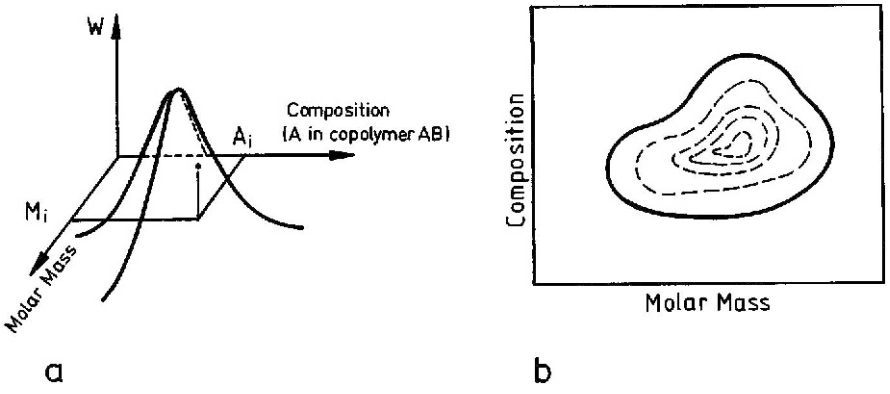

Fig. 3. Representation of the molecular heterogeneity of a random copolymer in a 3D diagram (**a**) and a contour plot (**b**)

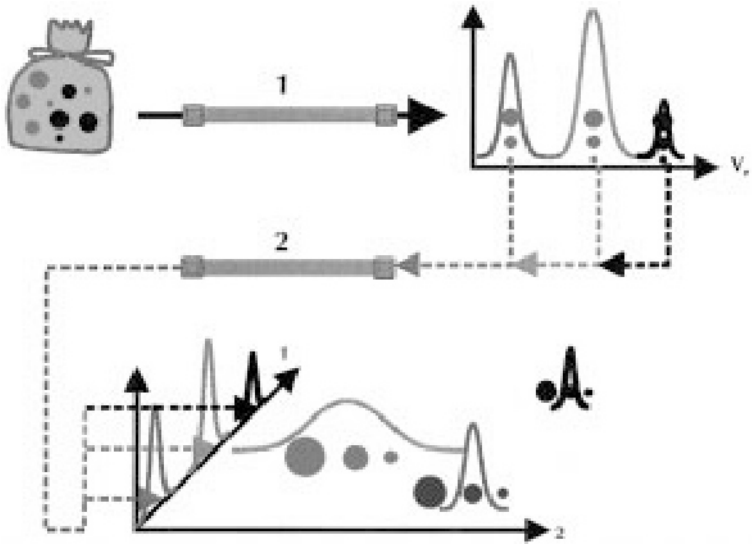

Fig. 4. Schematic separation protocol for the analysis of a complex polymer mixture

Much more important than GC are the different techniques of liquid chromatography. Using SEC, liquid adsorption chromatography (LAC), or liquid chromatography at the critical point of adsorption (LC-CC), polymers can be fractionated with respect to different aspects of molecular heterogeneity, including molar mass, functionality, and chemical composition. The advantage of these techniques over GC is that intact macromolecules are separated and analyzed. As will be shown in the following sections, liquid chromatography can be efficiently coupled to infrared spectroscopy [14–19], to mass spectrometry, and to nuclear magnetic resonance spectroscopy [20,21].

Another most efficient approach is the chromatographic separation of complex polymers by combining different separation mechanisms. This can be done by coupling two chromatographs in an off-line or on-line mode. Each of these chromatographs must operate in a mode which is selective towards one type of molecular heterogeneity. This two-dimensional chromatography has been termed "orthogonal chromatography" assuming the selectivity of each separation method with respect to one distribution function, e.g. MMD, FTD, or CCD [22]. The first truly automated 2D-chromatography setup for polymer analysis was proposed by Kilz et al. [23], who coupled gradient HPLC and SEC.

A possible separation protocol for a complex polymer mixture is presented in Fig. 4. The sample under investigation comprises molecules of different chemical compositions (different colors) and different sizes. In a first separation step this mixture is separated according to composition yielding fractions which are chemically homogeneous. These fractions are transferred to a size-selective separation method and analyzed with respect to molar mass. As a result of this two-

dimensional separation, information on both types of molecular heterogeneity is obtained.

3
Hyphenation of Size Exclusion Chromatography with Selective Detectors

Size exclusion chromatography is the premier polymer characterization method for determining molar mass distributions. In SEC, the separation mechanism is based on molecular hydrodynamic volume. For homopolymers, condensation polymers and strictly alternating copolymers, there is a correspondence between elution volume and molar mass. Thus, chemically similar polymer standards of known molar mass can be used for calibration. However, for SEC of random and block copolymers and branched polymers, no simple correspondence exists between elution volume and molar mass because of the possible compositional heterogeneity of these materials. As a result, molar mass calibration with polymer standards can introduce a considerable amount of error. To address this problem, selective detection techniques have to be combined with SEC separation.

3.1
General Considerations

When analyzing heterogeneous systems such as copolymers and polymer blends by SEC one must exercise extreme care. The dimensional distribution of macromolecules can in general be unambiguously correlated with MMD only within one heterogeneity type. For samples consisting of molecules of different chemical composition, the distribution obtained represents an average of dimensional distributions of molecules having a different composition and, therefore, cannot be attributed to a certain type of macromolecules.

The inadequacy of using SEC without further precaution for the determination of MMD of polymer blends or copolymers can be explained with reference to Fig. 5 [24]. For a linear homopolymer distributed only in molar mass, fractionation by SEC results in one molar mass being present in each retention volume. The polymer at each retention volume is monodisperse. If a blend of two linear homopolymers is fractionated, then two different molar masses can be present in one retention volume. If a copolymer is now analyzed, then a multitude of different combinations of molar mass, composition, and sequence length can be combined to give the same hydrodynamic volume. In this case, fractionation with respect to molecular size is completely ineffective in assisting the analysis of composition or MMD.

For demonstration, the SEC behavior of different polymethacrylates is given in Fig. 6. On silica gel as the stationary phase and methyl ethyl ketone as the eluent, all polymethacrylates elute in the SEC mode. The calibration curves of elution volume vs. molar mass for poly(methyl methacrylate) (PMMA), poly(*tert*-butyl methacrylate) (PtBMA), poly(*n*-butyl methacrylate) (PnBMA) and poly(decyl methacrylate) (PDMA) reflect the inability of the system to separate dif-

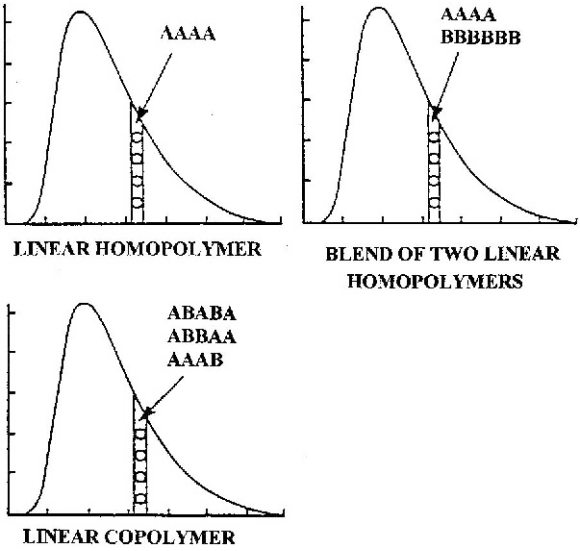

Fig. 5. SEC fractionation showing composition at a given retention volume

ferent polymethacrylates of similar molar mass. If for an unknown complex sample, e.g. a copolymer of methyl and decyl methacrylate, these calibration curves are used for molar mass determination, an elution volume of 3 ml would correspond to the following calculated molar masses: 107.000 g/mol (PnBMA calibration curve), 132.000 g/mol (PtBMA), 151.000 g/mol (PDMA), and 200.000 g/mol (PMMA). It is obvious that a huge error can result from using an inadequate calibration procedure.

To overcome the problems associated with classical SEC of complex polymers, molar mass-sensitive detectors are coupled to the SEC instrument. Since the response of such detectors depends on both concentration and molar mass, they have to be combined with a concentration-sensitive detector. The following types of molar-mass-sensitive detectors are used frequently [25–28]:

- differential viscometer
- low-angle laser light scattering (LALLS) detector
- multi-angle laser light scattering (MALLS) detector.

Another approach is the combination of SEC with multiple concentration detectors. If the response factors of the detectors for the components of the polymer are sufficiently different, the chemical composition of each slice of the elution curve can be determined from the detector signals. Typically, a combination of ultraviolet (UV) and refractive index (RI) detection is used; another possibility is the use of a diode-array detector. In the case of non-UV-absorbing polymers, a combination of RI and density detection yields information on chemical composition [29–31].

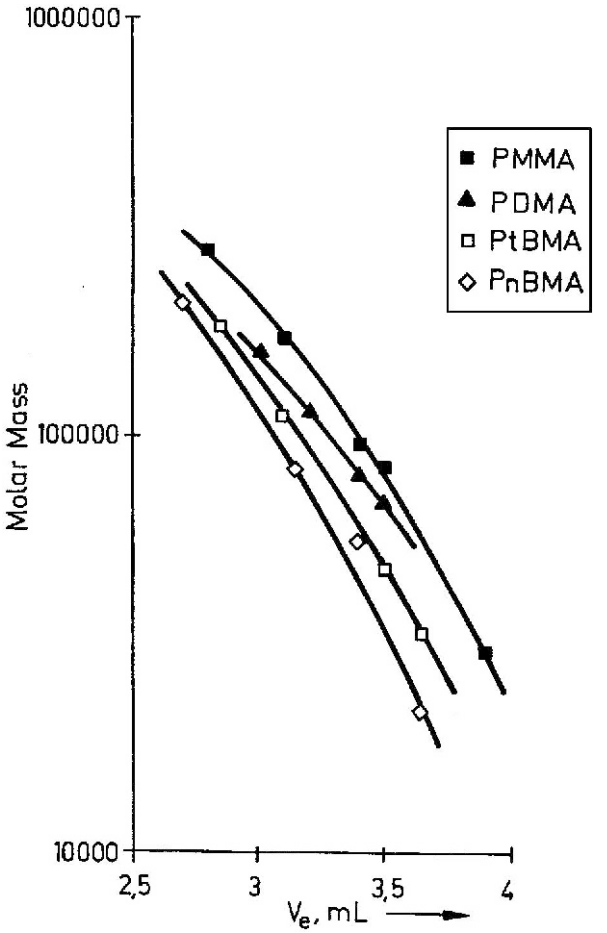

Fig. 6. SEC calibration curves of molar mass vs. elution volume for different polymethacrylates, stationary phase: LiChrosphere 300+1000 Å, eluent: methyl ethyl ketone

3.2
Coupling with Multiple Concentration Detectors

In the analysis of binary copolymers or polymer blends two different concentration detectors can be used. Typically, a combination of UV and RI detection is used, but other detector combinations have also been described. If the components of the copolymer have different UV-spectra, a diode-array detector will be the instrument of choice. One has, however, to keep in mind that non-linear detector response may also occur with UV detection.

The principle of dual detection is rather simple: when a mass m_i of a copolymer which contains the weight fractions w_A and w_B (=1–w_A) of the monomers A

and B is eluted in the slice i (with the volume ΔV) of the peak, the area $x_{i,j}$ of slice i obtained from detector j depends on the mass m_i (or the concentration $c_i = m_i/\Delta V$) of polymer in the slice, its composition (w_A), and the corresponding response factors $f_{j,A}$ and $f_{j,B}$, wherein j denotes the individual detector.

$$x_{i,j} = m_i\,(w_A f_{j,A} + w_B f_{j,B}) \tag{1}$$

The weight fractions w_A and w_B of the monomers can be calculated using

$$1/w_A = 1 - \{[(x_1/x_2) f_{2,A} - f_{1,A}]/[(x_1/x_2) f_{2,B} - f_{1,B}]\} \tag{2}$$

Once the weight fractions of the monomers are known, the correct mass of polymer in the slice can be calculated using:

$$m_i = x_i/[w_A(f_{1,A} - f_{1,B}) + f_{1,B}] \tag{3}$$

and the molar mass M_C of the copolymer is obtained by interpolation between the calibration lines of the homopolymers [32]:

$$\ln M_c = \ln M_B + w_A(\ln M_A - \ln M_B) \tag{4}$$

where M_A and M_B are the molar masses of the homopolymers which would elute in this slice of the peak (at the corresponding elution volume V_e).

It is clear that the interpolation between the calibration lines cannot be applied to mixtures of polymers (polymer blends). If the calibration lines are different, different molar masses of the homopolymers will elute at the same volume. The universal calibration is also not capable of eliminating the errors which originate from the simultaneous elution of two polymer fractions with the same hydrodynamic volume, but different composition and molar mass. Ogawa [33] has shown by a simulation technique that the molar masses of polymers eluting at the elution volume V_e are given by the corresponding coefficients K and a in the Mark–Houwink equation.

In SEC of a polymer blend, molar masses of the homopolymers eluting in the same interval can be calculated using:

$$\ln M = [AV_e/(1+a)] + [(B - \ln K)/(1+a)] \tag{5}$$

The architecture of a copolymer (random, block, graft) has also to be taken into account, as Revillon [34] has shown by SEC with RI, UV, and viscosity detection. Intrinsic viscosity varies largely with molar mass according to the type of polymer, its composition, and the nature of its components. Tung [35] found that for block copolymers in good SEC solvents the simpler first approach (Eq. 4) is more precise.

The common combination of an RI with a UV detector can only be applied if at least one of the monomers of the complex polymer absorbs a suitable wavelength, and if the UV spectra of both components are sufficiently different. Successful applications of this setup are the analysis of mixtures of polystyrene (PS) with PMMA, polybutadiene (PB), poly(vinyl chloride) or poly(butyl methacrylate). The RI detector provides the total elution profile, whereas the UV detector

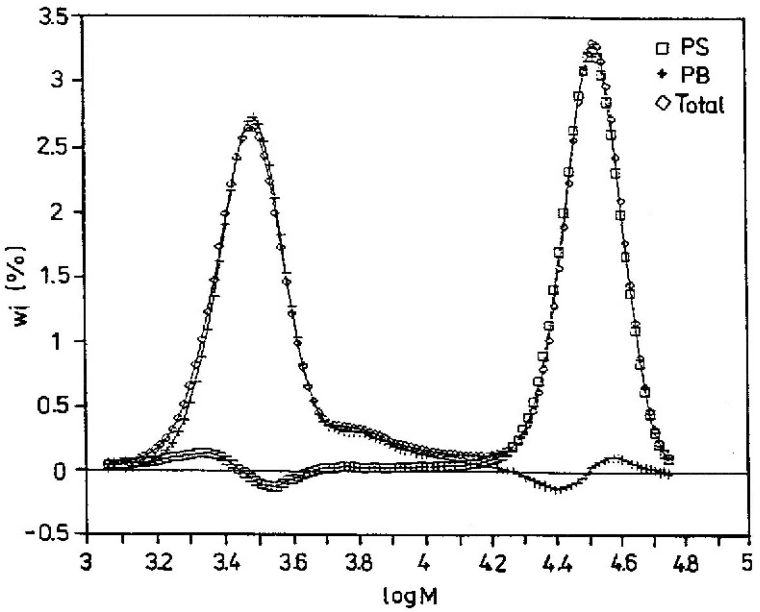

Fig. 7. Mass distribution and separated distributions of the components of a mixture of PS 50,000 and PB 3000 from SEC with D-RI detection, stationary phase: styragel, eluent: chloroform (from [31] with permission)

yields the elution profile of polystyrene. Subtracting the latter from the former, the elution profile of the non-absorbing component can be generated.

For polymer systems without UV activity the combination of a RI detector with a density (D) detector can be used. The working principle of the density detector is based on the mechanical oscillator method. Since this detector yields a signal for every polymer, provided that its density is different from the density of the mobile phase, this detector can be regarded as universal [29,30,36]. The separation of mixtures of polystyrene and polybutadiene by SEC with dual density-RI detection is presented in Figs. 7 and 8. In a first set of experiments, the response factors of both polymers in both detectors have to be determined. Then from the intensity of each slice of the elution curves in both detectors, the mass distribution of both polymers across the elution volume axis can be calculated. As can be seen in Fig. 7, a separation into the component peaks is obtained due to the fact that the molar masses of PS and PB are sufficiently different. For both components the individual elution profiles can be determined and using corresponding calibration curves for PS and PB the individual MMDs can be calculated. The same information can be extracted from an experiment where the molar masses of the components are similar and SEC separation does not work (see Fig. 8). Again the individual mass distributions are obtained and the MMDs for PS and PB can be determined.

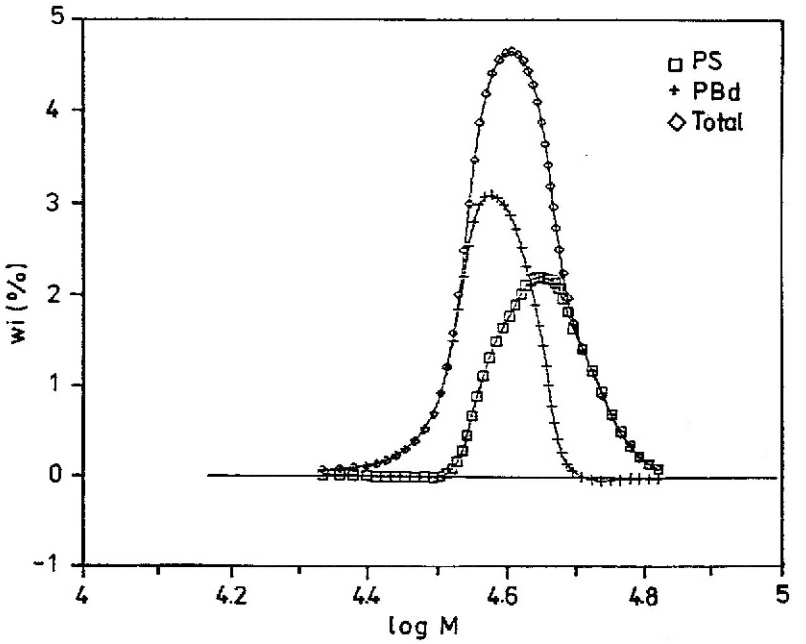

Fig. 8. Mass distribution and separated distributions of the components of a mixture of PS 50,000 and PB 31,400 from SEC with D-RI detection, stationary phase: styragel, eluent: chloroform (from [31] with permission)

Besides the overall composition of blends and random copolymers, valuable information can be obtained in the case of block copolymers. If a block copolymer contains a homopolymer fraction, a shoulder or second maximum in the MMD curve can be obtained that should have a different chemical composition. Figure 9 shows the MMD of a block copolymer of methyl methacrylate and decyl methacrylate, in which a second lower molar mass maximum can be identified as poly(decyl methacrylate) (PDMA) by dual detection [37]. The increase in the PDMA content with molar mass in the main fraction is reasonable and corresponds well with what is expected from the synthesis. It is worth noticing that this type of information can only be obtained by the D-RI detector combination, because both PDMA and PMMA have a similar low response in UV.

Further information on quantitative aspects of SEC with dual detection can be obtained from the work of Trathnigg et al. [38]. Different applications of dual detection SEC in the analysis of segmented copolymers [39], block copolymers [40,41], star polymers [42], and polymer blends [43,44] are also available. The limitation of SEC with dual detection is that only binary combinations of monomers can be investigated successfully. In the case of ternary combinations, more than two detectors must be used or one of the detectors must be able to detect two components simultaneously.

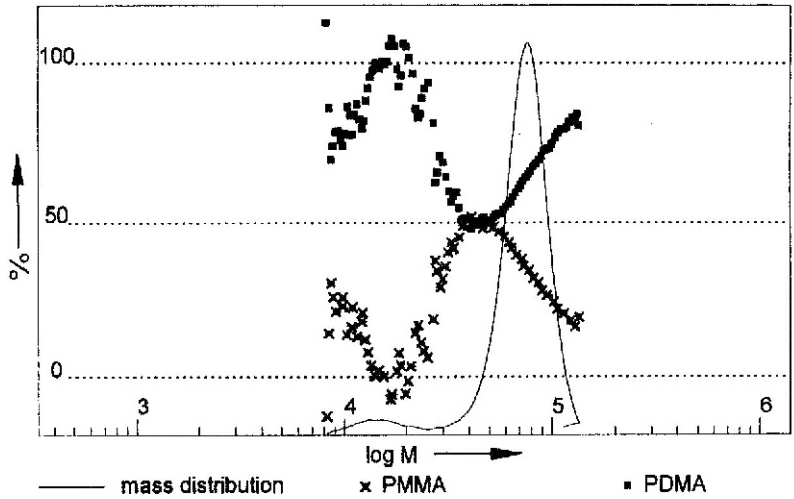

Fig. 9. Molar mass distribution and chemical composition of a PMMA-PDMA block copolymer from SEC with D-RI detection, stationary phase: styragel, eluent: chloroform (from [37] with permission)

3.3 Coupling with Molar-Mass-Sensitive Detectors

As has been pointed out, for SEC of complex polymers no simple correspondence exists between elution volume and molar mass. It is, therefore, useful to determine the molar mass not via a calibration curve but directly from the SEC effluent. This can be done by using molar-mass-sensitive detectors based on Rayleigh light scattering or intrinsic viscosity measurements [45].

In a light scattering detector, the scattered light of a laser beam passing through a cell is measured at angles different from zero. The (excess) intensity $R(\theta)$ of the scattered light at the angle θ is related to the weight-average of molar mass M_w:

$$K^* c/R(\theta) = [1/M_w P(\theta)] + 2A_2 c \tag{6}$$

where c is the concentration of the polymer, A_2 is the second virial coefficient, and $P(\theta)$ describes the scattered light angular dependence. K^* is an optical constant containing Avogadro´s number N_A, the wavelength λ_0, the refractive index n_0 of the solvent, and the refractive index increment dn/dc of the sample:

$$K^* = 4\pi^2 n_0^2 \, (dn/dc)^2/(\lambda_0^4 N_A) \tag{7}$$

In a plot of $K^* c/R(\theta)$ vs. $\sin^2(\theta/2)$, M_w can be obtained from the intercept and the radius of gyration from the slope. A multi-angle measurement provides additional information.

In most cases the injected concentration is small and A_2 can be neglected. Thus, if the optical properties (n_0 and dn/dc) of the polymer solution are known, the molar mass at each elution volume increment can be determined.

$$M_{w,i}=R(\theta)_i/K^*P(\theta)_i c_i \tag{8}$$

If a low-angle light scattering instrument is used, $P(\theta)$ is close to unity and $M_{w,i}$ can be calculated directly. For a multi-angle light scattering instrument, the mean-square radius of gyration $<R_g^2>$ at each elution volume can also be obtained from $P(\theta)$:

$$1/P(\theta)_i=1+q^2 <R_g^2>_i/3 \quad q=(4\pi/\lambda_0) \sin(\theta/2) \tag{9}$$

In practice, however, the radius of gyration can only be determined for molecules larger than 20 nm in diameter. By measuring the radius of gyration as a function of M_w, insight into the molecular conformation of the polymer can be obtained [1].

Molar mass determination requires the knowledge of the specific refractive index increment dn/dc which in the case of complex polymers depends on chemical composition. Copolymer refractive index increments $(\mathrm{d}n/\mathrm{d}c)_{copo}$ can be accurately calculated for chemically monodisperse fractions, if comonomer weight fractions w_i and homopolymer values are known:

$$(\mathrm{d}n/\mathrm{d}c)_{copo}=\Sigma\, w_i\, (\mathrm{d}n/\mathrm{d}c)_i \tag{10}$$

However, in some cases, additional effects on $(\mathrm{d}n/\mathrm{d}c)_{copo}$ must be considered. Due to cooperative interactions between the monomer units in the polymer chain, copolymer refractive index increments may deviate from the summation scheme. As a result of different sequence length distributions, different values of $(\mathrm{d}n/\mathrm{d}c)_{copo}$ can be obtained for the same gross composition. Copolymer $(\mathrm{d}n/\mathrm{d}c)_{copo}$ values can be obtained by multiple detection SEC providing the chemical composition at each slice of the elution curve.

Unfortunately, light scattering investigations of copolymers are even further complicated by the fact that SEC does not separate into chemically monodisperse fractions. Accordingly, due to compositional heterogeneity the refractive index increment of a particular scattering center may be different from the total dn/dc of the corresponding SEC slice. Therefore, in general, only apparent molar masses for copolymers can be measured [42]. Another influencing factor is the refractive index of the solvent. As has been shown by Kratochvil, the solvent refractive index should be significantly different from the values of the copolymer fractions and the corresponding homopolymers [46].

The evaluation of light scattering detectors for SEC was conducted by Jeng et al. with respect to precision and accuracy [47] and the proper selection of the light scattering equation [48]. The results obtained for polystyrene and polyethylene were compared for a low-angle and a multi-angle light scattering instrument. The application of SEC-light scattering has been discussed in a multitude of papers. In addition to determining M_w values, the formation of microgels has

been studied by Pille and Solomon [49]. Mourey et al. investigated high molar mass polystyrenes and branched polyesters, and discussed the problems encountered in molar mass and radius of gyration determination [50,51]. Grubisic-Gallot et al. proved that SEC-light scattering is useful for analyzing micellar systems with regard to determining molar masses, qualitative evaluation of the dynamics of unimer-micelles re-equilibration, and revealing the mode of micelle formation [52–54].

Another very useful approach to molar mass information of complex polymers is the coupling of SEC to a viscosity detector [55–60]. The viscosity of a polymer solution is closely related to the molar mass (and architecture) of the polymer molecules. The product of polymer intrinsic viscosity [η] times molar mass is proportional to the size of the polymer molecule (the hydrodynamic volume). Viscosity measurements in SEC can be performed by measuring the pressure drop ΔP across a capillary, which is proportional to the viscosity η of the flowing liquid (the viscosity of the pure mobile phase is denoted as η_0). The relevant parameter [η] is defined as the limiting value of the ratio of specific viscosity ($\eta_{sp}=(\eta-\eta_0)/\eta_0$) and concentration c for $c\rightarrow 0$:

$$[\eta]=\lim\,(\eta-\eta_0)/\eta_0 c=\lim\,\eta_{sp}/c \text{ for } c\rightarrow 0 \tag{11}$$

The viscosity of a polymer solution as compared to the viscosity of the pure solvent is measured by the pressure drop ΔP across an analytical capillary-transducer system. The specific viscosity is obtained from $\Delta P/P$, where P is the inlet pressure of the system. As the concentrations in SEC are usually very low, [η] can be approximated by η_{sp}/c.

A simple approach using one capillary and one differential pressure transducer will not work very well, because the viscosity changes $\Delta\eta=\eta-\eta_0$ will typically be very small compared to η_0, which means that a very small change in a large signal has to be measured. Moreover, flow-rate fluctuations due to pulsations of a reciprocating pump will lead to much greater pressure differences than the change in viscosity due to the eluted polymer. Instruments of this type should be used with a positive displacement pump.

A better approach is the use of two capillaries (C1 and C2) in series, each of which is connected to a differential pressure transducer (DP1 and DP2), and a sufficiently large holdup reservoir (H) in between. With this approach, the sample viscosity η is measured from the pressure drop across the first capillary, and the solvent viscosity η_0 from the pressure drop across the second capillary. Pulsations are eliminated in this setup because they appear in both transducers simultaneously. Another design is the differential viscometer, in which four capillaries are arranged similar to a Wheatstone bridge. In Fig. 10, both designs are shown schematically.

In the "bridge" design, a holdup reservoir in front of the reference capillary (C4) ensures that only pure mobile phase flows through the reference capillary when the peak passes the sample capillary (C3). This design offers considerable advantages: The detector actually measures the pressure difference ΔP at the dif-

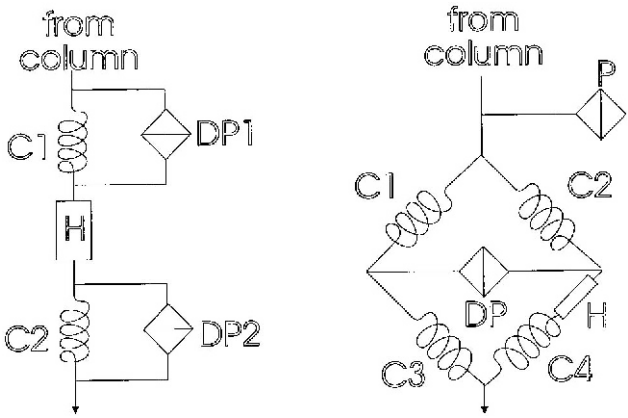

Fig. 10. Schematic representation of differential viscometers

ferential pressure transducer (DP) between the inlets of the sample capillary and the reference capillary, which have a common outlet, and the overall pressure P at the inlet of the bridge. The specific viscosity $\eta_{sp}=\Delta\eta/\eta_0$ is thus obtained from $\Delta P/P$. One concern with this type of detector is that the flow must be divided 1:1 between both arms of the bridge. This is achieved by capillaries 1 and 2, which must have a sufficiently high back pressure. Nevertheless, when a peak passes through the sample capillary, a slight deviation of the 1:1 ratio will be observed. A problem of flow-rate variations exists also in a single capillary viscometer: When the polymer peak passes through the measuring capillary, the increased back pressure leads to a peak shift [61].

Being able to determine [η] as a function of elution volume, one can now compare the hydrodynamic volumes V_h for different polymers. The hydrodynamic volume is, through Einstein's viscosity law, related to intrinsic viscosity and molar mass by $V_h=[\eta]M/2.5$. Einstein's law is, strictly speaking, valid only for impenetrable spheres at infinitely low volume fractions of the solute (equivalent to concentration at very low values). However, it can be extended to particles of other shapes, defining the particle radius then as the radius of a hydrodynamically equivalent sphere. In this case V_h is defined as the molar volume of impenetrable spheres which would have the same frictional properties or enhance viscosity to the same degree as the actual polymer in solution.

Assuming the validity of this approach, and in agreement with the SEC mechanism, similar elution volumes correspond to similar hydrodynamic volumes.

$$V_{e,1}=V_{e,2}\rightarrow M_1\,[\eta]_1=M_2\,[\eta]_2 \tag{12}$$

In a plot of log ($M[\eta]$) vs. V_e identical calibration lines should be found for the two polymers 1 and 2, irrespective of their chemical composition. This "universal calibration" approach was predicted and experimentally proved by Benoit et al. [62]. As a consequence, using the universal calibration curve established with

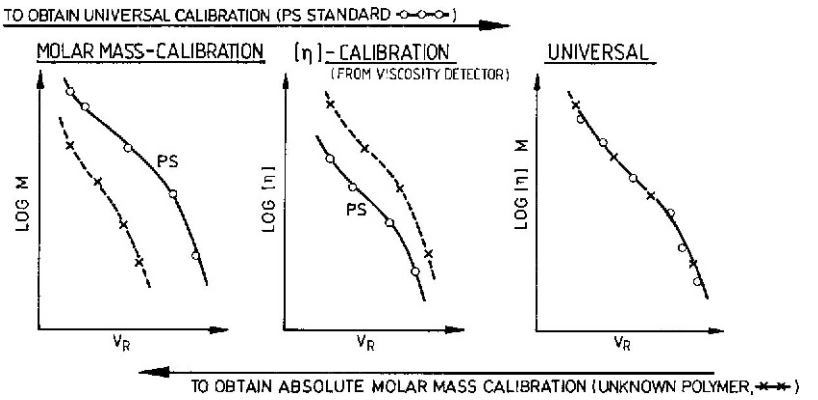

Fig. 11. Determination of absolute molar masses via universal SEC calibration

known calibration standards (for example polystyrene), one can obtain the SEC-molar mass calibration for an unknown polymer sample.

The intrinsic viscosity is a function of molar mass via the Mark–Houwink relationship, wherein K and a are coefficients for a given polymer in a given solvent at a given temperature.

$$[\eta]=K M^a \tag{13}$$

Combination of Eqs. (12) and (13) yields

$$K_1 M_1^{a(1)+1}=K_2 M_2^{a(2)+1} \tag{14}$$

If a column has been calibrated with polymer 1 (e.g. polystyrene), the calibration line for polymer 2 can be calculated, provided that the coefficients K and a are known for both polymers with sufficient accuracy:

$$\ln M_2=(1/1+a_2)\ln (K_1/K_2)+(1+a_1/1+a_2)\ln M_1 \tag{15}$$

Thus, the concept of universal calibration provides an appropriate calibration also for polymers for which no calibration standards exist. The limiting factor of this approach is the accuracy of determining K and a. There are very high variations in the values reported in the literature [63,64]. Even for such common polymers as polystyrene and poly(methyl methacrylate), the values may differ considerably.

If the Mark–Houwink coefficients are not available, a universal calibration curve is established using polystyrene calibration standards and the SEC-viscometer combination. The basic steps involved in the MMD analysis are summarized in Fig. 11. First, the universal calibration curve of the SEC separation system has to be established by using narrow molar mass standards as indicated by the top arrow pointing to the right. Once the universal calibration curve is established, the procedure can then be reversed, by going from right to left following the bottom arrow, to obtain the molar mass calibration curve of any unknown

polymer. The calibration curve is obtained literally by subtracting the [η] calibration curve of the unknown sample from the universal calibration curve. The [η] calibration curve for the unknown sample is obtained from the on-line viscometer [65].

The application of refractive index and differential viscometer detection in SEC has been discussed by a number of authors [66–68]. Lew et al. presented the quantitative analysis of polyolefins by high-temperature SEC and dual refractive index-viscosity detection [69]. They applied a systematic approach for multidetector operation, assessed the effect of branching on the SEC calibration curve, and used a signal averaging procedure to better define intrinsic viscosity as a function of retention volume. The combination of SEC with refractive index, UV, and viscosity detectors was used to determine molar mass and functionality of polytetrahydrofuran simultaneously [70]. Long chain branching in EPDM copolymers by SEC-viscometry was analyzed by Chiantore et al. [71].

One of the most difficult problems when characterizing copolymers and polymer blends by SEC-viscometry is the accurate determination of the polymer concentration across the SEC elution curve. The concentration detector signal is a function of the chemical drift of the sample under investigation. To overcome this problem, Goldwasser proposed a method where no concentration detector is required for obtaining M_n data [72]. In the usual SEC-viscometry experiment, the determination of the intrinsic viscosity at each slice of the elution curve requires a viscosity and a concentration signal:

$$[\eta]_i=(\ln \eta_{rel}/C)_i \tag{16}$$

where $\ln \eta_{rel}$ is the direct detector response of the viscometer. From Eq. (16) the molar mass averages can be calculated by:

$$M_n=\Sigma\, C_i/\Sigma\, [C_i/(V_{h,x}/[\eta])_i] \tag{17}$$

$$M_w=\Sigma\, C_i\, (V_{h,x}/[\eta])_i/\Sigma\, C_i \tag{18}$$

where $V_{h,x}=[\eta]_x M_x$ is the data retrievable from the universal calibration curve. By rearranging Eq. (17) using Eq. (16) the following expression is obtained:

$$M_n=\Sigma\, C_i/\Sigma\, (\ln \eta_{rel}/V_{h,x})_i \text{ or } M_n=\text{sample amount}/\Sigma\, (\ln \eta_{rel}/V_{h,x})_i \tag{19}$$

The sample amount can be easily determined from the injection volume and the sample concentration, and no information from a concentration detector is required. With this approach, the M_n value of any polymer sample can be determined by SEC using only a viscosity detector. Other molar mass averages, however, cannot be determined. The advantage of the Goldwasser M_n method is that it can access much wider molar mass ranges than other existing methods like osmometry or end-group methods.

Due to the problems encountered with SEC-LALLS and SEC-viscometry, a triple-detector SEC technology has been developed, where three on-line detectors are used together in a single SEC system. In addition to the concentration detector, an on-line viscometer and a LALLS instrument are coupled to the SEC

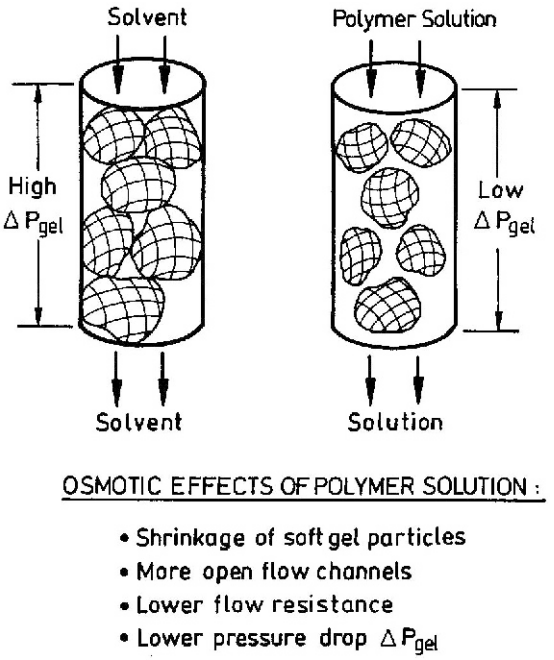

Fig. 12. Differential pressure measurement of osmotic effect on a soft gel column

(TriSEC). With TriSEC, absolute molar mass determination is possible for polymers that are very different in chemical composition and molecular conformation. The usefulness of the TriSEC approach has been demonstrated in a number of applications. It was shown by Pang and Rudin that using both viscometer and LS detection accurate molar mass distributions are obtained [73]. Wintermantel et al. have developed a custom-made multidetector instrument and demonstrated that it has great potential not only for absolute molar mass determinations but also for structure characterization of linear flexible, semiflexible, and branched polymers [74]. Degoulet characterized polydisperse solutions of branched PMMA [75], while Jackson et al. investigated linear chains of varying flexibility in order to prove universal calibration [76]. Yau and Arora discussed the advantages of TriSEC for the determination of Mark–Houwink coefficients, long-chain branching, and polymer architecture [77].

Finally, several attempts have been made to develop an absolute molar mass detector based on osmotic pressure measurements. Commercially available membrane osmometers are designed for static measurements, and the cell design with a flat membrane is not suited for continuous flow operation. Different from the conventional design, Yau developed a detector which measures the flow resistance of a column caused by osmotic swelling and deswelling of soft gel particles used for the packing (see Fig. 12) [65,78]. With a microbore gel column, a

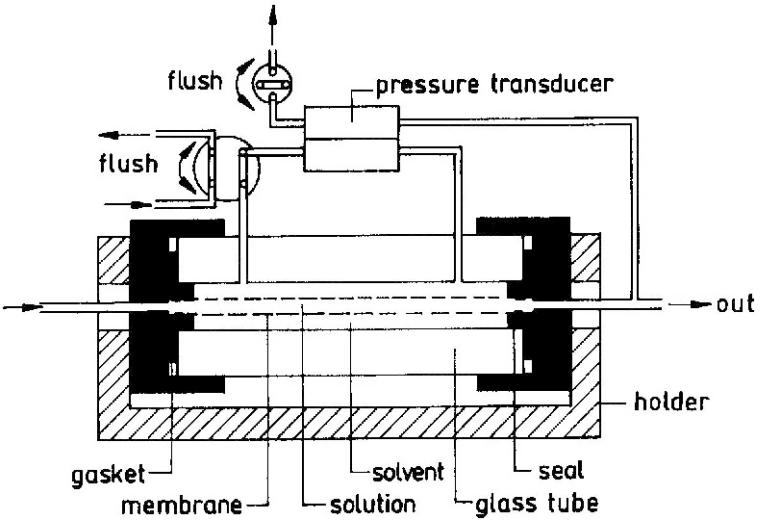

Fig. 13. Design of a concentric osmometric flow cell (from [80] with permission)

M_n-sensitive detector with a fast response was obtained which could be coupled to the SEC equipment. However, since the change in flow resistance could not easily be related to the osmotic pressure of the solution, absolute calibration was lost.

Recently, an osmometer based on a concentric design with a capillary-shaped membrane has been developed by Köhler et al. [79,80]. The flow cell volume is 12.2 µl, the response time approx. 15 s, and the molar mass cut-off is below 5000 g/mol. The design of the cell is given in Fig. 13. The cylinder symmetry and stiffness of the osmometer and the favorable properties of the membrane were combined to meet the requirements for on-line detection. Testing the instrument in both batch and continuous flow operation with polystyrene standards yielded reproducible results and good agreement with the nominal molar masses. However, the osmometer still caused a certain peak broadening, and the pressure noise level still strongly exceeded the noise of the concentration detector.

3.4 Conclusions and Outlook

As has been discussed, the combination of SEC and molar-mass-sensitive detectors is a powerful tool for the analysis of complex polymers. However, it is important to distinguish between claimed versus actual capabilities and between potential expectations and demonstrated performances. Tables 1 and 2, taken from a critical review of different techniques, summarize the informational content and additional details of SEC-light scattering and SEC-viscometry coupling

Table 1. SEC analysis using molar-mass-sensitive detectors

Method	Information content	
	Primary	Secondary
Regular SEC		Molar mass distribution
SEC-LALLS	Molar mass distribution	
SEC-MALLS	Molar mass distribution	Radius of gyration distribution
SEC-VIS	Intrinsic viscosity distribution	Molar mass distribution
		Radius of gyration distribution
		Copolymer M_n
SEC-VIS-LS	Intrinsic viscosity distribution	Copolymer M_n
	Molar mass distribution	
	Radius of gyration distribution	

Table 2. Generalization of molar mass-sensitive detectors

Intended measurements	LALLS/MALLS	Viscometer
Molar mass distribution	Requires precise n and dn/dc values, not affected by non-exclusion effects	Requires universal calibration and K, a parameters
Intrinsic viscosity distribution		Directly from experiment, not affected by non-exclusion effects
Radius of gyration distribution	MALLS only	Calculable from $[\eta]M$
Chain conformation and branching	R_g vs. M plot, MALLS only	$[\eta]$ vs. M plot, R_g vs. M plot
Chemically heterogeneous polymer analysis	Limited	Better
Noise, particulates, bubbles	Strongly affected	Less affected

[65]. The information content is classified into two categories. "Primary" information is of high precision and accuracy, insensitive to SEC operation variables, and not requiring molar mass or universal calibration. "Secondary" information is less precise and requires calibration.

In addition, the complex procedures related to SEC-light scattering and SEC-viscometry coupling are a potential source of error. According to Jackson and Barth [81] these include:

1. Accuracy of the universal calibration curve,
2. Detector configuration: arrangement of multiple detectors in series or in parallel can cause additional peak broadening, flow rate variations, back pressure variations,

3. Inter-detector volume: detectors are placed at different physical positions and their signals must be aligned very precisely,
4. Detector sensitivity: light scattering and viscosity detectors are very sensitive towards higher molar masses while RI detectors are most sensitive at lower molar masses,
5. Low molar mass fractions: polymer molecules may not adopt random coil conformation, the Mark–Houwink coefficients become functions of molar mass.

To summarize, although the principal limitation of SEC separating according to hydrodynamic volume and not molar mass cannot be overcome, the advantages of multidetector SEC in the accurate characterization of complex polymers are significant. However, in order to generate reproducible and accurate results on a routine basis, special care must be taken regarding the added complexity of the instrumentation. In addition to improving the design of multidetector SEC setups, important advances are expected from methods for determining the chemical composition across the molar mass distribution by interfacing SEC with Fourier transform infrared (FTIR) spectroscopy, mass spectrometry, and NMR.

4 Two-Dimensional Chromatography

As was pointed out in the introduction, complex polymers are distributed in more than one direction. Copolymers are characterized by the molar mass distribution and the chemical heterogeneity, whereas functional homopolymers are distributed in molar mass and functionality. Hence, the experimental evaluation of the different distribution functions requires separation in more than one direction.

The classical approach is based on the dependence of copolymer solubility on composition and chain length. A solvent/nonsolvent combination fractionating solely by molar mass would be appropriate for the evaluation of MMD, another one separating with respect to chemical composition would be suited for determining CCD or FTD. However, in reality, precipitation fractionation yields fractions which vary both in chemical composition and molar mass. Even high resolution fractionation would not improve the result. Narrower fractions can be obtained by cross-fractionation separating in two different directions. However, even in this case, it is almost impossible to obtain perfectly homogeneous fractions.

By the use of different modes of liquid chromatography it is possible to separate polymers selectively with respect to hydrodynamic volume (molar mass), chemical composition or functionality. Using these techniques and combining them with each other or with a selective detector, two-dimensional information on different aspects of molecular heterogeneity can be obtained. If, for example, two different chromatographic techniques are combined in a "cross-fractionation" mode, information on CCD and MMD can be obtained. Literally, the term "chromatographic cross-fractionation" refers to any combination of chromato-

graphic methods capable of evaluating the distribution in size and composition of copolymers. An excellent overview of different techniques and applications involving the combination of SEC and gradient HPLC has been published by Glöckner [64].

4.1 Orthogonal Chromatography

The molecular size of a copolymer molecule in solution is a function of its chain length, chemical composition, solvent and temperature. Thus, molecules of the same chain length but different composition have different hydrodynamic volumes. Since SEC separates according to hydrodynamic volume, SEC in different eluents can separate a copolymer in two diverging directions. This principle of "orthogonal chromatography" was suggested by Balke and Patel [82–84]. The authors coupled two SEC instruments together so that the eluent from the first one flowed through the injection valve of the second one. At any desired retention time the flow through SEC 1 could be stopped and an injection made into SEC 2. The first instrument was operated with tetrahydofuran (THF) as the eluent and polystyrene gel as the packing, whereas for SEC 2 polyether bonded phase columns and THF/heptane were used. Both instruments utilized SEC columns. However, whereas SEC 1 was operating so as to achieve conventional molecular size separation, SEC 2 was used to fractionate by composition, utilizing a mixed solvent to encourage adsorption and partition effects in addition to size exclusion.

The authors reported the investigation of random copolymers of styrene and *n*-butyl methacrylate, containing the parent homopolymers PS and PnBMA. While in SEC 1 fractions of different molecular size were obtained, a separation with respect to chemical composition into fractions of PnBMA, P(St/nBMA) and PS could be achieved in SEC 2, the elution order being PnBMA<P(St/nBMA)<PS. The explanation of this behavior is the synergistic effect of different separation mechanisms including size exclusion, adsorption and partition.

Strictly speaking, Balke's system combined SEC in the first dimension with a mixed mode separation in the second dimension. Since SEC separates with respect to hydrodynamic volume and not molar mass, the copolymers under investigation could not be quantified with respect to molar mass distribution (see discussion in Sect. 3). The effect of the SEC separation was simply to obtain fractions with narrower molar mass distribution as compared to the total sample. Considering this fact, it is clear that for chemically heterogeneous copolymers no quantitative data can be obtained from the first dimension. Only the second dimension, separating with respect to chemical composition, can provide quantitative information on the chemical composition distribution. Accordingly, a "coupled" information on both MMD and CCD was not available for this system.

Assuming that "orthogonality" means that each separation technique is selective towards a specific type of heterogeneity, it seems to be more advantageous

to use a sequence of methods, where in the first dimension the sample is separated according to chemical composition. From this type of separation, quantitative information on CCD can be obtained and the resulting fractions are chemically homogeneous. These chemically homogeneous fractions can then be subjected to SEC in the second dimension. In this case SEC separation is strictly with respect to molar mass, and quantitative data on MMD can be obtained.

4.2 Coupling of Liquid Adsorption Chromatography and SEC

Much work on chromatographic cross-fractionation has been carried out with respect to combination of SEC and gradient HPLC. In most cases SEC was used as the first separation step, followed by HPLC. In a number of early papers the cross-fractionation of model mixtures was discussed. Investigations of this kind demonstrated the efficiency of gradient HPLC for separation by chemical composition. Mixtures of random copolymers of styrene and acrylonitrile were separated by Glöckner et al. [85]. In the first dimension a SEC separation was carried out using THF as the eluent and polystyrene gel as the packing. In total, about 10 fractions were collected and subjected to the second dimension, which was gradient HPLC on a CN-bonded phase using iso-octane/THF as the mobile phase. Model mixtures of random copolymers of styrene and 2-methoxyethyl methacrylate were separated in a similar way; the mobile phase of the HPLC mode being isooctane/methanol in this case [86]. This procedure was also applied to real-world copolymers [85]. Graft copolymers of methyl methacrylate onto EPDM rubber were analyzed by Augenstein and Stickler [87]; whereas, Mori reported on the fractionation of block copolymers of styrene and vinyl acetate [88]. For all these experiments the same limitation with respect to the SEC part holds true: when SEC is used as the first dimension, true molar mass distributions are not obtained.

From the theoretical point of view, a more feasible way of analyzing copolymers is the prefractionation through HPLC in the first dimension and subsequent analysis of the fractions by SEC [89,90]. HPLC was found to be rather insensitive towards molar mass effects and yielded very uniform fractions with respect to chemical composition.

The major disadvantage of all early investigations on chromatographic cross-fractionation was related to the fact that both separation modes were connected to each other either off-line or in a stop-flow mode. Regardless of the separation order, SEC vs. HPLC or HPLC vs. SEC, in the first separation step fractions were collected, isolated, and then subjected to the second separation step. This procedure, of course, is very time-consuming and the reliability of the results at least to a certain extent depends on the skills of the operator.

A fully automated two-dimensional (2D) chromatographic system was developed by Kilz et al. [91–93]. It consists of two chromatographs, one which separates by chemical composition or functionality and an SEC instrument for subsequent separation by size. Via a storage loop system, fractions from the first

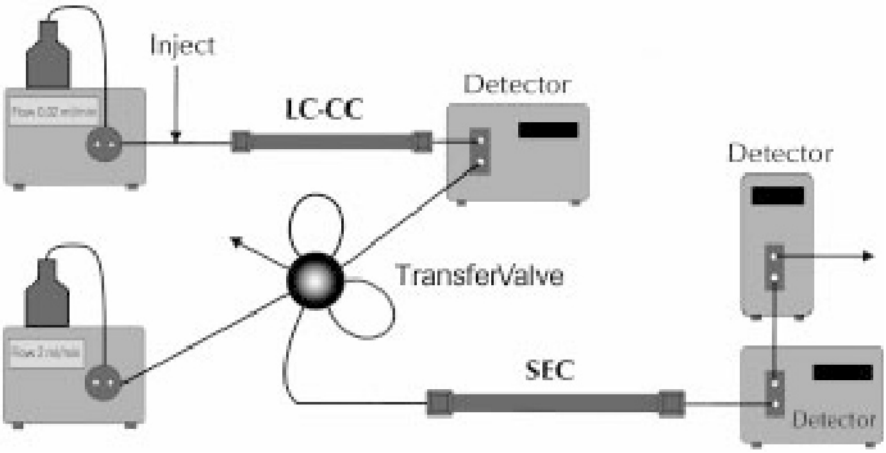

Fig. 14. Schematic representation of an automated 2D chromatographic system

separation step are automatically transferred into the second separation system. The operation of the column switching device is automatically driven by the software, which at the same time organizes the data collection from the detector. The principle design of a fully automated 2D system is presented schematically in Fig. 14.

Regardless of the sequence of the different separation modes, two different chromatographic systems comprising an eluent reservoir, a HPLC pump, an injector, and a column combination are required. Depending on the specific separation problem, one or more detectors may be used in both or only in the second chromatographic dimension. As already discussed, an important feature of a 2D chromatographic system is the sequence of the separations to be carried out. In many cases interaction chromatography as the first separation step is the best choice. From an experimental point of view, high flexibility is required for the first chromatographic dimension. This is better achieved by running the interaction chromatography mode in the first dimension due to the fact that (1) more parameters (mobile phase, stationary phase, temperature) can be used to adjust the separation according to the chemical nature of the sample, (2) better fine-tuning in HPLC gives more homogeneous fractions, and (3) sample load on HPLC columns can be much higher as compared with SEC columns.

The most sophisticated way of coupling the two chromatographs is a fraction transfer system comprising one eight-port injection valve (see Fig. 15). With two storage loops, it is possible to collect fractions continuously without losses. When starting the separation, loop 1 is in the "LOAD" position, whereas loop 2 is in the "INJECT" position. Each of the loops has a volume of 100–200 µl. When the first fraction leaves the HPLC system, it enters loop 1 and fills it. When loop 1 is completely filled with the fraction, the injection valves automatically switch to the opposite positions, i.e. loop 1 is then connected to the SEC system in the

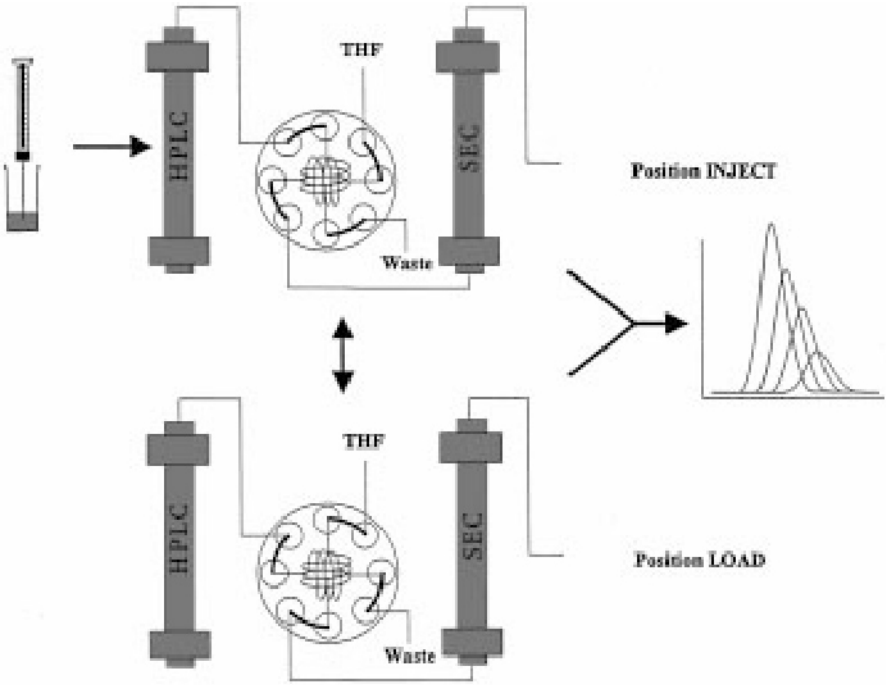

Fig. 15. Schematic representation of 2D chromatography using an eight-port injection valve and two storage loops

"INJECT" position, whereas loop 2 is connected to the HPLC system in the "LOAD" position. Now loop 2 is filled with the next fraction and loop 1 is emptied into the SEC for analysis. After filling loop 2, the injection valves are switched again, connecting loop 2 to the SEC and the emptied loop 1 to the HPLC to be filled with the next fraction. In this operational mode, the first separation step runs continuously, fractions are taken and continuously subjected to the second separation step, and each fraction is transferred without losses.

An important feature for such an automated system is the proper coordination of the flow rates of the HPLC and the SEC systems. Since fractions are continuously collected from HPLC and subjected to SEC, the collection time of one fraction must exactly equal the analysis time in the SEC mode. Depending on the number and size of the SEC columns, about 7–15 min are required for one SEC analysis. The flow rate in HPLC must be such that one storage loop is filled exactly within this time. In practice, typical flow rates are 20–40 µl/min and 1.5–2.5 ml/min for the first and second dimensions, respectively.

Each fraction from the HPLC separation represents a very dilute solution. When injecting this fraction into the SEC system, further dilution takes place. Accordingly, high sensitivity of the detector is required. In addition, the injection of the HPLC eluent into the SEC system (THF as the eluent) causes the for-

Table 3. Molar masses of the star copolymers

Sample	Butadiene content (wt%)	M_w (g/mol)	M_n (g/mol)
1	17	87,000	35,000
2	39	88,000	31,000
3	63	79,000	32,000
4	78	77,000	29,000

mation of a pronounced solvent peak at the void volume of the SEC chromatogram. This solvent peak appears very strongly when using a refractive index detector. Because of this solvent peak, in some cases, the component peak cannot be detected properly. In order to avoid the appearance of strong solvent peaks in the chromatograms the use of an evaporative laser light scattering detector (ELSD) is recommended. For the detection of UV-active components, a corresponding UV detector can be used; however, the UV absorption properties of the eluents must be considered in this case. The effect of sampling in comprehensive 2D chromatography has been studied by Murphy et al. [94]. Optimization of multidimensional separation systems requires an understanding of the relationship between system resolution and the number of second dimension injections across a first dimension peak.

One of the very few applications of 2D gradient HPLC-SEC was published by Kilz et al. describing the analysis of styrene-butadiene star polymers [92]. These 4-arm star polymers based on poly(styrene-*block*-butadiene) were prepared by anionic polymerization to give samples with well-known structure and molar mass control. In a first reaction step, a poly(styrene-*block*-butadiene) with a reactive chain end at the butadiene was prepared. This precursor reacted with a tetrafunctional terminating agent to give a mixture of linear (of molar mass *M*), 2-arm (2 *M*), 3-arm (3 *M*) and 4-arm (4 *M*) species. Four samples with varying butadiene content (about 20, 40, 60, 80%) were prepared in this way (see Table 3). A mixture of these samples was used for the 2D experiment. Accordingly, a complex mixture of 16 components, resulting from the combination of four different butadiene contents and four different molar masses (*M*, 2 *M*, 3 *M*, 4 *M*), had to be separated with respect to chemical composition and molar mass.

Initially, the 16-component star block copolymer was investigated by SEC. As can be seen in Fig. 16, four peaks were obtained. They correspond to the four molar masses of the sample consisting of oligomers with one to four arms. The molar masses were in the ratio *M*-2 *M*-3 *M*-4 *M*. Despite the high resolution, the chromatogram did not give any indication of the very complex chemical structure of the sample. Even when pure fractions with different chemical compositions were investigated, the retention behavior did not show significant changes as compared with the sample mixture. In each case a tetramodal molar mass distribution was visible indicating the different topological species. The SEC separation alone did not show any difference in chemical composition of the samples, which vary from 20 to 80% butadiene content.

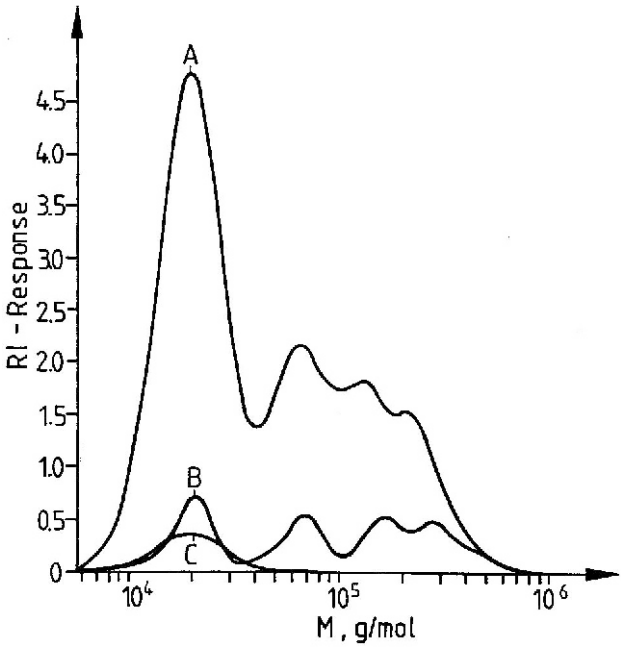

Fig. 16. SEC chromatograms of the 16-component sample (*A*) and the star polymers 1 (*C*) and 4 (*B*), stationary phase: SDV PSS 1000 and 10^5 Å, mobile phase: THF, RI detection (from [92] with permission)

Running the sample mixture in gradient HPLC gave poorly resolved peaks, which might suggest different composition, but gave no clear indication of different molar mass and topology (see Fig. 17). The combination of the two methods in the 2D setup dramatically increased the resolution of the separation system and gave a clear picture of the complex nature of the 16-component sample. A three-dimensional (3D) representation of the gradient HPLC-SEC separation is given in Fig. 18. Each trace represents a fraction transferred from HPLC to SEC and gives the result of the SEC analysis. Based on the composition of the sample, a contour map with the coordinates chemical composition and molar mass is expected to show 16 spots, equivalent to the 16 components. Each spot would represent a component which is defined by a single composition and molar mass. The experimental evidence of the improved resolution in the 2D analysis is given in Fig. 19. This contour plot was calculated from experimental data based on 28 transfer injections.

The contour plot clearly revealed the chemical heterogeneity (Y-axis, chemical composition) and the molar mass distribution (X-axis) of the mixture. The relative concentrations of the components were indicated by colors; 16 major peaks were resolved with high selectivity. These correspond directly to the components. For example, peak 1 corresponds to the component with the lowest

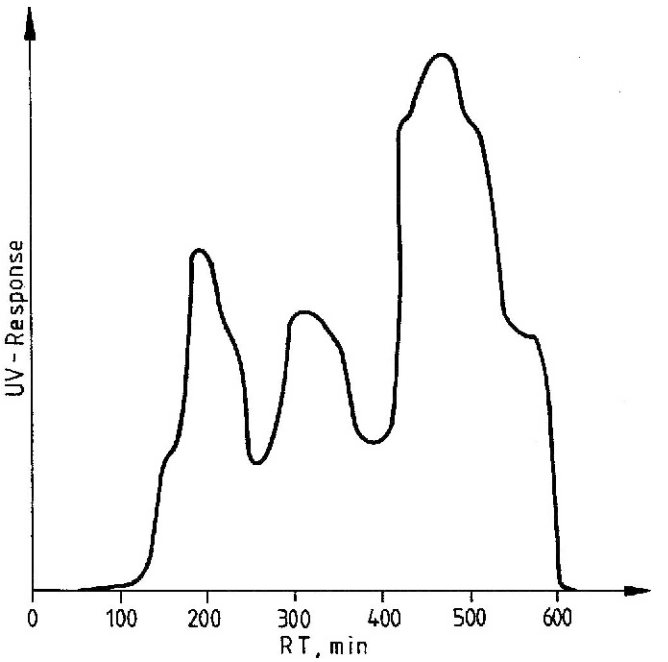

Fig. 17. Gradient HPLC chromatogram of the 16-component star polymer mixture, stationary phase: silica gel, mobile phase: i-octane/THF, linear, 20–100% THF (from [92] with permission)

butadiene content and the lowest molar mass (molar mass *M*) whereas peak 13 relates to the component with the lowest butadiene content but a molar mass of 4 *M*. Accordingly, peak 16 is due to the component with the highest butadiene content and a molar mass of 4 *M*. A certain molar mass dependence of the HPLC separation is indicated by a drift of the peaks for components of similar chemical composition, see peaks 1-5-9-13, for example. This kind of behavior is normal for polymers, because pores in the HPLC stationary phase lead to size-exclusion effects which overlap with the adsorptive interactions at the surface of the stationary phase. Consequently, 2D separations of this type will in general not be orthogonal but skewed, depending on the pore size distribution of the stationary phase. The quantitative amount of butadiene in each peak could be determined via an appropriate calibration with samples of known composition. The molar masses could be calculated based on a conventional SEC calibration of chromatograph 2.

The mapping of ethoxylated fatty alcohols and ethylene oxide–propylene oxide block copolymers by 2D chromatography was discussed by Trathnigg et al. [95]. They combined LAC and SEC and were able to determine the chemical composition distribution and the molar mass distribution of the polyethers.

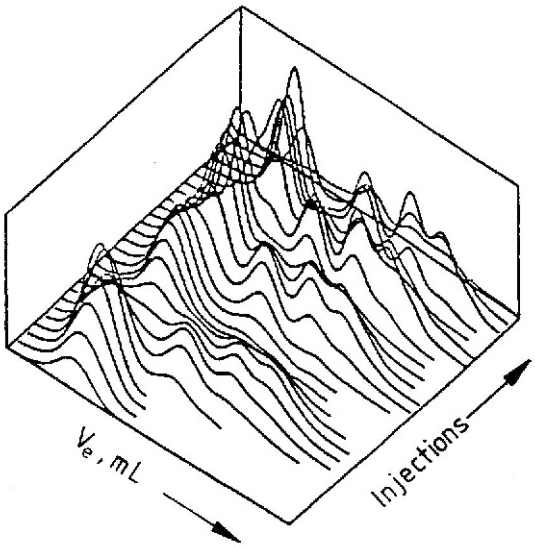

Fig. 18. 3D plot of the HPLC-SEC analysis of the 16-component star copolymer (from [92] with permission)

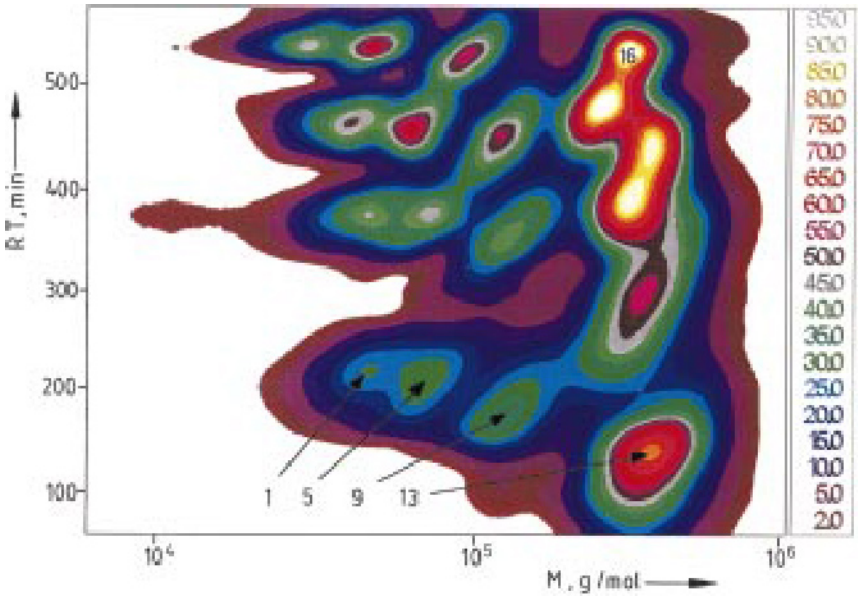

Fig. 19. Contour plot of the 2D separation of a 16-component styrene-butadiene star copolymer (from [92] with permission)

4.3 Coupling of Liquid Chromatography at the Critical Point of Adsorption and SEC

Liquid chromatography at the critical point of adsorption (LC-CC) relates to a chromatographic situation where the entropic and enthalpic interactions of the macromolecules and the column packing compensate each other. The Gibbs free energy of the macromolecule does not change when entering the pores of the stationary phase (ΔG=0). The distribution coefficient K_d is unity, regardless of the size of the macromolecules, and all macromolecules of equal chemical structure elute from the chromatographic column in one peak. To describe this phenomenon the term "chromatographic invisibility" is used, meaning that the chromatographic behavior is not directed by the size but by the inhomogeneities (chemical structure) of the macromolecules [96–103].

As the Gibbs free energy in general is influenced by the length of the polymer chain and its chemical structure, contributions ΔG_i for the polymer chain and ΔG_j for the heterogeneity may be introduced.

$$\Delta G=\Sigma(n_i\Delta G_i+n_j\Delta G_j) \tag{20}$$

For a homopolymer chain without chemical heterogeneity, ΔG equals the contribution of the polymer chain.

$$\Delta G=\Sigma n_i\Delta G \tag{21}$$

At the critical point of adsorption of the polymer chain of a complex polymer, however, the contribution ΔG_i becomes zero and chromatographic behavior is exclusively directed by the heterogeneity.

$$\Delta G=\Sigma n_j\Delta G_j \tag{22}$$

Under such chromatographic conditions it is possible to determine the heterogeneities of the polymer chain selectively and without any influence of the polymer chain length. LC-CC has been successfully used for the determination of the functionality type distribution of telechelics and macromonomers [104–109], for the analysis of block copolymers [111–114], macrocyclic polymers [115], and polymer blends [116–118].

Thus, LC-CC represents a chromatographic separation technique yielding fractions which are homogeneous with respect to chemical composition but distributed in molar mass. These fractions can readily be analyzed by SEC which for chemically homogeneous fractions provides true molar mass distributions without interference of CCD or FTD. Therefore, the combination of LC-CC and SEC in a 2D setup can truly be regarded as "orthogonal" chromatography provided that LC-CC comprises the first dimension. Consequently, for functional homopolymers being distributed in functionality and molar mass, coupled LC-CC vs. SEC can yield combined information on FTD and MMD. This type of dual information is of significant importance, for example, for the quality control of amphiphilic polyalkylene oxides.

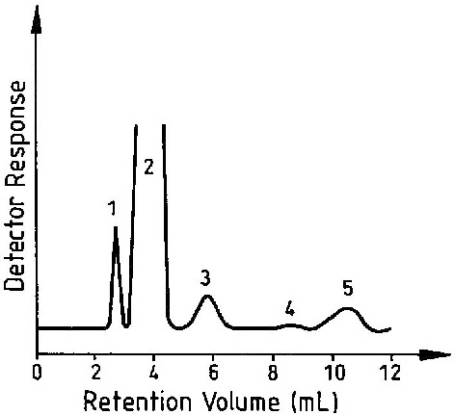

Fig. 20. LC-CC separation of octylphenoxy-terminated poly(ethylene oxide), stationary phase: Nucleosil RP-18, eluent: methanol/water 86:14 (v/v) (from [119] with permission)

The analysis of an octylphenoxy-terminated PEO with respect to FTD and MMD has been demonstrated by Adrian et al. [119]. A separation of the sample with respect to the terminal groups was achieved by LC-CC, similar to previous investigations [107,108], on a RP-18 stationary phase and a critical eluent composition of methanol/water 86:14 (v/v) (see Fig. 20) [119]. Five well-separated peaks appeared in the chromatogram, which were identified by matrix-assisted laser desorption/ionization (MALDI-TOF) mass spectrometry as being different functionality fractions. Accordingly, separation took place strictly with respect to the chemical structure of the terminal groups. Having this type of selective separation at hand, it was then combined with SEC as the molar mass selective technique using the experimental setup described in Fig. 14. As a result, a contour plot LC-CC vs. SEC was obtained (see Fig. 21) [119]. At the abscissa, the retention volume of the SEC runs (chromatograph 2) is given, whereas the ordinate gives the retention volume of the LC-CC (chromatograph 1). The peak height is assigned to a color code, meaning that equal colors are equivalent to equal peak intensities.

The contour plot clearly shows five spots corresponding to the five functionality fractions (cf. Fig. 20), fraction 2 being the main fraction containing the α-octylphenoxy-ω-hydroxy oligomers. In addition, α,ω-di(octylphenoxy) oligomer fractions and fractions having butylphenoxy end groups are obtained. It is obvious that the fractions have very similar molar masses.

The 2D experiment yielded separation with respect to functionality and molar mass, and FTD and MMD could be determined quantitatively. For calculating FTD, the relative concentration of each functionality fraction must be determined. These concentrations are equivalent to the volume of each peak in the contour plot. With the appropriate software this can be done easily. Determination of the MMD for each fraction was possible after calibrating chromatograph

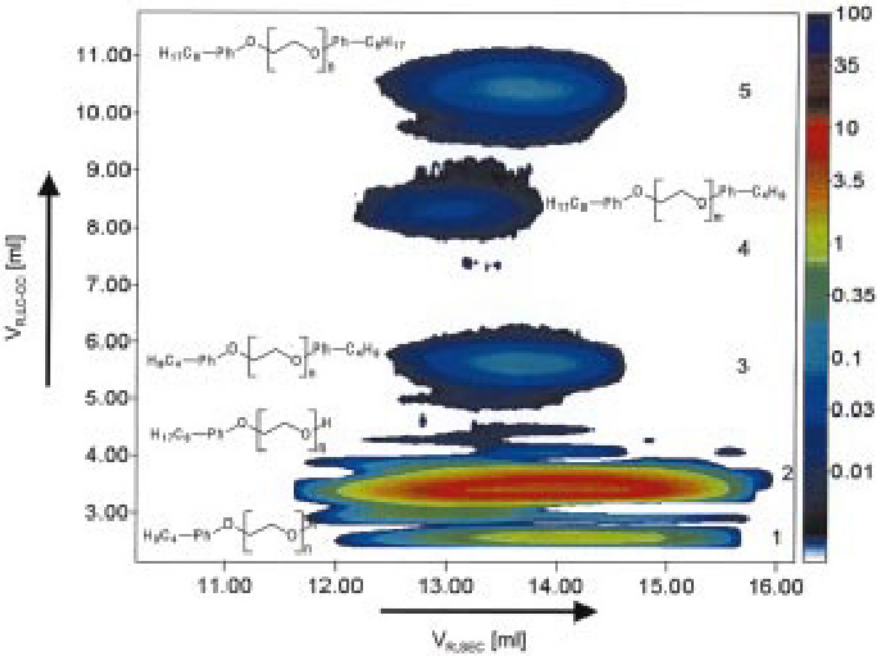

Fig. 21. Contour plot of the LC-CC vs. SEC separation of octylphenoxy-terminated poly(ethylene oxide) (from [119] with permission)

2 with PEO calibration standards. Calculation of the MMD could then be achieved in the usual way, taking one chromatogram for each functionality fraction, preferably from the region of the highest peak intensity.

In similar approaches, other polyalkylene oxides have been analyzed by 2D chromatography. Murphy et al. separated poly(ethylene glycols) and Brij-type surfactants according to chemical composition and molar mass by reversed-phase HPLC vs. SEC [120]. The analysis of methacryloyl-terminated poly(ethylene oxides) by LC-CC vs. SEC has been described by Krüger et al. [121]. The functionality type separation was conducted on a reversed-phase system at a critical eluent composition of acetonitrile/water 43:57 (v/v). The functionality fractions, including poly(ethylene glycol), α-methoxy-ω-hydroxy-, α-methoxy-ω-methacryloyloxy-, and α,ω-di(methacryloyloxy)-PEO, were identified by MALDI-TOF mass spectrometry. Finally, a technical C_{13},C_{15}-alkoxy-terminated PEO was analyzed by Pasch and Trathnigg using LC-CC vs. SEC [122].

The analysis of aliphatic polyesters with respect to FTD and MMD was demonstrated by Much, Schulz and Krüger [92,121]. Polyesters from adipic acid and 1,6-hexanediol are manufactured for a wide field of applications with an output of thousands of tons per year. They are intermediates for the manufacture of polyurethanes, and their functionality type distribution is a major parameter in

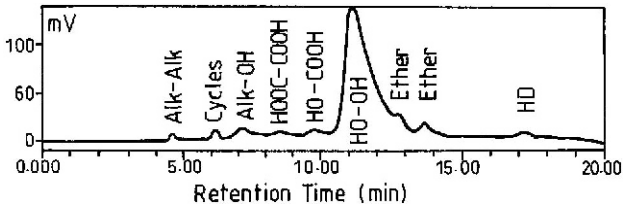

Fig. 22. LC-CC chromatogram of an aliphatic polyester, stationary phase: Tessek silica gel, eluent: acetone/hexane 51:49 (v/v) (from [121] with permission)

Table 4. Peak assignment of the polyester functionality chromatogram R^1-[-OC-$(CH_2)_4$-COO-$(CH_2)_6$-O-]$_n$-R^2

Fraction	Symbol	R^1	R^2
1	Alk-Alk	CH_2=CH$(CH_2)_4^-$	-X
2	Cycles	–	–
3	Alk-OH	CH_2=CH$(CH_2)_4^-$	-H
4	HOOC-COOH	HO-	-OC-$(CH_2)_4$-COOH
5	HOOC-OH	HO-	-H
6	HO-OH	HO-$(CH_2)_6$-O-	-H
9	1,6-hexanediol		
X: -OC-$(CH_2)_4$-COO-$(CH_2)_4$-CH=CH_2			

affecting the quality of the final products. In particular, nonreactive cyclic species are responsible for the "fogging effect" in polyurethane foams.

For the separation of the polyesters with respect to functionality, LC-CC was used; the critical point of adsorption of the polymer chain corresponding to an eluent composition of acetone/hexane 51:49 (v/v) on silica gel. The critical chromatogram of a polyester sample together with the functionality fraction assignment is given in Fig. 22 and Table 4. The "ether" peaks are obtained due to the formation of ether structures in the polyester samples.

$$HO\text{-}R^1\text{-}OH + HO\text{-}R^2\text{-}OH \rightarrow HO\text{-}R^1\text{-}O\text{-}R^2\text{-}OH$$

where R^1 and R^2 represent adipic acid-hexanediol polyester chains.

The molar mass distributions of the functionality fractions were determined by preparatively separating the fractions and subjecting them to SEC. The SEC chromatograms of fractions 1–9 are summarized in Fig. 23. For a number of fractions oligomer separations were obtained, which could be used to calibrate the SEC system.

The best way of fingerprinting the present very complex sample was a coupled 2D experiment in the coordinates LC-CC and SEC. As can be seen from the contour plot in Fig. 24, all structural features including the functionality fractions

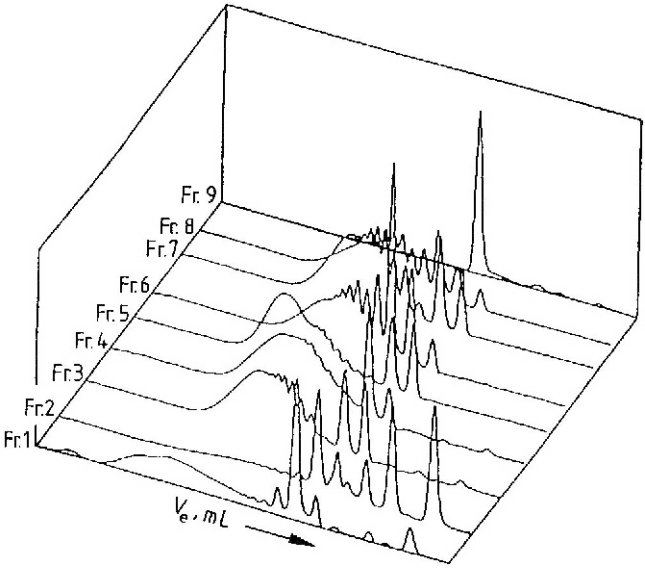

Fig. 23. SEC chromatograms of fractions 1–9 taken from LC-CC separation of the polyester, stationary phase: PL-gel, eluent: acetone (from [121] with permission)

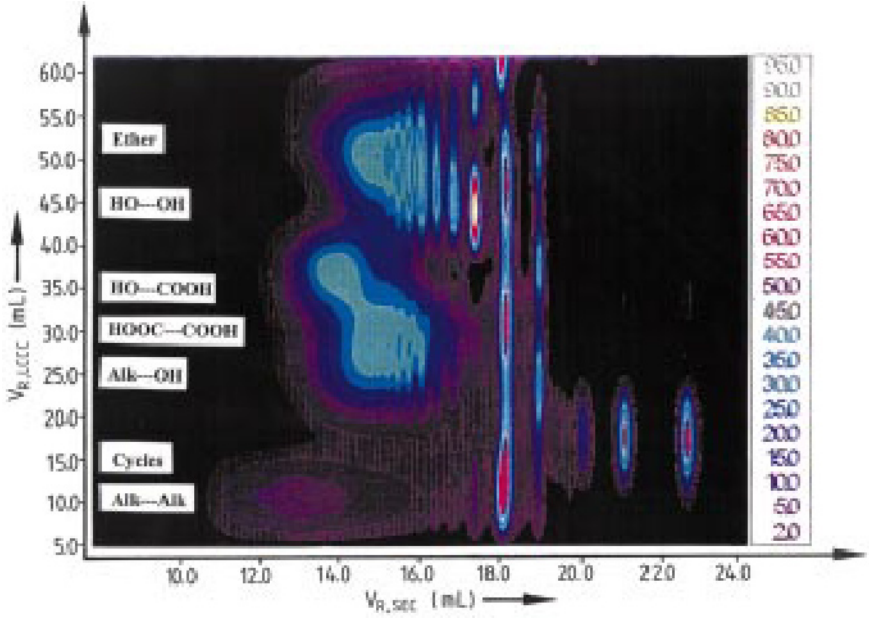

Fig. 24. Contour plot of the LC-CC vs. SEC separation of the polyester (from [121] with permission)

from LC-CC and the oligomer separations from SEC were well recognizable. Quantification of the contour plot yielded quantitative information on both FTD and MMD.

The application of liquid chromatography at the critical point of adsorption to block copolymers is based on the consideration that Gibbs free energy ΔG_{AB} of a block copolymer A_nB_m is the sum of the contributions of block A and block B, ΔG_A and ΔG_B respectively.

$$\Delta G_{AB}=\Sigma(n_A\Delta G_A+n_B\Delta G_B+\chi_{AB}) \tag{23}$$

where χ_{AB} describes the interactions between blocks A and B. Assuming no specific interactions between A and B ($\chi_{AB}=0$), the change in Gibbs free energy is only a function of the contributions of A and B.

$$\Delta G_{AB}=\Sigma(n_A\Delta G_A+n_B\Delta G_B) \tag{24}$$

By the use of chromatographic conditions corresponding to the critical point of homopolymer A, block A in the block copolymer will be chromatographically invisible, and the block copolymer will be eluted solely with respect to block B.

$$\Delta G_A=0 \tag{25}$$

$$\Delta G_{AB}=\Sigma n_B\Delta G_B \tag{26}$$

$$K_d^{AB}=K_d^B \tag{27}$$

At the critical point of homopolymer B, block B will be chromatographically invisible, and the block copolymer will be eluted solely with respect to block A.

$$\Delta G_B=0 \tag{28}$$

$$\Delta G_{AB}=\Sigma n_A\Delta G_A \tag{29}$$

$$K_d^{AB}=K_d^A \tag{30}$$

Triblock copolymers of the ABA' type may be analyzed similarly to the analysis of diblock copolymers. The two possible cases for this type of investigation are (1) the analysis with respect to the inner block B using the critical conditions of the outer blocks A and A', and (2) the analysis of the outer blocks A and A' using the critical conditions of the inner block B. It is particularly useful to carry out experiments at the critical point of A and A'. The separation then occurs with respect to the chain length of B, yielding fractions which are monodisperse with respect to B and polydisperse with respect to A and A'. These fractions can be analyzed selectively with respect to the outer blocks A and A' in separate experiments.

Based on this approach, a triblock copolymer of ethylene oxide (EO) and propylene oxide (PO), $HO(EO)_n(PO)_m(EO)_nOH$, was analyzed with respect to the PPO inner block and the PEO outer blocks by LC-CC and SEC. For the selective separation of the block copolymer with respect to the PPO block, experiments

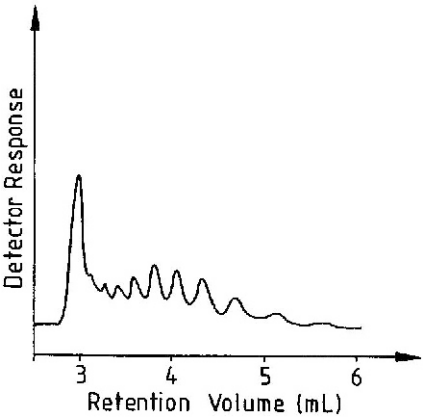

Fig. 25. LC-CC separation of a triblock copolymer $HO(EO)_n(PO)_m(EO)_nOH$ with respect to the PPO block, stationary phase: Nucleosil RP-18, eluent: methanol/water 86:14 (v/v) (from [119] with permission)

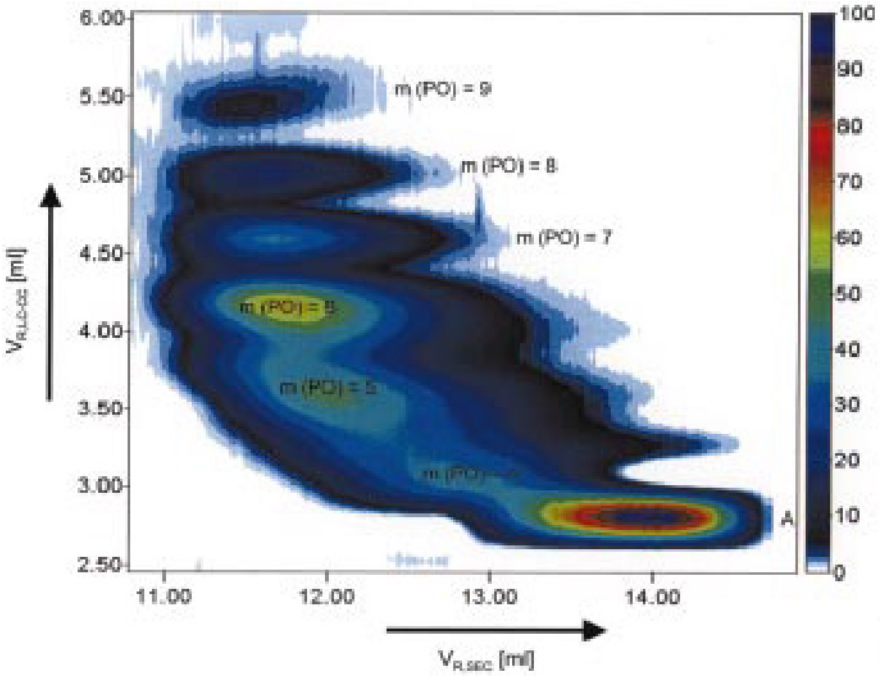

Fig. 26. Contour plot of the LC-CC vs. SEC separation of a triblock copolymer $HO(EO)_n(PO)_m(EO)_nOH$ (from [119] with permission)

were conducted using chromatographic conditions corresponding to the critical point of PEO. These were established on an RP-18 stationary phase when an eluent of methanol/water 86:14 (v/v) was used. The separation of the triblock copolymer at the critical point of PEO is shown in Fig. 25. Under these conditions, the poly(ethylene oxide) blocks behave as chromatographically "invisible" and retention of the block copolymer is solely directed by the poly(propylene oxide) block, yielding fractions of different degrees of polymerization (m) with respect to PPO. The assignment of the peaks was based on comparison with the chromatogram of a poly(propylene glycol). Every peak was uniform with respect to m but had a distribution in block length with respect to the PEO blocks (n). To identify fractions, they were collected and subjected to mass spectrometry. The first fraction contained poly(ethylene glycol) and block oligomers with a degree of polymerization m(PO)=1–3. The second fraction was homogeneous with respect to PO and contained m(PO)=4, while fraction 3 resulted from m(PO)=5.

The chromatogram in Fig. 25 reflects the oligomer distribution of the PO inner block, but does not give any information on the chain lengths of the PEO outer blocks or the total molar mass. This lack of information can be compensated for by 2D liquid chromatography. Figure 26 represents the contour plot of the 2D separation of the block copolymer in the sequence LC-CC vs. SEC. The separation with respect to the PO block length is now obtained along the ordinate, while the abscissa reflects the differences in total molar mass. As can be seen, the total molar mass of the fractions increases with the length of the PO block. As the molar mass of the PO block is known for each fraction, the molar mass of the EO blocks can be calculated from the total molar mass [119].

4.4 Conclusions and Outlook

Two-dimensional liquid chromatography is one of the most powerful methods for characterizing complex polymers in different coordinates of molecular heterogeneity. Using a chromatographic separation which is selective towards functionality or chemical composition in the first dimension and SEC in the second dimension, truly "orthogonal" separation schemes can be established. Thus, the combination of gradient HPLC vs. SEC yields quantitative information on CCD and MMD, while coupling LC-CC and SEC is useful for the analysis of functional homopolymers and block copolymers in the coordinates FTD-MMD and CCD-MMD, respectively. Even more complex systems, such as graft copolymers and polymer blends, in which each component may be chemically heterogeneous itself, can be analyzed, as has been shown by Pasch [123].

Although 2D liquid chromatography is experimentally more demanding than other chromatographic techniques, the complete characterization yields much more qualitative and quantitative information about the sample, and results are presented in an impressively simple way. The contour plot of a 2D separation maps all obtainable information and allows a fast and reliable comparison between two samples. For future development, the automated comparison of the

results of different samples can be considered as an important step to improve process control and quality management. It can be expected that, in addition to LAC and LC-CC, other separation modes will be combined with SEC. In an interesting application anion-exchange chromatography was coupled to SEC in order to analyze poly- and oligosaccharides [124].

5
Hyphenation of Liquid Chromatography with Spectroscopic Methods

The determination of compositional changes across the molar mass distribution of a polymer or the detection of a specific component in a complex polymer mixture is of considerable interest. This information allows the prediction of physical properties and ultimately the performance of the polymer. Several analytical techniques are of use in determining these properties. Mass spectrometry, NMR, and infrared spectroscopy can be used to provide data about the compositional details of the sample.

When only spectroscopic methods are used, they are able to identify polymer components with respect to their chemical nature. However, in many cases, they are unable to answer the question whether two chemical structures are combined to yield a copolymer or a blend or both. For example, analyzing a rubber mixture one is able to identify styrene and butadiene as the monomer units. However, using FTIR or NMR it is impossible to decide if the sample is a mixture of polystyrene (PS) and polybutadiene (PB), or a copolymer of styrene and butadiene, or a blend of a styrene-butadiene copolymer and PB. For the latter case, even the copolymer composition cannot be determined just by running a FTIR or NMR spectrum.

For the precise determination of the complex polymer composition including the chemical composition and MMD of the components in most cases a separation step is required. Only after obtaining fractions comprising the different polymer components, can an analysis with regard to chemical composition and MMD be conducted. The present section discusses different options which enable the use of liquid chromatography (SEC, HPLC, LC-CC) in conjunction with FTIR, mass spectrometry and NMR for the separation of complex polymers.

5.1
Coupling with FTIR Spectroscopy

Frequently, when analyzing a complex polymer, the first step must be the determination of the gross composition. Only when the chemical structures of the polymer components are known, can sophisticated separation techniques, such as gradient HPLC or LC-CC, be adapted to a specific analysis.

The most frequently used techniques for a "flash" analysis are infrared spectroscopy and SEC. Infrared spectroscopy provides information on the chemical substructures present in the sample, while SEC gives a first indication of the molar mass range. Information on both molar mass and composition is obtained

when SEC or a comparable chromatographic method is combined with an infrared detector. In the past, numerous workers have tried to use infrared detection of the SEC column effluent in liquid flow cells. The problems encountered relate to obtaining sufficient signal-to-noise (S/N) ratio even with Fourier transform infrared (FTIR) instruments, flow-through cells with minimum path lengths and mobile phases with sufficient spectral windows. Attempts to use FTIR detection with liquid flow-through cells and high-performance columns have not been very successful due to the requirement of considerably less sample concentration for efficient separation [125–132].

A rather broad applicability of FTIR as a detector in liquid chromatography can be achieved when the mobile phase is removed from the sample prior to detection. In this case the sample fractions are measured in a pure state without interference from solvents. Experimental interfaces to eliminate volatile mobile phases from HPLC effluents have been tried with some success [133–135] but the breakthrough towards a powerful FTIR detector has only been achieved by Gagel and Biemann, who formed an aerosol from the effluent and sprayed it on a rotating aluminum mirror. The mirror was then deposited in a FTIR spectrometer and spectra were recorded at each position in the reflexion mode [136–138].

Recently, Lab Connections Inc. has introduced the LC-Transform, a direct HPLC-FTIR interface based on the invention of Gagel and Biemann, and has discussed first applications in polymer analysis [139–141]. The design concept of the interface is shown in Fig. 27. The system is composed of two independent modules, the sample collection module and the optics module. The effluent of the liquid chromatography column is split, with a fraction (frequently 10% of the total effluent) going into the heated nebulizer nozzle located above a rotating sample collection disc. The nozzle rapidly evaporates the mobile phase while depositing a tightly focused track of the solute. When a chromatogram has been collected on the sample collector disc, the disc is transferred to the optics module in the FTIR spectrometer for analysis of the deposited sample track. A con-

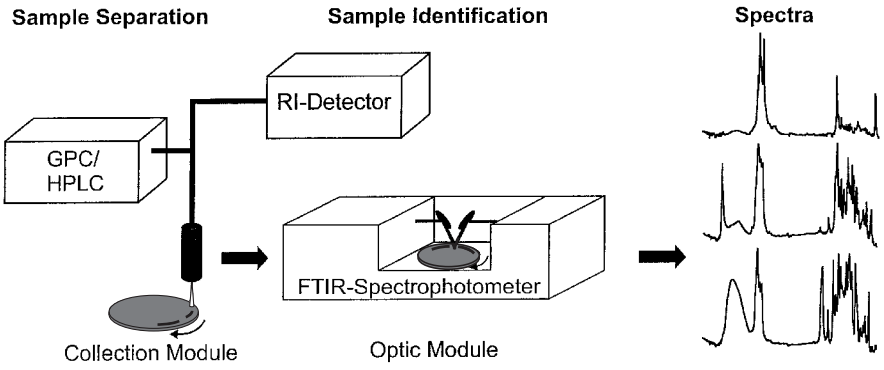

Fig. 27. Schematic representation of the principle of coupled liquid chromatography and FTIR spectroscopy

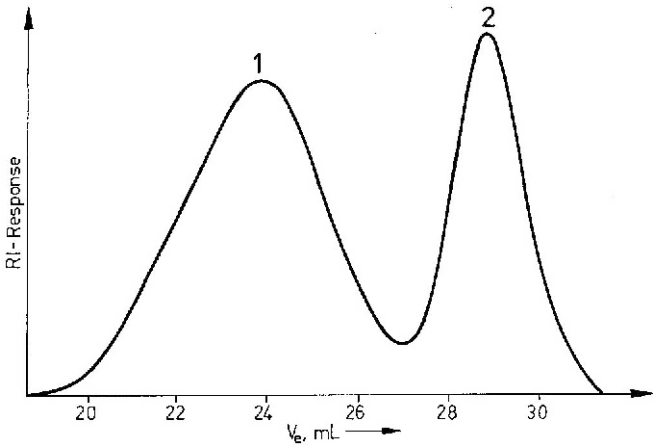

Fig. 28. SEC separation of a binary blend, stationary phase: Ultrastyragel 2×linear+10^5 Å, eluent: THF

trol module defines the sample collection disc position and rotation rate in order to be compatible with the run time and peak resolution of the chromatographic separation. Data collection is readily accomplished with software packages presently used for GC-FTIR spectrometry. The sample collection disc is made from germanium which is optically transparent in the range 6000–450 cm^{-1}. The lower surface of the disc is covered with a reflecting aluminum layer.

As a result of the investigation a complete FTIR spectrum for each position on the disc and, hence, for each sample fraction is obtained. This spectrum bears information on the chemical composition of each sample fraction. The set of all spectra can be arranged along the elution time axis and yields a three-dimensional plot in the coordinates elution time-FTIR frequency-absorbance.

One of the benefits of coupled SEC-FTIR is the ability to identify directly the individual components separated by chromatography. A typical SEC separation of a polymer blend is shown in Fig. 28 [142]. Two separate elution peaks 1 and 2 were obtained, indicating that the blend contained at least two components of significantly different molar masses. A quantification of the components with respect to concentration and molar mass, however, cannot be carried out as long as the chemical structure of the components is unknown.

The analysis of the chemical composition of the sample was conducted by coupled SEC-FTIR using the LC Transform. After separating the sample with respect to molecular size, the fractions were deposited on the germanium disc and FTIR spectra were recorded continuously along the sample track. In total, a set of about 80 spectra was obtained which was presented in a three-dimensional plot (Fig. 29). The projection of the 3D plot on the retention time-IR frequency coordinate system yielded a two-dimensional representation, where the intensities of the absorption peaks were given by a color code. Such a "contour plot" readily provides information on the chemical composition of each chromato-

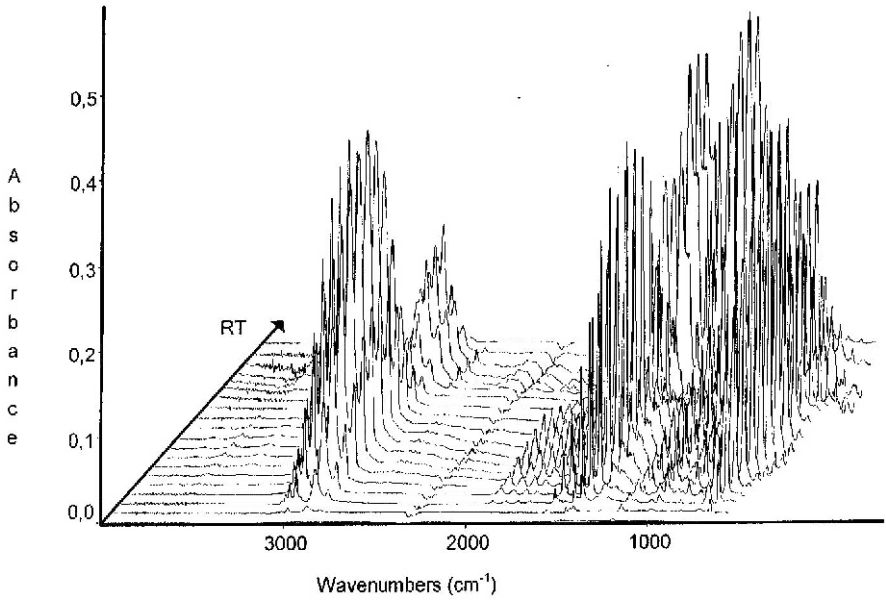

Fig. 29. SEC-FTIR analysis of a binary blend, "Waterfall" representation

graphic fraction (see Fig. 30). It is obvious that the chromatographic peaks 1 and 2 have different chemical structures. By comparison with reference spectra which are accessible from corresponding data bases, component 1 could be identified as polystyrene, while component 2 as poly(phenylene oxide). With this knowledge, appropriate calibration curves can be used for quantifying the composition and the component molar masses of the blend.

SEC coupled with FTIR becomes an inevitable tool when blends comprising copolymers have to be analyzed. Very frequently components of similar molar masses are used in polymer blends. In these cases resolution obtained by SEC is not sufficient to resolve all component peaks (see Fig. 31 for a model binary blend containing an additive). The elution peaks of the polymer components 1 and 2 overlap and, thus, the molar masses cannot be determined directly. Only the additive peak 3 at the low molar mass end of the chromatogram is well separated and can be quantified.

A first indication of the composition of the present sample was obtained from the contour plot in Fig. 32. Component 3 shows typical absorption peaks of a phenyl benzotriazole and can be identified as a UV stabilizer of the Tinuvin type. Component 2 exhibits absorption peaks which are characteristic for nitrile groups (2237 cm^{-1}) and styrene units (760, 699 cm^{-1}), while component 1 shows a strong ester carbonyl peak around 1740 cm^{-1} and peaks of styrene units. In agreement with the peak pattern of literature spectra, component 2 can be identified as a styrene-acrylonitrile copolymer. Component 1 is either a mixture of

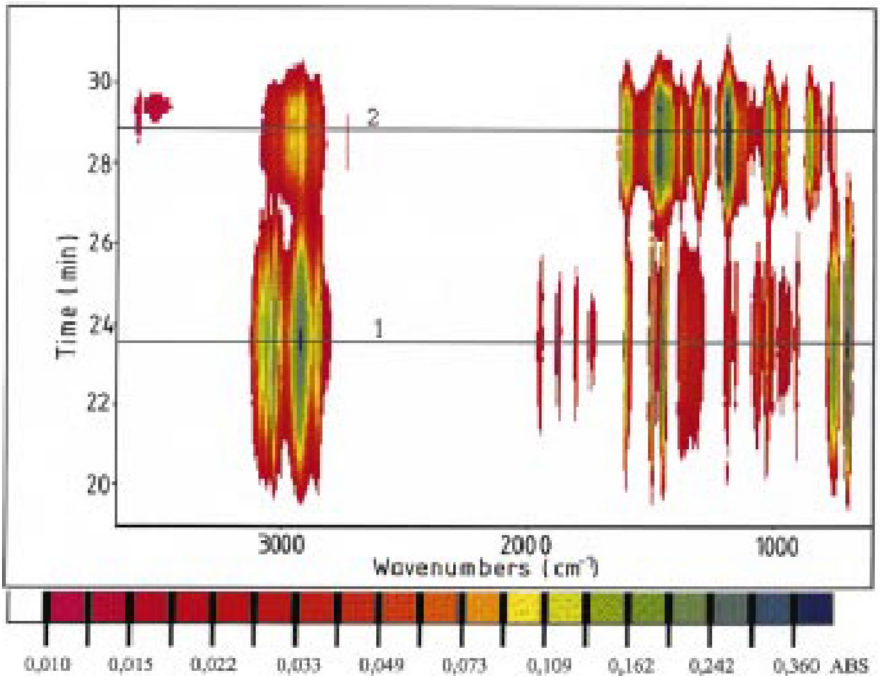

Fig. 30. SEC-FTIR analysis of a binary blend, "Contour plot" representation

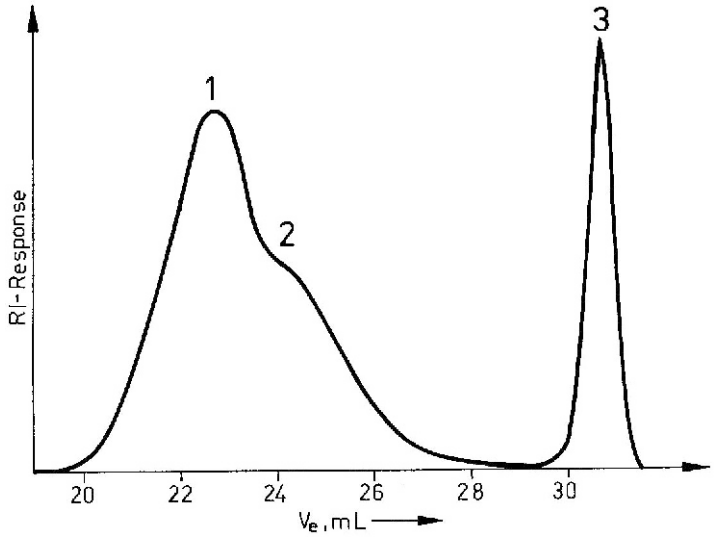

Fig. 31. SEC separation of a blend of two copolymers and an additive, chromatographic conditions see Fig. 28

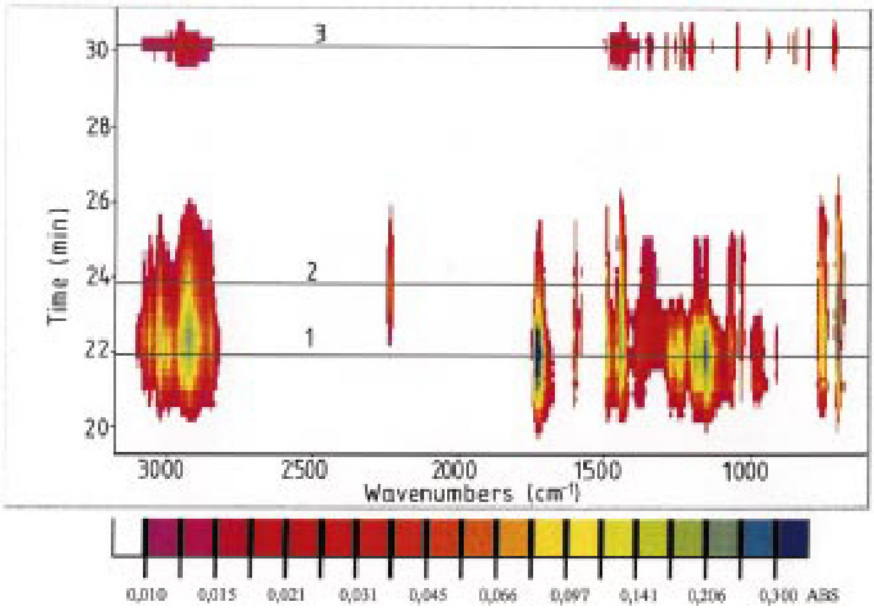

Fig. 32. Contour plot of the SEC-FTIR analysis of a blend of two copolymers and an additive

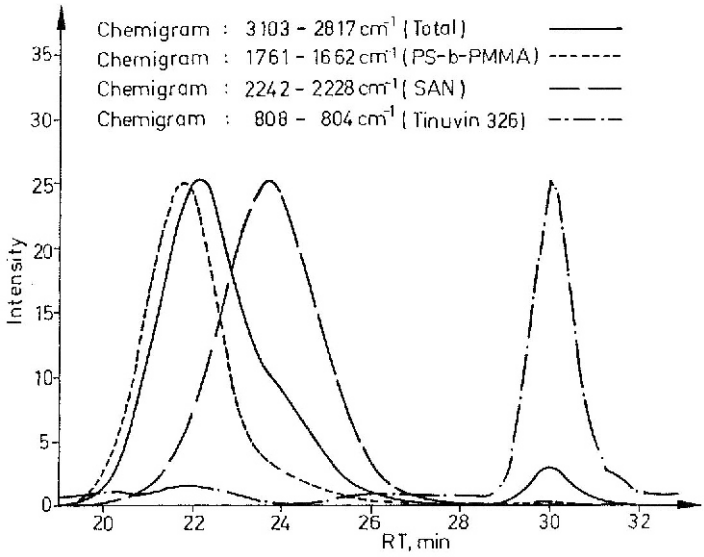

Fig. 33. Chemigrams taken from the contour plot in Fig. 32

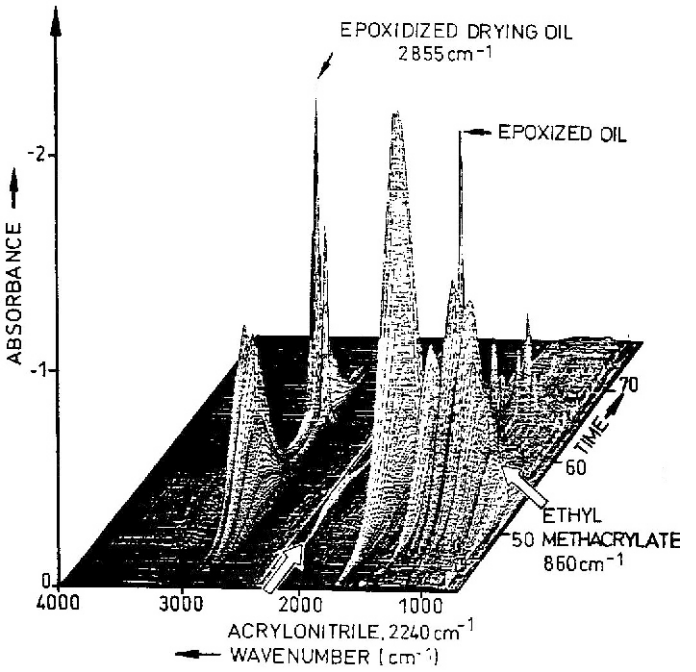

Fig. 34. 3D contour plot of a competitive modified vinyl sample obtained by SEC-FTIR

polystyrene and PMMA or a styrene-methyl methacrylate copolymer. Since the FTIR spectra over the entire elution peak are uniform, it is more likely that component 1 is a copolymer.

One important feature of the SEC-FTIR software is that from the contour plot specific elugrams at one absorption frequency can be obtained. Taking the elugram at 2230 cm^{-1}, which is specific for the nitrile group, the elution peak of the SAN copolymer could be presented individually. For the presentation of component 1 the elugram at the carbonyl absorption frequency was drawn. Thus, via the "chemigram" presentation the elution peak of each component is obtained (see Fig. 33). The total concentration profile could be obtained from the chemigram at the frequency of the C-H valence vibrations (2800–3100 cm^{-1}). The specific chemigrams, which are characteristic for one component each, represent the elution profile of this component. Accordingly, the chemigrams can be used for the calculation of the molar masses of the components.

In a relatively short period of time the Lab Connections Transform system found its way into a large number of laboratories. Applications of the technique have been discussed in various fields. Willis and Wheeler demonstrated the determination of the vinyl acetate distribution in ethylene-vinyl acetate copolymers, the analysis of branching in high-density polyethylene, and the analysis of the chemical composition of a jet oil lubricant [143]. Provder et al. [144] showed

that in powder coatings all additives could be positively identified by SEC-FTIR through comparison of the known spectra. Even biocides could be analyzed in commercial house paints. The comparison of a PS-PMMA blend with a corresponding copolymer gave information on the chemical drift. The analysis of a competitive modified vinyl polymer sample by SEC-FTIR is shown in Fig. 34. In the 3D plot some of the components of the binder could be identified readily (vinyl chloride, ethyl methacrylate and acrylonitrile), and an epoxidized drying oil additive was detected [144].

The quality of the results from SEC-FTIR strongly depend on the surface quality of the deposited sample fractions. Cheung et al. demonstrated that the surface wetting properties of the substrate dominate the deposit morphology [145]. The spectra fidelity, film quality, resolution and polymer recovery were considered by Balke et al. [146]. For different interface designs it was found that the morphology of the deposited polymer film was a key parameter for quantitative measurements.

5.2 Coupling with Mass Spectroscopy

From the very early stages of the development of modern mass spectrometry, the value of its combination with chromatography was quickly recognized. The coupling of GC with MS was a natural evolution since they are both vapor-phase techniques and, very quickly, GC-MS became accepted as a standard component of the organic analytical laboratory. It has taken considerably longer to achieve a satisfactory and all-purpose mode of HPLC-MS coupling. The difficulties with HPLC-MS are associated with the fact that vaporization of typically 1 ml/min from HPLC translates into a vapor flow rate of approx. 500–1000 ml/min. Other difficulties related to the eluent composition is the result of the frequent use of non-volatile modifiers, and the ionization of non-volatile and thermally labile analytes. However, over the last few years commercial interfaces have been developed which have led to a broad applicability of HPLC-MS [147–149]. The techniques necessary for the successful introduction of a liquid stream into a mass spectrometer are based on the following principles: electrospray ionization [150], atmospheric pressure chemical ionization [151], thermospray ionization [152], and particle beam ionization [153].

From the point of view of polymer analysis, a mass spectrometric detector would be a most interesting alternative to the conventional detectors because this detector could provide absolute molar masses of polymer components [154,155]. Provided that fragmentation does not occur, intact molecular ions could be measured. The measured mass of a particular component could then be correlated with chemical composition or chain length. However, the major drawback of most conventional HPLC-MS techniques is the limited mass range, preventing higher oligomers (molar mass above 2000–3000 g/mol) to be ionized without fragmentation [156–158].

The use of mass spectrometry for detailed polymer analysis has become more established due to the introduction of soft ionization techniques that afford intact oligomer or polymer ions with less fragmentation [159–162]. One of these techniques, electrospray ionization mass spectrometry (ESI-MS), has been widely applied in biopolymer analysis. Proteins and biopolymers are typically ionized through acid-base equilibria. When a protein solution (the effluent from a HPLC separation) is exposed to an electrical potential it ionizes and disperses into charged droplets. Solvent evaporation upon heat transfer leads to the shrinking of the droplets and the formation of analyte ions. Larger molecules acquire more than one single charge and, typically, a mixture of differently charged ions is obtained.

Unfortunately, ESI-MS has had limited application in polymer analysis [163,164]. Unlike biopolymers, most synthetic polymers have no acidic or basic functional groups that can be used for ion formation. Moreover, each molecule gives rise to a charge distribution envelope, thus further complicating the spectrum. Therefore, synthetic polymers that can typically contain a distribution of chain lengths and a variety in chemical composition or functionality furnish complicated mass spectra, making interpretation nearly impossible.

To overcome the difficulties of ESI-MS, Simonsick and Prokai added sodium cations to the mobile phase to facilitate ionization [165,166]. To simplify the resulting ESI spectra, the number of components entering the ion source was reduced. Combining SEC with electrospray detection, the elution curves of poly(ethylene oxides) were calibrated. The chemical composition distribution of acrylic macromonomers was profiled across the molar mass distribution. The analysis of poly(ethylene oxides) by SEC-ESI-MS with respect to chemical composition and oligomer distribution was discussed by Simonsick [167]. In a similar approach aliphatic polyesters [168], phenolic resins [169], methyl methacrylate macromonomers [169] and polysulfides have been analyzed [170]. The detectable mass range for different species, however, was well below 5000 g/mol, indicating that the technique is not really suited for polymer analysis.

Matrix-assisted laser desorption/ionization time-of-flight mass spectrometry (MALDI-TOF MS) is one of the newest soft ionization techniques that allows desorption and ionization of very large molecules even in complex mixtures. In polymer analysis, the great promise of MALDI-TOF MS is to perform the direct identification of mass-resolved polymer chains, including intact oligomers within a molar mass distribution, and the simultaneous determination of structure and end groups in polymer samples. This most promising method for the ionization of large molecules and the analysis according to their molar mass and functionality has been introduced by Karas and Hillenkamp [171–173]. Compared to other mass spectrometric techniques, the accessible mass range has been extended considerably, and the technique is fast and instrumentally very simple. Moreover, relatively inexpensive commercial instrumentation has become accessible. In principle, the sample to be investigated and a matrix solution are mixed in such a ratio that matrix separation of the sample molecules is achieved. After drying, a laser pulse is directed onto the solid matrix to photo-

excite the matrix material. This excitation causes the matrix to explode, resulting in the expulsion and soft ionization of the sample molecules. Once the analyte is ionized, it is accelerated and analyzed in a TOF mass spectrometer. As a result, the analyte is separated according to the molar mass of its components and, in the case of heterogeneous polymers, additional information on chemical composition may be obtained. In a number of papers it has been shown that polymers can be analyzed up to relative molar masses of about 500,000 Da [174–178]. It was also shown in a number of applications that functionally heterogeneous polymers can be analyzed with respect to the degree of polymerization and the type of functional groups [179–182].

The on-line combination of liquid chromatography and MALDI-TOF MS would be of great value for polymer analysis. In particular, for chemically or functionally heterogeneous polymers, liquid chromatography could provide separation with respect to chemical composition while MALDI-TOF would analyze the fractions with respect to oligomer distribution or molar mass. Unfortunately, MALDI-TOF is based on the desorption of molecules from a solid surface layer and, therefore, *a priori* not compatible with liquid chromatography. In an attempt to take advantage of the MALDI-TOF capabilities, a number of research groups carried out off-line LC separations and subjected the resulting fractions to MALDI-TOF measurements. Although this is laborious, it has the advantage that virtually any type of chromatographic separation can be combined with MALDI-TOF.

The different options for using MALDI-TOF as an off-line detector in liquid chromatography have been discussed by Pasch and Rode [183]. In SEC of low molar mass samples the separation into individual oligomers and the quantitative determination of the molar mass distribution via an oligomer calibration was achieved [see Fig. 35a for oligo(caprolactone)]. The lower oligomers appeared as well-separated peaks at the high retention time end of the chromatogram. For the analysis of the peaks, i.e. the assignment of a certain degree of polymerization (n) to each peak, MALDI-TOF MS was used. The SEC separation was conducted on the usual analytical scale and the oligomer fractions were collected, resulting in amounts of 5–20 ng substance per fraction in THF solution. The solutions were directly mixed with the matrix solution, placed on the sample slide and subjected to the MALDI experiments. As a large number of fractions may be introduced into the mass spectrometer at one time, sample preparation and MALDI-MS measurements take a very short period of time. In total nine fractions were collected from SEC and measured by MALDI-MS. For the lower oligomers the spectra consisted of a number of peaks of high intensity, having a peak-to-peak mass increment of 114 Da, which equals the mass of the caprolactone repeating unit. These peaks represented the $[M+Na]^+$ molecular ions, whereas the peaks of lower intensity in their vicinity were due to the formation of $[M+K]^+$ molecular ions. $[M+Na]^+$ and $[M+K]^+$ molecular ions were formed due to the presence of small amounts of $[Na]^+$ and $[K]^+$ ions in the samples and/or the matrix. Further peaks of low intensity indicated a functional heterogeneity in the samples. From the masses of the $[M+Na]^+$ peaks the degree of

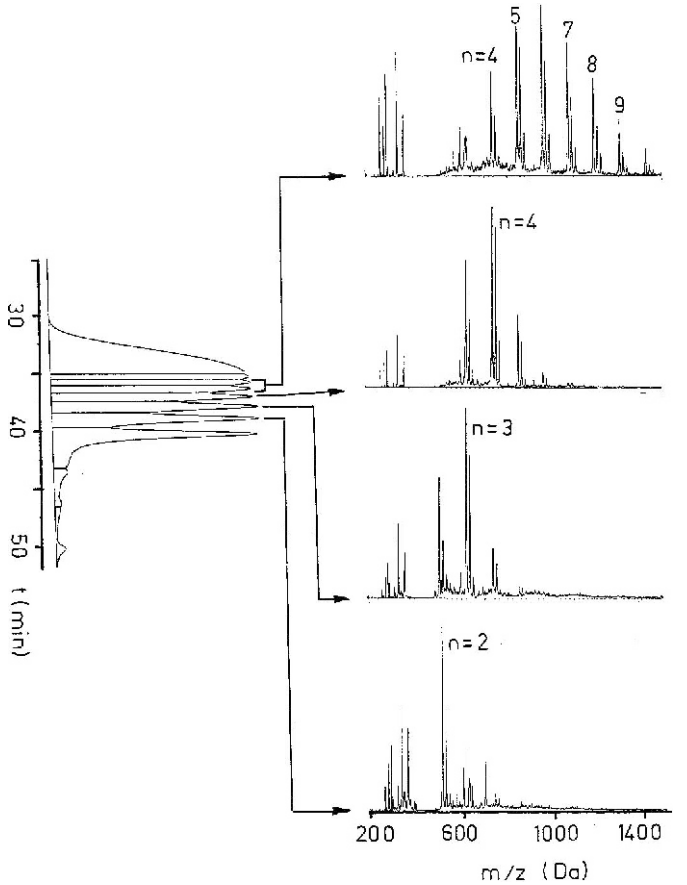

Fig. 35 a. SEC of oligo(caprolactone) and MALDI-TOF analysis of fractions (from [183] with permission)

polymerization of the corresponding oligomer was calculated. Using this procedure, the first peak in the chromatogram was assigned to n=1, the second peak to n=2, and so on. From the elution time and the degree of polymerization of each oligomer peak an oligomer calibration curve log molar mass vs. elution time was constructed. The conventional calibration curve based on polystyrene standards differed remarkably from the oligomer calibration curve, as can be seen in Fig. 35b.

A much more demanding task is the analysis of fractions from liquid chromatography, not only with respect to molar mass but also with respect to chemical structure. The separation of a technical fatty alcohol ethoxylate (FAE) by liquid chromatography under conditions where the chain length as well as the end groups direct the separation is presented in Fig. 36. Using this chromatographic technique, the FAE was separated into three main fractions, the first fraction ap-

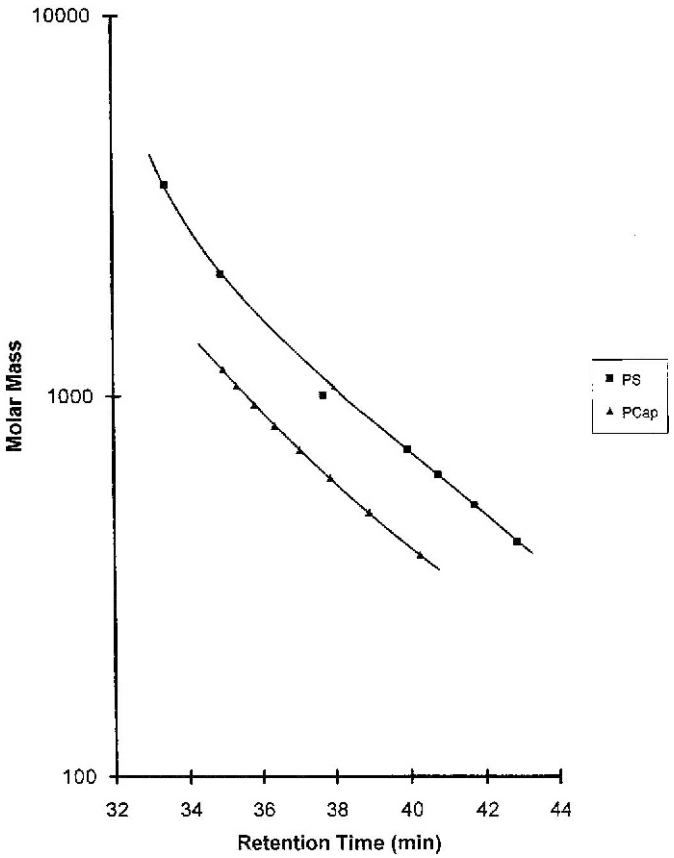

Fig. 35 b. SEC calibration graphs (from [183] with permission)

pearing as one peak at a retention time of about 60 s and fractions 2 and 3 showing oligomer separations. Fraction 1 was collected in total, whereas for fractions 2 and 3 the individual oligomer peaks were collected. The MALDI mass spectra of all three fractions gave a peak-to-peak mass increment of 44 Da, thus indicating that all fractions consisted of species with an ethylene oxide based polymer chain. From the masses assigned to the peaks and the peak-to-peak mass increment of the ethylene oxide repeating unit the mass of the end group for the different fractions was calculated. Provided the sample was a pure FAE, the end groups of fractions 1–3 could be identified as being poly(ethylene glycol) (PEG) (α,ω-dihydroxy end groups), C_{13}-terminated poly(ethylene oxide) (PEO) (α-tridecyl-ω-hydroxy end groups) and C_{15}-terminated PEO (α-pentadecyl-ω-hydroxy end groups), respectively. Using MALDI-TOF, the oligomer distribution of the PEG fraction was measured directly. For fractions 2 and 3 by determining the degree of polymerization of the oligomer peaks oligomer calibration curves were obtained, which were used for the molar mass calculation of the fractions.

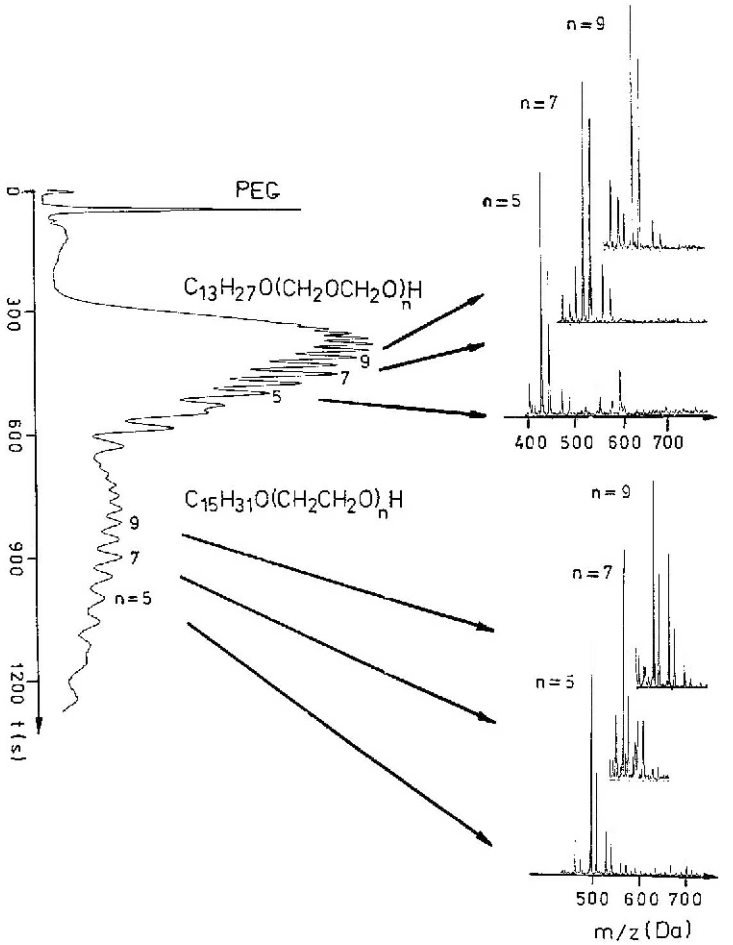

Fig. 36. Separation of a technical poly(ethylene oxide) by LC and analysis of fractions by MALDI-TOF, peak assignment indicates degree of polymerization *n* (from [183] with permission)

Thus, by combining liquid chromatography and MALDI-MS detection, complex samples can be analyzed with respect to chemical structure and molar mass.

Other examples of successful combinations of liquid chromatography and MALDI-TOF have been reported by Krüger et al. who separated linear and cyclic fractions of polylactides by LC-CC [184]. Just et al. were able to separate cyclic siloxanes from linear silanols and to characterize their chemical composition [185]. The calibration of an SEC system by MALDI-TOF was discussed by Montaudo et al. [186]. Poly(dimethyl siloxane) (PDMS) was fractionated by SEC into different molar mass fractions. These fractions were subjected to MALDI-TOF for molar mass determination. The resulting peak maximum molar masses were

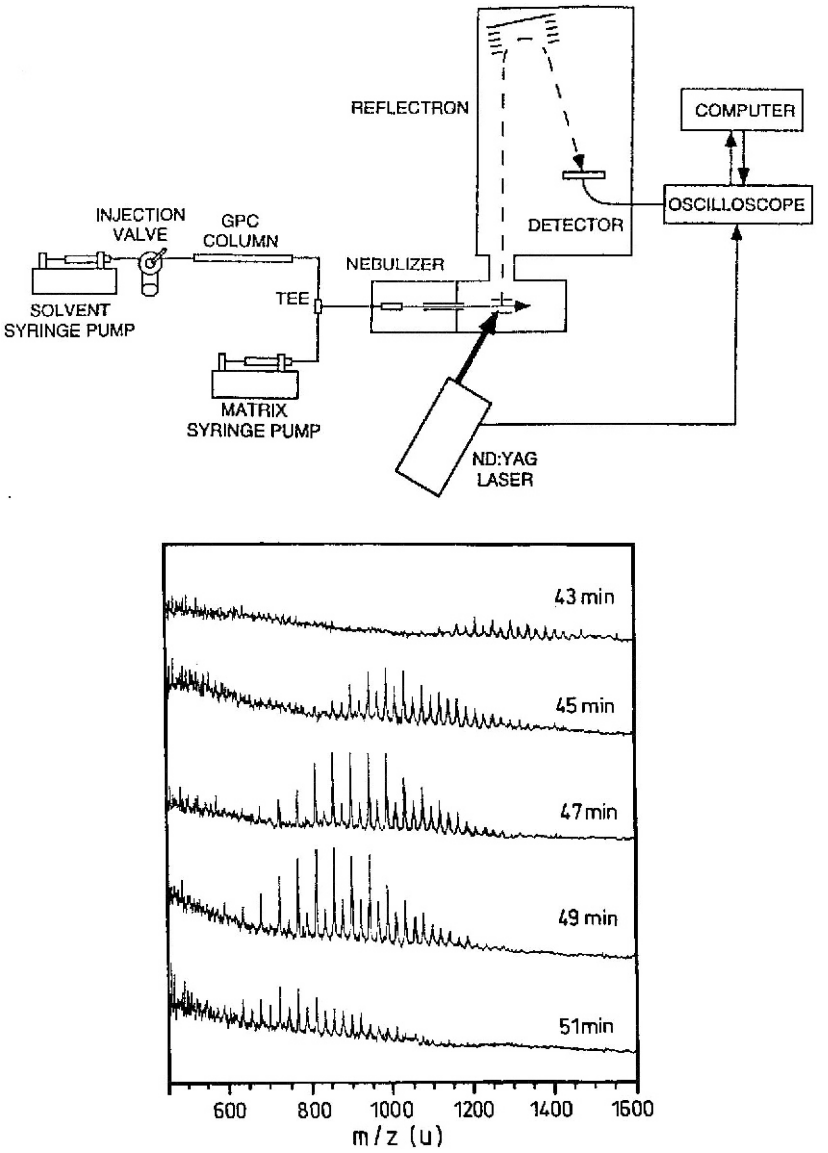

Fig. 37. Aerosol MALDI apparatus configured for on-line SEC-MS (**a**) and five spectra obtained during the separation of PEG 1000 (**b**) (from [191] with permission)

combined with the elution volumes of the fractions from SEC to give a PDMS calibration curve log M vs. V_e. The calibration of SEC by MALDI-TOF MS for PMMA, poly(vinyl acetate) and vinyl acetate copolymers has been discussed by Danis et al. In addition to obtaining proper calibration curves, band broadening

of the SEC system was detected [187]. The analysis of random copolyesters has been described recently by Montaudo et al. [188].

Considering the potential of MALDI-TOF in terms of versatility and sensitivity, on-line coupling with liquid chromatography would be a highly attractive possibility. Given the experiences with the direct introduction of small matrix containing liquid streams into high-vacuum instruments, it took a surprisingly long time before a device for liquid introduction to MALDI was described. In some recent papers Murray et al. have discussed the on-line coupling of SEC and MALDI-TOF MS [189–191]. In an aerosol MALDI-SEC experiment, the effluent from the SEC column was combined with a matrix solution and sprayed directly into a TOF mass spectrometer. Ions were formed by irradiation of the aerosol particles with pulsed 355 nm radiation from a frequency-tripled Nd:YAG laser. The ions were mass separated in a two-stage reflectron TOF instrument, and averaged mass spectra were stored every 11 s throughout the SEC-MS experiment. Well-resolved MALDI-TOF spectra were obtained from commercial PEG 1000 and PPG 1000 (see Fig. 37).

5.3 Coupling with Proton NMR

Nuclear magnetic resonance (NMR) spectroscopy is by far the most powerful spectroscopic technique for obtaining structural information about organic compounds in solution. Its particular strength lies in its ability to differentiate between most structural, conformational and optical isomers. NMR spectroscopy can usually provide all the necessary information to unambiguously identify a completely unknown compound. The NMR detection technique is quantitative with individual areas in spectra being proportional to the number of contributing nuclei. One major drawback of NMR spectroscopy is the relatively low sensitivity in comparison to MS; the other is the fact that structure elucidation of mixtures of unknown compounds with overlapping NMR signals is difficult and may be almost impossible in cases with overcrowded signals in a small chemical shift region of the NMR spectrum. Therefore, in many cases, it would be useful if a separation could be performed prior to the use of NMR. For more efficient procedures, a direct coupling of separation with NMR detection would be the method of choice [192].

The direct coupling of liquid chromatography with proton NMR has been attempted numerous times. Early experiments of coupled HPLC-^{1}H-NMR were conducted in a stop-flow mode or with very low flow rates [193–195]. This was necessary to accumulate a sufficient number of spectra per sample volume in order to improve the signal-to-noise ratio. Other problems associated with the implementation of on-line HPLC-NMR have included the need for deuterated solvents. However, with the exception of deuterium oxide, the use of deuterated eluents is too expensive for routine analysis. Therefore, proton-containing solvents, such as acetonitrile or methanol, must be used. To get rid of the solvent signals in the spectra, the proton NMR signals of the solvents have to be suppressed.

Recent rapid advances in HPLC-NMR provide evidence that many of the major technical obstacles have been overcome [196,197]. With the development of more powerful NMR spectrometers combined with new NMR techniques for solvent suppression it has become much easier to obtain well-resolved spectra in an on-flow mode. In particular, very efficient solvent suppression techniques have significantly improved the spectra during the HPLC-NMR run [198,199]. These techniques combine shaped radio frequency pulses, pulsed-field gradients, and selective ^{13}C decoupling to acquire high-quality spectra under on-flow conditions even with high HPLC gradients. Recently, even the direct coupling of supercritical fluid chromatography with ^{1}H-NMR [200–202] together with the monitoring of supercritical fluid extraction [203], as well as the coupling of capillary electrophoresis and ^{1}H-NMR [204–206], have been reported. An overview of the applications of on-line HPLC-^{1}H-NMR in organic chemistry was given by Albert [192].

The first steps of polymer analysis into coupled liquid chromatography-^{1}H-NMR were performed by Hatada et al. [207]. They linked a size exclusion chromatograph to a 500 MHz proton NMR spectrometer and investigated isotactic polymethyl methacrylate. Using deuterated chloroform as the eluent and running the chromatograph at a rather low flow rate of 0.2 ml/min they were able to accumulate well-resolved proton spectra. From the intensities of the proton signals of the end groups and the monomer units they determined the number-average molar mass across the elution curve. In further investigations they developed an absolute calibration method for direct determination of molar masses and molar mass distributions by on-line SEC-^{1}H-NMR [208]. Ute reported on the chemical composition analysis of EPDM copolymers as a function of molar mass, and the monitoring of stereocomplex formation for isotactic and syndiotactic PMMA [209].

The analysis of a technical poly(ethylene oxide) with respect to chemical composition and degree of polymerization has been performed by Pasch and Hiller [210]. This investigation was conducted under conditions which are common for HPLC separations, i.e. sufficiently high flow rate, moderate sample concentration, and on-flow detection. Using an octadecyl-modified silica gel as the stationary phase and an eluent of acetonitrile/deuterium oxide 50:50 (v/v), the sample was separated into different functionality fractions (see Fig. 38). The major fraction of the sample eluting between 14 and 25 min exhibited a partial oligomer separation.

For structural identification of the fractions, the ^{1}H-NMR spectrometer was directly coupled via capillary tubing to the chromatograph. The injection of the sample into the HPLC system was automatically initiated by the NMR console via a trigger pulse when starting the acquisition of NMR data. Using an appropriate pulse sequence, both solvent resonances (ACN at 2.4 ppm and water at 4.4 ppm) could be suppressed simultaneously. As a result of the on-line HPLC-NMR experiment, a contour plot ^{1}H chemical shift vs. retention time was generated (see Fig. 39). Due to the efficient solvent suppression, the obtainable structural information relates to the entire chemical shift region. From the contour

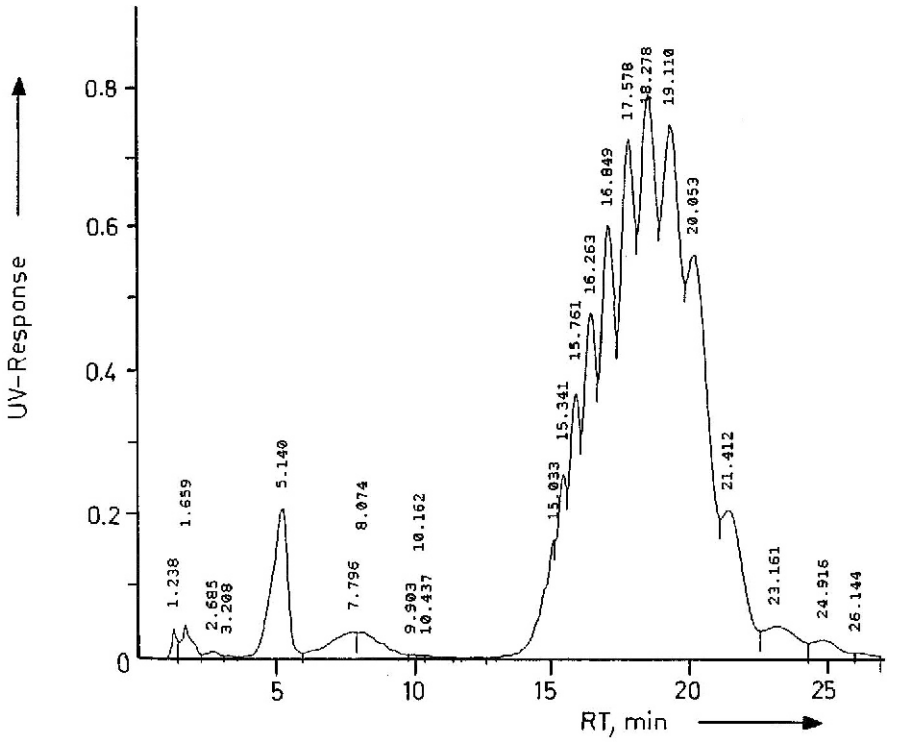

Fig. 38. HPLC chromatogram of a technical poly(ethylene oxide), stationary phase: RP-18, eluent: acetonitrile/deuterium oxide 50:50 (v/v) (from [210] with permission)

plot, four different elution peaks could clearly be identified and analyzed with respect to chemical composition. The remarkable feature of this investigation was that even the low concentration components in peaks 1–3 could clearly be identified in the contour plot.

Detailed structural information was obtained from the individual NMR spectra of the fractions at the peak maximum (see Fig. 40). The first peak was identified as being poly(ethylene glycol) while the other fractions were alkylphenoxy poly(ethylene oxides). From the intensities of the end groups and the ethylene oxide repeat units the average degree of polymerization for each fraction was calculated. Based on the total intensity distribution, a calculated chromatogram (or chemigram) was generated from the NMR contour plot. Comparing the real chromatogram (Fig. 38) with the chemigram (Fig. 39) an excellent agreement was obtained even recalling the oligomer separation pattern of the major fraction.

The analysis of fatty alcohol ethoxylate based surfactants by on-line HPLC-^{1}H-NMR has been described by Schlotterbeck et al. [211]. Using a reversed stationary phase and ACN/deuterium oxide as the eluent, surfactant mixtures were

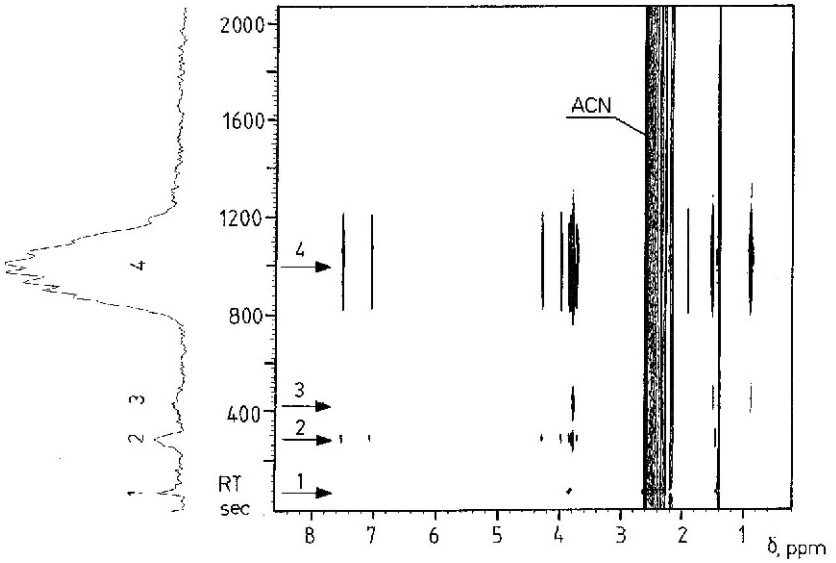

Fig. 39. Contour plot of chemical shift vs. retention time and chemigram of the on-line HPLC-NMR analysis of a technical poly(ethylene oxide) (from [210] with permission)

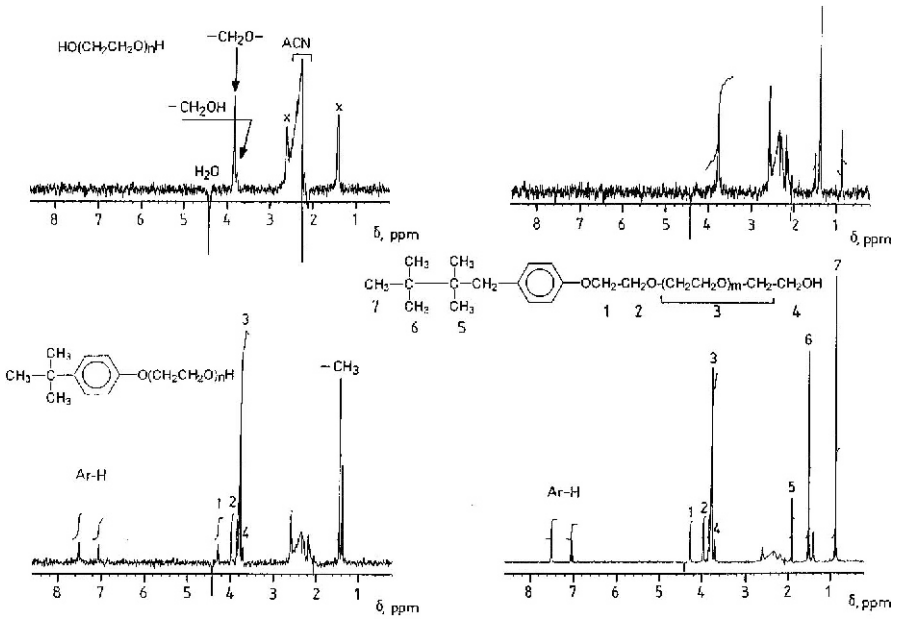

Fig. 40. Individual fraction spectra taken from Fig. 39

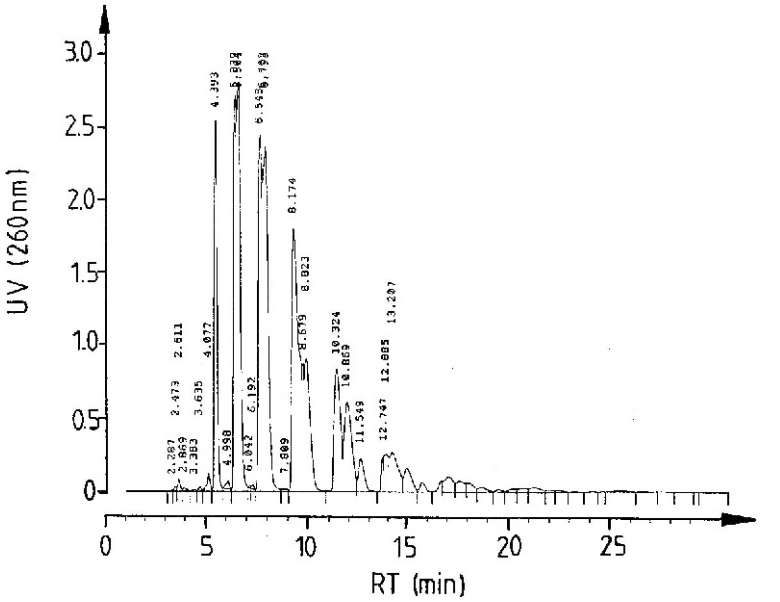

Fig. 41. HPLC chromatogram of an oligostyrene PS 530, stationary phase: RP-18, eluent: acetonitrile (from [212] with permission)

separated with respect to the fatty alcohol end groups. ^{1}H-NMR detection revealed the number of components, the chemical structure of the components end groups, and the chain length.

Finally, the investigation of the tacticity of oligostyrenes by on-line HPLC-^{1}H-NMR has been reported by Pasch et al [180]. The oligomer separation was carried out by hydrophobic interaction chromatography using isocratic elution with acetonitrile on a reversed phase RP-18 column. The chromatogram of an oligostyrene is shown in Fig. 41. The first oligomer peak could be identified as being the dimer (n=2), the next peak was identified as the trimer (n=3) and, accordingly, the following peaks could be assigned to the tetramer, pentamer etc. The dimer peak appeared uniform, whereas for the following oligomers a splitting of the peaks was obtained. For n=3 and n=4 a splitting into two peaks was observed. For n=5 and further a splitting into three or more peaks occured, which could be attributed to the formation of different tactic isomers.

The analysis of the isomerism of oligomers by HPLC-NMR is given in Fig. 42 [212]. In this experiment conventional HPLC grade acetonitrile was used as the eluent and no deuterium lock was applied. These conditions required high stability of the NMR instrument and a very efficient solvent suppression technique since 100% acetonitrile must be suppressed. The obtainable structural information related to the entire chemical shift region; however, residual signals of the eluent were obtained at 1.8–2.4 ppm and 1.3 ppm due to acetonitrile and its impurities. The contour plot clearly revealed two signal regions, which could be

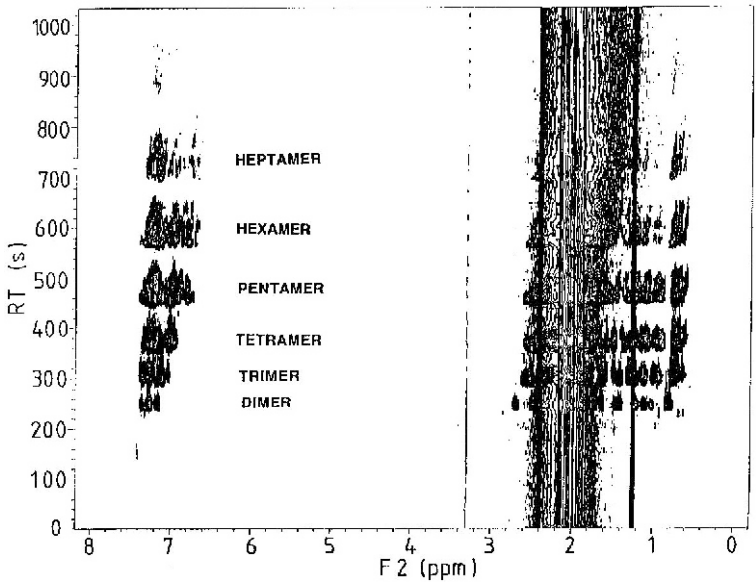

Fig. 42. Contour plot of chemical shift vs. retention time of the on-line HPLC-NMR analysis of PS 530 (from [212] with permission)

used for analysis. These were the region of the methyl protons of the *sec*-butyl end group at 0.6–0.8 ppm and the aromatic proton region of the styrene units at 6.5–8.0 ppm. For the generation of the contour plot every 8 s, a complete spectrum was produced by co-adding 8 scans. Accordingly, for the structural analysis, 128 spectra were available over the entire retention time range. For the analysis of a separated oligomer, a minimum of four spectra could be used. These spectra bear selective information on the tacticity, even without completely separating the tactic isomers chromatographically.

5.4 Conclusions and Outlook

As has been demonstrated, the combination of selective separation techniques with powerful spectroscopic detectors enables complex polymers to be analyzed with respect to all possible types of molecular heterogeneity. Chemical composition distribution can be monitored across the molar mass distribution. Steric and functional peculiarities can be detected over the entire molar mass range.

Despite a number of useful applications, LC-FTIR, LC-MS and LC-NMR cannot yet be regarded as mature techniques. One of the limitations to a broader application of these techniques, in particular of LC-NMR, is the relatively high price of the equipment. The minimum requirement for a highly efficient LC-NMR experiment is a 400–500 MHz instrument which is not affordable for every

laboratory. The other limitation is that for each technique very specific knowledge is required. To develop a proper LC-NMR experiment, LC expertise has to be combined with profound NMR experience. This requires an interdisciplinary problem solving approach.

However, due to the fact that polymer structures are becoming more and more complex and analysis time is one of the key efficiency factors, it is not difficult to predict a bright future for on-line coupling of liquid chromatography and spectroscopic techniques.

Acknowledgements. The assistance of J. Adrian and E. Esser in conducting some of the experimental work in coupled techniques and preparing the contour plots is gratefully acknowledged. The author would like to thank Ms. H. Eberle for carefully preparing the artwork.

References

1. Barth HG (1995) Hyphenated polymer separation techniques. Present and future role. In: Provder T, Barth HG, Urban MW (eds) Chromatographic characterization of polymers. Hyphenated and multidimensional techniques, chap 1. Adv Chem Ser 247, American Chemical Society, Washington, DC
2. Francuskiewicz F (1994) Polymer fractionation. Springer, Berlin Heidelberg New York
3. Cortes HJ (1992) J Chromatogr 626:3
4. Factor A, Carnahan JC, Dorn SB, van Dort PC (1994) Polym Degrad Stab 45:127
5. Ezrin M, Lavigne G (1992) Ann Tech Conf Soc Plast Eng 50:1717
6. Liu Y, Chou HC, Stoffer JO (1994) J Appl Polym Sci 53:247
7. Boinon B, Raihane M, Montheard JP (1994) Polym Degrad Stab 43:27
8. Jedlinski Z, Kowalczuk M, Kurcok P (1992) J Macromol Sci A29:1223
9. Matischek G, Stoffers H, Ohrbach KH, Kettrup A (1993) Polym Degrad Stab 39:381
10. Bell B, Beyer DE, Maecker NL, Papenfus RR, Priddy DB (1994) J Appl Polym Sci 54:1605
11. Farina M, Di Silvestro G, Sozzani P, Yuan CM (1991) Makromol Chem Macromol Symp 47:1
12. Liebman S, Levy E (1985) Pyrolysis and GC in polymer analysis. Marcel Dekker, New York
13. Geißler M (1997) Kunststoffe 87:194
14. Sabo M (1985) Anal Chem 57:1822
15. Hellgeth JW, Taylor LT (1987) Anal Chem 59:295
16. Hellgeth JW, Taylor LT (1986) J Chromatogr Sci 24:519
17. Griffiths PR, Conroy CM (1986) Adv Chromatogr 25:105
18. Gagel JJ, Biemann K (1986) Anal Chem 58:2184
19. Wheeler LM, Willis J (1993) Appl Spectrosc 47:1128
20. Lindon JC (1996) Progr Nucl Magn Res Spectrosc 29:1
21. Albert K (1995) J Chromatogr A703:123
22. Balke ST, Patel RD (1983) Adv Chem Ser 203:281
23. Kilz P (1992) Laborpraxis 6:628
24. Balke ST (1991) Characterization of complex polymers by SEC and HPLC. In: Barth HG, Mays JM (eds) Modern methods in polymer characterization, chap 1. Wiley Interscience, New York
25. Podzimek S (1994) J Appl. Polym Sci 54:91
26. Dayal U, Mehta SK (1994) J Liq Chromatogr 17:303
27. Dayal D (1994) J Appl Polym Sci 53:1557

28. Balke S, Rao B, Thiriratsakul R, Mourey TH, Schunk TC (1996) Prep 9th Int Symp Polym Anal Char (ISPAC 9), Oxford
29. Trathnigg B (1990) J Liq Chromatogr 13:1731
30. Trathnigg B (1991) J Chromatogr 552:505
31. Trathnigg B, Yan X (1992) Chromatographia 33:467
32. Runyon JR, Barnes DE, Rudel JF, Tung LH (1969) J Appl Polym Sci 13:2359
33. Ogawa T (1979) J Appl Polym Sci 23:3515
34. Revillon A (1980) J Liq Chromatogr 3:1137
35. Tung LH (1979) J Appl Polym Sci 24:953
36. Trathnigg B, Jorde C (1987) J Chromatogr 385:17
37. Pasch H, Augenstein M, Trathnigg B (1994) Macromol Chem Phys 195:743
38. Trathnigg B, Feichtenhofer S, Kollroser M (1997) J Chromatogr A 786:75
39. Johann C, Kilz P (1989) Proc 1st Int Conf Molar Mass Charact, Bradford
40. Dawkins JV (1995) Compositional heterogeneity of copolymers by coupled techniques with chromatographic columns and multidetectors. In: Provder T, Barth HG, Urban MW (eds) Chromatographic characterization of polymers. Hyphenated and multidimensional techniques, chap 15. Adv Chem Ser 247, American Chemical Society, Washington, DC
41. Meehan E, O'Donohue S, McConville JA (1993) Polym Mater Sci Eng 69:269
42. Gores F, Kilz P (1993) Copolymer characterization using conventional SEC and molar mass-sensitive detectors. In: Provder T (ed) Chromatography of polymers, chap 10. ACS Symp Ser 521, American Chemical Society, Washington, DC
43. Lee HC, Ree M, Chang T (1995) Polymer 36:2215
44. Lee HC, Chang T (1996) Bull Korean Chem Soc 17:648
45. Jackson C, Barth HG (1995) In: Wu CS (ed) Molecular weight sensitive detectors for size exclusion chromatography, chap 4. Marcel Dekker, New York
46. Kratochvil P (1987) In: Jenkins AD (ed) Classical light scattering from polymer solutions, Polym Sci Libr 5, Elsevier, Amsterdam
47. Jeng L, Balke ST, Mourey TH, Wheeler L, Romeo P (1993) J Appl Polm Sci 49:1359
48. Jeng L, Balke ST (1993) J Appl Polym Sci 49:1375
49. Pille L, Solomon DH (1994) Macromol Chem Phys 195:2477
50. Mourey TH, Coll H (1994) Polym Mater Sci Eng 69:217
51. Mourey TH, Coll H (1995) J Appl Polym Sci 56:65
52. Grubisic-Gallot Z, Gallot Y, Sedlacek J (1994) Macromol Chem Phys 195:781
53. Grubisic-Gallot Z, Gallot Y, Sedlacek J (1995) J Liq Chromatogr 18:2291
54. Zigon M, Grubisic-Gallot Z (1998) Proc 11th Int Symp Polym Anal Char, Santa Margerita Ligure, Italy
55. Yau WW, Abbott SD, Smith GA, Keating MY (1987) in: Provder T (ed) Detection and data analysis in size exclusion chromatography. ACS Symp Ser 352, American Chemical Society, Washington, DC
56. Styring M, Armonas JE, Hamielec AE (1987) in: Provder T (ed) Detection and data analysis in size exclusion chromatography. ACS Symp Ser 352, American Chemical Society, Washington, DC
57. Haney MA, Armonas JE, Rosen L (1987) in: Provder T (ed) Detection and data analysis in size exclusion chromatography. ACS Symp Ser 352, American Chemical Society, Washington, DC
58. Brower L, Trowbridge D, Kim D, Mukherjee P, Seeger R, McIntyre D (1987) In: Provder T (ed) Detection and data analysis in size exclusion chromatography. ACS Symp Ser 352, American Chemical Society, Washington, DC
59. Mori S (1993) J Chromatogr 637**:**129
60. Cheung P, Lew R, Balke ST, Mourey TH (1993) J Appl Polym Sci 47:1701
61. Lesec J, Millequant M, Havard T (1993) In: Provder T (ed) Chromatography of polymers. ACS Symp Ser 521, American Chemical Society, Washington, DC
62. Benoit H, Rempp P, Grubisic Z (1967) J Polym Sci B5:753

63. Kurata M, Tsunashima Y, Iwama, M, Kamada K (1975) In: Brandrup J, Immergut I (eds) Polymer handbook. Wiley, New York, p IV-1
64. Glöckner G (1991) Gradient HPLC of copolymers and chromatographic cross-fractionation. Springer, Berlin, Heidelberg, New York
65. Yau W (1990) Chemtracts-Macromol Chem 1:1
66. Sanayei RA, Suddaby KG, Rudin A (1993) Makromol Chem 194:1953
67. Puskas JE, Hutchinson R (1993) Rubber Chem Technol 66:742
68. Xie J (1994) Polymer 35:2385
69. Lew R, Suwanda D, Balke ST, Mourey TH (1993) J Appl Polym Sci Appl Polym Symp 52:125
70. Harrison CA, Mourey TH (1995) J Appl Polym Sci 56:211
71. Chiantore O, Lazzari M, Caldari S, Zecchi E (1998) Proc 11th Int Symp Polym Anal Char, Santa Margerita Ligure, Italy
72. Goldwasser JM (1989) Proc Int GPC Symp, Newton, MA
73. Pang S, Rudin A (1992) Polymer 33:1949
74. Wintermantel M, Antonietti M, Schmidt M (1993) J Appl Polym Sci Appl Polym Symp 52:91
75. Degoulet C, Nicolai T, Durand D, Busnel JP (1995) Macromolecules 28:6819
76. Jackson C, Chen YJ, Mays JW (1996) J Appl Polym Sci 61:865
77. Yau WW, Arora KS (1994) Polym Mater Sci Eng 69:210
78. Yau WW (1991) J Appl Polym Sci, Appl Polym Symp 48:85
79. Köhler W, Kühn A, Motsch A (1993) Acta Polym 44:238
80. Lehmann U, Köhler W, Albrecht W (1996) Macromolecules 29:3212
81. Jackson C, Barth HG (1994) Trends Polym Sci 2:203
82. Balke ST, Patel RD (1980) J Polym Sci B Polym Lett 18:453
83. Balke ST (1982) Sep Purif Methods 1:1
84. Balke ST, Patel RD (1983) Orthogonal chromatography. Polymer cross-fractionation by coupled gel permeation chromatographs. In: Craver CD (ed) Polymer characterization. Adv Chem Ser 203, American Chemical Society, Washington, DC
85. Glöckner G, van den Berg JHM, Meijerink N, Scholte TG (1986) In: Kleintjens L, Lemstra P (eds) Integration of fundamental polymer science and technology. Elsevier Applied Science Publ., Barking
86. Glöckner G, Stickler M, Wunderlich W (1989) J Appl Polym Sci 37:3147
87. Augenstein M, Stickler M (1990) Makromol Chem 191:415
88. Mori S (1990) J Chromatogr 503:411
89. Mori S (1988) Anal Chem 60:1125
90. Mori S (1981) Anal Chem 53:1813
91. Kilz P (1993) Labor Praxis 6:64
92. Kilz P, Krüger RP, Much H, Schulz G (1995) ACS Adv Chem 247:223
93. Kilz P, Krüger RP, Much H, Schulz G (1993) PMSE Preprints 69:114
94. Murphy RE, Schure MR, Foley JP (1998) Anal Chem 70:1585
95. Trathnigg B, Maier B, Yan X (1994) Proc 7th Int Symp Polym Anal Char, Les Diablerets, Switzerland
96. Entelis SG, Evreinov VV, Gorshkov AV (1986) Adv Polym Sci 76:129
97. Entelis SG, Evreinov VV, Kuzaev AI (1985) Reactive oligomers. Khimiya, Moscow
98. Tennikov MB, Nefedov PP, Lazareva MA, Frenkel SJ (1977) Vysokomol Soedin A19:657
99. Belenkii BG, Gankina ES, Tennikov MB, Vilenchik LZ (1976) Dokl Acad Nauk USSR 231:1147
100. Skvortsov AM, Belenkii BG, Gankina ES, Tennikov MB (1978) Vysokomol Soedin A20:678
101. Pasch H, Much H, Schulz G, Gorshkov AV (1992) LC-GC Int 5:38
102. Pasch H, Much H, Schulz G (1993) In: Trends in polymer science 3, Research trends. Trivandrum, India
103. Pasch H (1997) Adv Polym Sci 128:1

104. Filatova NN, Gorshkov AV, Evreinov VV, Entelis SG (1988) Vysokomol Soedin A30:953
105. Gorshkov AV, Verenich SS, Evreinov VV, Entelis SG (1988) Chromatographia 26:338
106. Gorshkov AV, Prudskova TN, Guryakova VV, Evreinov VV (1986) Polym Bull 15:465
107. Gorshkov AV, Much H, Becker H, Pasch H, Evreinov VV, Entelis SG (1990) J Chromatogr 523:91
108. Pasch H, Zammert I (1994) J Liq Chromatogr 17:3091
109. Pasch H, Brinkmann C, Much H, Just U (1992) J Chromatogr 623:315
110. Pasch H, Brinkmann C, Gallot Y (1993) Polymer 34:4099
111. Pasch H, Augenstein M (1993) Makromol Chem 194:2533
112. Pasch H, Augenstein M, Trathnigg B (1994) Makromol Chem 195:743
113. Pasch H, Gallot Y, Trathnigg B (1993) Polymer 34:4986
114. Pasch H (1993) GIT Fachz Lab 37:1068
115. Pasch H, Deffieux A, Henze I, Schappacher M, Rique-Lurbet L (1996) Macromolecules 29:8776
116. Pasch H (1993) Polymer 34:4095
117. Pasch H, Rode K (1996) Macromol Chem Phys 197:2691
118. Pasch H, Rode K, Chaumien N (1996) Polymer 37:4079
119. Adrian J, Braun D, Pasch H (1998) LC-GC Int 11:32
120. Murphy RE, Schure MR, Mink LP, Foley JP (1995) Proc Int Symp Polym Anal Char, A7, Sanibel Island, FL
121. Krüger RP, Much H, Schulz G (1996) Int J Polym Anal Char 2:221
122. Pasch H, Trathnigg B (1997) HPLC of polymers. Springer, Berlin Heidelberg New York
123. Pasch H (1997) Proc 11th Int Symp Polym Anal Char, Toronto, Canada
124. Suortti T (1997) J Chromatogr A763:331
125. Ross JH, Shank RL (1971) Polym Prepr 12:812
126. Vidrine DW, Mattson DR (1978) Appl Spectrosc 32:502
127. Vidrine DW (1979) J Chromatogr Sci 17:477
128. Brown RS, Hausler DW, Taylor LT, Carter BC (1981) Anal Chem 53:197
129. Wang CP, Sparks DT, Williams SS, Isenhour TL (1984) Anal Chem 56:1268
130. Johnson CC, Taylor LT (1984) Anal Chem 56:2642
131. Sabo M (1985) Anal Chem 57:1822
132. Hellgeth JW, Taylor LT (1987) Anal Chem 59:295
133. Robertson RM, de Haseth JA, Kirk JD, Browner RF (1988) Appl Spectrosc 42:1365
134. Griffiths PR, Conroy CM (1986) Adv Chromatogr 25:105
135. Hellgeth JW, Taylor LT (1986) J Chromatogr Sci 24:519
136. Gagel JJ, Biemann K (1986) Anal Chem 58:2184
137. Gagel JJ, Biemann K (1987) Anal Chem 59:1266
138. Gagel JJ, Biemann K (1988) Microchim Acta 11:185
139. Wheeler LM, Willis JN (1993) Appl Spectrosc 47:1128
140. Willis JN, Dwyer JL, Wheeler LM (1993) Polym Mat Sci 69:120
141. Willis JN, Dwyer JL, Lui MX (1995) Proc Int GPC Symp 1994, Lake Buena Vista, FL
142. Pasch H, Esser E, Montag P (1996) GIT Fachz Lab Chromatogr 16:68
143. Willis JN, Wheeler L (1995) Use of a GPC-FTIR interface for polymer analysis. In: Provder T, Barth HG, Urban MW (eds) Chromatographic characterization of polymers. Hyphenated and multidimensional techniques, chap 19. Adv Chem Ser 247, American Chemical Society, Washington, DC
144. Provder T, Kuo C, Whited M, Huddleston D (1995) Proc Int GPC Symp 1994, Lake Buena Vista, FL
145. Cheung PC, Balke ST, Schunk TC (1995) SEC-FTIR using a solvent-evaporative interface. In: Provder T, Barth HG, Urban MW (eds) Chromatographic characterization of polymers. Hyphenated and multidimensional techniques, chap 20. Adv Chem Ser 247, American Chemical Society, Washington, DC
146. Cheung P, Balke ST, Schunk TC, Mourey TH (1993) J Appl Polym Sci Appl Polym Symp 52:105

147. Balogh MP (1997) LC-GC Int 10:728
148. Smits R (1995) LC-GC Int 8:92
149. Niessen WMA, Tinke AP (1995) J Chromatogr A703:37
150. Dole M (1968) J Chem Phys 49:2240
151. Horning EC (1974) J Chromat Sci 12:725
152. Vestal ML, Ferguson GJ (1985) Anal Chem 57:2373
153. Willoughby RC, Browner RF (1984) Anal Chem 56:2626
154. Vouros P, Wronka JW (1991) In: Barth HG, Mays JW (eds) Modern methods in polymer characterization, chap 12. Wiley, New York
155. Vestal ML (1984) Science 226:595
156. Vargo JD, Olson KL (1985) Anal Chem 57:672
157. Vestal ML (1983) Mass Spectrom Rev 2:447
158. Vargo JD, Olson KL (1986) J Chromatogr 353:215
159. Leyen DV, Hagenhoff B (1989) J Vac Sci Technol A7:1790
160. Bletsos IV, Hercules DM (1991) Anal Chem 63:1953
161. Lattimer RP, Schulten HR (1985) Int J Mass Spectrom Ion Phys 67:227
162. Rollins K, Scrivens JH, Taylor MJ, Major H (1990) Rapid Commun Mass Spectrom 4:355
163. Fenn JB, Nohmi TJ (1992) J Am Chem Soc 114:3241
164. Kallos GJ, Tomalia DA (1991) Rapid Commun Mass Spectrom 5:383
165. Prokai L, Simonsick WJ (1995) SEC with electrospray mass spectrometric detection. In: Provder T, Barth HG, Urban MW (eds) Chromatographic characterization of polymers. Hyphenated and multidimensional techniques, chap 4. Adv Chem Ser. 247, American Chemical Society, Washington, DC
166. Prokai L, Simonsick WJ (1993) Rapid Commun Mass Spectrom 7:853
167. Simonsick WJ (1993) Polym Mater Sci Eng 69:412
168. Simonsick WJ, Ross CW (1996) Polym Prepr 37:286
169. Prokai L, Myung SW, Simonsick WJ (1996) Polym Prepr 37:288
170. Kemp TJ, Barton Z, Mahon A (1996) Polym Prepr 37:305
171. Karas M, Hillenkamp F (1988) Anal Chem 60:2299
172. Beavis RC, Chait BT (1989) Rapid Commun Mass Spectrom 3:233
173. Hillenkamp F, Karas M, Beavis RC, Chait BT (1991) Anal Chem 63:1193A
174. Bahr U, Deppe A, Karas M, Hillenkamp F, Giessmann U (1992) Anal Chem 64:2866
175. Danis PO, Karr DE, Mayer F, Holle A, Watson CH (1992) Org Mass Spectrom 27:843
176. Kahr MS, Wilkins CL (1993) J Am Soc Mass Spectrom 4:453
177. Montaudo G, Montaudo MS, Puglisi C, Samperi F (1994) Rapid Commun Mass Spectrom 8:1011
178. Danis PO, Karr DE, Xiong Y, Owens KG (1996) Rapid Commun Mass Spectrom 10:862
179. Pasch H, Unvericht R (1993) Angew Makromol Chem 212:191
180. Pasch, H, Gores F (1995) Polymer 36:1999
181. Braun D, Ghahary R, Pasch H (1996) Polymer 37:777
182. Pasch H, Deffieux A, Ghahary R, Schapacher M, Riquet-Lurbet L (1997) Macromolecules 30:98
183. Pasch H, Rode K (1995) J Chromatogr A699:21
184. Krüger RP, Much H, Schulz G (1996) GIT Fachz Lab 4:398
185. Just U, Krüger RP (1996) In: Auner N, Weis J (eds) Organosilicon chemistry II, VCH, Weinheim
186. Montaudo G (1995) Rapid Commun Mass Spectrom 9:1158
187. Danis PO, Saucy DA, Huby FJ (1996) Polym Prepr 37:311
188. Montaudo G (1998) Proc 11th Int Symp Polym Anal Char, Santa Margerita Ligure, Italy
189. Murray KK, Russell DH (1993) Anal Chem 65:2534
190. Murray KK, Russell DH (1994) J Am Soc Mass Spectrom 5:1
191. Fei X, Murray KK (1996) Anal Chem 68:3560
192. Albert K (1995) J Chromatogr 703:123

193. Dorn HC (1984) Anal Chem 56:747 A
194. Laude DA, Wilkins CL (1986) Trends Anal Chem 5:230
195. Albert K, Bayer E (1988) Trends Anal Chem 7:288
196. Albert K, Bayer E (1992) In: Patonay G (ed) HPLC detection: newer methods, VCH, New York
197. Hofmann M, Spraul M, Streck R, Wilson ID, Rapp A (1993) Labor Praxis 10:36
198. Smallcombe HS, Pratt LP, Keifer PA (1995) J Magn Reson A117:295
199. Ogg RJ, Kingsley PB, Taylor JS (1994) J Magn Reson B104:1
200. Albert K, Braumann U (1994) Anal Chem 66:3042
201. Albert K, Braumann U, Streck R, Spraul M, Ecker R (1995) Fresenius J Anal Chem 352:521
202. Albert K (1997) J Chromatogr A785:65
203. Braumann U, Händel H, Albert R (1995) Anal Chem 67:930
204. Wu N, Peck TL, Webb AG, Magin RL, Sweedler JV (1994) J Am Chem Soc 116:7929
205. Wu N, Peck TL, Webb AG, Magin RL, Sweedler JV (1994) Anal Chem 22:3849
206. Sweedler JV (1995) Proc 7th Int Symp High Performance Capillary Electrophoresis, Würzburg, Germany
207. Hatada K, Ute K, Okamoto Y, Imanari M, Fujii N (1988) Polym Bull 20:317
208. Hatada K, Ute K, Kashiyama M, Imanari M (1990) Polym J 22:218
209. Ute K (1998) Proc 11th Int Symp Polym Anal Char, Santa Margerita Ligure, Italy
210. Pasch H, Hiller W (1996) Macromolecules 29:6556
211. Schlotterbeck G, Pasch H, Albert K (1997) Polym Bull 38:673
212. Pasch H, Hiller W, Haner R (1998) 39:1515

Received: January 1999

Field-Flow Fractionation Techniques for Polymer and Colloid Analysis

Helmut Cölfen, Markus Antonietti

Max Planck Institute of Colloids and Interfaces, Colloid Chemistry Department, Am Mühlenberg 2, D-14476 Golm, Germany
E-mail: helmut.coelfen@mpikg-golm.mpg.de

Field-flow fractionation (FFF) is a family of flexible analytical fractionating techniques which have the great advantage that separation is achieved solely through the interaction of the sample with an external physical field and without a stationary phase. This has the advantage of avoiding the large variety of problems due to non-specific sample interactions with column materials associated with other chromatographic techniques. Furthermore, the range of information accessible is very broad and often complimentary when various FFF techniques are applied, so that even very complex systems with broad size distribution, heterogeneous mixtures or strongly interacting systems can be characterized. The range of particle sizes or hydrodynamic radii which can be separated is very broad ranging from 1 nm to 100 μm, covering the entire colloidal, polymeric and even most of the microparticle domain. No other fractionating technique can cover about 5 orders of magnitude of the particle size, even with complex distributions.
This review will introduce the basic principles, theory, and experimental arrangements of the various FFF techniques focusing on the most relevant for praxis: Sedimentation-FFF (S-FFF), Thermal-FFF (Th-FFF) and Flow-FFF (Fl-FFF). In a second part, selected applications of these techniques both to synthetic and biological samples will illustrate applications under a variety of conditions, where problems and potential pitfalls as well as recent developments are also considered.
Due to the wide spread of available information, an organized guide to the primary literature is given which contains the results from about 70% of the total literature published on FFF in listed journals so far.

Keywords: Field-flow fractionation, Chromatography, Separation, Polymers, Colloids

Advances in Polymer Science, Vol.150

List of Abbreviations

a_i	activity of component i in a solution
A_{Tot}	area of the accumulation wall
b	FFF channel breadth
b_0	channel width at the inlet
b_L	channel width at the outlet L
c	concentration
c^*	coil overlap concentration
c_0	concentration at the accumulation wall
d_H	hydrodynamic diameter
D	diffusion coefficient
D_T	thermal diffusion coefficient
E	electrical field strength
f	frictional coefficient
F	force
F_L	hydrodynamic lift force
F_{L_w}	hydrodynamic lift force by a near wall effect

F_{L_i}	inertial contribution to hydrodynamic lift force
$g(\dot{Y})$	zone spreading contribution to the FFF fractogram
G	gravitational/centrifugal acceleration
h(V)	experimental FFF fractogram
H_m	intensity of magnetic field
$\overline{H}$	theoretical plate height
J	flux density
k	Boltzmann's constant
l	average distance of the solute cloud from the accumulation wall
L	channel length
m	mass
m'	buoyant mass
M	molecular mass
n_c	peak capacity
N	plate number
N_A	Avogadro number
P	pressure
r	radius
r_c	radius from the center of rotation in S-FFF
$<r_G>$	radius of gyration
r_H	hydrodynamic radius
R	universal gas constant; also applied for the retention ratio
R_S	resolution between two separated components
s_0	fluid shear rate
S_m	mass based selectivity
S_D	diameter based selectivity
t	time
t_0	retention time of an unretained solute; void time
t_r	retention time
T	thermodynamic temperature
T_c	cold wall temperature in Th-FFF
$\lvert u_0 \rvert$	cross-flow velocity at the accumulation wall in A-Fl-FFF
U	solute drift velocity caused by the external field
v	flow velocity
$<v_s>$	mean velocity of the retained solute
<v>	mean velocity of the carrier fluid
$\overline{v}$	partial specific volume of the solute
$\overline{v}_i$	partial specific volume of component i in a multicomponent system
V	volume
V_0	volume of the separation channel
V_r	retention volume
$\dot{V}_c$	cross-flow rate for Fl-FFF
w	channel width

x	distance from the accumulation wall
y	distance perpendicular to the field axis and the carrier fluid flow
z	direction of the carrier fluid flow
z'	distance from the inlet to the focusing point for A-Fl-FFF
α	thermal diffusion factor=(D_T/D) T
χ_M	molar magnetic susceptibility
δ	distance of the particle bottom from the accumulation wall in hyperlayer FFF
ε_0	electrical permittivity of the free space
ε_m	relative electrical permittivity of the carrier medium
γ	thermal expansion coefficient
γ_s	steric correction factor
η	solvent viscosity
κ	thermal conductivity
κ_D	inverse of Debye length
κ_c	thermal conductivity at T_c
λ	retention parameter
μ_c^*	chemical potential
μ_e	electrophoretic mobility
ρ	solvent density
ρ_S	solute/particle density
σ	Gaussian half peak widths (time units) of eluting peaks
σ^*	complex conductivity
ω	angular velocity
ζ	ζ-potential
AC	adhesion chromatography
A-Fl-FFF	asymmetrical flow-field-flow fractionation
AUC	analytical ultracentrifugation
BSA	bovine serum albumin
CHDF	capillary hydrodynamic fractionation
DADMAC	diallyldimethylammonium chloride
DEP	dielectrophoresis
DEP-FFF	dielectrophoresis field-flow fractionation
DNA	desoxyribonucleic acid
DMSO	dimethyl sulfoxide
EAAS	electrothermal atomic adsorption spectroscopy
El-FFF	electrical field-flow fractionation
EM	electron microscopy
FFF	field-flow fractionation
Fl-FFF	flow-field-flow fractionation
GC-MS	gas chromatography coupled with mass spectrometry
Gr-FFF	gravitational field-flow fractionation
Gr-SPLITT-FFF	gravitational SPLITT-field-flow fractionation
HC	hydrodynamic chromatography

Helical Fl-FFF	three-dimensional flow-field-flow fractionation
HPLC	high performance liquid chromatography
ICP-MS	inductively coupled plasma mass spectrometry
IR	infrared
MALLS	multiangle laser light scattering
MS	mass spectrometry
MWCO	molar weight cut off
OFSC	opposed flow sample concentration
PCS	photon correlation spectroscopy
PEO	poly(ethylene oxide)
PET	poly(ethylene terephthalate)
PMMA	poly(methyl methacrylate)
PPO	poly(propylene oxide)
PS	polystyrene
PTFE	poly(tetrafluoroethylene)
P4VP	poly(4-vinylpyridine)
QELS	quasi-elastic light scattering
RI	refractive index
RNA	ribonucleic acid
RPM	revolutions per minute
SEC	size exclusion chromatography
S-FFF	sedimentation field-flow fractionation
S-Fl-FFF	symmetrical flow-field-flow fractionation
THF	tetrahydrofuran
Th-FFF	thermal field-flow fractionation

1 Introduction and Basic Principles

1.1 History/The Family of Field-Flow-Fractionation (FFF) Techniques

FFF techniques were pioneered by Giddings in 1966 [1]. Starting from this point, a remarkable development has taken place resulting in a diversity of different FFF methods. Figure 1 gives an overview of the different techniques with their time of invention. The number of different methods is directly related to the variety of force fields which can be applied for the separation of the samples. Practically, only three of those FFF methods are commonly used and commercially available at the present time; namely sedimentation-FFF (S-FFF), flow-FFF (Fl-FFF) and thermal-FFF (Th-FFF). The range of possible techniques was established in the early years whereas the main development of the last years is seen in a continuous optimization of the methodology and the instrumentation. This becomes most evident for the case of flow-FFF, where an asymmetrical channel with better separation characteristics has been developed.

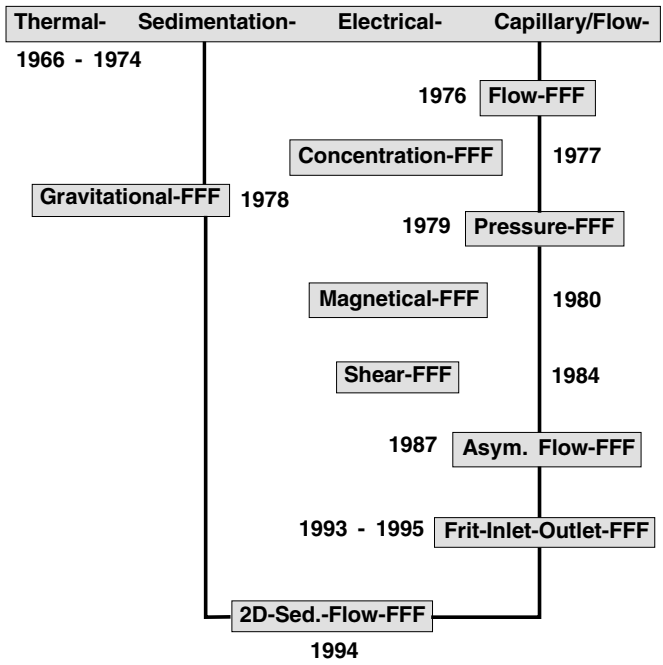

Fig. 1. A "family tree" of FFF methods with their date of birth

FFF techniques have also gained a broader and broader application, as reflected in the number of papers on the technique. This is shown in Fig. 2 in a plot of available papers versus time. Up to 1980, only few papers were published whereas there is a close to exponential increase afterwards. The FFF family has already been reviewed many times, covering both theoretical and practical aspects [2–26], and two books dedicated to FFF are available [27,28], the latter more generally treating separation techniques.

The first two experimental studies using FFF techniques were the fractionation of polystyrenes by Th-FFF [29] and the fractionation of *E. coli* bacteriophages and particles by sedimentation/gravitational-FFF [30–32]. Simultaneously, a theory of FFF was developed [33,34]. In 1972, electrical-FFF (El-FFF) was introduced as a technique for the separation of proteins [35,36]. The first flow-FFF setup was reported in 1974 applying circular tubes [37]. The experimental methodology and resolution of FFF were further improved by means of field programming which allowed the establishment of profiles of the applied physical field and thus an extension of the width of the separation range (see, e.g. [38–40]). Flow-FFF was introduced in 1976 in the principle setup which is still used today [41]. A year later the concepts for concentration FFF were published [42]. Other FFF methods, such as thermogravitational-FFF [43], pressure-FFF [44], magnetic-FFF [45] and shear-FFF [46], were developed but are rarely used

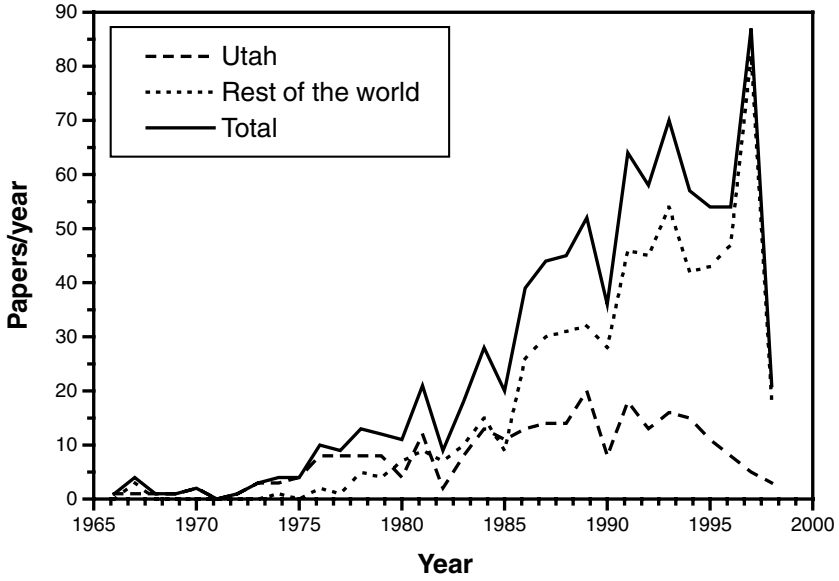

Fig. 2. Number of papers published on FFF. Source: Field-flow fractionation references web site update 14.10.1998 (see Sect. 6)

and are of minor importance. After 1984, principally flow-FFF was improved because it is the most simple and universally applicable FFF method for the whole range of systems. Asymmetrical flow-FFF was introduced in 1987 [47]. This technique has a better resolution than the so-far applied symmetrical flow-FFF due to the possibility of focusing the sample into a narrow band, whereas symmetrical flow-FFF could be improved by the introduction of frits for the sample injection [48–52]. Further improvement in the amount of accessible information of all FFF techniques was achieved by the modular combination of the fractionating FFF channel with an absolute molar mass measurement (multiangle laser light scattering; MALLS) at the beginning of the 1990s [53], a technique which can yield absolute molar mass distributions within a few minutes.

1.2 General Principles

The fundamental principle of FFF is illustrated in Fig. 3. The separation of the sample takes place inside a narrow ribbon-like channel. This channel is composed of a thin piece of sheet material (usually 70–300 μm thick Mylar or polyimide) in which a channel is cut and which is usually clamped between two walls of highly-polished plane parallel surfaces through which a force can be applied

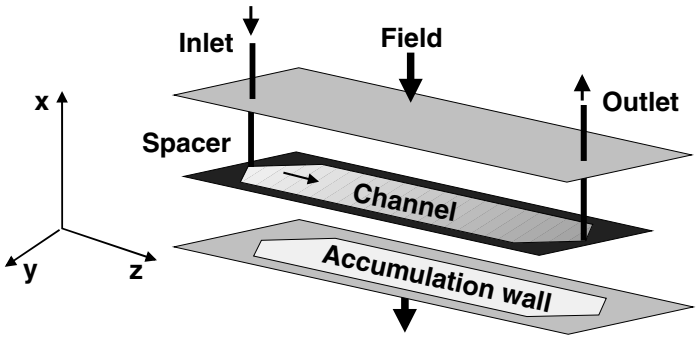

Fig. 3. Schematic representation of an FFF channel

(exceptions: flow- and electrical-FFF). The actual configuration varies with the type of field being utilized.

A carrier liquid is pumped through this channel from the inlet, where the sample is injected, to the outlet, to which a detector is connected. Inside the channel, a parabolic flow profile (laminar Newtonian flow) is established as in a capillary tube. Thus, flow velocities vary from zero at the walls to a maximum in the center of the channel. While the carrier liquid with the sample is flowing through the channel, an effective physical or chemical field is applied across the channel perpendicular to the flow direction of the carrier liquid. Interaction with the field concentrates the solute at one of the channel walls, called the accumulation wall. The center of gravity of the solute zones lies very near to the wall, usually extending only a few micrometers. Due to the established concentration gradient, a diffusion flux in the reverse direction is induced according to Fick's law. After a short time a steady state is reached, and the exponential distribution of the solute cloud across the channel can be described by a mean layer thickness (l). Due to the parabolic flow velocity profile, the solutes are transported in the direction of the longitudinal channel axis at varying velocities, depending on their distance from the channel walls. The nearer the solute is located to the accumulation wall, the later it will elute. Since smaller molecules (X) diffuse faster than larger ones (Y) and so establish a higher layer thickness l, the elution sequence proceeds from the smaller solutes to the largest ones. (See Fig. 4). Hence, the flow velocity profile of the carrier liquid amplifies very little distance differences between the solute clouds in the x-direction, leading to the separation. This FFF mode, when the intensity of driving forces induced by the applied outer field is homogeneous within the entire channel, is called classical or normal mode operation.

The intensity of the driving force can be varied in the course of the elution. This is called field intensity programming and permits analysis of very broadly distributed solutes (10^3–10^7 g/mol) [54] in one experiment over reasonable times with good resolution. The channel flow may also be programmed for shorter analysis times but with a cost to resolution.

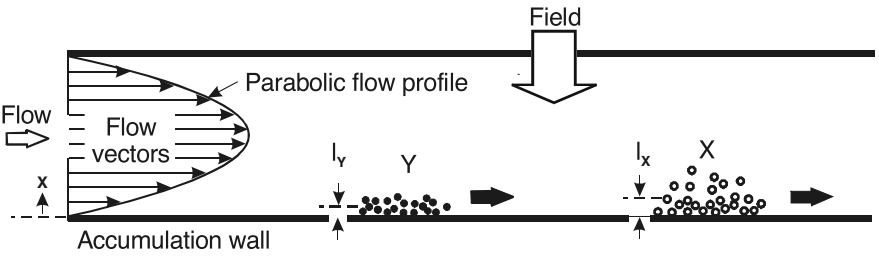

Fig. 4. Mechanism of an FFF separation of two components X and Y across the parabolic flow profile resulting in different flow velocities of X and Y. Reproduced from [14] with kind permission of the American Association for the Advancement of Science

The simple configuration with the defined channel geometry allows precise calculation of the flow hydrodynamics, unlike packed columns where flow patterns are very complex. In contrast to chromatography, the separation features of FFF techniques were conceived and developed from the beginning on theoretical grounds. Well-designed flow profiles were generated and different force fields were exploited to interact with a given specific particle property. Because of the theoretical basis of the resulting separation process, FFF is in principle also suited to determine absolute physicochemical properties of the sample components, such as the diffusion or thermodiffusion coefficient.

Compared to a packed high performance liquid chromatography (HPLC) column, the open channel also minimizes the shear effects exerted onto large molecules (as illustrated by the required pressure differences), and complex molecules and aggregates will remain intact. In addition, adsorption is kept to a minimum because of the greatly reduced surface area in an FFF channel. The carrier composition can affect the retention characteristics of polymers and particles in some cases. Factors including viscosity, ionic strength, type of detergent, and chemical composition have been discussed in the literature [55–62].

There are some special cases in FFF related to the two extreme limits of the cross-field driving forces. In the first case, the cross-field force is zero, and no transverse solute migration is caused by outer fields. However, because of the shear forces, transverse movements may occur even under conditions of laminar flow. This phenomenon is called the "tubular pinch effect". In this case, these shear forces lead to axial separation of various solutes. Small [63] made use of this phenomenon and named it "hydrodynamic chromatography" (HC). If thin capillaries are used for flow transport, this technique is also called capillary hydrodynamic fractionation (CHDF). A simple interpretation of the ability to separate is that the centers of the solute particles cannot approach the channel walls closer than their lateral dimensions. This means that just by their size larger particles are located in streamlines of higher flow velocities than smaller ones and are eluted first (opposite to the solution sequence in the classical FFF mode). For details on hydrodynamic chromatography, see [64–66].

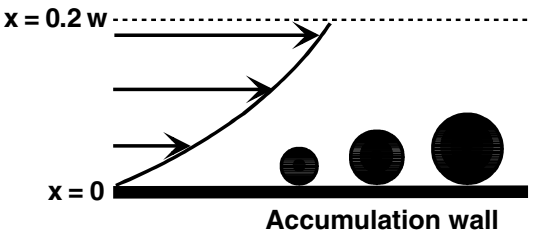

Fig. 5. Schematic representation of the steric-FFF mode

In the other limiting case of FFF, the intensity of the driving force is high enough to press all the solutes as close as possible to the accumulation wall of the channel, which is the basis of an independent FFF mode called steric field-flow fractionation [67]. This upper limit mode becomes operative when the mean diffusive layer thickness l is of approximately the particle size. As in hydrodynamic chromatography, the solute layer thickness is mainly controlled by steric exclusion of the particles from the accumulation wall. Again, larger particles are kept in streamlines of higher velocities than are smaller particles and are eluted more rapidly (see Fig. 5). In principle, any FFF technique can be operated in the steric-FFF mode by increasing the cross-field.

The transition between normal and steric-FFF mode depends on the particle size and lies for standard separation parameters at around 1 μm diameter (see Fig. 6). In this range, the elution behavior reverses, and the retention time is not any longer unique to a particle size. Consequently, the particle size determination of the size range can be erroneous, which can be a significant problem with polydisperse samples. However, most samples have sizes where the operation of one of the modes can be clearly assigned (see Fig. 6). The transition range between normal and steric-FFF mode has been considered in detail by Myers and Giddings [68].

For samples with a broad size distribution in the micron range, it is important to avoid the transition region between the normal and the steric mode during the measurement. This can be achieved by proper adjustment of the channel thickness, channel flow and the strength of the applied field [69]. The transition region in Fig. 6 can be experimentally determined by plotting the retention ratio vs. the particle size, as illustrated in Fig. 7 for the example of flow-FFF.

As the average velocity of the carrier in the channel increases, particles that are in close contact with the accumulation wall experience hydrodynamic lift forces which move them into a confined region from the wall that is thin relative to their size, or "focused," as shown in Fig. 8. This is the basis of another FFF operation mode called "hyperlayer mode" [71] which is characterized by an extremely high resolution in very short analysis times. However, the nature of the hydrodynamic lift forces is still only poorly understood.

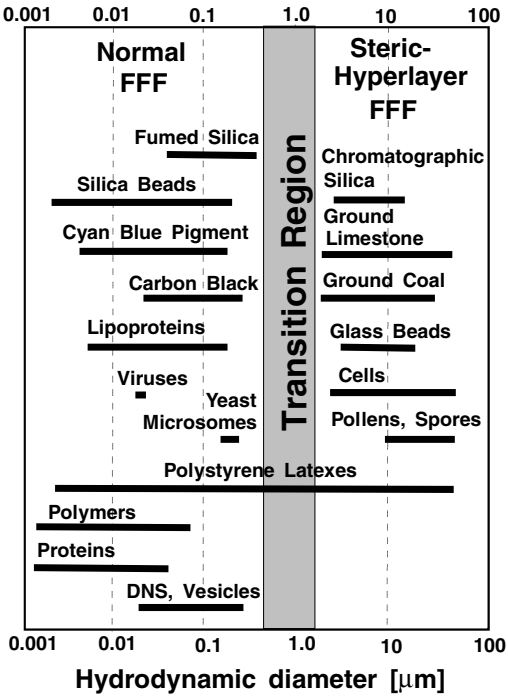

Fig. 6. Application of FFF to various materials spanning the whole range of applicability

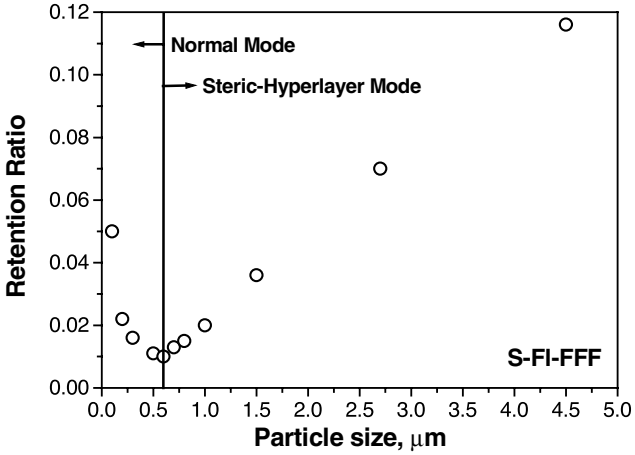

Fig. 7. Determination of the transition point between the normal and the steric mode for the example of S-Fl-FFF. Reproduced from [70] with kind permission of VCH Verlagsgesellschaft Weinheim

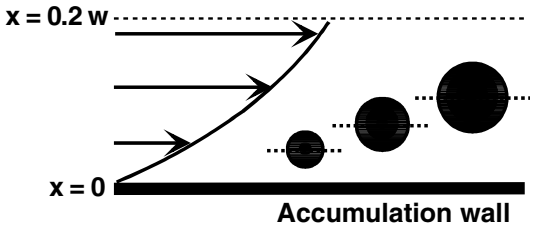

Fig. 8. Steric-hyperlayer mode

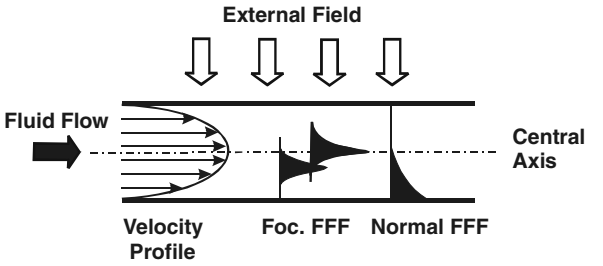

Fig. 9. Principle of focusing-FFF. Reproduced from [74] with kind permission of the American Chemical Society

Another FFF mode, focusing-FFF [71–74], exploits a counterbalance of the forces exerted on the solute via an external field gradient by dispersive diffusion processes. In contrast to classical FFF techniques, where the field strength is constant, the solute is focused to a position inside the channel where due to a balance of the driving force to the accumulation wall and the back diffusion the intensity of the driving force is zero. Thus a focused, Gaussian-shaped concentration distribution for each species is formed inside the channel, which migrate along the channel at different velocities and are longitudinally separated. Such a situation is shown schematically in Fig. 9. To illustrate the basic difference between the classical and all focusing-FFF methods, the exponential shape of the concentration profile of the solute in the case of classical FFF is also shown in Fig. 9.

1.3 Accessible Quantities

Depending on the separation mode, knowledge about the sample, and the FFF setup, four categories of operating an FFF experiment are identified:

1. Information about sample composition, homogeneity and purity from qualitative evaluation of the fractogram;

2. Application of the FFF channel as a separation column and determination of physicochemical quantities by following characterization (either on or off line);
3. Measurement of forces acting in the FFF channel;
4. Determination of absolute physicochemical quantities of the sample via the retention times in the FFF channel.

1. The simplest analytical information that can be obtained with the aid of FFF is the homogeneity of the sample or evidence for the presence of a compound of interest in the fractionated sample by the appearance of a peak in the expected interval of retention volume. In some cases, comparison of the retention volume and the peak shape of the investigated component with the peak shape of a reference sample can provide sufficient qualitative analytical information on sample purity and homogeneity. The peak areas in the fractogram can be used to evaluate quantitatively concentrations of the detected components provided that the relationship between detector response and concentration or quantity of the detected component is known. This relationship is usually determined by a calibration procedure. However some sample is lost in the void peak so that it is not possible to relate the detected concentration to that of the original sample; consequently, concentration determinations can more advantageously serve to compare the relative concentrations of the fractionated components.

2. Coupling FFF with other techniques can enhance measurement capabilities. Here, the possibility of taking fractions after the FFF separation is of great advantage. The use of photon correlation spectroscopy, for example, to determine the size of spheres eluted from sedimentation FFF yields both size and density [75]. Further comparison can be achieved with electron microscopy. In principle, every analytical technique (spectroscopy, microscopy, chemical analysis, etc.) can be performed off-line on fractions from FFF.

It is, however, more convenient to couple absolute flow-through detectors online with an FFF channel. For example, coupling multiangle laser light scattering (MALLS) with FFF has become highly popular among FFF researchers in recent years and is treated in detail in Sect. 4.3.2. Here, the molar mass distribution as well as the radii of gyration for each species are obtained on an absolute basis.

If a continuous viscosity detector is coupled to an FFF channel, viscosity distributions and intrinsic viscosities can be measured without calibrating the channel [76]. The coupling of one FFF instrument to another opens the possibility of obtaining two-dimensional property distributions of complex materials: the combination of sedimentation- and flow-FFF provides the size-density distribution of complex colloids, whereas a combination of thermal- and flow-FFF yields the composition-molecular weight distribution of copolymers.

3. FFF in an absolute configuration can be used to determine the often very weak cross-forces by the retention times which helps to understand the funda-

mental physicochemical phenomena which are reflected in these forces. For example, for poorly understood forces (e.g. hydrodynamic lift forces) or coupled transport phenomena (thermal diffusion), the measurement of forces exerted on model particles can help to explore and understand the principles. An FFF separation is sensitive to these very weak forces, and retention of colloids and macromolecules is induced by forces as little as 10^{-16} to 10^{-14} N per particle [77]. Thus forces as small as 10^{-16} N can be determined by measuring t_r. Force increments as low as 10^{-17} N can be detected as measurable shifts in t_r of 0.1 to 1 min (from $(\Delta t_r/t_0)=w\Delta F/6kT$; a change ΔF in F of 10^{-17} N at T=300 K with w=250 μm thus shifts the retention time by $\Delta t_r=0.106\ t_0$. Typically, the void time t_0 is 1 to 10 min, giving $\Delta t_r \approx 0.1$ to1 min) [14]. These forces are eight to nine orders of magnitude less than the force required to rupture one C–C bond (ca. 0.8×10^{-8} N [78]). The very high resolution of observable net forces is a result of the fact that they are balanced or "weighted" by similarly small entropic forces such as back diffusion due to the concentration gradient and so forth.

For micrometer-sized particles subject to steric- or lift-hyperlayer-FFF, the driving forces are higher (10^{-14} to 10^{-8} N per particle) but are not balanced by back diffusion as in the normal FFF mode. Steric- and lift-hyperlayer-FFF provide powerful means for the investigation of hydrodynamic lift forces [79]. Here, retention times have been measured for well-characterized particles such as latex spheres under widely varying conditions, and the hydrodynamic lift force F_L has been determined.

4. The dimensionless retention parameter λ of all FFF techniques, if operated on an absolute basis, is a function of the molecular characteristics of the compounds separated. These include the size of macromolecules and particles, molar mass, diffusion coefficient, thermal diffusion coefficient, electrophoretic mobility, electrical charge, and density (see Table 1, Sect. 1.4.1.) reflecting the wide variablity of the applicable forces [77]. For detailed theoretical descriptions see Sects. 1.4.1. and 2. For the majority of operation modes, λ is influenced by the size of the retained macromolecules or particles, and FFF can be used to determine absolute particle sizes and their distributions. For an overview, the accessible quantities for the three main FFF techniques are given (for the analytical expressions see Table 1, Sect. 1.4.1):

Sedimentation-FFF. Retention measurements give the effective particle mass m' (buoyant mass). If the particle density is known, the particle mass m, particle volume V_p, and hydrodynamic diameter d_H can be calculated [80,81]. Apart from the particle dimensions, the density can be determined as well [82] as the difference in the densities of the solute and the solvent, $\Delta\rho$, is linearly correlated to λ. Fractionation can be used in regions where the solvent density is lower than the solute density ($\rho<\rho_s$) as well as where $\rho>\rho_s$. The determination of particle density in a single experiment is possible by sedimentation-flotation focusing-FFF [72,73,83] analogous to density gradient ultracentrifugation.

Flow-FFF. The measurement of retention in flow-FFF directly yields the diffusion coefficient D and the related hydrodynamic diameter d_H which is related to D by the Stokes–Einstein equation $D = \frac{kT}{3\pi\eta d_H}$. As the solute density does not influence retention, information from flow-FFF can be advantageously combined with that of sedimentation-FFF yielding particle size and density distributions.

Thermal-FFF. The retention rate directly yields the Soret coefficient D_T/D. If D is known (for example from flow-FFF), the thermal diffusion coefficient D_T can be obtained which can give information about the chemical sample composition. Unfortunately, no context is known which analytically relates D_T with the sample composition [84]. On the other hand, for known D_T values (material constant), the diffusion coefficient distribution is directly obtained.

1.4 General Theoretical Considerations

If the geometry of an FFF channel is known exactly and a parabolic flow profile in the channel can be assumed (see Sect. 1.2), it is possible to make exact predictions about the separation of the sample as well as the separation efficiency. In this section, only the general theoretical expressions universally applicable to all FFF techniques operating in the normal mode are provided. Specialities of the different FFF methods are given during their detailed discussion in Sect. 2.

1.4.1 *Elution in an FFF Channel*

The theory of FFF has undergone significant developments since the general introduction of the "non-equilibrium theory of FFF" by Giddings in 1968 [33] especially motivated by the various FFF techniques. Examples that include general discussions for FFF are [5,25,30,85–102], Th-FFF [34,103], magnetic-FFF [45] dielectrical-FFF [104], S-FFF [105,106], hyperlayer-S-FFF [83,107], focusing-FFF [108], Fl-FFF [41] and shear-FFF [46].

For the concentration profile of a sample which has been driven towards the accumulation wall by the physical field, the general transport theory yields for the flux density J_x of the solute:

$$J_x = \underbrace{Uc(x)}_{\substack{\text{External}\\ \text{field}}} - \underbrace{D\frac{dc(x)}{dx}}_{\text{Diffusion}} \qquad (1)$$

where D is the translational diffusion coefficient, x is the distance from the accumulation wall, c(x) is the concentration gradient and U is the drift velocity of

the solute caused by the external field. As indicated in Eq. (1), there are two contributions to the flux density of the solute: (a) the flux caused by the solute drift due to the external field and (b) the back diffusion away from the accumulation wall according to Fick's law due to the established solute concentration gradient. After a short time, a steady state is established. Due to the transport character of the solute distribution, this is not an equilibrium state as erroneously stated in many literature references but in fact a stationary non-equilibrium state. In the steady state, the resulting flux vanishes and by integration of Eq. (1) the following relationship is obtained:

$$c(x) = c_0 \exp\left(-\frac{x|U|}{D}\right) \tag{2}$$

where c_0 is the concentration at the accumulation wall. The diffusion coefficient can be related to the frictional coefficient f by the Stokes–Einstein relation:

$$D = \frac{kT}{f} \tag{3}$$

where k is the Boltzmann constant and T is the temperature. The frictional coefficient furthermore relates the drift velocity U to the force F which acts on the solute by:

$$U = \frac{F}{f} \tag{4}$$

A parameter $l=D/|U|$ can now be introduced which is a measure of the average distance of the solute from the wall. From Eqs. (3) and (4) the following relationship for l is obtained:

$$l = \frac{kT}{F} \tag{5}$$

or in the form of the dimensionless retention parameter λ

$$\lambda = \frac{l}{w} = \frac{kT}{Fw} \tag{6}$$

where w is the channel thickness. The parameter λ is not directly experimentally accessible, but can be related to experimental quantities. This can be done by using the retention ratio R. R is defined as the ratio of the retention time of an unretained solute t_0 to the retention time of the retained solute t_r or equivalently in terms of retention volumes $R=V_0/V_r$ of the two species. V_0 is the volume of the separation channel which in the ideal case can be calculated from its geometry, but is experimentally obtained from the position of a low molecular weight sol-

ute. R can also be defined as the ratio of the mean velocity of the retained solute $<v_s>$ to the mean velocity of the carrier fluid $<v(x)>$.

$$R = \frac{t_0}{t_r} = \frac{V_0}{V_r} = \frac{< v_s >}{< v(x) >} = \frac{< c(x)v(x) >}{< c(x) >< v(x) >} \tag{7}$$

or as the integral form:

$$R = \frac{\int_0^w c(x)v(x)dx}{\int_0^w c(x)dx \int_0^w v(x)dx} \tag{8}$$

For the isothermal, isoviscous flow profile v(x) of a Newtonian liquid between two parallel infinite plates, one obtains:

$$v(x) = \frac{\Delta P}{2\eta L} x(w - x) \tag{9}$$

where ΔP is the pressure drop along the channel with length L and η is the viscosity of the solvent. For a parabola-shaped flow profile, the mean velocity $<v(x)>$ is 2/3 of the maximum velocity in the center of the channel at x=w/2. Thus, $<v(x)>$ can be written:

$$< v(x) >= \frac{\Delta P w^2}{12\eta L} \tag{10}$$

Using Eqs. (9) and (10), the integrals in Eq. (8) can be solved and a relationship between λ and the experimentally accessible R obtained [34]:

$$R = 6\lambda \left[\coth\left(\frac{1}{2\lambda} \right) - 2\lambda \right] \tag{11}$$

For small values of λ, one can approximate $\coth(2\lambda)^{-1}=1$ and thus Eq. (11) is simplified:

$$R = 6\left(\lambda - 2\lambda^2 \right) \tag{12}$$

or if λ approaches 0 by:

$$\underbrace{\lim}_{\lambda \to 0} R = 6\lambda \tag{13}$$

For $\lambda<0.3$, deviations from the exact Eq. (11) are negligible [85]. Once λ is known, it can be related to physicochemical quantities of the solute depending

Table 1. Relationship between λ and the physical solute properties using different FFF techniques [27,109] with R=gas constant, ρ=solvent density, ρ_s=solute density, $\omega^2 r$=centrifugal acceleration, V_0=volume of the fractionation channel, $\dot{V}_c$=cross-flow rate, E=electrical field strength, dT/dx=temperature gradient, M=molecular mass, d_H=hydrodynamic diameter, D_T=thermal diffusion coefficient, μ_e=electrophoretic mobility, χ_M=molar magnetic susceptibility, H_m=intensity of magnetic field, ΔH_m=gradient of the intensity of the magnetic field, $\Delta\mu^*_c$ = total increment of the chemical potential across the channel

FFF technique	Expression for λ	Physicochemical parameters
Sedimentation-FFF	$\lambda = \frac{RT}{\omega^2 r M\left(1-\frac{\rho}{\rho_s}\right)w}$	ρ_s, M
	$\lambda = \frac{6kT}{\pi d_H^3 \omega^2 rw\left(\rho_s-\rho\right)}$	d_H
Thermal-FFF	$\lambda = \frac{D}{D_T(dT/dx)w}$	D, D_T
Electrical-FFF	$\lambda = \frac{D}{\mu_e E w}$	D, μ_e
Flow-FFF	$\lambda = \frac{DV_0}{\dot{V}_c w^2}$	D, d_H
Steric-FFF	$\lambda = \frac{d_H}{2w}$	d_H
Magnetic-FFF	$\lambda = \frac{RT}{Mw\chi_m H_m \Delta H_m}$	M, χ_m
Concentration-FFF	$\lambda = \frac{RT}{\Delta\mu^*_c}$	$\Delta\mu^*_c$

on the nature of the applied physical field. For the various FFF techniques, these relationships can be found in Table 1.

The theoretical treatment above was based on the following assumptions: (a) The channel is placed between infinite parallel plates, (b) the flow profile is parabolic, (c) a steady state concentration profile of the sample is established after action of the physical field, (d) uniform force of the physical field in the channel, and (e) absence of extraneous non-uniform forces. These assumptions are usu-

ally fulfilled for the various FFF techniques, but significant errors and artifacts can be generated in the other cases (see also Sect. 4.2.1).

1.4.2
Resolution, Theoretical Plate Heights and Peak Capacity

Successful separation of two components requires that a difference Δt_r in retention time t_r is generated by sufficiently different molecular parameters of the components subjected to fractionation. However, separation also requires a consideration of peak broadening so that peaks with a finite Δt_r do not overlap. In FFF, theoretical guidelines can be developed to reach band broadening and resolution objectives through optimization of the flow rates V and $\dot{V}_c$.

As in chromatography and related techniques, the resolution R_s between two components can be defined by [28]:

$$R_s = \frac{t_{r2} - t_{r1}}{2\sigma_2 + 2\sigma_1} \cong \frac{\Delta t_r}{4\sigma} \tag{14}$$

where σ_1 and σ_2 are the Gaussian widths (in time units) of the two eluting peaks. For well-defined, neighboring components with similar properties one can assume that the σ values are similar [41], and a mean common σ is used which is the average of the σ_i. In elution methods such as FFF and chromatography, σ is – in analogy to fractionation systems – related to the height equivalent of a theoretical plate, $\overline{H}$, by [28]:

$$\overline{H} = \frac{L\sigma^2}{t_r^2} = \frac{\sum_i L_i \sum_i \sigma_i^2}{\left(\sum_i t_{r,i}\right)^2} \tag{15}$$

where L is the channel length. The plate number N can be calculated from $\overline{H}$ by $N = L/\overline{H}$. $\overline{H}$ is only an average value as several contributions to the average plate heights exist:

$$\overline{H} = \overline{H}_{neq} + \overline{H}_{long} + \overline{H}_{inj} + \sum \overline{H}_i \tag{16}$$

where the non-equilibrium term $\overline{H}_{neq}$ is due to the velocity profile, $\overline{H}_{long}$ due to longitudinal diffusion, $\overline{H}_{inj}$ is caused by the broadness of the sample zone when starting elution and $\sum \overline{H}_i$ is due to the sum of instrumental effects. The last three terms are for a modern instrument usually small and can be neglected as compared to the magnitude of the first one.

A combination of Eqs. (14) and (15) gives:

$$R_s = \frac{L^{1/2}}{4} \frac{\Delta t_r}{t_r \overline{H}^{1/2}} \tag{17}$$

which relates the resolution R_s to the plate height $\overline{H}$.

Furthermore, R_s is related to the peak capacity n_c which is the number of peaks that can be separated at a specified resolution R_s over the channel length L by [28]:

$$n_c = \frac{L}{4\sigma R_s} = \frac{(L\overline{H})^{1/2}}{\sigma t_r} \tag{18}$$

To make use of Eqs. (17) and (18), $\overline{H}$ needs to be related to the experimental parameter λ. Hence, an expression for the plate height must be sought which varies for each FFF technique. In general, $\overline{H}$ can be expressed as [28]:

$$\overline{H} = \chi \frac{w^2 \langle v \rangle}{D} \tag{19}$$

where <v> is the mean cross-sectional fluid velocity and χ a dimensionless parameter. χ equals 24 λ^3 for small λ and l [85].

For example, in the case of Fl-FFF, the non-equilibrium contribution to the plate height, which is the minimum value of $\overline{H}$, is closely approximated by [41]:

$$\overline{H} = \frac{2}{3} R^2 (1 - R) \frac{V}{\dot{V}_c} L \cong \frac{2}{3} R^2 \frac{V}{\dot{V}_c} L \tag{20}$$

where the final approximation is applicable for R (or λ) <<1. When this latter approximation is substituted into Eq. (17), we obtain:

$$R_s = \frac{1}{4} \left(\frac{3\dot{V}_c}{2V} \right)^{1/2} \frac{\Delta t_r}{t_r R} \tag{21}$$

1.5 Comparison of FFF with Other Analytical Techniques

1.5.1 *Comparison of FFF (Th-FFF and Fl-FFF) with SEC*

As FFF is similar to other chromatographic techniques it is interesting for the reader to compare their performance. The most extensive comparison is with size exclusion chromatography (SEC). The reason for this is that SEC and Th-FFF have similar application ranges, mainly synthetic polymers in organic solvents, and were developed at about the same time. Both FFF and SEC are used to obtain molecular weight information, but they use different fundamental mechanisms and therefore have different capabilities and limitations. For example, SEC can be advantageously applied to low molecular weight polymers while, for Th-FFF, very high temperature gradients are needed for the retention of these oligomers/polymers. On the other hand, Th-FFF is more

suited to ultrahigh molecular weight polymers susceptible to shear degradation in the packed SEC column. In this respect, SEC and Th-FFF are complimentary.

A significant difference can be found in the theoretical basis of the separation. The open Th-FFF channel allows retention to be precisely related to physicochemical parameters and experimental variables (even if the nature of thermal diffusion is not yet completely understood), whereas separation conditions in SEC channels lack the possibility of a rigid physicochemical basis. But although Th-FFF has a more rigorous theoretical background than SEC and a much wider application range with regard to separable molar masses, and although both techniques require almost the same supplemental equipment, it is astonishing to note that SEC has found widespread application and was the subject of intense research whereas Th-FFF was more or less a "Cinderella" in the analytical ballrooms. Both techniques were established in the 1960s but, even today, the application of FFF is in general by no means comparable with that of SEC. The following discussion compares SEC and FFF in detail, including calibration procedures, separation efficiencies and the general applicability of both techniques to polymer analysis.

Methodology and Universal Calibration. FFF calibration curves relating the retention of the solute to the molar mass can be expressed as:

$$\log V_r = a + S_m \log M \tag{22}$$

where a and S_m are constants; S_m is referred to as the mass based selectivity. Since the V_r of a component is related to its transport coefficients (D in Fl-FFF and D/D_T in Th-FFF), the calibration constants contain the inherent dependence of these transport coefficients on M; the appropriate algebraic scaling relations are well known in polymer and colloid physics:

$$D/D_T = \phi_0 M^{-n} \text{ for Th-FFF and} \tag{23}$$

$$D = AM^{-b} \text{ in case of FI-FFF} \tag{24}$$

The parameters ϕ_0, n, A and b are universal constants for a given polymer-solvent system. (Since D_T is independent of M and the degree of branching for a given polymer-solvent system [110,111], n≈b.) Differences between n and b arise primarily from the temperature dependence of the transport coefficients, which plays a role in Th-FFF and makes n slightly larger than b [112].

Combining Eq. (23) with the expression for $l = \frac{wD}{D_T \Delta T}$ for Th-FFF and, respectively, Eq. (24) with $l = \frac{w^2 D}{\dot{V}_c}$ for Fl-FFF yields the following universal calibration equations:

$$\lambda = \frac{\phi_0}{\Delta T} M^{-n} \tag{25}$$

for Th-FFF and

$$\lambda = \frac{wA}{\dot{V}_c} M^{-b} \tag{26}$$

for FI-FFF.

The parameter λ can be calculated from experimental values of V_r using Eq. (11), or M can be directly related to V_r by using the approximation $R \cong 6\lambda$ (accurate to within 2% when $R<0.06$):

$$V_r = \frac{V_0 \Delta T}{6\phi_0} M^n \text{ for Th} - \text{FFF and} \tag{27}$$

$$V_r = \frac{V_0 \dot{V}_c}{6Aw} M^b \text{ for FI} - \text{FFF} \tag{28}$$

A comparison of these separation equations with the universal calibration curve (Eq. 22) leads to the prefactors of Eq. (22):

$$a = \log \frac{V_0 \Delta T}{6\phi_0} \text{ and } S_m = n \text{ for Th} - \text{FFF} \tag{29}$$

$$a = \log \frac{V_0 \dot{V}_c}{6Aw} \text{ and } S_m = b \text{ for FI} - \text{FFF} \tag{30}$$

It is seen that for all FFF techniques the dependence of the retention volume on molecular weight is not linear. Practically, this restricts the accessible range of particle sizes in one single normal mode separation to about one order of magnitude. Broad molar mass distributions can be efficiently analyzed by FFF in a single run in the field programming mode. Theoretical guidelines and examples (including temperature programming) that can be found in the literature [15] show how experimental time and fractionating power in Th-FFF can be manipulated through changes in flow rate and ΔT. In contrast to FFF, the elution volume in SEC is proportional to the logarithm of hydrodynamic size or molecular weight of the sample, and molecular weight distributions can be as broad as five orders of magnitude in weight and are still accurately determined. Such molecular weight ranges, however, require connection of several columns in series, which significantly increases both run time and operating pressure.

FFF calibrations are universal in the sense that calibration constants apply to all other FFF setups under a wide range of experimental conditions [113] which are somewhat different from SEC as explained below. For characterizing molecular mass distributions with SEC, the calibration constants must be determined empirically for a whole set of standard samples. FFF channels are also calibrated empirically with standards for polymer-solvent systems where the Mark–Houwink coefficients for the dependence of the transport coefficients on M are un-

known. When this dependence is accessible, Fl-FFF does not require calibration, and since D_T is independent of M, universal calibration in Th-FFF can be performed with a single standard of known M to determine D_T. Once the calibration constants have been determined, no additional information is needed to characterize the molar mass distribution of a given polymer on every Th-FFF apparatus.

Both FFF and SEC require careful control of the temperature for universal calibration. For SEC and Fl-FFF, this means controlling the temperature of the room or of the channel/column. For Th-FFF, it is important to maintain the specified cold-wall temperature, T_c. Fortunately, the temperature at the center of gravity of a component is independent of the field strength in Th-FFF, so that universal calibration constants do not change when ΔT is tuned to optimize the analysis of a particular range in M, provided T_c is held constant.

The resolution of polymer components in FFF and SEC is governed by two factors: the change in retention with M and the plate height $\overline{H}$. The former is defined by the selectivity S_m and governed by transport coefficients and the separation mechanism; the latter is used to define the extent of remixing of separated zones [114]. If the remixing occurs more slowly than the retention, a net gain in the separation of different components is obtained. Plate height varies with experimental conditions, with lower $\overline{H}$ corresponding to more efficient separations. Selectivity in FFF depends on the polymer-solvent system but is as high as 0.5–0.65; this compares favorably with SEC where S_m is 0.1–0.2.

The higher selectivity of FFF results in more precise values of M compared with SEC [115]. However, SEC has a lower plate height, so the question of which technique is superior cannot be answered definitely. Several workers have compared Th-FFF with SEC in a systematic fashion. Early studies [115] focused on the mass-based fractionating power F_m, defined as the smallest relative molecular weight increment ($\Delta M/M$) that can be separated with unit resolution. For low molecular weight polymers, the greater efficiency of SEC leads to a superior fractionating power. In addition, Th-FFF is not applicable below 10^4 g/mol because the ratio of the transport coefficients (D/D_T) becomes too unfavorable for significant retention to occur. However, SEC efficiency deteriorates with M so that, around 10^5 g/mol, the higher selectivity of Th-FFF more than compensates for its lower efficiency. The advantages of Th-FFF over SEC continue to increase with increasing M.

Time requirements have been the subject of more recent comparisons between Th-FFF and SEC [116,117]. The time required to separate two components that differ in molecular mass by ΔM can be expressed as [118]:

$$t_r = \left(\frac{4R_S}{b} \frac{M}{\Delta M} \right)^2 \frac{\overline{H} V_r}{V_0 \langle v \rangle} \tag{31}$$

Here, R_s is the resolution defined in Eq. (17). When the resolution between two components is unity, the components are almost completely resolved. In

FFF, $\overline{H}$ can be precisely related to experimental parameters, allowing a closed form for t_r to be obtained:

$$t_r = \frac{1}{D}\left(\frac{4V_0 w}{3bV_r}\frac{M}{\Delta M}R_S\right)^2 \tag{32}$$

This equation indicates that faster separations are achieved with thinner channels and higher levels of retention. However, V_r is generally limited to under 20–50 times the channel volume in order to avoid undesirable interactions with the accumulation wall. For polymers in the size range of 10^6 g/mol, a 20% difference in molecular mass can be separated with unit resolution in about 6 min, while smaller differences and larger molecular weights require more time. Although channels as thin as 51 μm have been used to increase efficiency, as t_r is proportional to w^2, problems with sample overloading increase [119–121], particularly for polymers with $M>10^6$ g/mol. As more sensitive detectors become available, smaller sample loads become possible and, thereby, overloading problems diminish so that thinner channels may be used with increasing separation efficiency.

An analysis of separation time in SEC on an exact basis is not possible because column efficiency cannot be theoretically derived. Stegemann et al. [116] used empirical efficiency models to compare the time requirements of Th-FFF, SEC and hydrodynamic chromatography, and a critical M value of 10^5 g/mol was obtained above which Th-FFF is superior to SEC.

For Th-FFF, column dispersion is well defined and can therefore be accounted for and removed from the elution profile [122,123]. In removing the effects of column dispersion, the smaller fractionating power of Th-FFF for $M<10^5$ g/mol can be partially compensated. Similar findings were also published by Gunderson and Giddings [115] who found that, after dispersion corrections, Th-FFF shows a better resolution than SEC with the exception of low molar mass samples.

For laboratories that analyze a broad range of polymers on a routine basis, it is important to have a technique that can be tuned to maximize the efficiency of each particular analysis. In FFF the field strength is variable, while in SEC the column must be changed. Although several SEC columns can be purchased for the price of a single FFF channel, the SEC columns must be replaced periodically as a result of degradation of the packing material. Other advantages also make Th-FFF more attractive than SEC for a universally broad application: First, since the FFF channel is open, it has little tendency to clog, even in the presence of particles (including gels) up to 75 or 100 μm diameter, which is the typical range for the channel thickness. Secondly, the absence of a separation gel which can degrade also allows harsh chromatographic conditions. In this respect Th-FFF is particularly promising for high temperature polyolefin analysis. Another important aspect of the comparison is shear sensitivity. For random coil polymers with $M>10^6$ g/mol, SEC starts to become unreliable because shear forces in the packed column can degrade single polymer strands, whereas the FFF flow pattern subject shear-sensitive molecules to less disruptive conditions [124,125].

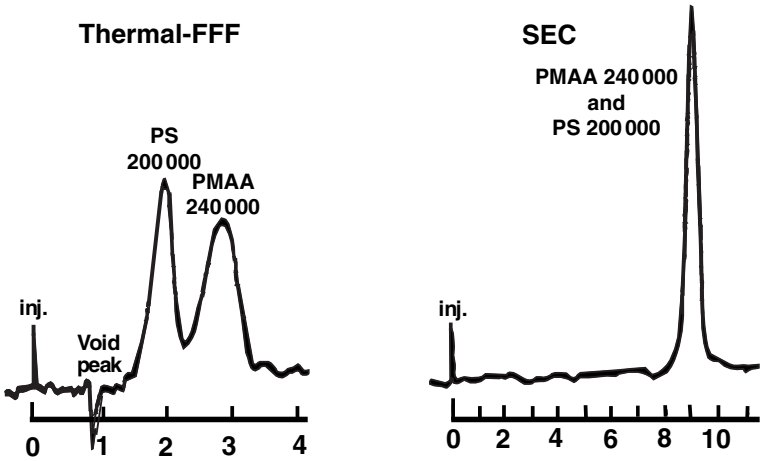

Fig. 10. Elution profiles of similarly sized polystyrene and poly(methyl methacrylate) polymers by Th-FFF and SEC illustrating the chemical selectivity of Th-FFF. Reproduced from [2] with kind permission of Pergamon Press

Th-FFF has been used successfully on many occasions to fractionate polymers with $M>10^6$ g/mol and in one case for $M>10^7$ g/mol [126].

One of the unique characteristics of Th-FFF is that retention depends not only on the molar mass but also on the chemical composition of the polymer. This "chemical" differentiation is due to the dependence of the underlining thermal diffusion process on polymer (and solvent) composition [84]. This effect can likely be used to determine compositional distributions in copolymers and blends [111]. Figure 10 compares the resolving power of Th-FFF and SEC on two polymers of similar molecular weight but varying chemical composition. The polymers coelute in SEC because their sizes are similar; whereas Th-FFF resolves the polymers because they differ in chemical composition.

1.5.2
Comparison of FFF (Th-FFF and Fl-FFF) with Other Analytical Techniques

The theoretical separation capabilities of Th-FFF have also been compared with those of capillary hydrodynamic fractionation (CHDF) [116]. Th-FFF was found theoretically to have the highest separation potential (also compared with SEC) and high selectivity which, however, is not fully accessible due to experimental restrictions. For CHDF, low selectivity but high efficiency as well as a very high analysis speed was predicted for samples with lower M but, experimentally, capillaries with very small tube diameters are not available in sufficient quality. In addition, such capillaries are very sensitive to clogging with minor amounts of impurities, e.g. dust. SEC was found to reach selectivities between Th-FFF and CHDF and had a high separation speed for lower molar masses $M<10^5$ g/mol.

S-FFF has been compared with analytical ultracentrifugation (AUC) with respect to the fractionation of a 10-component latex standard mixture with narrow particle size distribution, known diameters (67–1220 nm) and concentration [127]. With an analytical ultracentrifuge, the particle sizes as well as their quantities could be accurately determined in a single experiment whereas in S-FFF deviations from the ideal retention behavior were found for particles >500 nm resulting in smaller particle size determination in the normal as well as in the programmed operation. It was concluded that, without a modified retention equation which accounts for hydrodynamic lift forces and steric exclusion effects, S-FFF cannot successfully be used for the size characterization of samples in that size range.

Another comparison of AUC and FFF was reported for the Fl-FFF separation of native ferritin which exhibits a particle size distribution (monomer, dimer, trimer) as well as a density distribution due to non-uniform amounts of FeOOH in the core [128]. Such samples are notoriously difficult to characterize by sedimentation techniques like S-FFF and AUC because size and density distributions are superimposed whereas Fl-FFF was found to yield baseline resolved peaks for each of the oligomers due to the separation dependent only on diffusion coefficients.

Several authors [9,129–131] have to a certain extent compared S-FFF with hydrodynamic chromatography HC [129], disk centrifugation [9,129,130] and with some other non-separating methods such as transmission electron microscopy [9,130], light scattering [9], quasi-elastic light scattering [9,131], among others. Approximately 5–50 times higher resolution of S-FFF, in comparison with SEC or HC, was reported. In the majority of cases these authors concluded that the advantages of FFF were more important than the minor drawbacks.

1.6 Experimental Methodology

The setup of an FFF system and the experimental procedure are discussed in the following section.

1.6.1 *General Equipment for FFF*

The basic experimental equipment for FFF is, except for the channel and its support, in general identical to the equipment used for liquid chromatography. It is usually composed of a solvent reservoir, a pump, and an injection system; the chromatographic column is replaced by the FFF channel, followed by a detector. The FFF channel can require additional supporting devices, such as a centrifuge for sedimentation FFF or a power supply, and other electronic regulation devices for electrical FFF. If necessary, this basic equipment is complemented by a flow meter at the end of the separation system. For special semipreparative purposes, a fraction collector can be attached to the system.

In the following subsections, the different components of an FFF system apart from the FFF channel are given. A more detailed description is available elsewhere [27].

Solvent Reservoir. The requirements for the solvent reservoirs are similar to those in liquid chromatography. Regarding the applied solvent, the reservoirs must be manufactured of an inert material and must neither change the solvent properties nor react with the mixed solvent components. Filling and emptying the reservoir must be easy, as must be the solvent exchange and cleaning. It is necessary in some cases to keep the solvent under an inert gas to prevent dissolution of the air components in the solvent. Bubbling through with an inert gas, ultrasonic or vacuum treatment, or a combination of these methods can be used to degas the solvent as well as using a commercially available degasser.

Solvent Delivery System. Solvent delivery systems provide the flow rate of the carrier liquid through the whole separation system. Highly stable liquid flow rates free of pulsations, a broad range of adjustable flow rates, repeatability, and reproducibility of the adjusted flow rate are their most important parameters. A broad range of adjustable flow rates is important. The pumps must be corrosion resistant and inert to the solvents used. The channels for FFF have very low hydrodynamic resistance and, consequently, the solvent delivery systems should not rely on high pressure operation. Furthermore, it is very important that the flow rate is free of pulsation. The stability of the flow rate and, consequently, of the velocity profile inside the separation channel is the most important requirement for the validity of all the theoretical relationships for retention and dispersion and thus for the choice of the solvent delivery system.

Sample Injection. In principle, the samples can be injected in two ways: with a syringe through a septum, or through a multiport valve at the channel inlet. The septum material must be inert to the solvent, but usually cannot withstand more than 30 punctures before replacement is necessary. Furthermore, the septum variant of injection complicates the entire FFF operation and is rarely used anymore. Sample injection by multiport valves does not suffer from these complications.

Elution Volume Measurements. The majority of commercially available pumps provide a high constancy of flow rate and reproducibility of setting. In these cases, measurement of the retention times and knowledge of the flow rate in a given time interval make it possible to calculate the retention volumes and/or retention ratios directly from the retention times (see Eq. 7). Nevertheless, an independent flow rate or retention volume measurement at the end of the separation system is often useful. This applies especially for S-FFF, focusing S-FFF, and Fl-FFF. Small but fluctuating solvent leakage through the rotary passage sealing at the head of the separation system may occur in the first two cases, and the determination of the retention volume from the flow rate may cause serious errors.

Several commercially available devices can be employed at the outlet of the separation system. The use of an optical drop counter is advantageous if aqueous solvents are used as eluents. With respect to usually very low concentrations of separated substances in the eluate, the surface tension and the size of the droplets are usually not affected. A siphon equipped with a photo-optical sensor may also be used to measure the retention volume. If water is used as the eluent, there are problems with the drops adhering to the inner siphon surface.

Detectors. Most detectors for liquid chromatography can also be used in FFF systems. Refractive index detectors [132] are the most popular for soluble macromolecules. Designed as differential detectors, they measure differences in refractive indices of eluate relative to pure eluent, Δn_r. This difference is proportional to the solute concentration in the eluate through the refractive index increment dn_r/dc. The major problem associated with the use of a refractometer is the dependence of the refractive index on temperature and pressure, which can cause baseline drifts and fluctuations.

Photometric detectors focus on the interaction of light with the solute, e.g. absorption of light, fluorescence, optical rotation, or light scattering. A combination of these phenomena (e.g., both absorption and light scattering) may sometimes occur even for simple absorption optics. The notation "photometric detector" describes the fact that light intensity is always measured photometrically after passing through a measuring cell filled with the detected sample.

Absorption photometers operating in the ultraviolet (UV) or visible (VIS) range have gained the widest application. Detectors operating in the infrared (IR) range are also commercially available. The foregoing photometric detectors are designed to operate at one or more fixed wavelengths, or they may be equipped with a source of polychromatic light and a monochromator that makes it possible to vary the wavelength continuously.

Fluorescence detectors measure the intensity of the fluorescence of the eluate, stimulated either by monochromatic light or a laser. As most polymers and colloids do not exhibit fluorescence, applications of this detector have been very limited.

The final group of photometric detectors are instruments that measure the intensity of scattered light either from non-homogeneous dispersions (turbidimetric detectors, nephelometers) or from molecularly homogeneous systems (light scattering photometers). Depending on the ratio of the mean particle size to the wavelength of the scattered light, three basic regions of light scattering are distinguished: the region of Rayleigh scattering, where the particle diameter is substantially less than the wavelength of the applied light (approximately 20-fold); the region of Mie scattering, where the diameters of the scattering particles are roughly comparable with the wavelength of the light and; finally, the geometric region, where the particle diameter is significantly greater than the wavelength of the light. All these three regions of particle sizes are accessible by FFF so that a quantitative determination of a particle size distribution is very difficult at the limits of each domain. For the same reasons, the interpretation of the response of turbidimetric detectors is also not easy to evaluate.

A low-angle laser light scattering (LALLS) detector was developed for use in size exclusion chromatography [133] and has been used coupled with FFF [134]. The advantage of this detector is that it can, in combination with a concentration detector (refractometer, UV/VIS, or IR photometric detector), provide direct data on molar masses of the eluted sample.

In recent years, multiangle laser light scattering (MALLS) detectors have become highly popular in SEC and also in FFF (see, e.g. [135–140]), since they also determine molar masses and molecular dimensions on an absolute basis. Here, the scattered light is simultaneously detected at various angles so that an extrapolation to zero angle is possible. Such instruments are commercially available from several companies. As an important development, the FFF-MALLS combination is discussed in a separate chapter (see Sect. 4.1.2).

An interesting alternative to the use of the conventional laser-light-scattering detector are evaporative light scattering detectors [141], which are also commercially available. The eluent containing particles after FFF separation is sprayed, the solvent is vaporized, and the light scattering of the aerosol is measured.

A viscometric detector together with a concentration detector can provide information on molar masses of macromolecules emerging from the FFF system [76,134,142–144] using the Mark-Houwink-Kuhn-Sakurada coefficients. If these coefficients are not available, an intrinsic viscosity distribution can still be determined without calibration. Detailed features of this distribution are unique to a given polymer sample, and are not affected by changes in experimental conditions [145]. In fact, since the intrinsic viscosity distribution is more directly related to end-use properties, its measurement is preferred in certain applications.

Detectors capable of continuously measuring the density of the flowing liquid have been designed by Kratky et al. [146]. They are based on the measurement of frequency oscillations of a quartz tube through which the eluate flows. The oscillation frequency depends on the tube mass and, thus, for the given eluent, on the concentration and density of the solute. Their application to size exclusion chromatography has been described by Trathnigg and Jorde [147]. Kirkland applied such a detector for FFF [148].

Beckett described inductively coupled plasma mass spectrometry (ICP-MS) as an off-line detector for FFF which could be applied to collected fractions [149]. This detector is so sensitive that even trace elements can be detected making it very useful for the analysis of environmental samples where the particle size distribution can be determined together with the amount of different elements/pollutants, etc. in the various fractions. In case of copolymers, ICP-MS detection coupled to Th-FFF was suggested to yield the ratio of the different monomers as a function of the molar mass. In several works, the ICP-MS detector was coupled on-line to FFF [150,151]. This on-line coupling proved very useful for detecting changes in the chemical composition of mixtures, in the described case of the clay minerals kaolinite and illite as natural suspended colloidal matter.

In a recent paper, electrospray mass spectrometry was applied as a detection system for Fl-FFF [152]. This detector is especially useful for low molar mass

samples as the MALLS detector suffers from poor sensitivity at molar masses below 10^4 g/mol [153]. The method was tested with poly(styrene sulfonate) standards (M_w=1.4×10^3–4.6×10^4 g/mol) and poly(ethylene glycol) standards (M_w= 1.0×10^3–4.0×10^3 g/mol). For the polyelectrolyte samples, the high ionic strengths were a problem as matrix ion clusters and adducts formed a background in the mass spectra. However, this detector is complementary to the MALLS detector and also provides molar mass distributions on an absolute basis together with the diffusion coefficient distribution from the retention behavior. Another advantage is that in cases of mixtures of different polymers, the molecular weight distribution of each individual polymer can be obtained by their mass chromatograms.

Many other on-line detectors suitable for SEC columns as reviewed [154], including chemiluminescent nitrogen detection, dynamic surface tension detection, high frequency detection and Fourier transform infrared detection, can be applied to FFF; the latter being capable of delivering polymer compositions on-line.

There are also many possibilities for the off-line combination of FFF with various detectors, and virtually any analysis technique can be applied to the fractions as long as the sample quantity is sufficient. One useful combination is electron microscopy on fractions collected from an FFF channel [155]. Electrothermal atomic adsorption spectroscopy (EAAS) [156] has also been described.

1.6.2 *The FFF Experiment*

An FFF experiment involves several phases. In most FFF experiments, the carrier liquid flow is started and the cross-field is adjusted. The sample is then injected and a careful procedure of sample introduction and relaxation must be followed [28,97]. This procedure is illustrated in a schematical FFF fractogram (Fig. 11). One can see five basic phases of an FFF experiment. Special care must be taken to determine the time the sample spends in the tubing and connections outside the channel, t_{extra}, as this shifts the void peak as well as the sample peak towards longer retention times.

1.6.2.1 Relaxation

After the sample has entered the channel it relaxes into a steady-state concentration profile at the accumulation wall under the influence of the applied field (step 2 in Fig. 11). The carrier liquid flow is stopped just after the sample injection because otherwise it would experience the full range of flow velocities existing across the channel, in turn causing extensive band broadening. Although the flow can be stopped by simply turning off the pump, the pressure pulse associated with restarting the pump can result in severe baseline distortions. Therefore, it is better to interrupt the channel flow during sample relaxation, routing

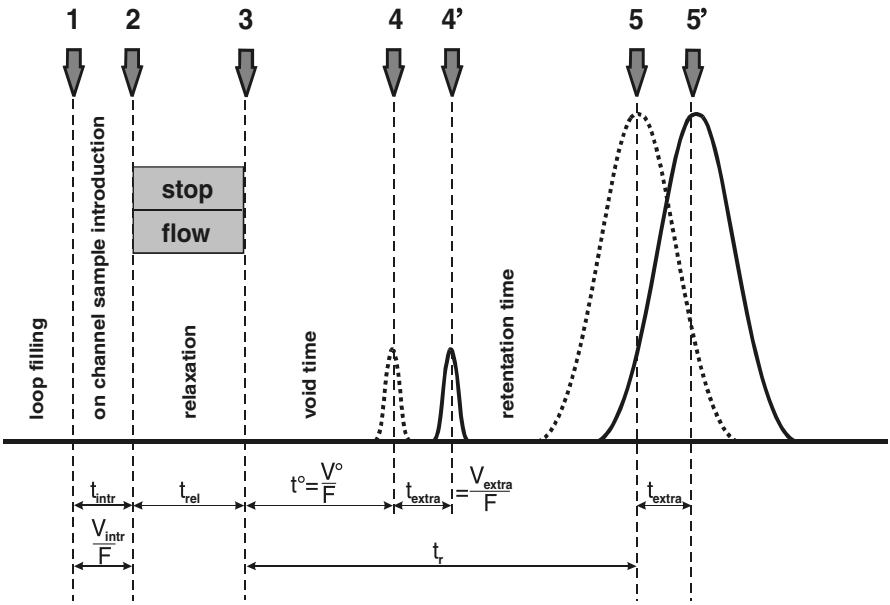

Fig. 11. Schematic FFF fractogram with the different phases of an FFF experiment. Reproduced from [157] with kind permission of Societá Chimica Italiana

flow around the channel with a pair of three-way valves and a pressure matching device.

As an alternative to stopping the flow, the sample can be rapidly compressed against the accumulation wall by flow rather than field-driven transport [48]. After compression, the sample zone quickly relaxes into its steady-state concentration profile without appreciable zone broadening. This method requires a special inlet configuration where either a splitter divides the channel thickness into two flow spaces near a pair of inlets located on opposite walls [158,159], or the carrier substream enters the channel through a frit imbedded in the wall opposite the accumulation wall [160]. The advantages and disadvantages of the two configurations for hydrodynamic relaxation have been summarized [160]. The most important advantage of the frit inlet is the gentle relaxation limiting sample adsorption on the membrane and decreased shear effects, but it requires careful sample introduction. While the flow splitter can be used in any FFF subtechnique, the frit inlet was designed for flow-FFF, where it is easily implemented into the existing design. Figure 12 shows the two methods for hydrodynamic relaxation.

1.6.2.2 Field Programming

If samples to be fractionated are very polydisperse, a high external field strength must be applied in order to separate the least retained macromolecules or par-

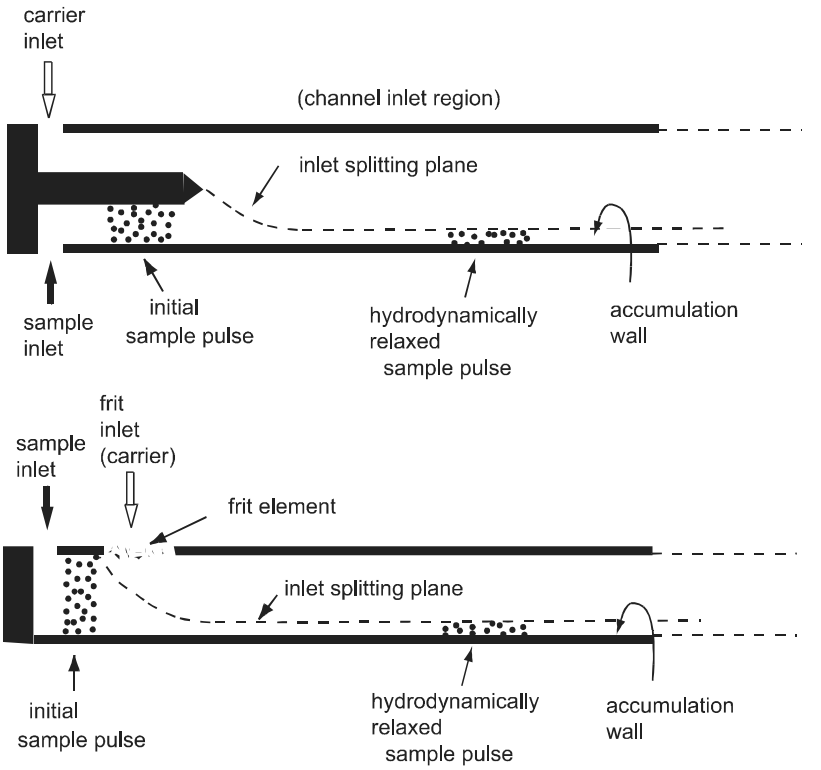

Fig. 12. Schematic illustration of hydrodynamic relaxation achieved in a split inlet system (*above*) and a frit inlet system (*below*). Reproduced from [160] with kind permission of the American Chemical Society

ticles [161]. As a result, well-retained species leave the fractionation channel after an excessively long period. This problem can be solved by gradually decreasing the intensity of the forces affecting the retained solute. In principle, there are two ways possible: decreasing the external field strength, or changing the solute property that is decisive for its retention [162]. For various FFF techniques the means for such variations can be deduced directly from equations for λ. However, other possibilities even exist which are not expressed explicitly by these equations but can be employed effectively.

Yang et al. [38] classify programming into two basic categories: uniform programming and solvent programming. Uniform programming means that some parameters (e.g. external field strength) are being changed equally and simultaneously throughout the channel. Changes in the physical field can be, for example, a change in the temperature gradient for Th-FFF, the speed of rotation or the density of the used carrier liquid for S-FFF, the electric field gradient for El-FFF, the ratio of longitudinal flow to cross-flow for Fl-FFF, the gradient of magnetic field strength for magnetic-FFF, and so on.

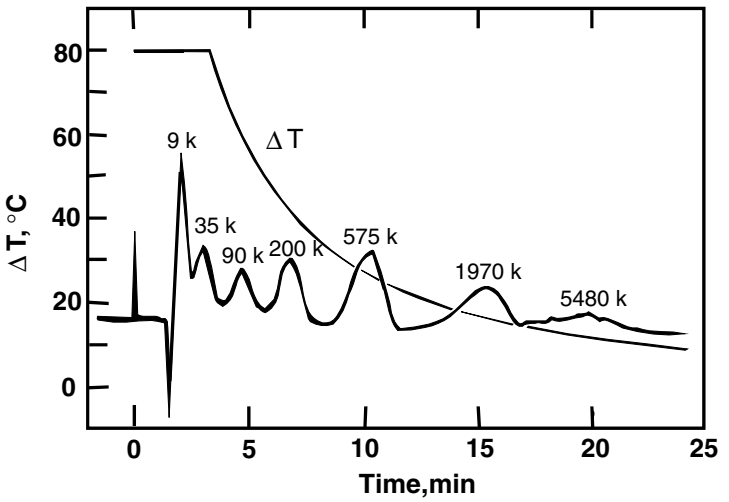

Fig. 13. Separation of seven polymers of indicated molar mass by power-programmed Th-FFF. Reproduced from [54] with kind permission of the American Chemical Society

In solvent programming the change is induced by the inflowing carrier liquid and continues gradually in time and distance from the beginning of the channel (e.g. the change in the carrier liquid density in sedimentation-FFF). The change in solute properties can be influenced by, for example, changing pH and thereby altering the diffusion coefficient and/or electrophoretic mobility in El-FFF.

Programming, however, not only complicates the evaluation of the experimental data [27,38,39] but, furthermore, secondary relaxation phenomena [91], solute-solute and solute-accumulation channel wall interactions occur at high field strength and, thus, high solute concentrations in the vicinity of the accumulation wall must also be considered. Thus whether to use programming or not is always a compromise between the speed versus precision of the measurement. Advantages and disadvantages of such programming procedures have been discussed by Giddings and Caldwell [163]. Experimental results [38,39,164–166] confirmed the utility of the programming in FFF, and good agreement of experimental retention with the theoretical values was found [89,167].

Several mathematical functions have been used for programming field decays in both thermal- [39,54,164,168] and flow-FFF [165]; these include linear [39,165], exponential [164,165,167,168], parabolic [39], and power [54,169] functions. The exponential decay function produces a linear calibration plot of log M versus retention time, that provides convenient and accurate calibrations over a wide molar mass range without the need for frequent recalibration [168]. The effects of operating parameters on the accuracy of the determined molar masses were investigated so that nomographs containing optimum operating conditions could be given on the basis of a preliminary separation [170]. The

power function can be used to maintain a fractionation power that is independent of molecular weight, which is desirable for the characterization of highly polydisperse samples. The power program developed by Williams [169] gives nearly constant fractionating power over the entire separation which is not provided by the other types of programs. Figure 13 illustrates the use of power programming to separate seven polymers ranging in molecular weight from 9.0×10^3 to 5.5×10^6 g/mol.

Kirkland et al. [6,167,171] dealt with the programming of S-FFF in an analysis of particle size distribution. They also used time-delayed exponential decay programming of the centrifugal force intensity, which allowed them to linearize the dependence of retention time to a logarithm of solute dimensions. Moreover, the total analysis time was shortened without sacrificing the resolution.

Flow-rate programming was elaborated theoretically and verified experimentally [40]. Slowing down the channel flow, field programming, and an increase in the field strength applied [172] have provided a higher resolution of particle separation by S-FFF within three orders of magnitude of masses in a single experiment.

1.6.2.3 Optimization of the FFF Experiment

Once an FFF measurement has been completed, it is useful to investigate the same sample under different experimental conditions (such as field strength, etc.). If the same distribution is obtained at markedly different retention times, one can exclude the presence of artifacts. Another approach is to compare the fractionation of a narrowly distributed sample with a sample whose size distribution is broader and that spans the entire size range of the narrower sample under identical fractionation conditions. This technique is described in the literature [173].

It has already been stated that a simple way to enhance the resolution of an FFF measurement is to reduce the channel thickness. This however can lead to other problems as the effects of surface irregularities are enhanced, due to the increase of the surface-to-volume ratio of the channel, and lead to increasing, unpredictable solute–wall interactions, etc. Furthermore, non-uniformities in the channel planarity will also be a problem with very small channel thicknesses, especially in Fl-FFF where the accumulation wall is a membrane. Another possibility for the reduction of $\overline{H}$ is to reduce the flow velocity of the carrier liquid <v> which, in turn, leads to longer retention times and slower separation. However, in Fl-FFF, one has the possibility to increase the flow rate with cost to resolution but simultaneously increase also the cross-flow rate. Nevertheless, this enhances sample absorption onto the membrane. The third possibility for the reduction of $\overline{H}$ is to increase the solute diffusion. This can be done by decreasing the solvent viscosity by increasing the temperature.

Another method for experiment optimization concerns the sample. Here, it is desirable to inject the sample with the lowest detectable concentration, as high

concentrations increase sample–sample interactions or overloading effects (see Sect. 4.2.1). Significant effort has been spent on concentrating the sample past FFF so that it is possible to operate at much lower sample concentrations (see, e.g. the frit outlet system, Sect. 4.3.3). It is also important to choose a suitable carrier liquid to prevent coagulation of particles or phase separation of polymers.

Thus the optimization of an FFF experiment depends greatly on the analytical demands. If a rapid separation is required, one would apply field programming with cost to resolution and precision of the measurement. For very precise measurements, on the other hand, one must consider long experimental times as well as repetitions of the experiment under partly significant differing conditions. Sometimes many problems have to be addressed before a suitable fractionation can be achieved. For a good description of such a method optimization process see [166].

2 FFF Techniques and Modes of Operation

The different FFF techniques all have their special applications and compliment each other in a favorable way. As well as discussing the various FFF methods, the typical application ranges of the most important FFF techniques are given in Table 2.

Table 2. Typical application ranges of various FFF techniques

FFF technique	Typical application range	Modes
S-FFF	Polymers $>10^6$ g/mol, and colloids or particles >30 nm, useful for particular matter and biological applications. Applicable to water and organic solvents. The only technique operating in all modes of FFF	Normal, steric, focusing, adhesion
Gr-FFF	Particles >1 μm. Applicable to water and organic solvents	Steric, adhesion
Th-FFF	Lipophilic synthetic polymers $>10^4$ g/mol. Very useful for large shear sensitive polymers or aggregates. Applicable to water and organic solvents	Normal, steric
Fl-FFF	Polymers, colloids and particles from 1000 g/mol or 1 nm to ≈50 μm. Most universal of all FFF techniques. Applicable to water and organic solvents	Normal, steric
El-FFF	Biopolymers and colloids from 40 nm to >1 μm. Applicable to water	Normal, steric

2.1 Sedimentation-FFF (S-FFF)

S-FFF is one of the oldest FFF techniques (see Fig. 1). It was designed in theory independently by both Giddings [1] and Berg et al. [30–32] and experimentally realized a few years later in the principal arrangement still used today [174]. Either gravitational or centrifugal forces act as the effective field.

The sedimentation force F acting on the solute particles or macromolecules is given by the relationship:

$$F = \frac{\pi d_H^3 G |\Delta\rho|}{6} \tag{33}$$

where G is the gravitational/centrifugal acceleration and $|\Delta\rho|$ the difference in the densities of the particles and the solvent used. Note that the sign of the density difference just determines the direction of movement in the field. A positive value means sedimentation whereas a negative value indicates flotation.

If Eq. (33) is combined with Eq. (6) a relationship is obtained for the retention parameter [174]:

$$\lambda = \frac{6kT}{\pi d_H^3 G w |\Delta\rho|} \tag{34}$$

Thus, colloidal particles can be separated (see Eqs. (33) and (34)) based on differences in m',d_H or $|\Delta\rho|$, with the separation adjustable by the spin rate of the rotor used to control $G=\omega^2 r$ where ω is the angular velocity and r is the distance from the axis of rotation.

Berg and Purcell [30] presented an elementary theoretical analysis of the fractionation of particles by using gravitational or centrifugal forces in the centrifuge. In their first experimental paper [32] they described the fractionation of polystyrene (PS) latex with particle sizes of 0.796 and 1.305 μm. Their experimental arrangement was quite simple, but the time of the analysis was very long (76 to 125 h). In a subsequent paper [31] the separation of R17 *E. coli* bacteriophage with a molar mass of 4×10^6 g/mol was described. The time of the analysis was substantially shorter in this case, approximately 4 to 12 h due to a higher centrifugal field.

Finally, Giddings et al. [174] described an S-FFF device in which the channel was coiled along the internal wall of the centrifuge basket (see Fig. 14A,B and also Fig. 15). The basic theoretical and experimental aspects of S-FFF were discussed and the fractionation of a series of monodisperse spherical polystyrene latexes was demonstrated [174]. The principle of a rotor for S-FFF capable of being applied at low centrifugal fields corresponding to speeds up to 6000 rpm is shown in Fig. 15 [175].

The channel itself, in which separation proceeds, is formed between two stainless steel polished strips that include a stainless steel spacer. The stainless

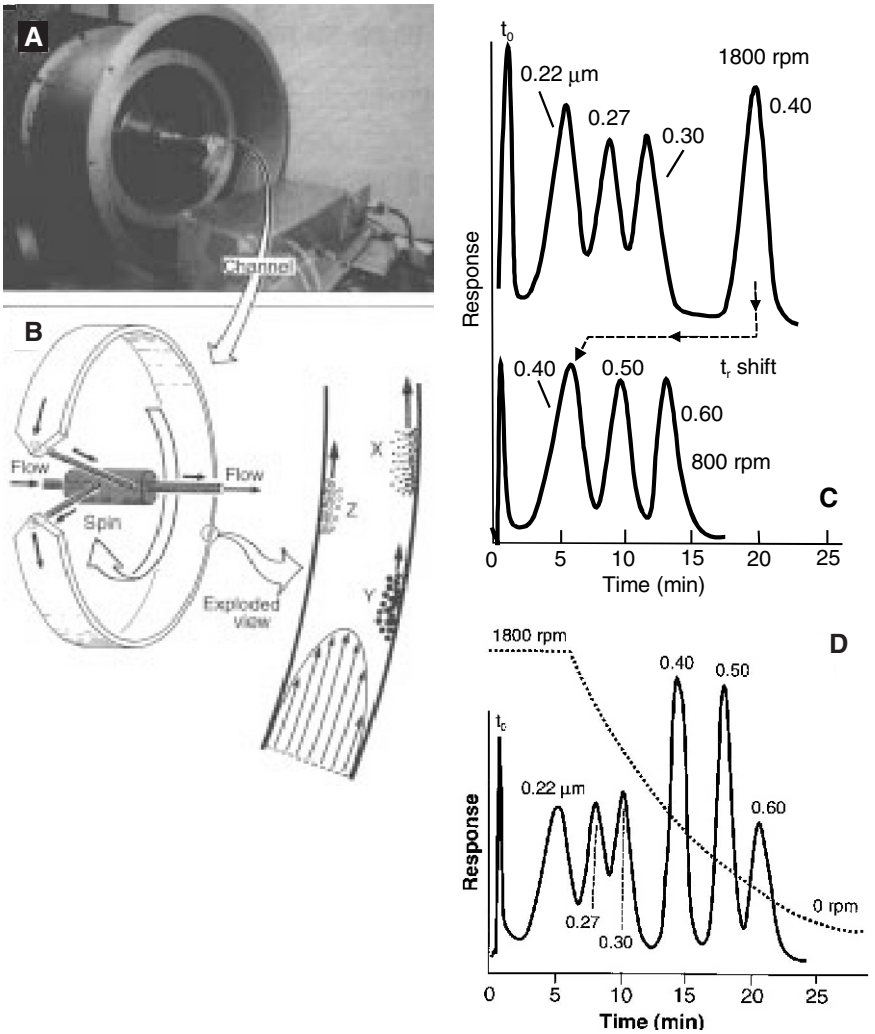

Fig. 14. S-FFF apparatus designed by Giddings' group (**A**) the separation principle with smaller particles (*X)*, bigger particles (*Y*) and floating particles (*Z*) with a density smaller than that of the solute [These particles are equally well separated as retention depends on $|\Delta\rho|$ (**B**)]. **C** Fractogram of a separation of polystyrene latexes of different sizes at two different rotational speeds. The ability to shift retention by changing the rotational speed is demonstrated. **D** The same mixture analyzed by a programmed field run demonstrating that a wider particle size range can be condensed into a reasonable elution span. Reproduced from [14] with kind permission of the American Association for the Advancement of Science

steel strips are coiled into a ring whose outer diameter adjoins closely the inner surface of the rotor basket. The strips are welded together, coiled into a ring and placed properly in the rotor basket. Inlet and outlet tubes are welded to the beginning and the end of this channel. An injection port with a septum is situated

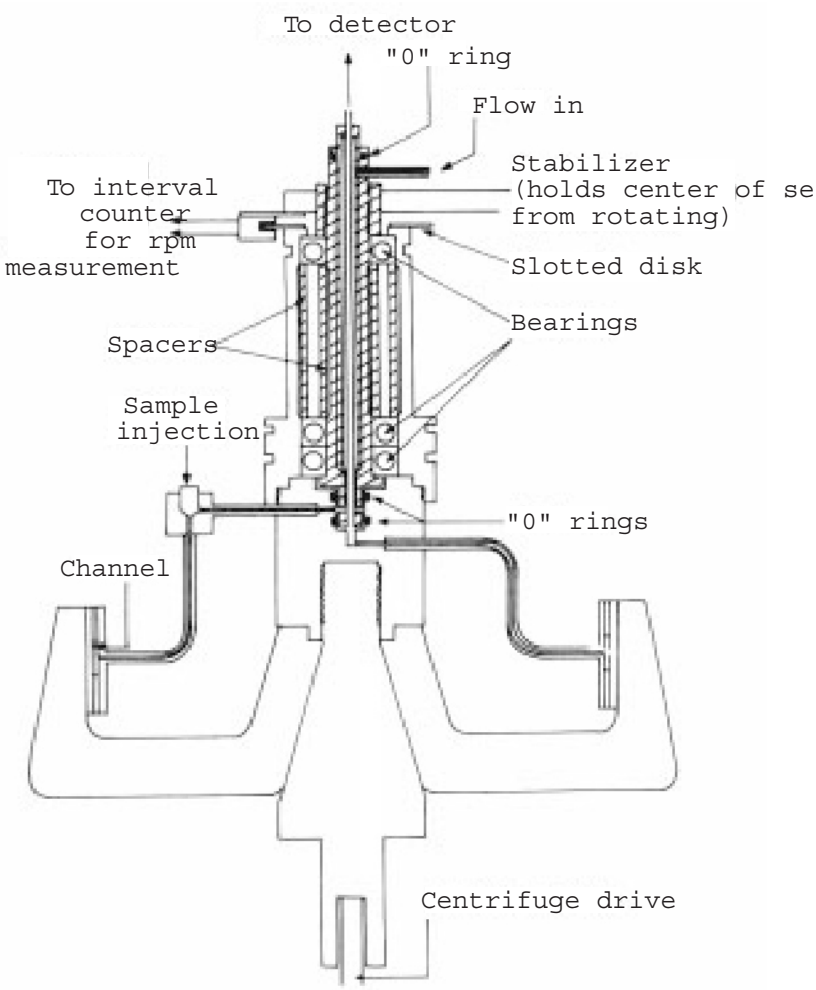

Fig. 15. Schematic representation of a rotor for S-FFF. Reproduced from [175] with permission of John Wiley and Sons

at the inlet tube. Both inlet and outlet tubes must be connected to a rotary passage. Solvent is introduced to the rotor and channeled into the detector by a system of two concentric tubes inside the rotary passage. The rotor is further equipped with an element permitting measurement of the rotation speed. The sealing rings and the whole rotary sealing unit, made of ethylene-propylene rubber, are a critical and troublesome part of the instrument. This rotor design allows injection of the sample only with the rotor at rest. The flow of liquid must then be stopped and the rotor set to the required rotation with the flow stopped

in the course of relaxation. Only then can the pump with an adjusted flow rate be put into operation and the separation performed. Prior to subsequent injection, the rotor must again be stopped. Common dimensions of the S-FFF channel are as follows: thickness, approximately 250 μm; width, about 20 mm; and length, approximately 500 mm. The radius of coiling is usually 80–100 mm.

Improvements in the rotor design by Kirkland et al. [6] using a split ring, which expands during rotation, thereby sealing the channel itself permitted an increase in centrifugal acceleration up to 20,000 rpm. Further improved channels for sedimentation-FFF made it possible to work up to 32,000 rpm which, at the given rotor dimensions, corresponded to an acceleration of about 100,000 gravitational units [176].

The separation of a mixture of different sized PS latex beads at two different spin rates is shown in Fig. 14C. As predicted (Eqs. 33 and 34), t_r increases with both d_H and G. The rough proportionality of t_r to the particle mass and thus to d^3_H explains why particles differing only slightly (down to 5 to 10%) in size can be well separated. In some respects, the size selectivity ($S_d \cong 3$) is too great. A fivefold size difference elutes over a t_r range of ~125-fold, making t_r excessively long for larger particle sizes. The long separation time is unacceptable. This problem can be circumvented by programming the decreasing field strength so that late-eluting particles hasten out of the channel [38] (Fig. 14D). The resolution is most uniform when G is reduced with time according to a special power program [169] but other types of field programming have also been successfully employed (see Sect. 1.6.2.2). When programming is used, Eqs. (11) and (34) are no longer valid as the retention behavior is complicated by the varying field. This is an important difference to analytical ultracentrifugation (AUC) which can also make use of field programming to fractionate particles in the size range of 30 nm to 10 μm in a single experiment (see, e.g. [177,178]). This ultracentrifuge technique is common laboratory practice today and the theory remains the same for the programmed field, in contrast to FFF, as the sedimentation coefficient is calculated on the basis of the run time integral $\int \omega^2 t$ which is continuously monitored by the ultracentrifuge.

Elution in S-FFF requires rotating seals which are troublesome at high spin rates and, therefore, S-FFF is difficult to apply to particles smaller than 10 to 30 nm in size (for usual density differences) and polymers $<10^6$ to 10^7 g/mol, i.e. for most linear polymers. Thus, S-FFF is more attractive for biological applications, large colloids and microparticles, and several applications have been described [179].

For new systems, the particle density ρ_s is often unknown. This uncertainty is resolved by measuring retention at two or more carrier liquid densities ρ [82] in analogy to corresponding procedures in AUC which yield particle size and density distributions [180,181]. Measurements made close to the point of neutral buoyancy yield ρ_s to four digits accuracy which is equivalent to the maximum accuracy of density gradient ultracentrifugation. Carrier densities far removed from neutral buoyancy provide ρ_s by extrapolation. This approach, used for viruses [182,183], can yield ρ_s without exposing fragile particles to highly modified dense media but at the cost of accuracy.

S-FFF can be advantageously used to characterize complex particulate objects. For example, for a superstructure the overall weight is $m'=\sum m'_I$, where m'_I is the effective mass of the component i. Examples for such composed systems include core-shell latexes and filled liposomes [184], where m'= m'(shell)+m'(core). If the carrier density is adjusted to make the core neutrally buoyant, m'(shell) and its distribution can be obtained from retention measurements. However, this is not a simple task, as physically attached solvent also contributes to the shell density. For liposomes, where the shell is a uniform phospholipid bilayer, m'(shell) gives a measure of the shell area A. On the other hand, if the shell is made neutrally buoyant, m'(core) can be measured. This can then be used to measure the loading of a substance like a drug in the liposome or to determine the core volume [184]. Such measurements are otherwise only possible with contrast variation scattering techniques such as neutron scattering using very expensive equipment. Nevertheless, care must be taken with any technique relying on variation of the solvent density as density variation of a solvent always requires the addition of either another solvent or a salt which in turn can lead to extensive conformation changes. The addition of the same solvent in the deuterated form, such as H_2O/D_2O, is feasible for such purposes.

If the change in m' is measured in two different solvents (see the note of caution above), the mass or thickness of adsorbed layers on particles can be determined [185,186]. Before adsorption, only the effective particle mass is determined. After adsorption, the measured gain $\Delta m'$ corresponds to the adsorbed layer. Eqs. (33) and (34) give for $\Delta m'$:

$$\Delta m' = \frac{6kT\Delta t_r}{Gwt_0} \tag{35}$$

The detectable amount of adsorbed species can be extremely low. A retention time shift of $\Delta t_r=0.3\ t_0$ at a modest G (10^3 g) with w=250 μm results in only ~10^{-17} g of adsorbed mass (density 1.4 g/cm^3). This mass corresponds to a very small layer, only ~0.6 Å thick on a 0.2 μm sphere [186]. The above approach has been used to measure protein adsorbed on latex surfaces [186–188], which is relevant to immunodiagnostic assays and biomedical implants. Complete adsorption isotherms can be measured [186] and antigen–antibody binding ratios determined [187].

When the diluted sample of solute is injected during rotation, it is concentrated at the beginning of the channel, due to the fact that the average volume flow rate of the retained solute is lower than the average flow rate of the injected solution. Hence diluted colloidal samples can be concentrated by sedimentation-FFF [189]. One can even operate such that the injection is run at a higher field force and, after the entire sample solution is injected, the field force is decreased to the required value.

The good agreement between theory and experiment in S-FFF was confirmed by experiments with standard samples [81]. Good agreement was also found for the determination of molar masses of different biopolymers [171] and sizes of

poly(vinyl chloride) latex fractions compared with those from electron microscopy [190]. The underlying theory of retention and dispersion in S-FFF was experimentally verified by measurements of polystyrene standard latexes in comparison with electron microscopy [191]. Differences in the sizes could be attributed to shrinkage of the latex in the electron beam of the microscope.

2.2 Gravitational-FFF (Gr-FFF)

Gr-FFF is based on the same principle as S-FFF. However, as the applied field is simply the Earth's gravitational field, it is clear the lower separable particle size is limited depending on the particle density. In fact, particles with sizes lower than 1 μm are usually not well retained so that, in Gr-FFF, particles usually elute only in the steric mode (see Fig. 6).

The channel for Gr-FFF has the simplest design of all FFF methods and is also the cheapest to make (material cost of ca. 20 US$). It can be formed by cutting the required shape of the channel into a cellulose acetate, Teflon or Mylar foil. The channel foil, equipped with inlet and outlet tubes, can be clamped between two plates of glass or Plexiglas with the aid of screws. Such a channel was described by Giddings et al. [175]. Dimensions should be chosen depending on the size of separated particles. The channel is usually 70–250 μm thick, 10–25 mm wide, and up to 2000 mm long. An example of the design of a channel of this type is shown in Fig. 16. The spacer is sandwiched between two mirror-finished

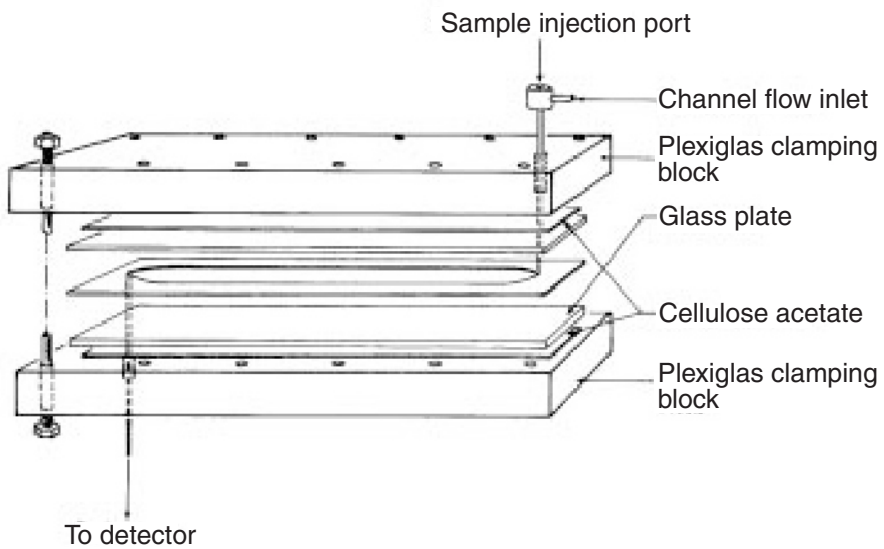

Fig. 16. Schematic representation of a channel for steric-FFF in the natural gravitational field. Reproduced from [175] with permission of John Wiley and Sons

plates made of either floating glass or polycarbonate. The foils between the glass or Plexiglas plates function as cushions that balance the pressure on the edges and in the center of the glass or Plexiglas plates. It is advisable to use rubber washers under the screws to distribute the local pressure and avoid cracking.

Giddings theoretically suggested a gravitational-FFF operating with a cyclical field by rotating the channel frequently 180° around its long axis [192]. This method however never gained importance.

2.3 Thermal-FFF (Th-FFF)

Like S-FFF, Th-FFF is one of the oldest FFF techniques [29,193]. Thompson described a basic experimental arrangement and a successful fractionation of polystyrene (PS) standards with narrow distribution of molar masses [29,193] followed by studies on some fundamental theoretical and experimental aspects of Th-FFF [34,194]. The theory of the retention of macromolecules in Th-FFF was advanced later [195]. The dependence of retention on the molar mass of polystyrene samples was proven experimentally [109,194], since D is a linear function of M of the form $D=A\times M^{-b}$. It was possible to find a linear dependence of λ values on $M^{-0.5}$ [194]. Analogous experimental results, confirming theoretical relationships for retention in Th-FFF, were also reported for other polymers [196,197]. In a critical review of polymer analysis by Th-FFF, Martin and Reynaud [197] specified the requirements for successful separation.

A channel for Th-FFF is relatively simple. It is usually composed of two metallic blocks (with high heat conductivity, preferably copper) with highly polished even surfaces between which a spacer is clamped. The actual dimensions of the metal block are usually 40–60 cm length, 3–6 cm width and a thickness of 2–3 cm. Electrolytic nickel and chromium plating increases the mechanical and corrosion resistance. In both blocks side holes are drilled into which thermistors, which serve for control and regulation of the temperature of both blocks and thus also of the temperature gradient between the two main channel walls, can be inserted.

One or both blocks are equipped with holes to which tubes are soldered for the solvent inlet, including sample injection and eluate outlet. Figure 17 illustrates the case in which inlet and outlet capillaries are placed in the upper heated block. It is, however, more advantageous to situate these capillaries in the lower cooled block for the reason that the lower wall is the accumulation wall of the channel so that the sample, after being injected, is transferred to the vicinity of this wall. In this way equilibration at the head of the channel is facilitated and the time required for primary relaxation is reduced. At the channel end, the solute is concentrated at the accumulation wall, and its exit is easier if the capillary is situated in this block so that the sample does not have to overcome the field strength.

The channel shape is properly cut into a spacer foil of low thermal conductive material which is inserted between the metal blocks. The material of the foil must be resistant to the solvents used within the range of operating tempera-

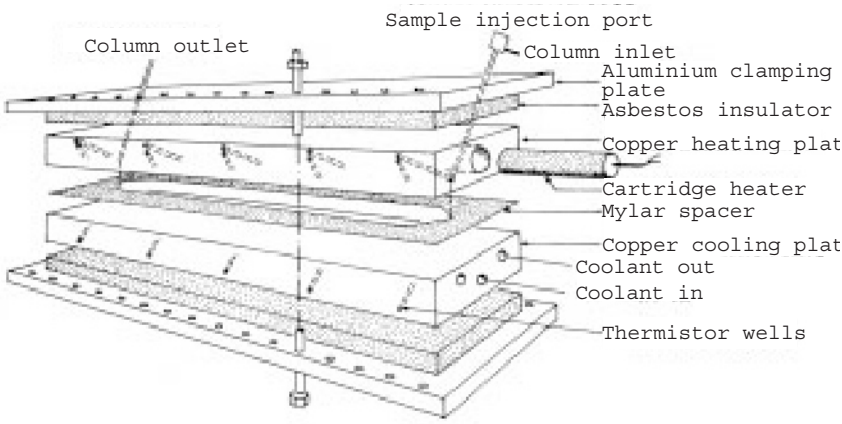

Fig. 17. Schematic representation of a Th-FFF channel. Reproduced from [175] with kind permission of John Wiley and Sons

tures, and the mechanical properties of the material must provide perfect sealing when the entire system is clamped. The channel is cut out of commercially available polymer foils made of engineering plastics (e.g., Mylar, Kevlar) which have proved best for these purposes. Channel shapes can be altered as required. In addition to the shape illustrated in Fig. 17, hairpin-shaped channels [198,199] with a higher channel length have been used. This geometry provides a more effective separation for the rather compact dimensions of the setup, but also restricts the experiment to lower loads.

This system of metal blocks and spacer is then layered between two heat-insulating plates of low-thermal-conductivity material and another two plates with high mechanical rigidity (e.g. of light aluminum alloy). The overall system is fixed with a system of torque-controlled screws, the balanced pressure providing channel sealing.

The applied field is a temperature gradient perpendicular to the solvent flow in a thin (≈100 μm) channel between a hot (upper) and cold (lower) metal block. The upper block is heated with electric cartridges; the lower one is cooled. A regulating transformer or controllable thyristor power supply can be used to feed the heating elements. Common thyristors combined with simple power supply regulators are sufficient to maintain the desired experimental parameters ΔT and T_c. The cold block temperature is kept constant by a circulating liquid with the aid of a thermostat with the same strength as the heating cartridges. This can lead to very high temperature gradients, exceeding 10,000 K/cm, as the temperature differences between the hot and the cold wall are up to 100 K in normal operation and even up to 150 K in extreme cases [200]. A typical Th-FFF channel is shown in Fig. 17.

From the theoretical viewpoint, Th-FFF is the most complicated of the FFF techniques suffering from numerous assumptions and approximations, al-

though the effective driving force $|F|$ per polymer molecule can be defined by a quite simple relationship:

$$|F| = kT\frac{D_T}{D}\frac{dT}{dx} \tag{36}$$

where D_T is the coefficient of thermal diffusion. Combining this equation with Eq. (6) yields a simple dependence of t_r on the molecular weight with $D \cong AM^{-b}$ ($b \approx 0.6$ for random coils):

$$\frac{t_r}{t_0} \cong (D_T / A)\Delta T M^b \tag{37}$$

in which ΔT has replaced $w \times dT/dx$.

However, such treatment neglects the numerous deviations from the assumed ideal behavior so that significant errors can occur. Therefore, possible deviations from ideal behavior, as well as the appropriate corrections, are treated below.

The movement of macromolecules in a temperature gradient is always in the direction from the hot to the cold region [43,197]. This movement is caused by thermal diffusion, exploited as the driving force in Th-FFF, and called the Soret effect, known already for over 50 years [201–203]. The transport (Eq. (1)) has to be extended by a term taking the thermal diffusion into account. Thus the flux density J_x can be expressed by [34,194]:

$$J_x = -D\left[\frac{dc}{dx} + c\left(\frac{\alpha}{T} + \gamma\right)\frac{dT}{dx}\right] \tag{38}$$

where γ is the thermal expansion coefficient and α the thermal diffusion factor $\alpha = (D_T/D)T$. The thermal diffusion factor α can be maximized through solvent adjustment, although a poor understanding of thermal diffusion limits the ability to predict this factor from polymer and solvent parameters. However, certain trends have been established. For example, thermal diffusion appears to increase with polymer density and the thermal conductivity difference of the polymer and carrier liquid [110]. Thermal diffusion also correlates inversely with the solvating power of the carrier liquid.

As already stated in Sect. 1.4.1, the resulting flux vanishes after the steady state has been established so that Eq. (38) can be rearranged:

$$\frac{1}{c}\frac{dc}{dx} = -\left(\frac{\alpha}{T} + \gamma\right)\frac{dT}{dx} \tag{39}$$

The bracketed term can be simplified, since the γ of liquids is usually in the range of $0.2–1.5 \times 10^{-3}$ and negligible compared to the values of α/T which can be up to 1000-fold [34]. The temperature dependence of the remaining terms $-(\alpha/T) \times (dT/dx)$ partially cancel each other out, since α/T decreases with in-

creasing temperature, whereas dT/dx increases [204,205]. The weak influence of temperature has been empirically explored for different conditions [109]. In the case of a weakly retained sample (R=0.5) in ethylbenzene using ΔT=100 K (T_c= 20 °C, with T_c=temperature of the cold wall), 85% of the solute molecules are distributed in temperature regions with ΔT=24.6 K which results in a difference of 17% in the $-(\alpha/T)\times(dT/dx)$ term. In the case of a strongly retained sample (R= 0.1) under the same conditions but with T_c=45 °C, 85% of the solute molecules are distributed in a range <1 K resulting in a difference in the $-(\alpha/T)\times(dT/dx)$ term of only 0.75%. Hence, $(\alpha/T)\times(dT/dx)$ can be considered as temperature independent for strongly retained samples ($R\leq 0.1$).

Equation (39) may be integrated:

$$c(x) = c_0 \exp\left(\frac{-x}{l}\right) \text{ with } \frac{1}{l} = \left(\frac{\alpha}{T} + \gamma\right)\frac{dT}{dx} \tag{40}$$

Applying the definition of the retention parameter λ (see Sect. 1.4.1), one can define the average concentration $\langle c(x)\rangle$ over the channel width as:

$$\langle c(x)\rangle = c_0\lambda(1-\exp(-1/\lambda)) \tag{41}$$

The average drift velocity of molecules in a region in the channel is determined by the magnitude of the temperature gradient at the distance l from the accumulation wall $(dT/dx)_{x=l}$. As l varies very slightly, only some microns even in the case of strong retention, the relevant temperature gradient for the separation is usually determined at the cold wall [206]. In the case of relatively small temperature gradients (ΔT<40 K), (dT/dx) can be approximated by $\Delta T/w$. With the above-discussed neglection of γ and inserting $\alpha=(D_T/D)T$, one obtains for λ:

$$\lambda = \left[\left(\frac{w \cdot D_T}{D}\right)\frac{dT}{dx}\right]^{-1} \approx \frac{D}{D_T \cdot \Delta T} \tag{42}$$

In Th-FFF the field strength is determined by the temperature difference ΔT between the channel walls. According to Eq. (42), the value of λ is a linear function of $1/\Delta T$. This fact was verified experimentally for a wide range of ΔT values for polystyrene samples of various molar masses [109,194]. It also follows from Eq. (42) that if the channel thickness w changes and ΔT remains constant, retention will not change, since the temperature gradient dT/dx will change accordingly. Furthermore, the ratio of D/D_T, the Soret coefficient, is important for the separation in Th-FFF. Janca and Klepárník [199] discussed the interchange of Th-FFF and the Soret effect (thermal diffusion) [207] and the possibility of fractionating polyelectrolytes [208].

Equation (42) shows that Th-FFF can be used to measure thermal diffusion coefficients [209] by plotting, for example, the elution volume vs. 1/D for a set of narrow standards with known D. However, only a few polymer/solvent combinations have been evaluated this way. Recently, Beckett has shown that excellent

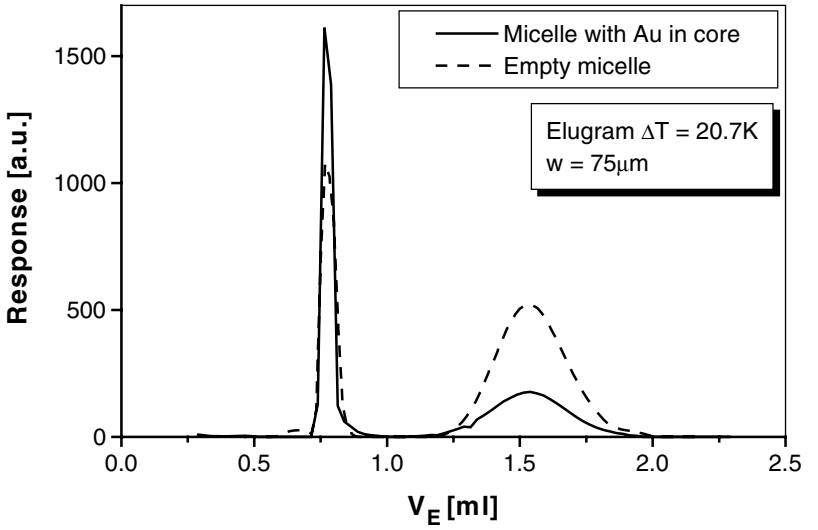

Fig. 18. Th-FFF measurements of polystyrene-poly-4-vinylpyridine (PS_{123}-b-$P4VP_{118}$) micelles in toluene [216]. The core consists of poly(4-vinylpyridine) which can be used as a nanoreactor for Au synthesis to generate a significantly different D_T of the core. However, the detected D_T is that of polystyrene

calibration curves can be obtained using four well-characterized (in terms of M_w) broad standards [210–212].

Experimental evidence was obtained showing that D_T itself may be temperature dependent [109]. Another method to determine D_T is the measurement of thermodiffusion in polymer solutions by "forced Rayleigh" light scattering [213]. This technique has the advantage that the employed temperature gradients are very small so that the coefficients are determined close to thermal equilibrium.

For polymers, D_T is found to be virtually independent of chain length and chain branching, but it is strongly dependent on polymer and solvent composition [84]. For random copolymers, D_T varies linearly with monomer composition; block copolymers display more complex behavior [111,214]. For segregated block copolymers like micelles, D_T seems to be determined by the monomers located in the outer region (see Fig. 18). For particles, D_T appears to be both composition and size dependent [215].

The two factors (D and D_T) controlling polymer retention are strictly orthogonal: D depends only on the size and geometry, whereas D_T depends on chemical composition. Th-FFF has been used mainly to discriminate between chain length differences (reflected in D) within polymer families, yielding molecular weight distributions (MWDs) [15,168]. The promise of compositional differentiation and measurement based on D_T has been little exploited but certainly has future potential as illustrated by the example in Fig. 10.

Complications in the theoretical description of retention in Th-FFF arise from deviation from isoviscous flow due to the temperature gradient resulting in a non-parabolic flow profile [194,217]. An exact analysis of the flow profile of a non-isothermal and thus non-isoviscous flow was published by Westerman-Clark [218]. The consequences of a temperature gradient on the form of the flow profile as well as on retention and peak broadening have been published by Gunderson et. al. [205].

A further source of complications is the assumption of solvent incompressibility, which is a severe simplification for any organic solvent. Using this simplification, Westerman-Clark defined the flow of an incompressible Newtonian fluid between two parallel plates in dependence of the distance from the accumulation wall x as [218]:

$$\frac{d}{dx}\left(\eta\frac{dv(x)}{dx}\right)=-\frac{\Delta p}{L} \tag{43}$$

where $\Delta p/L$ is the pressure drop over the channel length L. This equation can be solved when it is assumed that the flow velocities at both walls are zero ($v(o)=v(w)=0$) resulting in an expression for the flow velocity profile which is much more complicated than the general expression for v(x) in Eq. (9) in Sect. 1.4.1:

$$v(x)=-\frac{\Delta p}{L}\left[\int_0^x\frac{x}{\eta(x)}dx-\frac{\int_0^w\frac{x}{\eta(x)}dx}{\int_0^w\frac{1}{\eta(x)}dx}\int_0^x\frac{1}{\eta(x)}dx\right] \tag{44}$$

Considering the applied high temperature gradients of up to 10000 K/cm, the proper calculation of v(x) very much depends on the proper description of the temperature dependence of the viscosity $\eta(x,T)$. This dependence can be described by a virial expansion of the form:

$$\frac{1}{\eta}=a_0+a_1T+a_2T^2+a_3T^3 \tag{45}$$

The temperature coefficients a_x are solvent-specific thus complicating a universal description of flow properties in a Th-FFF channel.

The temperature gradient across the channel is only in a first approximation a linear function of x, because dT/dx is a function of the thermal conductivity κ which again depends on the temperature:

$$\kappa=\kappa_c+\frac{d\kappa}{dT}\left(T-T_c\right) \tag{46}$$

Equation (45) describes the situation at a defined T and T_c where κ_c is the thermal conductivity at T_c. If $d\kappa/dT$ is taken as constant in the applied ΔT, the

temperature profile across the channel can be described as a complicated function of x [205]:

$$T(x) = T_c + \frac{-1 + \sqrt{1 + \frac{2x}{w}\frac{1}{\kappa_c}\frac{d\kappa}{dT}\Delta T + \frac{x\Delta T^2}{w}\left(\frac{1}{\kappa_c}\frac{d\kappa}{dT}\right)^2}}{\frac{1}{\kappa_c}\frac{d\kappa}{dT}} \tag{47}$$

It is very difficult to determine $\eta(x)$ by substituting Eq. (47) into Eq. (45). Expansion into Taylor series simplifies further calculations and differs by only 0.25% from the exact solution [109]:

$$T(x) = T_c + x\left(\frac{dT}{dx}\right)_c + \frac{x^2}{2!}\left(\frac{d^2T}{dx^2}\right)_c + \frac{x^3}{3!}\left(\frac{d^3T}{dx^3}\right)_c + \ldots\ldots \tag{48}$$

Finally, using Eqs. (44), (45) and (48) yields the flow profile in the channel of Th-FFF:

$$v(x) = -\frac{\Delta p}{L}\sum_{i=1}^{5} h_i \left(\frac{x}{w}\right)^i \tag{49}$$

where h_i is a calculated polynomial coefficient. The average flow velocity $<v(x)>$ is:

$$< v(x) >= -\frac{\Delta p}{L}\sum_{i=1}^{5} h_i \frac{h_i}{(i+1)} \tag{50}$$

Now, the retention ratio R can be calculated using Eqs. (40), (41), (49) and (50) according to the general equation in Sect. 1.4.1, Eq. (7):

$$R = \frac{1}{\sum_{i=1}^{5} h_i \frac{h_i}{(i+1)}}\left\{\frac{1}{\left(1-\exp(-1/\lambda)\right)}\left[\sum_{i=1}^{5} h_i \sum_{j=1}^{i-1}\frac{i!}{(i-j)!}\lambda^j\right] + \sum_{i=1}^{5} i! h_i \lambda^i\right\} \tag{51}$$

For very high retention ($R \rightarrow 0$), the limiting value of Eq. (51) becomes:

$$R = \frac{\lambda}{\sum_{i=1}^{5} \frac{h_i / h_1}{(i+1)}} \tag{52}$$

The retention, which is determined via Eqs. (51) and (52), is larger than the value which would result from the corresponding simplified treatment in Sect. 1.4.1 using a parabolic flow profile which is explained by the reduced flow velocity near the cold wall. Exact velocity profiles in Th-FFF were numerically

computed for several solvents and ΔT-values increasing the accuracy of the retention prediction by two orders of magnitude compared to the parabolic flow profile [219].

Th-FFF can be applied to almost all kinds of synthetic polymers, like polystyrene, polyolefins, polybutadiene, poly(methyl methacrylate), polyisoprene, polysulfone, polycarbonate, nitrocelluloses and even block copolymers [114,194,220]. For some polymers like polyolefins, with a small thermal diffusion coefficient, high temperature Th-FFF has to be applied [221]. Similarly, hydrophilic polymers in water are rarely characterized by Th-FFF, due to the lack of a significant thermal diffusion (exceptions so far: poly(ethylene oxide), poly(vinyl pyrrolidone) and poly(styrene sulfonate)) [222]. Thus Th-FFF has evolved as a technique for separating synthetic polymers in organic solvents [194]. More recently, both aqueous and non-aqueous particle suspensions, along with mixtures of polymers and particles, have been shown to be separable [215].

Th-FFF, like S-FFF, is an FFF technique which takes significant advantage of field programming [164]. As already discussed, field programming is especially advantageous for solutes with a very broad molar mass distribution beginning with high ΔT for small solutes continuously decreasing to low ΔT for the high molecular polymers. Usually, significant separation problems occur for polymers with $M<10^4$ g/mol [200]. These restrictions were partially circumvented by the use of a pressurized system operating at elevated temperatures. This provided an effective fractionation of low molar mass PS [200]. The potential of this technique was shown for the fractionation of polymers with an extremely wide range of molar masses, from 4×10^3 to 7×10^6 g/mol in a single experiment [39]. A big advantage of Th-FFF is that ultrahigh molecular mass polymers can be separated in the absence of shear degradation. Velocity gradients are expected to be an order of magnitude less than those in SEC, and extentional shear is virtually absent. The ability of Th-FFF to maintain the integrity of the polymer has been clearly demonstrated by reinjecting well-retained fractions of a polymer standard having a molecular weight of 20.6×10^6 g/mol [126]. Miniaturization of the channel for Th-FFF and some other design modifications made it possible to reduce the time of analysis to several minutes and even down to several tens of seconds [118], and to increase the resolution [198].

Subsequent studies were oriented towards an explanation of the factors that cause and affect zone spreading in Th-FFF [223] as well as the determination of the precise polydispersity of polymer samples [224] by measuring at various carrier solvent velocities and extrapolating to zero velocity. Improved separation can be obtained by using a thermogravitational effect, that is, by using thermal convection in a non-horizontal channel [43]. The resulting velocity profile formed under such conditions has a more complicated non-parabolic shape [43]. Martin and Hes [134] demonstrated the advantage of coupling the Th-FFF channel with low-angle laser light scattering for the analysis of polymers.

To summarize, Th-FFF is especially well suited for the precise analysis of very high molecular weight macromolecules, macromolecular assemblies or species subject to shear degradation [125], copolymers, polymers prone to surface interaction,

polymers needing corrosive solvents, high-temperature polymer solutions, and narrow polymer samples requiring an accurate determination of polydispersity.

2.4 Flow-FFF (Fl-FFF)

Fl-FFF is the most universally applicable FFF technique as the separation only relies on differences in the diffusion coefficients. Thus, it nicely complements S-FFF or Th-FFF with respect to size distribution analysis [225]. Fl-FFF is capable of separating almost all particles (up to ≈50 μm [226] or even much larger) and colloids and polymers down to ≈2 nm [17] or 10^3 g/mol [227]. The lower limit is determined by the pore size of the membrane material. The need for such membrane covering the accumulation wall is the principle disadvantage of Fl-FFF due to possible interactions with the solute and the danger of a membrane-induced non-uniformity in the channel thickness, especially since thinner channels are highly favored for faster separations. However, the advantages of Fl-FFF usually more than balance the potential pitfalls and sources of error. Consequently, Fl-FFF is the FFF technique which has been developed the most in recent years in instrumentation [48] and has found the most widespread distribution.

Fl-FFF is flexible in channel design and each of the different existing variants has its merits. A secondary cross-flow of the solvent, perpendicular to the flow of the solvent in the channel, creates the external field [41,228–230] while the channel design is flexible. The channel can be set up either by two permeable walls (S-Fl-FFF), only one permeable wall (A-Fl-FFF) [231–233], or in a hollow fiber which may serve as the channel [234]. For S-Fl-FFF, the setup for the channel flow and cross-flow is simple and straightforward [41,228] so that thinner channels can be used leading to a faster separation and a distinct fractionation in the steric hyperlayer mode. A-Fl-FFF on the other hand has the advantage of a simpler construction of the fractionation channel itself and the possibility to focus the sample prior to elution to minimize zone broadening complications. A third Fl-FFF arrangement, of elution though a hollow ultrafiltration fiber, has been demonstrated [234–239] but this technique will not be discussed in detail here as the system properties depend almost exclusively on the characteristics of the hollow fiber and thus any improvement in this system relies on the availability of high quality hollow fibers.

2.4.1 *Symmetrical Flow-FFF (S-Fl-FFF)*

The design of a S-Fl-FFF channel is shown in Fig. 19. Both cross- and longitudinal-flows are provided by separate pumps. To provide the required ratio of cross- and longitudinal-flow rates, the exits of cross- and longitudinal-flows are equipped with metering valves. The metering valve on the longitudinal-flow exit should be placed after the detector in order to prevent higher extra-channel zone broadening.

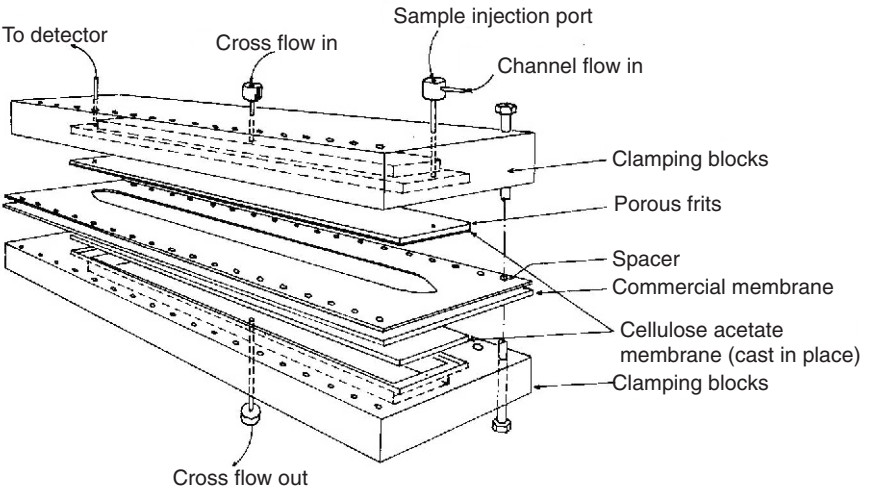

Fig. 19. Schematic presentation of an S-Fl-FFF channel. Reproduced from [175] with kind permission of John Wiley and Sons

Lee and Lightfoot [229] developed the theoretical basis of Fl-FFF. This theory has been confirmed by numerous works on the fractionation of model systems, including monodisperse spherical polystyrene latexes and a number of proteins [41,228,229,240], some polydextrans [229], viruses [241], and other spherical particles and macromolecules [242,243].

The driving force $|F|$ in Fl-FFF is the viscous force exerted on a particle by the cross-flow stream. Application of Stokes law gives for $|F|$ [17]:

$$|F| = fU = 3\pi\eta U d_H \tag{53}$$

where d_H is the hydrodynamic diameter of the particle, η the viscosity of the carrier liquid, and U is the velocity of the cross-flow stream. The quantity U is related to the experimentally accessible flow rate $\dot{V}_c$ of the cross-flow stream by [41]:

$$U = \frac{\dot{V}_c}{bL} \tag{54}$$

where b is the breadth and L the length of the channel. The substitution of Eqs. (53) and (54) into Eq. (6) shows that λ is inversely proportional to d_H:

$$\lambda = \frac{kTbL}{3\pi\eta\dot{V}_c w}\frac{1}{d_H} \tag{55}$$

Flow-FFF provides the best resolution and speed when $\lambda << 1$ which is achieved by a high $\dot{V}_c$ so that validity of Eq. (13) can be assumed under usual Fl-FFF operating conditions [41,244]. When Eq. (55) is substituted into Eq. (13), the retention time t_r is found to be directly proportional to d_H:

$$t_r = \frac{\pi\eta t_0 \dot{V}_c w d_H}{2kTbL} \tag{56}$$

The void time t_0 is by definition equal to the void or channel volume, V_0=bLw, divided by the channel flow rate V, which leads to:

$$t_r = \frac{\pi\eta w^2}{2kT}\frac{\dot{V}_c}{V}d_H \text{ or } \lambda = \frac{2kTV}{\pi\eta\dot{V}_c w^2 d_H} \tag{57}$$

This expression relates the experimental quantity t_r directly to d_H provided that all other parameters are known. Alternate expressions can be obtained relating t_r to the friction coefficient f or to D through use of the Stokes–Einstein equation D=kT/f giving:

$$t_r = \frac{w^2}{6kT}\frac{\dot{V}_c}{V}f \text{ or } \lambda = \frac{6kTbL}{w\dot{V}_c f} \tag{58}$$

and

$$t_r = \frac{w^2}{6D}\frac{\dot{V}_c}{V} \text{ or } \lambda = \frac{6bLD}{w\dot{V}_c} \tag{59}$$

The above equations are applicable when the two flow rates are held constant throughout the run. In some cases it is desirable to program $\dot{V}_c$ in order to expand the range of applicability [165,233]. This programmed field technique, however, complicates the above derived equations and results obtained in a way that is beyond the scope of this review; the interested reader is referred to the original literature here.

The first part of Eq. (11), respectively Eq. (13), yields that the product $t_r R$ is proportional to t_0. Using this and employing Eq. (56) to get t_r, the resolution expression is obtained:

$$R_s = \frac{\pi}{8}\left(\frac{3}{2}\frac{\dot{V}_c^3}{V}\right)^{1/2}\frac{\eta w^2}{kTV_0}\Delta d_H \tag{60}$$

where Δd_H is the difference in hydrodynamic diameters between the two species being fractionated. Equation (60) shows that the resolution R_s can be enhanced by increasing the cross-flow rate $\dot{V}_c$ or decreasing the channel flow rate V. As $\dot{V}_c$ affects R_s to the 3/2 power, it is, like the decrease in w, a major parameter for the optimization of R_s. However, the resulting gain in resolution is in turn achieved by longer run times. This is confirmed by Eq. (57) which shows that t_r has a similar dependence on $\dot{V}_c$ and V as R_s does.

Several modifications to the Fl-FFF method have been developed to enhance operation. Shortly after the introduction of Fl-FFF, the effect of relaxation on the retention and resolution was studied [245]. A substantial improvement in the

fractionation of viruses was achieved using the stop-flow technique [245]. A further improvement was the introduction of the outlet stream splitter which enables the sample stream near the accumulation wall to be led to the detector and thus enhance the concentration of the detected material for a better detector response [165,246]. This outlet stream splitter can, in principle, be applied to the other FFF techniques as well. Frit inlet Fl-FFF [52] allows the system to reach the steady-state more quickly thus eliminating the necessity for the stop-flow step [49]. This is achieved by utilizing a very high cross-flow in the first centimeter as the sample enters the channel to force the sample close to the accumulation wall. Furthermore, if a frit is applied as a channel outlet (frit outlet Fl-FFF) eluted samples can be concentrated by approximately five times which is a clear advantage if detector sensitivity is a problem. An extremely useful combination for a number of analyses has been frit outlet Fl-FFF and MALLS.

If the channel for Fl-FFF is utilized such that cross-flow is due to a solvent of different composition that has the solvent flowing in an axial direction, continuous separation of high-molar-mass components from low-molar-mass contaminants, migrating through the accumulation membrane, can be achieved. The ratio of cross-flow rate to axial-flow rate must be suitably adjusted. The function of a continuous Fl-FFF channel as a dialysis or ultrafiltration cell was described theoretically and demonstrated in practice for the separation of bovine serum albumin from low-molar-mass methylene blue [247].

2.4.2
Asymmetrical Flow-FFF (A-Fl-FFF)

Asymmetrical flow-FFFA (A-Fl-FFF) was introduced by Wahlund and Giddings in 1987 [47]. The same system was independently suggested slightly earlier by Granger et al. [237,248], but their application of the technique suffered from a lack of a primary relaxation step preceding separation [47]. A-Fl-FFF is notable for a channel which has only one permeable wall so that the solvent can leave the channel only via the accumulation wall and thus generates a cross-flow. The permeable wall is usually a sintered metal plate or ceramic frit covered by an ultrafiltration membrane (see Fig. 20).

The channels are initially of the same rectangular geometry as the symmetrical variant and the breadth remains constant along the channel length. The continuous loss of carrier fluid through the membrane as it flows down the channel leads to a gradual fall in volumetric flow rate between the inlet and outlet leading to a gradient in the mean channel flow velocity in channels with constant breadth. This variation of flow velocity must be taken into account in the determination of sample component properties from observed elution times, but poses no great difficulty. There is also an unavoidable gradient in the cross-flow velocity across the channel thickness, but this gradient is negligible for strongly retained material [47]. To compensate for these undesired effects, a trapezoidal channel [249] was introduced, and is almost exclusively applied now. In a recent paper, Williams proposed a theoretical channel which exponentially decreases

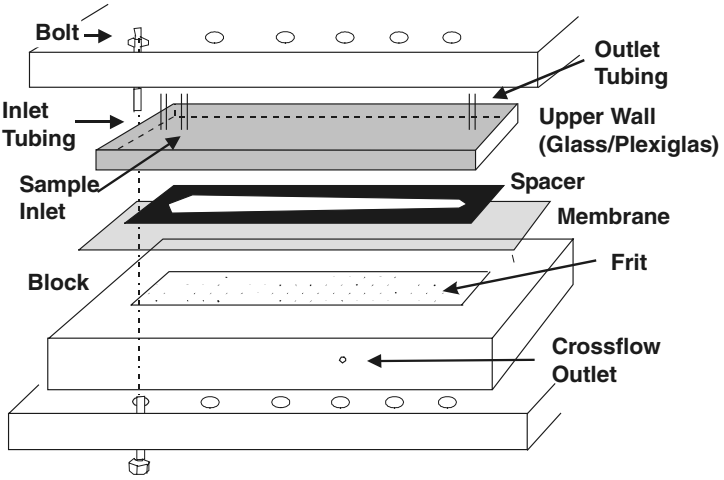

Fig. 20. Schematical presentation of an A-Fl-FFF channel

in breath along its length so that a constant flow velocity can be achieved throughout the channel length under certain flow conditions [250].

Due to the differences in the cross-flow generation compared with S-Fl-FFF, and the possibility of sample focusing, the experimental methodology differs from that applied for most other FFF techniques (stop-flow for sample relaxation). Thus, a short description of an A-Fl-FFF experiment as well as the whole experimental setup is necessary to understand its merits.

The A-Fl-FFF experiment is based on three different phases: (1) relaxation/focusing; (2) elution, and (3) backflushing. During the first phase, the flow is directed to enter the channel from the inlet and the outlet only exiting through the membrane. At a certain position in the channel determined by the counteracting flows, termed the focusing point, the axial velocity will be zero. The focusing point is made visible by a colored substance, e.g. bromophenol blue, which is injected into the channel during the relaxation/focusing mode. A sample, which is injected during this phase, is focused at this point, the exponential profile of the concentration distribution being established. Some samples can show altered retention behavior at different focusing times due to a pronounced interaction tendency with either themselves or with the ultrafiltration membrane [251,252]. After determination of the focusing point, the channel thickness needs to be calibrated using a protein with a well-known diffusion coefficient [253].

The next phase is the elution phase, where the flow enters the channel from the inlet end and exits, both through the membrane (cross-flow) and through the channel outlet end (outlet flow). The balance between the cross-flow rate $\dot{V}_c$ and the outlet flowrate $\dot{V}_{out}$ according to Eq. (69) can be adjusted by needle valves. V_{out} is measured by a flowmeter, the value of $\dot{V}_c$ is either measured directly by a

second flowmeter or simply calculated from the known V_{in} and V_{out} according to $\dot{V}_c = \dot{V}_{in} - \dot{V}_{out}$. Accurate knowledge of $\dot{V}_{out}$ is necessary. The elution phase is followed then by the third phase, backflushing, the flow entering the channel from the outlet end and flushing retained materials out of the channel [253].

A specific advantage of the asymmetrical channel design in A-Fl-FFF is the possibility to focus the sample into a very sharp band prior to separation resulting in higher separation resolution and improved accuracy of particle size measurements. Further advantages are that the construction of A-Fl-FFF channels is technically simple compared with S-Fl-FFF; the effects of heterogeneity and uneven permeability of the upper frit and unevenness of its surface are eliminated; and the glass/PMMA wall allows visual observation of the migration of suitable samples. The ability to observe the flow pattern of an injected dye aids in troubleshooting non-uniform flows that can occur with membranes that become uneven with deterioration or poor installation. Later, it was pointed out [249] that A-Fl-FFF channels also have an advantage in terms of reduced dilution of sample components during elution. Early studies indicate greater efficiency of the A-Fl-FFF channels compared to S-Fl-FFF [231,232], possibly because of irregular cross-flow in early S-Fl-FFF channels associated with an non-homogeneous upper frit. However, with good frits now available for S-Fl-FFF, there is no difference between these two geometries concerning the regularity of the cross-flow.

Drawbacks of the asymmetrical design associated with the non-uniform flow velocities are being reduced with innovative channel designs and continued theoretical development [249]. Due to the different generation of the cross-flow, the theoretical description of the flows acting in A-Fl-FFF and thus the whole retention theory is more difficult. Instead of the simple Eq. (54) for S-Fl-FFF, the following relationship is obtained for the cross-flow velocity U in the x-direction:

$$U = -|u_0|\left(1 - \frac{3x^2}{w^2} + \frac{2x^3}{w^3}\right) \tag{61}$$

where $|u_0|$ is the cross-flow velocity at the accumulation wall. Assuming a constant cross-flow, the average flow velocity in the z-direction $\langle v \rangle$ can be expressed by:

$$\langle v \rangle = \langle v \rangle_0 - \frac{|u_0|}{w} z \tag{62}$$

where $\langle v \rangle_0$ is the flow velocity at the channel inlet.

In a trapezoidal channel, the expression is more complicated.

$$\langle v \rangle = \frac{\dot{V}_{in} - |u_0| A(z)}{w b(z)} \tag{63}$$

where A(z) is the area of the accumulation wall from the inlet up to z and b(z) the width of the channel at z:

$$b(z) = b_0 - \frac{z(b_0 - b_L)}{L} \tag{64}$$

where b_0 and b_L are the channel widths at 0 and L. A(z) is given by:

$$A(z) = \int_0^z b(z)d(z) = b_0 z - \frac{z^2\left(b_0 - b_L\right)}{2L} \tag{65}$$

Combining Eqs. (63) and (65), the average flow velocity can be calculated by:

$$< v >= \frac{\dot{V}_{in} - |u_0|\left(b_0 z - \frac{z^2\left(b_0 - b_L\right)}{2L}\right)}{w\left(b_0 - \left(b_0 - b_L\right)\frac{z}{L}\right)} \tag{66}$$

The concentration profile in the x-direction c(x) can be obtained by combining Eqs. (1) and (61) and integration (see Eq. 2):

$$c(x) = c_0 \exp\left(\frac{-|u_0|x}{D}\left[1 - \frac{x^2}{w^2} + \frac{x^3}{2w^3}\right]\right) \tag{67}$$

To calculate the retention ratio R, one needs to know the void time t_0 (See Eq. (7)) which for an asymmetrical channel is given by [249]:

$$t_0 = \frac{V_0}{\dot{V}_c} \ln\left(1 + \frac{\dot{V}_c}{\dot{V}_{Out}}\left[1 - \frac{w\left(b_0 z' - \frac{b_0 - b_L}{2L} z'^2 - y\right)}{V}\right]\right) \tag{68}$$

where z' is the distance from the inlet to the focusing point, $\dot{V}_c$ and $\dot{V}_{out}$ the cross-flow, respectively, outlet flow rate, V_0 is the void volume and y the area excluded by the tapered inlet end. Using Eq. (65), Eq. (68) simplifies to:

$$t_0 = \frac{V_0}{\dot{V}_c} \ln\left(1 + \frac{\dot{V}_c}{\dot{V}_{Out}}\left[1 - \frac{A(z') - y}{A_{tot}}\right]\right) \tag{69}$$

where A(z') is the area from the inlet to the focusing point and A_{tot} is the area of the accumulation wall. For asymmetrical channels, the retention parameter λ is given by:

$$\lambda = \frac{DV_0}{\dot{V}_c w^2} \tag{70}$$

λ can be related to R by the simple approximation R=6λ (see also Sect. 1.4.1). The error is usually ≤5% for λ for sufficiently high retention (t_r/t_0)≥5.3 [47,254]. In the latter reference, a more detailed consideration of the relative errors caused by the approximation R=6λ is given for different levels of retention.

If R=6λ is assumed, Eq. (70) can be expressed as:

$$t_r = \frac{t_0 \dot{V}_c w^2}{6DV_0} \tag{71}$$

which shows that the diffusion coefficient can be determined directly and in an absolute fashion by measurement of t_r in A-Fl-FFF. Combining Eq. (70) with the Stokes–Einstein relationship and assuming R=6λ gives the relation of t_r to the hydrodynamic diameter d_H:

$$d_H = \frac{2kTV_0}{\pi\eta \dot{V}_c w^2 t_0} t_r \tag{72}$$

2.5 Electrical-FFF (El-FFF)

Electrical field-flow fractionation belongs to the most sophisticated experimental techniques of FFF although the schematical setup looks quite simple (see Fig. 21). However, the electrical fields are difficult to implement in practice and extensive problems, discussed below, can occur. Therefore, relatively few papers on El-FFF exist even though the first publication appeared as early as 1972 [35], and the high intensity and manipulability (such as through pH changes) of electrical forces principally promise a high potential of El-FFF [35,255].

The experimental setup is shown in Fig. 21. Two PMMA blocks with chambers that enable buffer solution to flow through are the main parts of the channel. The channel walls consisting of semipermeable flexible membranes of wet regenerated cellulose permit the passage of small ions and separate the channel volume from the electrode compartments in the blocks [175]. This layered setup is necessary because the applied high voltages needed to achieve highly selective separations even of small proteins and nucleic acids lead to the electrolysis of solutes and solvent. Placing the electrodes outside the channel ensures the generated gas bubbles do not perturb the desired flow profile The two membranes

are separated by the spacer foil, into which the channel is cut. Channel dimensions, as well as solvent transport, is similar to Fl-FFF. The entire channel is clamped together by a system of screws. Circulation of the buffer electrolyte prevents an accumulation of electrolysis products in both chambers. A channel designed in this manner has a very low electrical resistance but is very sensitive to even slight fluctuations of the flow inside, resulting in deflection of membranes leading to deformation of the channel shape and volume changes. A channel with walls composed of membranes of cellulose acetate cast on the surface of plastic frits is more mechanically resistant [256] but suffers from increased electrical resistance.

Recently, an improved channel design has been described, which makes use of solid electrodes as channel walls instead of the former applied membrane system [257–259]. The applied voltages are also much lower and beneath the electrolysis limit (ca. 1–2 V across the channel). Although such a setup was expected to generate fields of sufficient strength to separate colloidal particles, the inevitable electrode polarization limits the working field in the channel to a small fraction of the nominal field. The exact magnitude of the field responsible for retention in El-FFF must therefore be determined by calibration.

A third channel design has been reported [37,229,260–262] where the channel is composed of a circular semipermeable tube, and the electrical field is applied perpendicularly to the central axis of the channel. As with the corresponding circular Fl-FFF channel, such a system relies on the availability of suitable hollow fiber material.

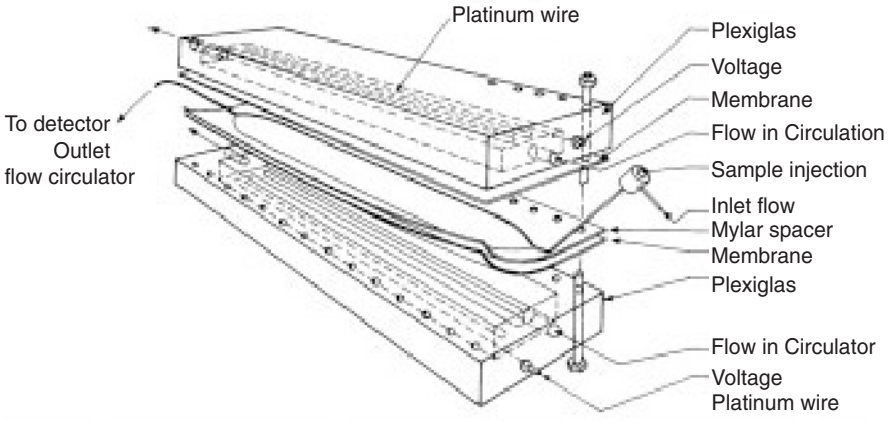

Fig. 21. Schematic representation of an El-FFF System. Reproduced from [175] with kind permission of John Wiley and Sons

El-FFF uses an electrical field E across the channel as the driving force for the particle separation. As the drift velocity U of a macromolecule with electrophoretic mobility μ_e is defined by:

$$U=\mu_e E \tag{73}$$

the force F acting on the sample according to Eq. (4) is $F=f\mu_e E$, finally leading to the expression for λ [36]:

$$\lambda = \frac{D}{\mu_e E w} \tag{74}$$

Kesner et al. [36] indicated a discrepancy between the theoretical retention and experimental values for some proteins in a channel with flexible membrane walls. These deviations were probably caused by the flexible membrane walls as such effects were not observed for a channel with rigid walls [256]. Nevertheless, the experimental data of Kesner et al. [36] was in reasonable agreement with the El-FFF theory [87,263] with respect to both retention and dispersion. Deviations were attributed to an electrical field gradient in the vicinity of the membrane interface [263]. Calculation of the dependence of λ on 1/E from literature data on electrophoretic mobilities and diffusion coefficients confirmed the validity of the retention theory in El-FFF.

For particles, the electrophoretic mobility μ_e is related to their surface charge density, which is best expressed in terms of the ζ-potential. For moderately charged particles (ζ-potential $<\pm 25$ mV), this relationship is given by Eq. (75), where the function $f(\kappa_D d_H)$ varies smoothly between 1.0 and 1.5 as κ_D varies between very small and very large values [264]:

$$\mu_e=\zeta(2\varepsilon/3\eta)f(\kappa_D d_H) \tag{75}$$

Here, κ_D is the inverse of the Debye length. Even though the ζ-potentials for latex spheres may exceed ± 25 mV and, therefore, require a more complex equation to relate to mobility (as per O'Brien and White [265]), the low ionic strength (small κ_D) of El-FFF measurements should still ensure a proportionality between μ_e and ζ. From the retention data, it is possible to obtain quantitative information regarding either the ζ-potential of samples with known particle size eluting from the channel or the particle size, if the electrophoretic mobility is known.

Despite the potential advantages that El-FFF offers, there are a number of serious drawbacks and limitations which restrict its use. First, the processes involved in the separation are much more complex than is assumed in the theory of El-FFF as pointed out by studies of the influence of experimental parameters on the retention of proteins [260,266–268], underlining the importance of solvent parameters and solute–solute interactions.

In two papers, Palkar and Schure studied the mechanism of electrical field-flow fractionation in detail [269,270]. An electrical circuit of the channel was

presented, discussing potential problems including voltage drops in the channel as well as their sources and suggesting an explanation as to why the electrical field in the channel differs from the calculated field. It was pointed out that it is of crucial importance to understand the internal electrical field in El-FFF which depends on the electrode material and electrode geometry, as well as the carrier liquid composition and even flow rate. In the second paper, the effect of the sample conductivity on the retention was studied, which results in a very strong concentration dependence of the retention, even at very low solute concentrations. Due to the conductivity differences between the sample and the carrier liquid, the electrical field in the channel is locally dependent. All these problems are true also for the newer El-FFF channel designs [257–259] such that El-FFF still has definite limitations.

2.6 Other Experimentally Tested FFF Techniques

The FFF techniques described in this section are already more or less specialities developed or suitable only for a limited amount of samples. Some of them have only been used a few times and are yet only poorly understood. However, they are presented here because they may be the technique of choice for special applications.

2.6.1 *Magnetic-FFF*

Magnetic-FFF is the obvious choice for ferromagnetic particles. In addition, it was theoretically proposed that various dia- and paramagnetic biological samples could also be separated by magnetic-FFF though requiring long separation times [271,272].

In magnetic-FFF, a magnetic field supplies the force for the separation of the sample:

$$F = \frac{M\chi_m H_m dH_m}{dx} \tag{76}$$

where χ_m is the molar magnetic susceptibility, H_m the intensity of the magnetic field, and ΔH_m the gradient of the intensity of the magnetic field dH_m/dx. If Eqs. (76) and (6) are combined, one obtains for λ:

$$\lambda = \frac{RT}{Mw\chi_m H_m \Delta H_m} \tag{77}$$

One possible magnetic-FFF channel arrangement is the classical FFF setup of a channel clamped between two glass plates [273]. The channel is then placed in the center of an electromagnet with a maximal magnetic field of approx. 300 to

450 G. The second arrangement was described by Vickrey and Garcia-Ramirez [45] who used a Teflon capillary of 1.5 mm diameter and 3040 mm length for separation. The capillary was coiled (coil diameter 5.6 cm) around an electromagnet (400 G).

Magnetic-FFF has been studied in only a few works [45,273,274] dealing with the separation and retention of BSA in the presence of Ni(II) ions and retention of metal oxides. The comparison of experimental retentions with the theoretical model indicated [45] that in addition to the effect of the magnetic field on the macromolecules, other yet unknown parameters seem to be present. Furthermore, the investigation of metal oxide particles in magnetic-FFF indicated that the slow velocity of relaxation processes probably influences the quality of the separation [273]. Even the surface nature of particles plays a role in retention [274]. In summary, magnetic-FFF remains an immature technique.

2.6.2 *Dielectrophoresis-FFF (DEP-FFF)*

Separation is not only obtained by a homogeneous electrical field (as applied in El-FFF) but the field can also be of an nonhomogeneous nature, leading to dielectrophoresis (DEP). Dielectrophoresis is the movement of particles in non-uniform electrical fields [275,276]. Here, the separation force F_{dep} is the result of the interaction between the dipole induced in the particle by the field and the field gradient over the particle. DEP is observed for charged and uncharged particles as well as in AC or DC electrical fields. The magnitude of the DEP force F_{dep} is described by:

$$F_{dep} = 0.25\pi\varepsilon_0\varepsilon_m d_H^3 \left(\frac{\sigma_p^* - \sigma_m^*}{\sigma_p^* + 2\sigma_m^*} \right) \nabla E^2(\text{rms}) \tag{78}$$

in which ε_0 is the permittivity of free space (8.854×10^{-12} F m^{-1}), ε_m the relative permittivity of the suspending medium, d_H the (hydrodynamic) diameter of the particle, σ^*_p and σ^*_m the complex conductivity of the particle and the medium, and ∇E the field gradient.

The combination of dielectrophoresis with field-flow fractionation (DEP-FFF) is potentially a very gentle and selective method for the separation of cells and other large particles. A large number of different designs of DEP channels has been used and proposed for the separation of particles [104,275,276]. However, the most successful designs [276–281] employ the typical FFF channel geometry containing large arrays of microelectrodes so that relatively small voltages can be used to generate the high field gradients needed to induce DEP. Microelectrodes not only simplify the equipment needed to generate the electrical fields, but also reduce secondary effects such as heating.

The solute particles are held at the accumulation wall by a DEP force which depends on the dielectric properties of the particles and the surrounding medium, the frequency and magnitude of the electrical field, and the electrode geometry. DEP-FFF is an unconventional FFF technique in that the DEP force is inherently non-uniformly distributed over the channel, not only in the plane of the electrodes/channel wall, but also across the channel above the electrodes [282]. Since solute particles themselves are a source of local field non-uniformities, mutual attraction occurs due to DEP forces between the particles which in extreme cases can lead to what is called pearl-chain formation. As a consequence, DEP-FFF can be considerably disturbed by interparticular interactions [57].

Most dielectrophoretic separations of cells to date have used steric-DEP-FFF. The cells are usually effectively immobilized in potential energy minima [282] near the electrodes by a combination of gravity and electrical field forces. Afterwards, the applied hydrodynamic flow forces transport those particles that are held less strongly at the electrodes.

Hyperlayer-DEP-FFF has the advantage of making better use of the parabolic velocity profile of the fluid since flow at different heights in the channel is exploited; as in steric-DEP-FFF the particles essentially stay in the layer near the channel wall. In addition, the hyperlayer mode minimizes the adhesion of the particles to the channel wall, which also suppresses the aggregation of cells into pearl-chains.

2.6.3 *Pressure-FFF*

Pressure-FFF is similar to Fl-FFF. In fact, some of the channel designs described for Fl-FFF can also be used for pressure-FFF. The difference between the two techniques is that in Fl-FFF, the flow field is applied externally, whereas in pressure-FFF the lateral flow across the channel wall(s) is initiated by an internal pressure drop in a liquid pumped along the channel with semipermeable walls on two sides of a hollow fiber membrane. Pressure-FFF has the advantage of increased solute concentration relative to Fl-FFF because of solvent leakage through the semipermeable walls during elution. In the case of the S-Fl-FFF channel, the cross-flow through both walls is oriented outwards from the channel and the membranes are sufficiently fixed on a porous, mechanically rigid support by the pressure so that the channel dimensions are well defined. Adjustment of the ratio of the transverse and longitudinal flows is also simplified analogous to A-Fl-FFF. The combination of a single pump and a metering valve on the cross-flow exit is already sufficient to operate a S-Fl-FFF channel for pressure-FFF. The arrangement of pressure-FFF with a hollow fiber serving as membrane is also straightforward [37]. To the exit of the circular tube, a metering valve is connected so that the required portion of the solvent passes through the capillary wall.

Although pressure-FFF was described as early as 1974, extensive examination was performed much later [234]. In the first work on pressure-FFF, the ba-

sic theoretical model of the separation in circular semipermeable tubes was developed, and blue dextran and human plasma were fractionated [37]. Later, the theory of pressure-FFF was improved on the basis of the general dispersion theory for a circular tube [283] and the description of the pressurized flow in a circular tube or a rectangular channel [44]. However, some complications arising from the transport phenomena in a pressure-FFF channel have yet to be solved.

2.6.4
Three-Dimensional Fl-FFF (Helical-Fl-FFF)

Helical-Fl-FFF belongs to a set of multidimensional FFF techniques where separating forces and flows operate in three dimensions. The separation occurs in the annular space between two rotating concentric circular cylinders ("Taylor-Couette device"). The inner cylinder is fixed, while the outer rotates at a constant angular velocity (Fig. 22A). A pressure gradient drives the carrier flow along the axis of rotation to elute for detection, so that a helical flow is generated. The helical flow multiplies migration differences in a radial direction for a large separation (Fig. 22B). It has recently been suggested theoretically that the separation mechanism could be refined further by applying a radial field, for example, a thermal, electrical or sedimentation field or other driving force used in normal FFF [284]. During a helical-Fl-FFF separation the solutes travel simultaneously in the direction of the outer cylinder which is the accumulation wall with linearly increasing azimuthal velocity by virtue of the applied field, and along the cylinder axis with the carrier liquid. As soon as the solutes have passed the region of the maximum axial flow velocity, their velocity in the axial flow di-

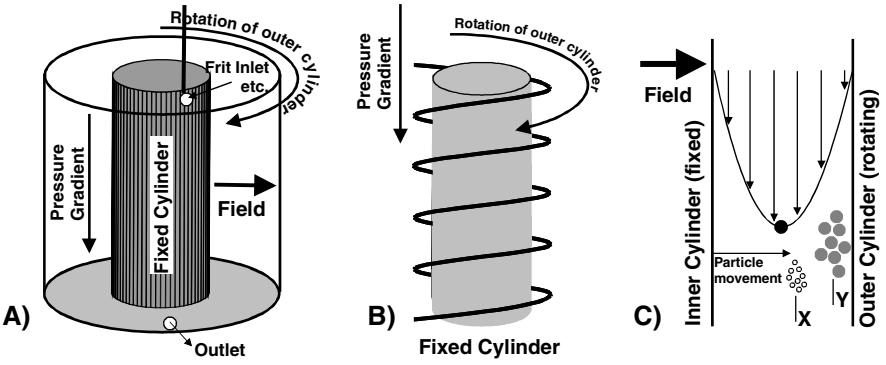

Fig. 22. Schematic presentation of a helical-Fl-FFF device (**A**), the generation of a helical flow in the annular space between a fixed and a constantly rotating cylinder (**B**) and the separation mechanism (**C**). The larger particles *Y* migrate faster towards the outer cylinder and are thus located in regions with lower axial velocity than the slower migrating ones

rection will decrease, although their azimuthal velocity increases. This has the consequence that the solutes which interact less with the field are located in the region of higher axial flow velocities as in classical FFF and thus elute first (Fig. 22C).

The two advantages of helical-Fl-FFF are (1) the amplification of the separation compared to a parallel plane FFF arrangement with concurrent improved resolution, and (2) that the fractionator body is smaller. Experimental verification of the helical-Fl-FFF concept was attempted using an electrical field across the concentric cylinders [285].

2.6.5 *Acoustic-FFF*

Acoustic-FFF was proposed and experimentally verified by preliminary measurements by Semyonov and Maslow applying a standing acoustic wave field as external force [286]. The particles can be pressed against the wall or be focused within the channel depending on the sign of the adiabatic compressibility difference between sample and solvent. The difference between the sample adiabatic compressibilities or alternatively the particle size can be determined from this FFF technique.

2.6.6 *Photophoretic-FFF*

Recently, Kononenko et al. proposed particle photophoresis (particle movement under the action of light) as a suitable field for FFF [287,288] as already suggested by Giddings in 1988 [77]. Initial experiments with carbon black showed that the elution curve changed when light was applied. These results indicate some potential for the practical introduction of photophoretic-FFF to the family of FFF techniques.

2.7 Theoretically Proposed FFF Techniques

In theory, almost any kind of physical effect may lead to a separation of a sample, and is thus suitable as the driving force in FFF. Therefore, the list of FFF techniques in this chapter is by no means complete. Here, then, are a few examples of FFF techniques provided which have been theoretically proposed but not yet demonstrated due to experimental difficulties, if not impossibilities.

2.7.1 *Concentration-FFF*

The separation force in concentration-FFF is a chemical potential field established by a concentration gradient of a mixed solvent across the channel in order

to induce effective chemical forces [42]. This technique is very difficult to realize experimentally.

The solute concentration distribution across the channel is determined by the chemical potential gradient caused by the varying solvent composition. For the chemical potential gradient dμ*/dx, the value of λ is determined by

$$\lambda = \frac{RT}{\Delta\mu_c^*} = \frac{1}{\ln c_0 / c_w} \tag{79}$$

where $\Delta\mu^* = (d\mu^*/dx)w$ is the total increment of the chemical potential across the channel and c_0 and c_w the concentrations near both walls (0 and w), respectively. The $\alpha_c = c_0/c_w$ required for an effective separation was calculated to exceed at least 10 to 100 which means the establishment of very large concentration gradients across the channel.

Substituting Eq. (79) into Eq. (11) yields the retention ratio [27]:

$$R = \frac{6}{\ln\alpha_c}\left(\frac{\alpha_c + 1}{\alpha_c - 1} - \frac{2}{\ln\alpha_c}\right) \tag{80}$$

Hence, it should be possible to measure differences in the chemical potential for the solute. The proposed channel for concentration-FFF is placed between two semipermeable membranes like in S-Fl-FFF permitting lateral flux of the binary solvent components. The reservoirs of the mixed solvent at various concentrations of active components are in contact with these membranes from opposite sides so that the solute should concentrate at the wall, displaying the minimum chemical potential.

2.7.2 *Shear-FFF*

Shear-FFF utilizes shear forces to drive a separation [46]. Such shear can be induced in the annular space between two concentric cylinders that are in relative rotational motion. This technique is in parts similar to helical-Fl-FFF (see Sect. 2.6.4) and is intended for the separation of large macromolecules and globular particles. The fluid flow in the axial direction is superposed over the angular flow caused by relative rotation [46] such that the shear flow generated causes the inward migration of solute macromolecules and particles. Two limiting cases differing in the freedom of fluid flow through random coil macromolecules were considered theoretically with several simplifications. The scope and limitations of shear-FFF have been discussed by Giddings [46].

2.8 Steric-FFF

Unlike the preceding FFF techniques, steric-FFF invokes a new mechanism but not a new field. Steric-FFF is a mechanism applicable to larger particles (~0.5 to 200 μm) and can be applied with any FFF technique provided that the acting forces are high enough to force the particles against the accumulation wall. The mechanism of steric-FFF has already been discussed in Sect. 1.2. In contrast to the normal mode, in steric-FFF larger particles elute first. An advantage of steric-FFF is the separation speed. Figure 23 shows an example of a separation of seven latexes within 3 min.

On the other hand, the mechanism of steric-FFF is complicated by a number of hydrodynamic phenomena [79]. The most important are the hydrodynamic lift forces that drive particles away from the wall and thus counteract the physical field [289–291]. This effect can even lead to an increase in the separation

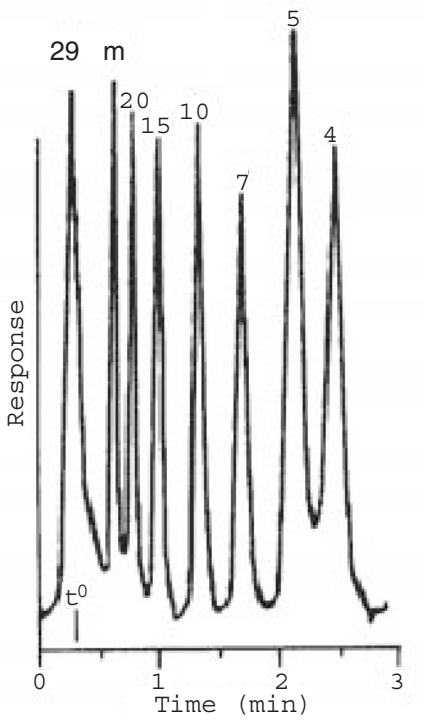

Fig. 23. High-speed separation of seven polystyrene latex beads by steric-S-FFF. Reproduced from [14] with kind permission of the American Association for the Advancement of Science

speed, as shown for the high-speed focusing-FFF of polystyrene latex particles [292].

The occurrence of hydrodynamic lift forces principally leaves two options to perform the FFF experiment: either the field force is increased to offset the lift forces and confine the particles close to the wall [226], or they can be adjusted to allow the particles to gain a significant elevation above the wall, where they form hyperlayers. The first mechanism preserves the steric mechanism, whereas the latter is the mechanism of lift-hyperlayer FFF (see Sect. 2.8.2). From these considerations, it becomes clear that the mechanism of steric-FFF is more complicated than the normal mode operation, necessarily requiring a calibration prior to measurement. This calibration is performed using a double logarithmic plot of the retention time t_r vs. the known hydrodynamic diameter d_H of a standard particle. From the slope and intercept, one can obtain the calibration constants S_d and t_{r1} by using the equation [293]:

$$\log t_r = -S_d \log d_H + \log t_{r1} \tag{81}$$

where S_d is the diameter-based selectivity and t_{r1} is a constant representing the retention time of a particle of unit diameter. The value of t_{r1} depends on the field strength and, for S-FFF, also on the particle density which enables density determinations from steric-S-FFF measurements. Using the calibration parameters S_d and t_{r1}, the particle size weight distribution, m(d) can be obtained directly from the elugram using:

$$m(d) = c(t_r)\langle v\rangle S_d t_{r1}\left(\frac{t_r}{t_{r1}}\right)^{(s_d+1)/s_d} \tag{82}$$

where $c(t_r)$ is the fractogram signal at retention time t_r and <v> is the flow rate through the channel.

Although steric-FFF can in principle be performed with any FFF technique, it was most successfully carried out with sedimentation forces which allowed the possibility to offset hydrodynamic lift forces (see Fig. 23). The calibration of steric-S-FFF is complicated because the sedimentation force depends on the density difference against the solvent, unless performed with standards which have the same density as the sample. This makes it difficult to use a simple diameter-based calibration method as indicated by Eq. (81). The approach towards a successful calibration in such cases is the density compensation principle [293] in which particles of an identical diameter but different densities can be eluted at the same retention time by adjusting the field strengths to compensate for the density difference between the particles [293,294]. This can be done by adjusting the field strength of a steric-S-FFF run inversely proportionally to the change in density difference by using the relationship:

$$(\mathrm{rpm})_{\mathrm{sample}} = \left\{\frac{\Delta\rho_{\mathrm{std}}}{\Delta\rho_{\mathrm{sample}}}\right\}^{1/2} (\mathrm{rpm})_{\mathrm{std}} \tag{83}$$

where $(rpm)_{sample}$ represents the rotational speed for a run with the sample, $(rpm)_{std}$ is the corresponding speed of the standard run, $\Delta\rho_{std}$ is the density difference between the standards and the carrier liquid, and $\Delta\rho_{sample}$ is that between the sample and the carrier.

However, even sophisticated calibration procedures cannot account for wall effects of the sample which might be absent for the calibration standard. The term "wall effects" summarizes all kinds of forces, both attractive and repulsive, which can become significant as the colloidal particles are usually forced to be in direct contact with the accumulation wall. Therefore, any information from such experiments can become error prone, so it is recommended to reduce the field or to alter the carrier flow rate in order to switch from the steric to the hyperlayer mode.

In addition, quantitative evaluation of steric-FFF experiments usually relies on special detectors, since the particles being separated are very large. A standard UV-detector, for instance, cannot be used, unless it accounts for the Mie scattering or Fraunhofer diffraction. A special photometric detector has been designed especially for steric-FFF [295].

2.8.1 *Hydrodynamic Lift Forces*

In contrast to the simple retention theory of steric-FFF, the retention ratios were found to depend experimentally not only on size but also on flow rate [296] and particle density. In 1979 Caldwell et al. [297] attributed this observation to flow-dependent hydrodynamic lift forces that elevate the particles away from the wall. These forces have the same origin as the forces governing the separation mechanism in hydrodynamic chromatography and were theoretically described prior to their observation in steric-FFF measurements [289–291]. Hydrodynamic lift forces increase with the carrier liquid flow rate and keep the particles a short distance from the accumulation wall and thus into regions with a higher flow velocity in the parabolic flow profile [79,298]. These lift forces decrease with higher field strengths and increasing particle size [299] and, in certain cases, they can also cause the loss of resolution [300]. Hydrodynamic lift forces have also been observed in other FFF techniques than S-FFF or Gr-FFF, for instance, A-Fl-FFF [231]. The action of hydrodynamic lift forces is outlined in Fig. 8.

As hydrodynamic lift forces are as yet only very poorly understood [79], they cannot yet be incorporated into a closed retention theory. However, early studies suggest that the retention ratio R in steric-FFF can be expressed by a quite simple relationship [294]:

$$R = \frac{t_0}{t_r} = \frac{3\gamma_S d_H}{w} \tag{84}$$

where γ_S is the steric correction factor which is related to the hydrodynamic lift forces. According to Eq. (84), it is shown that the prediction of particle retention

in steric-FFF requires a clear understanding of this steric correction factor. Therefore, attempts were made to quantitatively express the hydrodynamic lift forces. Different relationships were used over the years, the first originating from Caldwell et al. where the lift force $F_L(x)$ was described as [297]:

$$F_L(x) = 20.3(\eta\rho)^{0.5} \frac{d_H^2}{R_c} \left[3 < v(x) > x\right]^{0.5} \Delta v(x) \tag{85}$$

with x=0 in the center of the channel differing from the normal convention, R_c is the radius of the circular S-FFF channel, and $\Delta v(x)$ is the difference between the particle and the fluid velocity at the position of the particle center of gravity.

Recent systematic studies used steric-S-FFF with well-characterized latex beads of diameters 2–50 μm where the sedimentation force was adjusted to exactly counterbalance the lift force F_L [79,301] to provide a measure of F_L. This has led to a more subtle view of the hydrodynamic lift forces than expressed by Eq. (85). There are indications that the hydrodynamic lift force is presumably composed of two different contributions: (a) the lift force due to the fluid inertial effect F_{L_i}, which may be described by the theory of hydrodynamic lift forces [289–291], and (b) the hydrodynamic lift force by a near-wall effect F_{L_w} [61,62,79,301,302]. The latter was experimentally found to be a function of particle diameter d_H, the distance of the particle bottom from the wall δ, the fluid shear rate s_0, and the fluid viscosity η by:

$$F_{L_w} = C \frac{d_H^3 \eta s_0}{8\delta} \tag{86}$$

with C being a dimensionless coefficient. The origin of this incremental force is unclear but may be related to lubrication phenomena.

If the external field strength is kept so low that the particles are significantly elevated from the wall by the action of the hydrodynamic lift forces, the fluid inertial contribution of the hydrodynamic lift force F_{L_i} can be investigated [289–291,301]. Observed inertial lift forces were in reasonable agreement with values predicted by the inertial lift force theory expressed by:

$$F_{L_i} = 13.5\pi \frac{\langle v \rangle^2 d_H^4 \rho}{16 w^2} g(x/w) \tag{87}$$

where <v> is the mean flow velocity and g(x/w) is a function of (x/w) [302]. Combining Eqs. (86) and (87), a general expression of the overall active hydrodynamic lift force F_L is obtained [301]:

$$F_L = \underbrace{C\frac{d_H^3 \eta s_0}{8\delta}}_{\text{Near wall contribution}} + \underbrace{13.5\pi \frac{\langle v \rangle^2 d_H^4 \rho}{16 w^2} g(x/w)}_{\text{Inertial contribution}} \quad (88)$$

When particles are close to the channel wall, the first term dominates whereas the second does when particles are at some distance from the accumulation wall. Thus, steric-FFF is also a very promising technique to study particle hydrodynamics in the vicinity of the wall.

The behavior of particles under the simultaneous effect of field forces and lift forces can vary with the nature of different applied primary field forces [298]. The force acting on the particles is proportional to the third power of the particle diameter in S-FFF, but only to the first power of the particle diameter in Fl-FFF thus indicating that S-FFF is probably best suited for a fine balance between the external field and hydrodynamic lift forces.

On the other hand, retention in lift-hyperlayer FFF only depends on the particle size and is independent of density which makes the calibration easier. Lift-hyperlayer FFF is a very fast technique applicable to a particle size range from 0.5–50 μm if cross-flow forces are applied [226,303]. A further advantage of lift-hyperlayer FFF is that the particles are held well away from the wall during separation and thus particle–wall interactions are omitted.

2.8.2 *Capillary Hydrodynamic Fractionation (CHDF)*

CHDF is similar to steric-FFF in respect to the elution mode (larger particles elute more rapidly) but the separation characteristics are different. In CHDF, long capillaries (ca. 100 m) with internal diameters as small as only a few microns are used for the separation of particles and polymers in the size range of 30 nm up to several μm, depending on the capillary used. The underlying principle of hydrodynamic chromatography had already been put forward in 1970 [304], before the first experiments using non-porous silica columns were performed [63]. By 1974 the first separation of macromolecules in a capillary was reported [305]. There are only a few papers dealing with CHDF separations (for an example, see [306]), nevertheless, the setup is commercially available and has found application in several laboratories.

Advantages of CHDF include fast separations in a matter of minutes, easy handling and a very good reproducibility of the measurements. A problem of CHDF is the necessarily long capillary length required for a successful separation because the effectivity of the separation can be described by:

$$\Delta r = 3.039 \left(\frac{R_{cap.}^3}{L_{cap.}} \right)^{1/2} \left(1 - \frac{d_H}{2 R_{cap.}} \right)^{3/2} \quad (89)$$

where d_H is the hydrodynamic particle diameter, $R_{cap.}$ the internal radius of the capillary, and $L_{cap.}$ the length of the capillary. Thus the resolution of the measurement (small Δr) can be enhanced by the choice of long capillaries of small internal radii. On the other hand, such conditions promote the influence of diffusion in the flow direction resulting in band broadening. Furthermore, the influence of ill-defined colloidal forces (the "wall-forces") become more important for long capillaries and are often the dominant source of the separation. Therefore, the elution behavior cannot be predicted and relies at least on the calibration with standard samples. For all these reasons, CHDF can be regarded as a limiting case of steric-FFF separation but without the corresponding resolution or versatility.

2.9 Focusing-FFF

Focusing-FFF is a special mode of FFF where a gradient of a physicochemical quantity like density in S-FFF in the channel balances the external force. This leads to a focusing of the sample band at a defined position above the accumulation wall, where the external force is exactly counterbalanced. In the case of focusing S-FFF, the focusing would be at the position where the sample density is equal to the local density in the gradient, analogous to isopycnic ultracentrifugation. This principle has recently been generalized to demonstrate that other perichoric gradients and a variety of the fields could be combined to produce a focusing effect [18]. The principle of focusing-FFF is illustrated in Fig. 9. In the FFF literature, the term hyperlayer-FFF instead of focusing-FFF was suggested by Giddings and is also used.

The retention theory for focusing-FFF was developed for focusing-S-FFF but can be transferred to other focusing mechanisms [72,73]. Janca and Chmelik developed this theory for several shapes of fractionation channels [74] and found that it is advantageous to form axially asymmetrical velocity profiles in channels with modulated cross-sectional permeability [83].

2.9.1 *Focusing-S-FFF*

Focusing-S-FFF is based on the isopycnic centrifugation principle where a substance bands in a density gradient at a position where its density is equal to the local gradient density. The density gradient can be created by centrifugal forces acting on a liquid composed of two or more components differing in their effective densities. Diffusion processes disperse the formed zone of the banded solute so that a Gaussian concentration distribution is obtained with a width depending on the diffusion coefficient. For detailed reference about the underlying principles refer to the literature of isopycnic ultracentrifugation [307]. When the parabolic flow profile in the FFF channel is formed, the solute zone moves with a velocity of the streamline at the altitude corresponding to the coordinate of

equal densities [72,73]. Therefore, retention in focusing-S-FFF is just determined by the solute density whereas in normal S-FFF, it also depends on the size. In contrast to isopycnic sedimentation in an ultracentrifuge, the focused zone is laterally transported which improves the resolution. Furthermore, the migration distance in the thin FFF channel is magnitudes smaller than in an ultracentrifuge and, thus, the time for solute equilibration is shorter reducing the experimental time.

The density gradient, $d\rho/dx$, formed by the action of a centrifugal force can be calculated neglecting the pressure gradient according to [307]:

$$\frac{d\rho}{dx} = \frac{\partial\rho}{\partial c_i}\left(\frac{\partial c_i}{\partial a_i}\right)\frac{a_i M_i\left[1-\bar{v}_i\rho(x)\right]\omega^2 x}{RT} \tag{90}$$

where a_i or $\bar{v}_i$ is the activity, respectively, the partial specific volume of the i^{th} component of the density gradient. The force acting on the solute particles or macromolecules can be defined with knowledge of $d\rho/dx$ as:

$$F(x) = \bar{v}\omega^2 x_0 \frac{d\rho}{dx}(x_0 - x) \tag{91}$$

where $\bar{v}$ is the partial specific volume of the solute species and x_0 the coordinate where the force onto the solute is 0. F(x) has the meaning of a force per mass unit of the solute. Hence, the general equation for the Gaussian concentration distribution function c(x) of the sample in the direction of the focusing forces becomes for S-FFF [72, 73]:

$$c(x) = c_{max}\exp\left[\frac{-\bar{v}\omega^2 x_0(d\rho/dx)(x_0 - x)^2}{2RT}\right] \tag{92}$$

Experimentally, focusing-S-FFF can be carried out with the normal S-FFF equipment. The carrier liquid contains both components for the density gradient which is is established under the influence of the centrifugal forces.

There are two different philosophies about the optimum channel design for focusing-S-FFF reported in the literature. Whereas Janca et al. utilized channels with trapezoidal or parabolic cross sections [83,308–315], resulting in a variation of the fluid flow velocity across the channel width, Giddings [316] favored the classical rectangular cross section with a parabolic fluid velocity profile.

Focusing S-FFF suffers from the problem that the density gradient has to be formed instantaneously which is not the case in practice even for thin channels [107]. This may be the reason why published results obtained with focusing S-FFF are rare [27,74,83,308–315].

Focusing- S-FFF seems promising especially for the separation of samples due to structural changes. For example, polymers can be analyzed in terms of

tacticity or degree of branching due to the density differences for chains having the same molar mass but different structures. Also for biopolymers, the fractionation due only to density differences is advantageous as these substances are very often monodisperse with respect to molar mass, but exhibit differences in structure and the related density.

2.9.2 *Isoelectric-Focusing-FFF*

Isoelectric focusing-FFF is appropriate for the separation of amphoteric particles, since their electrophoretic mobility depends on pH and is zero at the isoelectric point. If a stable pH gradient is formed in the FFF channel due to an applied electrical field [317], the amphoteric solute will be focused into the position of its isoelectric point. Isoelectric-focusing-FFF was first proposed as a concept and experimentally verified five years later [314,315,318–321].

2.10 Adhesion-FFF/Potential-Barrier FFF

Adhesion-FFF is a very interesting FFF mode for colloidal samples which addresses colloidal forces. So far it has only been applied with Gr-FFF and S-FFF but can, in principle, be generalized. Adhesion-FFF makes use of the variation of colloidal forces by pH, surface tension, ionic strength, temperature or dielectric constant of the suspending medium of the carrier liquid and thus affects the Hamaker constant, surface potential and Debye–Hückel length [57,322–326]. If these parameters are properly adjusted, colloids adhere or detach from a solid surface. Thus it is possible to totally absorb or desorb colloidal particles onto or from the accumulation wall. This FFF variant is named potential-barrier FFF [269,270,322–325,327]. The total release of adherent particles is accomplished either by reducing the field strength, increasing the solvent velocity, or by varying the potential energy of interaction between the colloidal particles and the column material, for instance, by changing the ionic strength of the carrier solution. Adhesion-FFF is very useful for the study of possible aggregation processes as the particle size distributions prior and after adhesion to the accumulation wall can be compared [284]. This is illustrated in Fig. 24 by means of a typical experimental elution profile.

Unless aggregation is studied, potential-barrier FFF is restricted only to particles which fully adsorb in a reversible way on the channel wall. Thus, the material of the channel walls needs to be properly selected which is a difficult task. One major advantage of potential-barrier FFF is the possibility to separate and characterize dilute colloidal samples of the same size but differing surface potentials or Hamaker constants.

Another variant of adhesion-FFF is cellular adhesion chromatography (AC) which can be used to separate cells in a preparative manner. It utilizes selective

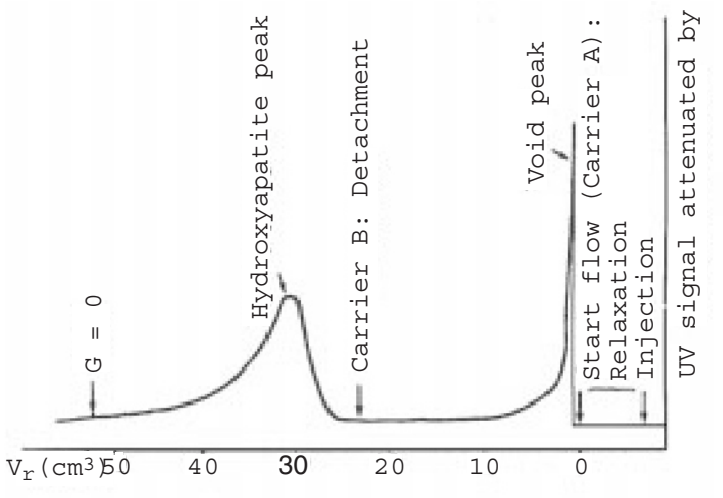

Fig. 24. Attachment and detachment of hydroxyapatite particles from a Hastelloy C surface in an S-FFF channel in carrier A: 10^{-3} M KNO_3 (pH 6.8) and carrier B: 0.5% v/v Fl-70+0.02% w/w NaN_3 (pH 9.4). Reproduced from [328] with kind permission of John Wiley and Sons

adhesion of cell groups to an FFF accumulation wall for separation which requires chemical surface modifications or even surface design [329–331].

Cellular adhesion FFF combines the controllable hydrodynamic shear forces of FFF and the selective adhesion of AC. The hydrodynamic shear is used to detach selectively and evenly adhered cells or particles from the surface and allows an estimation of the differences in cell/surface adhesion forces. The channel for cellular adhesion FFF is constructed in the same way as that used for Gr-FFF but is smaller in size and with the modification that the accumulation wall consists of either bare or polymer-coated surfaces. After the cell suspension is filled into the channel allowing sufficient time for cell adhesion, the flow is applied and fractions are collected. Despite the collection of fractions, cellular adhesion FFF can also be used as a tool to study rapid kinetics of cell surface adhesion, a largely unexamined area [332].

2.11 Preparative and Micropreparative FFF

Considering the mass of injected sample of some micrograms and the danger of solute–solute interactions, it is obvious that FFF is in general only an analytical method. However, some strategies have been employed to apply FFF principles for preparative separations as well.

Repeated sample injections allow at least micropreparative fractionation, which was described for polymer latex particles by S-FFF [333]. Preparative separations can however also be achieved by applying continuous sample feed. One possibility is to use SPLITT channels (see Sect. 2.12) but classical FFF methods

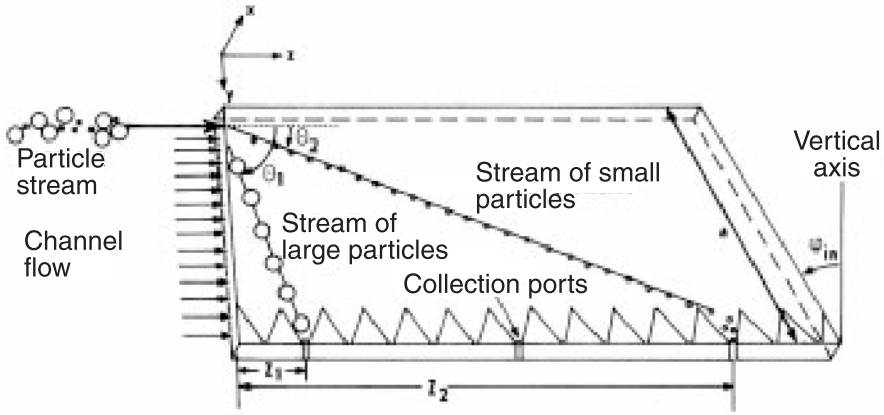

Fig. 25. Schematic representation of an inclined channel for continuous steric-Gr-FFF. Reproduced from [334] with kind permission of Elsevier Science Publishers

have also been described that work with continuous sample feed. For example, continuous steric-Gr-FFF was performed by inclining the transversal axis of the channel and by injecting the sample into the upper part [334]. The separated particles are carried by the flow and slide towards the lower regions of the channel into collectors situated along the channel (see Fig. 25), where the particles are trapped according to their size: larger particles are trapped in a shorter distance.

The distance from the injection point Z where the particles are trapped in the pocket can be calculated from:

$$Z = \frac{54\langle v \rangle \eta}{w^2 d_H \Delta\rho \, G \cos\varphi_{in}} \tag{93}$$

where <v>is the fluid flow rate, G the gravitational acceleration, and ϕ_{in} the inclination angle. This continuous fractionation was used for the separation of coal fly ash [335].

A continuous Fl-FFF channel analogous to a dialysis cell or ultrafiltration cell [247] was described theoretically and later demonstrated in practice for the separation of bovine serum albumin from methylene blue, various viruses, proteins, and colloidal silica particles.

Focusing-FFF can be applied as a preparative separation technique if the channel is equipped with several outlet capillaries situated at various heights above the accumulation wall of the focused samples, and the sample is fed continuously [74].

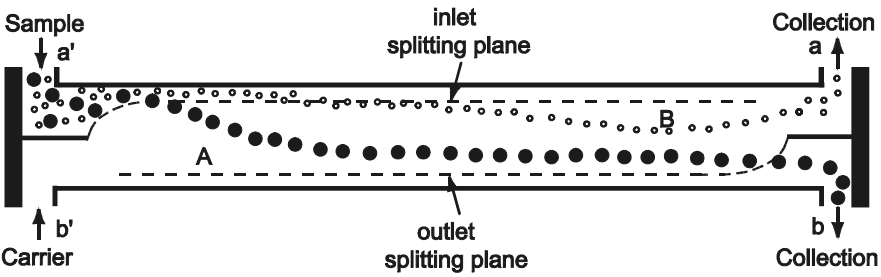

Fig. 26. Schematic representation of Gr-SPLITT-FFF

2.12 SPLITT-FFF

SPLITT-FFF uses stream splitters at the channel inlet and outlet which enables the separation of a mixture into two fractions. Although the separation of the sample is also achieved by the action of an external field, the mechanism of separation is different from FFF. The separation in FFF is along the flow axis of the channel because of the different flow velocities of each component, whereas in SPLITT separation is over the thinnest dimension of the channel. While conventional FFF is an analytical tool requiring operation with very small samples, SPLITT is a preparative tool which can be operated with continuous sample feed [336,337]. SPLITT channels are similar to FFF channels but with two carrier inlet streams a' and b' and two outflow streams a and b as illustrated in Fig. 26.

Control of the inlet and outlet flow rates determines the positions of the inlet and outlet splitting planes and allows the adjustment of the cut-off point between the two fractions and enhancement of the efficiency of the separation [338,339]. The feed stream enters through a', while the flow from b' compresses the sample feed flow upward into a band sometimes only 10 or 20 μm thick. This compression is determined by the flow rate ratio. Similarly, the outlet splitting is controlled by the ratio of flow rates from a and b. Conditions for successful separations in SPLITT channels by modifications to the inlet and outlet splits has been discussed in detail by Giddings [340].

Although SPLITT has the advantage of being a very rapid preparative fractionating technique due to the short transport paths of only a few hundred μm needed to achieve separation, the disadvantage is that only two fractions smaller or larger than a given cut size can be collected depending on the conditions used. Thus, only subsequent treatment of the fractions under different flow conditions can yield a narrow distribution of particles. Applying this procedure, SPLITT can also be used as an analytical tool to reconstruct the particle size distribution, although this is a very tedious method [69].

2.12.1 *Gravitational-SPLITT-FFF (Gr-SPLITT-FFF)*

Gr-SPLITT-FFF is the most simple design of a SPLITT channel and the most widely used among the different SPLITT techniques. The function of a Gr-SPLITT-FFF channel is illustrated in Fig. 26. Here, the fractionation is achieved according to the particle size and density analogous to Gr-FFF so that the smaller particles emerge through the upper outlet a while the larger ones leave at the lower outlet b.

2.12.2 *Electrical- and Magnetic-SPLITT-FFF*

In an electrical-SPLITT-FFF channel, an electrical field is applied which consequently leads to a SPLITT separation of differently charged particles or molecules [341]. The separation mechanism, however, is more similar to that of electrophoresis than El-FFF. Components with high mobility are driven through the outlet splitting plane and emerge through the outlet splitter. Adjustment of both the electrical field strength and the outlet stream splitting ratio tunes the cut point between the collected species. The electrical SPLITT cell can also be operated in the equilibrium mode by adjusting the pH such that some species go to the anodic wall and others to the cathodic wall. This is most useful for amphoteric samples with different isoelectric points, like proteins.

A magnetic SPLITT fractionation system extends the merits of SPLITT-FFF to magnetic samples [342]. Here, permanent magnets act as the driving force perpendicular to the solvent flow for the separation in the SPLITT channel. The system was experimentally tested using mixtures of silica particles, labelled silica particles and magnetic particles leading to a complete separation of particle mixtures with high and low magnetic susceptibilities. In the continuous mode, the throughput was around 0.1 g/h with a sample recovery of nearly 99%.

2.12.3 *Diffusion-SPLITT-FFF*

Diffusion can also be used as a driving force in SPLITT channels. If one uses a SPLITT channel analogous to a gravitational-SPLITT-FFF channel where the sample is injected into inlet a' (Fig. 26), the higher diffusion of smaller molecules allows them to cross the outlet splitting plane and thus to exit the lower outlet b, whereas larger molecules have a lower diffusion coefficient and exit from the upper outlet a. This method has been applied for continuous separations and diffusion coefficient determinations of a number of proteins [343,344].

3 Selected Applications of FFF

This section lists selected applications of the various FFF techniques demonstrating the possibilities of FFF for various samples. For simplicity, the section is structured into the major substance classes which are suitable for analysis by FFF distinguishing between samples of synthetic or natural origin.

3.1 Polymers

3.1.1 *Synthetic Polymers*

3.1.1.1 S-FFF

Although S-FFF is usually applied to particles or large biopolymers, its use for the analysis of synthetic polymers with high molecular weight (M) was demonstrated for polyacrylamide [176]. This is, however, a rare application.

3.1.1.2 Th-FFF

As Th-FFF is the technique of choice for synthetic polymers in organic solvents, there are many studies reported in the literature. Th-FFF has been found applicable to virtually every type of lipophilic polymer in the range $M=10^4$–10^7 g/mol using ΔT~10–100 K, but only to a very limited amount of hydrophilic polymers where Fl-FFF has its traditional strengths. Exceptions include poly(vinyl pyrrolidone) and poly(ethylene glycol) [222].

The list of examples of successful Th-FFF separations of lipophilic polymers is extensive and includes polystyrene [29,34,76,118,144,164,165,168,196,200,345–350], polyisoprene [55,110,144,196,349,350], polytetrahydrofuran [144,196,349,350] and poly(methyl methacrylate) [55,110,144,196,349,350], polybutadiene [349], poly(ethyl methacrylate), poly(*n*-butyl methacrylate), poly(octadecyl methacrylate), poly(α-methylstyrene), poly(dimethylsiloxane), poly(vinyl acetate), poly(vinyl chloride) and poly(vinyl carbazole) [144], polyethylene [351] and other polyolefins [221]. The polyolefin separations were achieved in a special high temperature channel [15,351]. Asphaltenes have also been separated with Th-FFF [352].

From the Th-FFF retention data, it is possible to obtain a molar mass distribution after a suitable calibration for the determination of the Mark–Houwink constants (straight-line plot of $\log(D/D_T)$ vs. $\log M$ [15]). Another possibility is to couple an absolute molar mass detector like MALLS (see Sect. 4.3.2) or a suitable detector combination such as an on-line viscometer coupled with a refractive index detector. This possibility does not require prior knowledge of D_T

[144]. A large variety of samples was investigated with the latter technique including polystyrene, poly(methyl methacrylate), poly(ethyl methacrylate), poly(*n*-butyl methacrylate), poly(octadecyl methacrylate), polyisoprene, poly(α-methylstyrene), poly(dimethylsiloxane), poly(vinyl acetate), poly(vinyl chloride) and poly(vinyl carbazole). Another advantage of coupling a continuous viscosity detector to the Th-FFF channel is that viscosity distributions can be measured resulting in a measurement of absolute intrinsic viscosities without the need for calibration [76]. If copolymer samples are investigated in Th-FFF coupled with a viscometer, both the average molecular weight and the average composition are accessible [142].

Th-FFF is also a good technique if polydispersities of very narrow samples from anionic polymerization need to be determined. This was demonstrated for polystyrene from band broadening data in Th-FFF with a higher accuracy than the results from SEC on the same samples [123].

Whereas polymers in the range $M=10^4$–10^7 g/mol are well resolved by Th-FFF, polymers of lower molecular weight (~10^3 g/mol) need an inconveniently high ΔT (~150 K) for retention, and problems of boiling solvent, etc. arise. However, successful separations of polystyrene down to 600 g/mol have been described using very high temperature gradients in a pressurized Th-FFF channel [200].

On the other hand, the upper end of accessible molar masses $M\approx10^7$ g/mol [126] can be significantly shifted to higher values if more compact structures such as branched, cross-linked, or particulate samples are investigated since the D_T of the sample is low. The fractionation of ultrahigh molar mass samples is a very promising application for Th-FFF as these polymers are often fragile and thus sensitive to shear degradation which can be mainly circumvented in the open FFF channel. Consequently, this type of application is on the rise [126].

Janca and Martin [353] studied the influence of various operational parameters on the retention of ultrahigh molecular weight polystyrenes (0.6–30×10^6 g/mol) in Th-FFF, finding that at high flow rates (1.5 ml/min) the retention was not strictly proportional to the molecular weight for polymers with $M>3\times10^6$ g/mol, although the samples did not suffer from shear degradation as demonstrated by reinjection. Such reversal in the M-dependence of retention at high flow rates had already been observed for high molar mass polymers [354], and can be explained by shear-induced entropic effects. By the action of such effects, the high molecular weight components are transported into the center of the channel where the velocity gradient across the polymer coil is reduced.

Another promising field of application of Th-FFF is the investigation of gel/microgel mixtures with polymers as pioneered by Lee et al. [355,356]. A major advantage is that for the Th-FFF experiment no filtration is required to endanger material loss. For example, microgels or particles which are problematic for SEC separations can be separated from a polymer, so that the major constituents of composites such as acrylonitrile-butadiene-styrene (ABS) rubber are quantitatively accessible.

Other examples include the monitoring of the degradation of poly(methyl methacrylate) (PMMA) by an electron beam [355] or the investigation of the

physicochemical difference between two acrylate elastomers that have been manufactured by the same procedure but show different mechanical properties [355]. These differences are not distinguished by SEC, even in combination with viscometry or light scattering. Composite polymers where particles are mixed with a polymer have also been examined [357].

The dependence of retention in Th-FFF on chemical composition of the polymers and solvent [84] also opens a wide field of application for Th-FFF, especially for copolymers. According to Eq. (42), retention in Th-FFF can be used to determine the thermal diffusion factor α_T which was demonstrated for polystyrene in toluene [209]. Later, this study was extended to other solvents (ethyl acetate, 2-butanone, *p*-dioxane, cyclohexane, dimethylformamide, chloroform, and ethylbenzene) [204].

The ability of Th-FFF to separate polymers by chemical composition [2] was demonstrated in the separation of polystyrene, polyisoprene and polybutadiene polymers of similar molecular weight [349] and extended to polytetrahydrofuran [350]. An impressive example of the ability to separate according to chemical composition was reported for two polymers indistinguishable by SEC (See Fig. 10).

Recent studies [111,214] indicate that Th-FFF can even be used to determine the relative chemical composition of two components in random copolymer and linear block copolymers whose monomers do not segregate due to solvent effects. However, this application is limited by the unpredictable nature of thermal diffusion. Nevertheless, combining information from Th-FFF with those derived on fractions by independent detectors selective to composition (such as an IR spectrometer) can yield further insight into the dependence of D_T on the chemical composition. Even more powerful is the combination of Th-FFF with SEC as, here, the chemical composition (from Th-FFF) can be studied as a function of the molar mass (from SEC). This was demonstrated by van Asten et al. by cross fractionating copolymers and polymer blends with SEC and Th-FFF [358].

Kirkland et al. [359] reported the possibility of varying the retention behavior in Th-FFF by the application of a solvent mixture, later supported by other workers [58,360]. The retention enhancement so achieved was attributed to a synergistic effect involving the thermal diffusion of both polymer and solvent.

Of all solvent mixtures examined thus far, the retention of polystyrene is highest in mixtures of THF and dodecane. This is illustrated in Fig. 27 where the separation of five polystyrene standards ranging in molecular weight from 2.5×10^3–17.9×10^4 g/mol in a mixture of 45 vol% THF in dodecane is shown [360]. This fractogram represents the lowest molecular weight polymer ever resolved from the void peak with a standard Th-FFF channel.

The extension of the application range of Th-FFF using exponential temperature programming was described by Kirkland, Yau et al. for the fractionation of polystyrene and poly(methyl methacrylate) and standard mixtures [164,168], whereas Giddings separated mixtures of polystyrene standards in ethylbenzene over a wide range of molar masses (9×10^3–1.97×10^6 g/mol) using high speed power programming with various field profiles of Th-FFF [54].

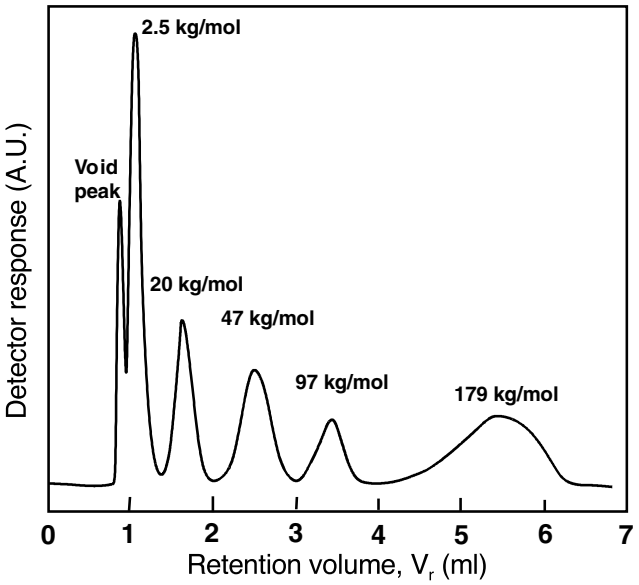

Fig. 27. Separation of polystyrene standards using a mixture of 45 vol% THF in dodecane as carrier liquid. Reproduced from [360] with kind permission of the American Chemical Society

The use of ultrathin (50 μm) channels for high speed separation by Th-FFF was demonstrated by Giddings [118] who separated mixtures of polystyrene standards in experimental times of less than a minute.

3.1.1.3 Fl-FFF

Fl-FFF is most attractive for water-soluble polymers [59] and can directly deliver the diffusion coefficient distribution and also a molar mass distribution via the relationship $D=AM^{-b}$. This was exploited for poly(ethylene oxide), poly(styrene sulfonate) and poly(vinyl pyrrolidone) and other polymers using published Mark–Houwink constants [361]. Many papers just report on the fractionation of polymers or the determination of the hydrodynamic size distribution of polymers. Examples include poly(styrene sulfonates) [59,165,243], poly(acrylic acid) [243] and poly(2-vinylpyridine) [59].

Polyelectrolytes are a substance class notoriously difficult to analyze. This problem also exists for Fl-FFF due to polymer–polymer or polymer–wall/membrane interactions. Benincasa and Giddings [59] completed a systematic study of ionic-strength effects in the application of Fl-FFF to both cationic and anionic polyelectrolytes over a broad molecular weight range. Poly(2-vinylpyridine) was effectively characterized in a 20 mM solution of nitric acid (pH 2), while the best results on poly(styrene sulfonate) were obtained in a dilute (6.5 mM) solution of

sodium sulfate. With tris(hydroxymethylaminomethane) buffer, anomalous behavior was observed. Thus, it becomes clear that a suitable carrier liquid is vital for the investigation of polyelectrolytes. Tank and Antonietti described a universal carrier fluid for Fl-FFF (deionized water containing 0.02% NaN_3 and 0.01% Tween 20) which simplifies the experimental conditions if large varieties of samples are to be investigated spanning from cationic to anionic polyelectrolytes [362]. With this solvent, polycations as poly(1-vinyl-2-pyrrolidone) and polyanions as poly(styrene sulfonates) were successfully fractionated. The results for an industrial poly(1-vinyl-2-pyrrolidone) sample agreed very well with the results from other absolute techniques like analytical ultracentrifugation on the same sample although an indication of absorption of high molar mass polymers to the membrane was reported. Other reports dealt with the aggregation behavior of charged amphiphilic graft copolymers in dependence on pH or of different salt concentrations as studied by A-Fl-FFF [251,252,363]. Shear sensitive commercial ultrahigh molar mass polyacrylamides in the range $0.35–9\times10^6$ g/mol were characterized in terms of molar mass distributions, shear effects, alteration of the solvent, degradation, and agglomeration and their effects on mineral flocculation [166,364]. These polymers, though industrially important as flocculants, are very difficult to characterize due to their polydispersity, high molar mass and shear sensitivity.

Although most applications of Fl-FFF have been reported for aqueous carrier liquids, a few studies have been carried out in organic liquids as well (for a more detailed discussion see also Sect. 4.3.1). Brimhall et al. [365,366] were the first to report non-aqueous polymer separations by Fl-FFF by separating polystyrene in ethylbenzene. Poly(ethylene oxide) and poly(methyl methacrylate) were characterized in THF [367] and, recently, a so-called universal fractionater also capable of high-temperature fractionations has been reported and applied to the separation of a variety of polymers and particles by Fl-FFF in non-aqueous carrier liquids, including the separation of polyethylene [368].

3.1.2 *Biopolymers*

3.1.2.1 S-FFF

S-FFF has successfully been applied to separate and characterize a number of biopolymers, including DNA [176,369], proteoglycans [370], cartilage proteoglycans [371], dextrans [141] and fibrinogen [176]. Further applications concerned preparative S-FFF of DNA-plasmid from crude cellular lysates [372].

3.1.2.2 Th-FFF

Th-FFF is also suitable for the separation of biomolecules, although the use of organic solvents restricts statements about the native state of aqueous-based

buffer. Also, extensive conformational changes and even denaturation can occur which significantly restrict the range of applicable samples. Nevertheless, dextrans, ficolls, pullulans, cellulose and the starch polymers amylose and amylopectin have been separated by Th-FFF using DMSO as a solvent [373]. These polysaccharide samples have a wide range of industrial applications. Examples include pullulans: coating materials, packaging agents, plasma additives and gelling agents; dextrans: blood substitutes, chromatographic media and immunological testing equipment, etc. Nevertheless, these samples are difficult to separate by SEC without complications of sample adsorption, shear degradation and clogging of the column.

Although thermal diffusion is weak in aqueous systems, mixtures of water and dimethyl sulfoxide can be used to fractionate dextrans by Th-FFF [204]. The retention was found to increase linearly with the dimethyl sulfoxide (DMSO) content which again underlines that D_T depends on the solvent composition.

Th-FFF was also applied for the characterization of natural rubber to avoid shear degradation and allow full characterization of the gel phases present [356]. More recently, similar studies applied Th-FFF/MALLS for the determination of the molar mass distribution of microgel ($M=10^{10}$ g/mol) containing natural rubber without filtering prior to the measurement. The largest molecules detected in the sample were found to be more than three orders of magnitude greater than indicated by SEC [374].

3.1.2.3 Fl-FFF

The most commonly biopolymers separated by Fl-FFF are proteins [49]. Fl-FFF is capable of separating proteins differing by just 15% in size within 3 to 10 min. S-Fl-FFF has been applied to a variety of proteins, including albumin, ovalbumin, γ-globulin, hemoglobin, ferritin, lysozyme, β-casein, apoferritin, human and rat blood plasmas and elastin [41,240,247]. Fl-FFF was also used to investigate the structural transformations of proteins [240].

More recently, A-Fl-FFF was used for highly efficient protein separations [231,249] and for the high-speed separation of biopolymers [232]. Other biopolymers and mixtures thereof were fractionated and characterized by Fl-FFF including bovine serum albumin, albumin, γ-globulin, thyroglobulin, protein conjugates, lipoproteins from blood plasma and DNA [60,232,233], nucleic acids [231], dextrans [237], ferritin and aldolase [109,362], molar mass distributions of dextrans and pullulans [361] as well as diffusion coefficients of linear and circular DNAs [375]. Protein complexes also exhibit baseline resolution by Fl-FFF. Figure 28 shows an example of such a separation. Protein dimers elute as satellite peaks at ~1.4 t_r and monoclonal antibody aggregates can also be resolved.

Humic acids, a mixture of amphiphilic heterogeneous macromolecules from soil which vary widely in composition and molecular weight, are soluble in neutral or alkaline water – distinct from fulvic acids. They are usually quite small macromolecules, but they heavily interact with any column material, thus re-

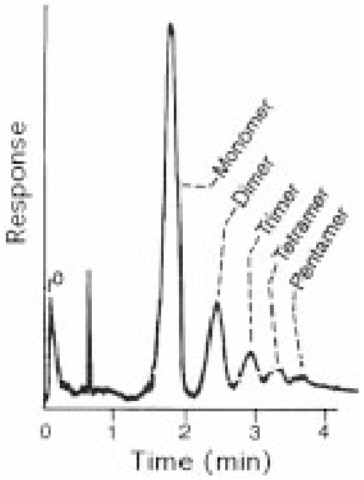

Fig. 28. Separation of a monoclonal antibody from its higher oligomers showing separable peaks up to pentamer aggregation. Reproduced from [14] with kind permission of the American Association for the Advancement of Science

stricting the use of SEC. Humic acids have been successfully studied by Fl-FFF [376]. Beckett et al. characterized humic and fulmic acids in terms of molar mass distributions [11,227,377]. Schimpf and Wahlund investigated the influence of pH, ionic strength, humic acid concentration and bridging by Ca^{2+} addition on the molar mass and size distribution of humic acids [378], whereas the complexation ability of humic acids was studied by van den Hoop and van Leeuwen [379]. In a related study, Beckett et al. studied the size and molar mass distribution of pulp and paper mill effluents by Fl-FFF [380,381].

3.1.2.4 Other FFF Techniques

El-FFF is a technique devoted to the fractionation of proteins which is reflected in the number of papers applying this technique to protein separations. The possibilities of El-FFF were first demonstrated by Caldwell for the separation of albumin, lysozyme, hemoglobin, and γ-globulin in two different buffer solutions (pH 4.5 and 8.0) [35]. Later, the performance of an El-FFF channel with flexible membranes [36], a channel with rigid membranes [256], or a circular channel [260] for the separation of proteins were described. In these studies, human and bovine serum albumin, γ-globulin (bovine), cytochrome C (horse heart), lysozyme (egg white) and soluble ribonucleic acid (t-RNA), as well as denaturated proteins, were successfully separated.

Dielectrophoresis in combination with fluid flow through an open chamber with interdigitated sinusoidally corrugated electrodes was used for the separation of proteins and DNA [382].

Pressure-FFF was found to be suitable for the fractionation of blue dextran and human plasma in a circular semipermeable capillary, 0.2 cm in diameter [37], whereas magnetic-FFF was applied to the study of the retention behavior of bovine serum albumin in the presence and absence of nickel nitrate [45]. In the presence of nickel(II) ions, the retention time of the BSA sample was 6% higher with the magnetic field than it was without the field while the retention times reported for BSA samples both with and without a magnetic field in action did not differ in the absence of nickel(II) ions.

3.2 Colloids

3.2.1 *Synthetic Colloids*

3.2.1.1 S-FFF

S-FFF can be most advantageously applied to address questions related to colloids. The fractionation according to the particle size and particle density is not necessarily problematic but can be turned into an advantage either by seeking independent size information or by a proper design of the experimental conditions. In a trilogy of papers from 1983, Giddings et al. explored the capabilities and methodology of colloid characterization by S-FFF for the investigation of monodisperse samples [81], particles having size distributions [130] and emulsions [383]. Apart from polystyrene latexes, which are the most common standards for particle sizing techniques, polymerized serum albumin microspheres. [183,384], polychloroprene [6,384], poly(methyl methacrylate) [6], poly(vinyl chloride) [130,190], poly(glycidyl methacrylate) [131], poly(vinyl chloride) [130] and polychloroprene [6] latexes have been fractionated.

Apart from latexes, S-FFF has been used to fractionate and determine the size distribution of numerous industrial colloids including water-based titanium dioxide dispersions [6,171], carbon black dispersions [6], phthalocyanine blue [6], various silica sols [141,171,176], gold and silver sols [385], pigments, metal and ceramic particles, clay and a host of latexes [294]. Gold, palladium, silver and copper particles in the size range 0.3–15 μm were separated by steric-S-FFF and their size distributions determined in less than 12 min [69].

Similar studies which adress colloidal phenomena like aggregation were reported [386]. For a partially aggregated poly(methyl methacrylate) latex, singlet, doublet and triplet particle clusters could be cleanly resolved. Remarkably, there were two detected doublet peaks that differed by ~10% in mass suggesting a two-stage latex growth process, the lighter doublets forming after first-stage growth and the heavier doublets after the second stage (see Fig. 29). These observations were confirmed by electron microscopy. Other studies on aggregated PMMA latexes [387] and other colloids have also been reported [16,251,388,389].

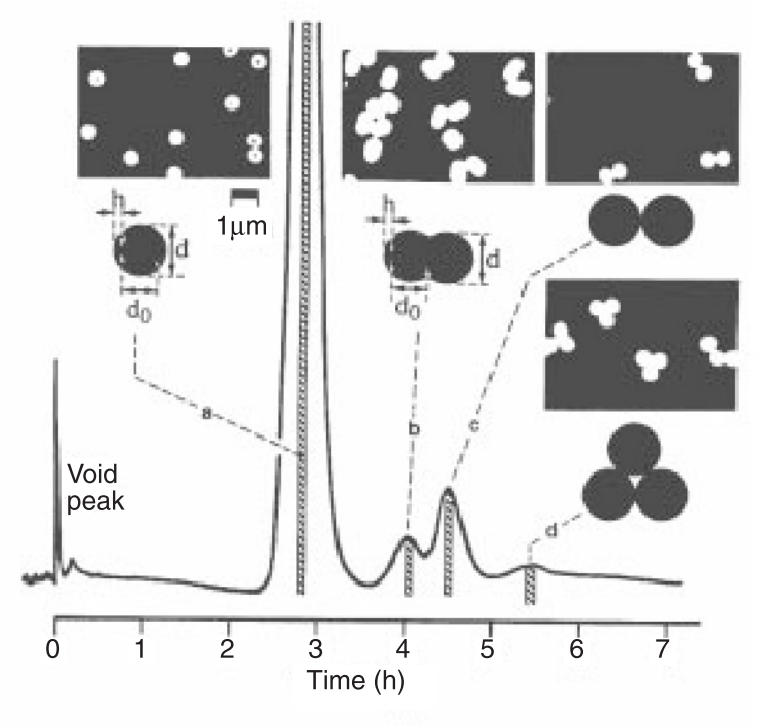

Fig. 29. Separation of components of partially aggregated latex by S-FFF. Reproduced from [386] with kind permission of the American Chemical Society

Li and Caldwell used S-FFF to determine the mass and surface concentration of absorbed PEO-PPO-PEO triblock copolymers (Pluronics) onto PS latex standards [185]. Fl-FFF was found to work equally well for this problem. As experimental absorption problems are widespread and extremely relevant, it is expected that FFF will play an important future role in such studies, as long as the mass of the absorbed layer is sufficiently high.

Another promising application of S-FFF is the characterization of emulsions and S-FFF is used as the standard technique for emulsion characterization in some laboratories [390]. Manifold emulsions or organelles have been fractionated with S-FFF [75,383,391–396] including perfluorocarbon blood substitutes [391].

Other reported applications of S-FFF include the characterization of samples of environmental samples like diesel exhaust soot [384]. The first successful experimental implementation of focusing-S-FFF fractionated a mixture of polystyrene latex with poly(glycidyl methacrylate) latex differing in density which was eluted with Percoll as the carrier fluid [309].

3.2.1.2 Th-FFF

Colloid characterization is not the classical application of Th-FFF. Nevertheless, Th-FFF was first applied to silica particles suspended in toluene testing a correlation between thermal diffusion and thermal conductivity [397]. Although a weak retention was achieved, no further studies were carried out until the work of Liu and Giddings [398] who fractionated polystyrene latex beads ranging from 90 to 430 nm in acetonitrile applying a low ΔT of only 17 K. More recently, polystyrene and polybutadiene latexes with particle sizes between 50 μm and 10 μm were also fractionated in aqueous suspensions despite the weak thermal diffusion [215] (see Fig. 30). Th-FFF is also sensitive to the surface composition of colloids (see the work on block copolymer micelles), recent effort in this area has been devoted to analyzing surfaces of colloidal particles [399,400].

3.2.1.3 Fl-FFF

Many papers report the fractionation of polystyrene latexes or mixtures thereof, as such commonly available spherical latex standards are an ideal system to test FFF setups or evaluations (for an example, see [362,401]). Recent coupling of Fl-FFF to MALLS enables a very high precision in particle size determinations. One example is shown in Fig. 31, where two Duke standard latex batches of a nominal size of 100 nm were investigated by Fl-FFF/MALLS, underlining both separation power and resolution. Using traditional techniques such as photon correlation spectroscopy (PCS) and classic Fl-FFF detection, these samples seem to be identical. However, with Fl-FFF/MALLS, the batches could be separated as two discrete size distributions with a peak size that differed by 3 nm. However, it is not stated if a precise temperature control was maintained so that, critically considered, the observed differences could also have their origin in slight temperature

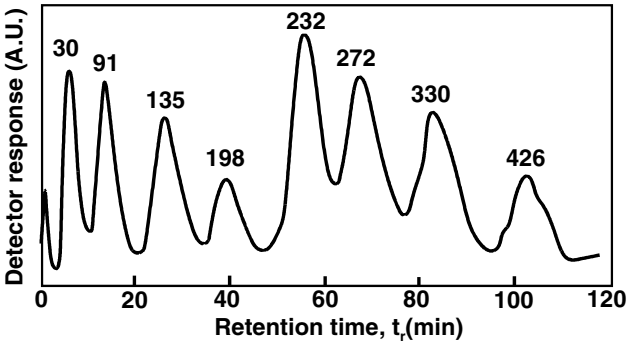

Fig. 30. Separation of eight polystyrene latex particles in aqueous suspension by Th-FFF. The numbers above each peak correspond to the particle diameter in nm. Reproduced from [215] with kind permission of Elsevier Science Publishers

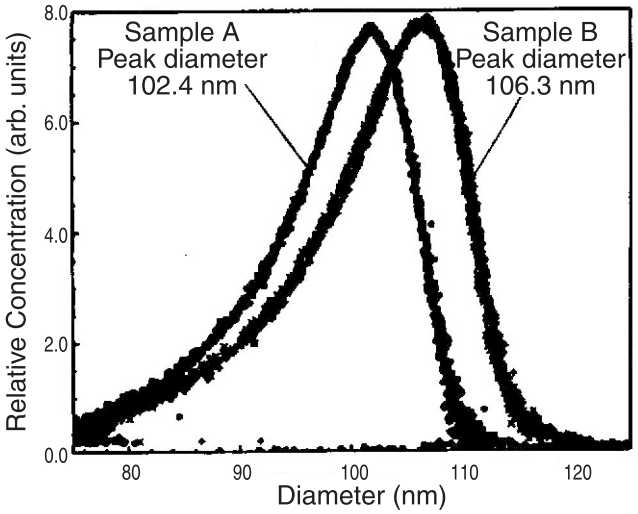

Fig. 31. Fl-FFF-MALLS particle size distribution for two Duke standard latexes of nominal size 100 nm but from two different batches. Reproduced from [374] with kind permission of John Wiley and Sons

differences between the measurements. Unfortunately, no information about the reproducibility of a measurement on an identical sample was given.

Other colloids which have been fractionated and characterized by Fl-FFF include colloidal silica of 10–130 nm diameter [242] or down to 2 nm [17], Xylophene (emulsion), Stabisol (silica sol), Ludox (colloidal silica) and emulsion paints [237].

Complex colloids can be characterized advantageously by a combination of Fl-FFF with different analytical or other FFF techniques, yielding supplemental information. Examples reported in the literature are combinations of Fl-FFF and S-FFF for size (Fl-FFF) and density (S-FFF) as well as the thickness and density of the shell of core shell latexes [402], El-FFF for the charge and composition of emulsions [403], Th-FFF for the characterization of the size and composition of core shell latexes [404] and, finally, with SEC for the particle size distribution and stoichiometry of gelatin complexes with poly(styrene sulfonate) and poly(2-acrylamido-2-methylpropane sulfonate) [405].

3.2.1.4 Other FFF Techniques

Colloid characterization by El-FFF has been attempted. First trials of the separation of polystyrene latexes were not successful as the samples were strongly adsorbed when an electrical field was applied, while the fraction of adsorbed particles increased at greater field intensity [36]. With the improved El-FFF channel working with lower electrical fields, uncoated and protein-coated poly-

styrene latexes and mixtures thereof could be characterized [257]. As the relaxation of the highly charged PS latex standards occurs rapidly (within minutes or less) in El-FFF, it was suggested that this method could be a convenient means to gain insight into the early phase of adsorption reactions which was later experimentally verified for absorption of Pluronic F108 onto a PS latex [406]. Even minor amounts of adsorbed polymer were found to significantly change the retention behavior of the particle in El-FFF.

Magnetic-FFF was applied for the fractionation of iron oxide particles (Fe_2O_3) suspended in acetonitrile [273,274] but only with poor resolution. The effect of the surface modification of Fe_2O_3 particles by the addition of a surfactant in a magnetic field has been studied [274].

3.2.2
Natural Colloids

3.2.2.1
S-FFF

One important application of S-FFF is the fractionation of natural colloids in river water which exhibit a very broad particle size distribution [407,408]. These studies show that different river sources exhibit different size and mineralogy distribution patterns, which are characteristic for the river source. For such investigations S-FFF is used to provide fractions, and these fractions are investigated by further techniques to yield the morphology by EM, elemental content by energy-dispersive X-ray analysis, and mineralogy by X-ray diffraction, to name just a few. By using S-FFF, twenty or more fractions in the size range 0.1–2 μm can be generated in 60 to 100 min, whereas traditional centrifugation or ultrafiltration procedures take days. Modern on-line coupling of FFF and inductively coupled plasma MS has simplified and improved the sensitivity of measuring elemental profiles for different particle sizes [150]. Despite the above characterizations, it is often important to address pollutant adsorption onto the colloids in the river water to understand the transport mechanisms of these pollutants. Colloids from soils, for example, are thought to play a major role in the transport of pollutants through soil profiles and ground waters [409]. Such questions can be addressed if the particle size distribution is known and, thus, S-FFF delivers the amount and surface density of adsorbed materials across the particle size range of colloids [410]. S-FFF has also been applied to the characterization of liposomes [184,384,411,412].

3.3
Particulate Matter

Due to the size of these particles (>1 μm) most applications described in this section apply steric- or hyperlayer-FFF if not stated otherwise. Furthermore, the transition between colloids and particles is not strictly defined so that some experiments are described in the section about colloids, others here in this section.

3.3.1 *Synthetic Particles*

3.3.1.1 S-FFF/Gr-FFF

For particle sizes >1 μm, natural gravitation suffices for separation. A simple Gr-FFF apparatus has been utilized for particles larger than 1 μm [413–422]. Steric-Gr-FFF was applied to separate large polystyrene latexes up to 100 μm in diameter [299], residues from coal liquefaction [423] and fine coal particles [424]. The Gr-FFF channel in combination with a standard HPLC setup is furthermore already being used for an effective determination of the particle size distribution of spherical and irregular chromatographic silica particles in the range 4–7 μm [422]. Information about the porosity of such chromatographic silicas can be obtained by coupling the information from S-FFF with an independent technique for particle size determination, such that the S-FFF data deliver the particle density and thus their porosity. This was demonstrated for a combination of S-FFF/steric-S-FFF and microscopy to evaluate the particle density of fractions of chromatographic supports (d=2–12 μm) [425].

Steric-S-FFF has also been used for numerous fast fractionations including gold, palladium, silver and copper particles in the size range 0.2–15 μm [69,294,385], alumina, low-porosity 7–65 μm poly(vinyl chloride) latex [426] or quartz [427]. Many of these samples were fractionated in times of only 1–5 min.

3.3.1.2 Fl-FFF

One important application of Fl-FFF is the determination of the particle size distribution of chromatographic silica for HPLC packings [226,428,429] which, in combination with S-FFF, allows characterization of the porosity of the samples and particle size distribution.

S-Fl-FFF and A-Fl-FFF were found to be suitable techniques for the characterization of paint components, namely pigments, binders and fillers with their very broad and overlapping size distributions [70]. Both normal FFF and the hyperlayer-FFF mode could be successfully applied.

3.3.2 *Natural Particles*

3.3.2.1 S-FFF

Many environmental samples are particularly well suited for S-FFF or Gr-FFF due to their large sizes, and many successful fractionations of such samples have been reported, including silt-sized particles and river-borne particulates [377], as already discussed in the section on colloids. Another promising application is

the fractionation of subcellular biological compartments. For example, streptococcal cell wall fragments were investigated [430], and the collected fractions were further investigated by PCS. However, differences between the results obtained by the two methods were observed and attributed to the sensitivity of the QELS method to the shape of particles measured. Other examples of successfully analyzed subcellular particles include mitochondria and microsomes [431] or cell wall fragments by coupling S-FFF to gas chromatography-mass spectrometry (GC-MS) [432].

Many samples of interest for medical applications can be fractionated and characterized by S-FFF. Reported examples include viral aggregates (singlets, doublets, and so forth) of the gypsy moth nuclear polyhedrosis virus [433], protein particles including those responsible for optical clouding in cataractous human lenses [434], and for the size determination of the Kreutzfeldt–Jakob disease agent [435]. Other successfully fractionated samples of natural origin are wheat, corn and oat starch granules [436], 2–70 μm starch granules [426] or clays [156].

3.3.2.2
Fl-FFF

Lipoproteins which are difficult to investigate by techniques relying on the particle density as well as on the particle size (S-FFF, ultracentrifugation, etc.) can be successfully separated by Fl-FFF which yields the particle size distribution of high, low and very low density lipoproteins [437,438]. Furthermore, Fl-FFF has been used to fractionate ground minerals by size [439].

3.4
Other Samples

3.4.1.1
S-FFF

S-FFF has been applied for the separation of living cells such as human, sheep, rabbit, and horse blood cells or HeLa cells [12,296,420,440–444] which, furthermore, could give insight into the growth and cell cycle distribution of cells in cultivation broths [444] or an estimation of the bacterial biomass in natural waters [445]. Blood components have been separated in the same apparatus [446]. Cardot, Martin, and co-workers have shown that abnormal blood cells (from anemia or transfusions) can be distinguished from healthy erythrocytes in Gr-FFF [413,415]. In such channels, a prevalent parasite can be isolated from blood, suggesting a possibility for rapid diagnosis [414].

Another sample class that is well separable by S-FFF are viruses [182,433]. Molar masses were determined [80,433,447] including T2 bacteriophage [80,171,174], R17 *E. coli* bacteriophage [31] and the T4D virus, for which it was shown that the infectivity of the virus remained essentially unaffected by its passage through the FFF channel and detector system.

Furthermore, S-FFF has been applied to nuclear-energy-related materials [448,449] and Gr-FFF for residues from coal liquefaction processes [423].

3.4.1.2 Th-FFF

Giddings et al. applied a pressurized Th-FFF channel to increase the temperature range of Th-FFF and used very high temperature gradients (up to $\Delta T = 158\ ^{\circ}C$) for the extension of this FFF technique to lower molar mass samples. This allowed the successful separation of several crude oils and asphalts [200] as well as asphaltenes [450].

3.4.1.3 Fl-FFF

Fl-FFF, in the lift-hyperlayer mode, was applied for the high-speed (2 to 3 min) fractionation of normal and abnormal erythrocytes from various species [12] as illustrated in Fig. 32. Furthermore, various viruses were successfully separated including bacteriophage Qβ, MS2, f2 and ϕx174 [231,241].

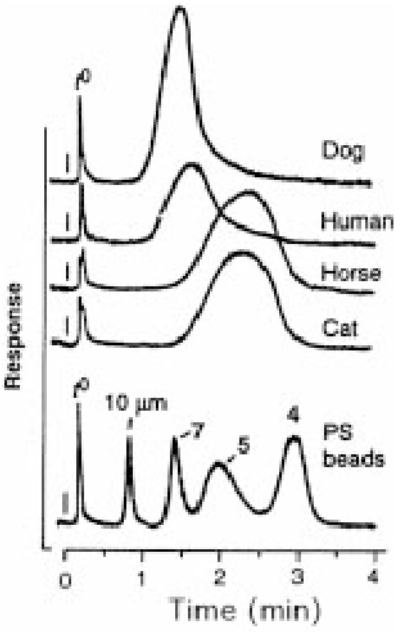

Fig. 32. Separation of different mammalian red blood cells and polystyrene latexes of the indicated diameters by hyperlayer-Fl-FFF. Reproduced from [12] with kind permission of the American Chemical Society

3.4.1.4 Other FFF Techniques

A hybrid technique of FFF and adhesion chromatography was used to study the rapid biological kinetics of cell surface adhesion of B and T lymphocytes to HA13 surfaces. Since cell adhesion is critical in many areas, including cancer metastasis and thrombosis research, a tool for the study of adhesion kinetics is highly desired [332]. Cells [281] and yeast cells [451] were successfully separated by DEP-FFF.

SPLITT-FFF has been applied in environmental studies and oceanography [452,453] for fractionating water samples into a number of fractions which were then analyzed by other methods.

Coal fly ash [335] was fractionated on a preparative scale by the technique of continuous steric-FFF.

4 Possibilities and Limits

In this section, recent developments of the FFF methodology are presented which might have a significant impact on the possibilities of FFF separations. On the other hand, problems which are associated with FFF measurements in general are discussed. These problems and possible artifacts have to be kept in mind when interpreting FFF results, regardless of the technique or detection system used.

4.1 Advantages of FFF

The main advantages of FFF measurements include: speed (from a few minutes to few hours); the small quantity of material required (typically: 10 μL of a 1 wt% solution corresponding to 100 μg sample) and the fractionating power which makes FFF suitable for impure and mixed species. Further advantages are the minimal effort needed for sample preparation and the possibility of sample recovery in order to take fractions after separation since FFF is generally a non-destructive method.

The application range of the FFF family is wider than that of any other analytical method for the characterization of particle sizes or molar masses and includes macromolecules in solutions, emulsions and particles in suspension: the accessible molar mass for macromolecules extends from 10^3 to 10^{18} g/mol, a size range for particles from 1 nm to 100 μm. Even very complex mixtures with components spanning many orders of magnitude of particle sizes and molar masses can be successfully characterized. A particular advantage, mainly exploited in Th-FFF and Fl-FFF, is the absence of shear degradation as ultrahigh molecular weight polymers are only exposed to gentle tangential shear forces with the possible exception of higher shear forces at the inlet valve which needs to be considered.

4.2
Problems and Potential Pitfalls

As in every analytical measurement, one must be aware of the problems or potential weaknesses of an FFF measurement as well as of sources of experimental artifacts. There are a number of studies which have investigated theoretical predictions and the experimental results and pointed out error sources which lead to deviations between experiment and theory.

4.2.1
Experimental Artifacts

The numerous reasons which can account for various deviations from the ideal FFF retention theory were discussed in the corresponding sections. Here, additional problems are treated which can complicate FFF measurements and significantly distort the results obtained. General requirements for a successful FFF measurement include precise flow control and flow rate; precise temperature measurement; precise determination of t_0 and t_r; correct relaxation procedure; control of sample overloading and integrity and control of mixed normal and steric retention effects as well as wall adsorption control. Some of these complications cannot be avoided so one must correct for these effects, usually in a semiempirical and partially very complicated fashion.

On the other hand, the average FFF experiments are not designed to vary the numerous parameters which detect deviations from the ideal behavior. Therefore, the user will often not be aware of the complicating phenomena and thus get erroneous results. Hence, it appears necessary to routinely run several experiments with the same sample under varying conditions to get correct physicochemical quantities. This is a severe disadvantage which spoils the picture of FFF being a very fast and convenient absolute technique.

4.2.1.1
Artifacts Due to Sample Non-idealities/Overloading

Transport properties like the diffusion coefficient of polymers and particles depend in part drastically on the sample concentration. For random-coil polymers, the effect of concentration is especially large near the critical overlap concentration c^* [454]. In the semidilute regime, polymer coils interact and tangle with one another so that their transport through a solution is limited and, consequently, the magnitude of the diffusion coefficient drops dramatically. The higher the molecular weight and the better the solvent quality, the lower is c^*. According to these considerations, it is important to keep the polymer concentration within the channel below c^* so that diffusion and thus retention is not influenced. Above c^* overloading effects occur, such as peak "fronting", and a shift towards higher retention volumes. Excessive overloading can even result in additional peaks at higher retention volumes, probably due to polymer entan-

glements and aggregation. To estimate if the applied polymer concentration is below c*, one can calculate the sample concentration c_0 at the accumulation wall which is the highest sample concentration in the channel. Practically, c_0 can be related to the injected concentration c_{inj} by [121]:

$$c_0 = \frac{c_{inj}}{\lambda\left(1-\exp\left(-1/\lambda\right)\right)} \cong \frac{c_{inj}}{\lambda} \tag{94}$$

Substituting c_0 by the critical concentration c* in Eq. (94) gives:

$$c_{inj,max} \cong c^{*}\lambda \tag{95}$$

The maximum injectable concentration will be somewhat higher than that predicted by Eq. (95) due to zone broadening which occurs immediately after injection with consequent dilution of the sample. If it is impossible to inject concentrations below $c_{inj,max}$ due to an inadequate detection limit, or if this value is unknown, the injected concentration must be varied and the elution profiles examined in order to trace indications of sample overloading. For example, in the analysis of high molecular weight polymers ($>1\times10^6$ g/mol), concentrations below 1 mg/ml are usually required to prevent overloading. In the case of detection problems at sample concentrations below the overload concentration, especially in the case of broad distributions, the outlet stream can be split by a stream splitter (see Fig. 12 for the inlet analogon) which concentrates the outlet stream and leads to improved detector response [165,246].

The effect of sample overloading is reported to be different for the various FFF techniques. In S-FFF, sample overloading leads to earlier elution with a tailing peak shape [57]; for polymers in organic solvents, the overloading effect is opposite [121] while, for Fl-FFF, overloading results in completely distorted peaks [232] or in later sample elution [231]. This effect, however, is strongly dependent on the ionic strength of the carrier liquid. At low ionic strengths, overloading results in earlier elution whereas, at high ionic strengths, the opposite is observed [455].

Beside overloading effects, charge interaction effects play an important role in the retention behavior of polyelectrolytes [243]. In such cases, a strong dependence of the retention data on the concentration and volume of the injected polymer sample can also be observed. This phenomenon related to intermolecular interactions complicates quantitative evaluation of distributions from FFF retention data. Such effects can be partly suppressed by the addition of an electrolyte but investigations of polyelectrolytes are still complicated. Other sample–sample interactions can significantly change the effective size of the polymer and thus also its retention behavior [456]. Such interactions are common with biopolymers as they are very often part of their biological function.

The three effects mentioned above, overloading, charge effects and solute–solute interactions, were observed experimentally for various FFF techniques

early on [171,194,241] but have not as yet been satisfactorily included in the retention theory of FFF.

4.2.1.2 Solvent Effects

The carrier liquid can also influence the FFF results as it can alter solute–solute or solute–wall interactions as well as the extension of a polymer in solution [266]. This in turn influences the diffusion and retention of the sample. Limited efforts have been made to describe these phenomena so that their influence still cannot be quantitatively treated. The practical importance of solvent effects becomes clear for the example of proteins which can be switched from positive to negative polyelectrolytes by pH variation. In any case, the pH should be chosen outside the range of the isoelectric point to avoid adsorption problems.

4.2.1.3 Sample–Wall Interactions

There are many forces which can account for the interaction of a sample with the accumulation wall. Numerous electrostatic, colloidal or other forces, both of attractive and repulsive nature, influence the interaction of the sample with the wall. These effects are summarized under the term "wall effects". Recently a correction for such wall effects was presented in terms of a semiempirical correction parameter [457]. It is however not easy to determine whether or not such effects disturb the results of a particular FFF measurement. Only measurements under different conditions and with different sample concentrations and solvent compositions can show an alteration of the retention behavior caused by such wall effects.

The other important class of solute–wall interactions are the repulsive forces which are generated when a particle is driven towards the accumulation wall equal to the particle radius. This "steric exclusion" effect leads to an earlier elution of the particle [67].

A third class of solute–wall interactions is the sample adsorption to the accumulation wall which may become particularly problematic in Fl-FFF since the accumulation wall consists of a membrane. The severity of adsorption differs significantly among the limited number of membranes that have been used in Fl-FFF, so that as additional membranes are explored, one can expect improvements. A number of membranes has been tested for use for Fl-FFF with respect to sample adsorption including polypropylene, polysulfone, several supported regenerated celluloses and their derivatives and polycarbonate membranes [166]. The extent of sample adsorption obtained with the wrong membrane material is demonstrated in Fig. 33.

Sample–wall interactions may also be encountered with all other FFF techniques. The sample interaction with the accumulation wall can become a problem especially if thin channels are used to shorten elution times and to improve efficiency. For such cases, a rinsing procedure has been suggested [455].

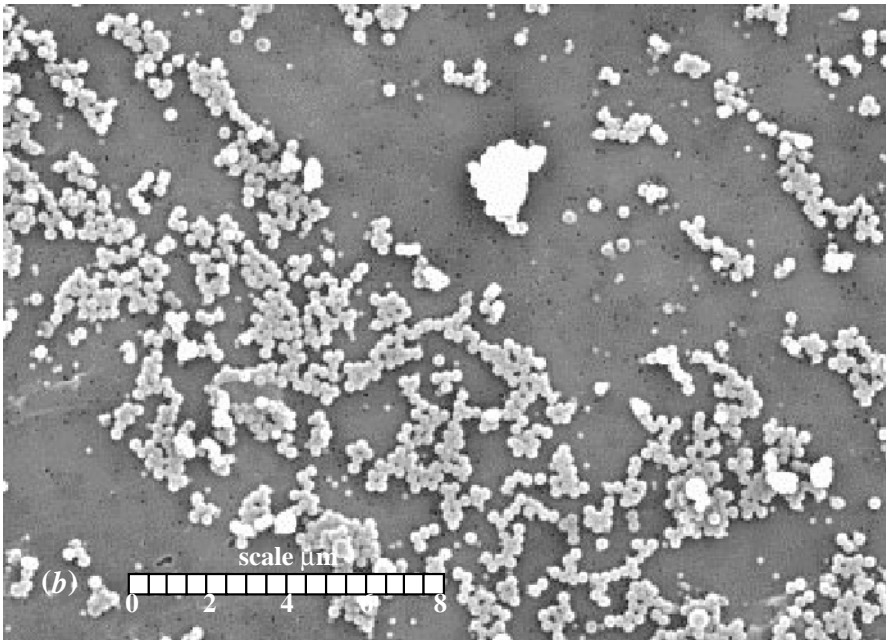

Fig. 33. SEM micrograph of a polycarbonate Fl-FFF membrane after the fractionation of a mixture of 121, 265 and 497 nm polystyrene standards. Reproduced from [166] with kind permission of the author

Another source of deviations to the ideal behavior is the smoothness of the channel surface which, in reality, is hardly perfect. The surface quality affects substantially both retention and zone dispersion. Smith et al. [223] illustrated this fact experimentally for Th-FFF. Dilks et al. [458] studied experimentally the effect of sample injection and flow pattern on the zone shape inside the channel by performing measurements in a transparent channel and photographing the colored zones formed under various conditions of injection, flow, and geometric channel irregularities. One important result was that even apparently minor channel irregularities can give rise to considerable distortion of the zone formed. In Fl-FFF, the membrane is the critical parameter as ideally it has to fulfill the requirements of pressure and mechanical stability, even surface, uniform pore size, inert behavior with respect to solvent and samples and sufficient counter pressure to achieve smooth and uniform flow rates. A membrane fulfilling all the above requirements does not exist so that the choice of a membrane for Fl-FFF is always a compromise and depends on the analytical problem. In addition, for all other FFF techniques, the surface quality, in particular the smoothness of the channel accumulation wall, substantially affects both retention and zone dispersion. Smith et al. [223] illustrated this fact experimentally for Th-FFF.

4.2.1.4 Field Programming

When using field programming, serious alterations to the retention behavior can be induced. For example, due to the initially strong fields used in programming, high molecular weight components are severely compressed early in the experiment, which can lead to chain entanglement. Therefore, when deriving quantitative information from the elution profile, it is important to change the field programme, sample concentration, or carrier flow to verify the derived distribution function of the measured quantity.

In the case of Fl-FFF, cross-flow programming may be accompanied by a "threshold" migration effect. This effect is represented by an abrupt and total cessation of zone migration when the cross-flow rate exceeds a certain threshold value, and is only poorly understood. However, the immobilization appears to reversible. In one such study [165], three poly(styrene sulfonate) standards ranging in molecular weight from 4×10^4 to 1.3×10^6 g/mol were immobilized in a Fl-FFF channel for 16 h. After the initiation of a field-decay program, the polymers were immediately released and eluted with near-baseline resolution.

4.2.1.5 Other Problems

Litzén and Wahlund systematically studied error sources like temperature effects, sample overloading, sample adsorption to the accumulation wall membrane and influences of the carrier liquid composition, that occur with Fl-FFF [455]; the latter has already been discussed above. It was shown that preservation of constant channel temperature is very important as repeated measurements of an identical sample resulted in gradually decreasing retention times due to increasing channel temperature caused by frictional heat, especially when using high flow rates. As constant channel temparature is usually not fulfilled with the standard Fl-FFF channels, which simply operate at room temperature without any temperature control, this is an important point to consider.

Non-uniform field strengths can also affect FFF results. For example in S-FFF, the centrifugal field strength inside the channel is heterogeneous due to finite channel thickness and thus different distance from the axis of rotation [105]. However, as the channel thickness is usually many times less than the radius of its coiling, this influence is negligible but will come into play if rotors with smaller diameter are designed. For El-FFF the generation of a uniform field can be a problem.

Another experimental artifact of FFF is the occurrence of "ghost peaks". Granger et al. speculated for the case of A-Fl-FFF that such peaks can occur if the sample does not reach its steady state concentration distribution and is thus transported by pure convection in the flow field which can occur at high flow rates [248]. The other peak is that for the separation by diffusion and fits well with theory.

A further experimental problem is caused by the action of hydrodynamic lift forces in A-Fl-FFF. As the mean carrier fluid velocity varies along the channel length in the rectangular channel geometries, the equilibrium positions of the particles also vary. Hence conditions may be encountered where the carrier velocity close to the outlet of a rectangular A-Fl-FFF channel falls to such a low level that lift forces are unable to counter the drag of the flow through the membrane. These particles then make contact with the membrane and do not elute [250].

4.2.2 Zone Spreading

As in every transport-based fractionating technique, zone spreading of the concentrated sample zone must occur in FFF due to the generated concentration gradient which causes diffusion according to Fick's law. Therefore, the width of a peak in an FFF fractogram consists both of the polydispersity of the sample and zone spreading due to diffusion. It is clear that significant overestimations of the sample polydispersity can be made especially if the samples are small and thus have high diffusion coefficients. In methods which study time-dependent transport processes via snapshots at a fixed time, like sedimentation in an analytical ultracentrifugation cell, a correction for zone broadening due to diffusion is possible.

In FFF, however, the fractogram is recorded in dependence of time so that a correction via extrapolation to infinite time in order to eliminate diffusion effects is not possible. A different strategy may be used for the correction of zone spreading which suffers from a number of assumptions and restrictions. A number of authors, reviewed by Janca [459], have dealt with the methods of correction for zone spreading which was found to be particularly extensive at high flow rates or low retentions. The results are summarized below.

An FFF fractogram represents the dependence of the detector response h(V) on the retention volume V. The value of h(V) at every point of the fractogram is the sum of the relative concentration of a fraction in this retention volume and of spreading contributions of the neighboring fractions of the separated solute. A relation between the experimental fractogram h(V) and the fractogram corrected for zone spreading g(Y) is given by Eq. (96).

$$h(V) = \int_{-\infty}^{+\infty} g(Y)G(V,Y)dY \tag{96}$$

where G(V,Y) is the spreading function, whose physical meaning can be explained as the zone broadening caused in the separation system and diffusion processes.

There are at least two significant contributions to the separation system: The first is the channel geometry which influences the flow patterns. Giddings et al. [89] reported, theoretically and experimentally, the intrachannel contributions to zone dispersion appearing in the triangular end pieces of an FFF channel re-

sulting in a process where parts of the solute zone follow flow paths of different lengths. The second contribution is caused by extra-channel elements of the separation system such as the injector, the detector cell, and the tubing connecting between the channel and the separation system. These contributions cannot be excluded but they must be minimized.

Equation (96) can analytically be solved only for a uniform spreading function which is a severe restriction. In such cases Eq. (96) becomes a convolution integral:

$$h(V) = \int_{-\infty}^{+\infty} g(Y) G(V - Y) dY \tag{97}$$

For many cases, especially if the spreading is small, the spreading function can be approximated by the normal Gaussian distribution function G in the form:

$$G = \left(\frac{1}{2\pi\sigma^2} \right)^{1/2} \exp\left[-\frac{(V - Y)^2}{2\sigma^2} \right] \tag{98}$$

where σ is the standard deviation of the spreading function. Its magnitude is very often considered to be constant within a very limited range of elution volumes meaning practically that Eq. (98) can be used for narrowly distributed samples only. For samples with wider distributions, a non-uniform spreading function can be used:

$$h(V) = \int_{-\infty}^{+\infty} g(Y) \left[\frac{1}{2\pi\sigma(Y)^2} \right]^{1/2} \exp\left[-\frac{(V - Y)^2}{2\sigma(Y)^2} \right] dY \tag{99}$$

which can be approximated and solved numerically by:

$$h(V) = \left[\frac{1}{2\pi\sigma(Y)^2} \right]^{1/2} \int_{V_i}^{V_f} g(Y) \exp\left[-\frac{(V - Y)^2}{2\sigma(Y)^2} \right] dY \tag{100}$$

V_I and V_f are the initial and final retention volumes between which the integration of experimental fractograms is performed.

The dependence of $\sigma(Y)$ for FFF can be calculated from the theoretical equation:

$$\sigma(Y) = \left[\frac{\chi(\lambda) w^2 < v(x) > L}{D} \right]^{1/2} \tag{101}$$

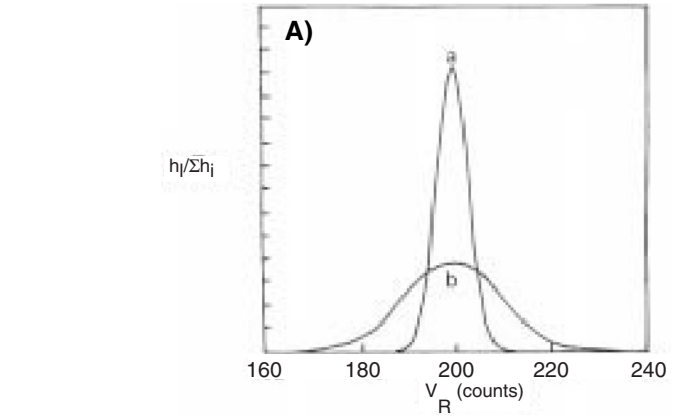

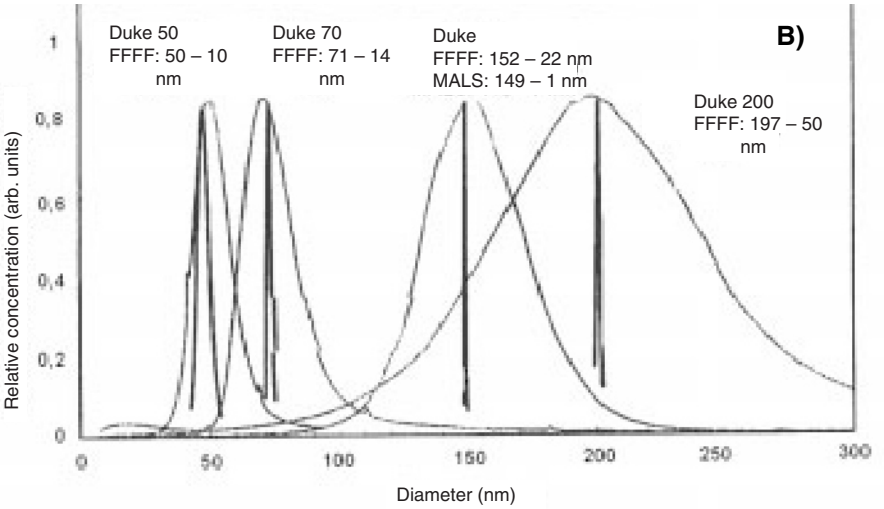

Fig. 34.A Correction for zone broadening of a model fractogram. *a* represents the original curve and the corrected one whereas *b* is the uncorrected fractogram. Reproduced from [460] with kind permission of the American Chemical Society. **B** Comparison of differential particle size distributions of narrowly distributed polystyrene latex standards derived by MALLS and Fl-FFF without correction for zone broadening. Reproduced from [461] with kind permission of Academic Press

where $\chi(\lambda)$ is a dimensionless parameter which depends on λ in a complex manner. If $\lambda \to 0$, then $\lim_{\lambda \to 0} \chi = 24\,\lambda^3$ [34] and if $\lambda \to \infty$, $\lim_{\lambda \to \infty} \chi = \frac{1}{105}$ [347].

The efficiency of the presented correction method was verified on model fractograms for different conditions. A very good correlation between the original distribution and the corrected fractogram was found for simulated data. The ne-

cessity of a correction for zone dispersion can be seen in Fig. 34 where corrected and uncorrected model fractograms are shown together with the known distribution. Figure 34B, in particular, shows the dramatic effect of band broadening.

4.2.3 *Elution of Non-Spherical Samples*

Steric hyperlayer-FFF is well established as a fast separation technique for micron-sized particles, although the hydrodynamic lift forces are not yet well understood. This is worse for the steric elution of non-spherical particles. Despite over thirty years of application of FFF techniques, only very little has been reported about the fractionation of non-spherical particles by any FFF mode. The few available studies so far reported are the investigation of coal particles [423,424], inorganic colloids [462], metal particles [69] and doublets of polystyrene beads, rod-shaped glass fibers, compressed latex discs and quartz particles with complex shape [427]. In the latter paper, systematic studies of particle shape on the retention behavior of non-spherical particles are reported with the result that the qualitative major retention behavior of spheres and other shapes is equal (e.g. response to increase in the field strength, etc.). However, the quantitative differences in the retention behavior were found to depend on numerous factors in a complex way so that no quantitative relation between the hydrodynamic radius and the retention ratio could be established.

In a recent paper, Beckett and Giddings have extended the general retention equation for the normal and steric FFF mode to include an entropy contribution associated with the orientation of non-spherical particles during the elution process [463]. The result is an increase in the mean cloud thickness l which results in an earlier elution of the sample. Interestingly, it was stated that the normal mode of S-FFF is thought to be independent of particle shape whereas some shape dependencies could be expected for Fl-FFF although the discussed entropic contributions on particle retention should be applicable to any FFF technique. Nevertheless, the independence of the normal S-FFF mode on the particle shape for moderately sized samples (axial ratio <10) was experimentally confirmed by results of Kirkland et al. [464]. They showed that for S-FFF, the shape of separated particles has only a negligible effect on retention and zone dispersion. Only with an extreme axial ratio does the dependence of retention on flow rate change. This was reported to be caused by the orientation of such particles in the flow gradient of the carrier liquid (e.g. rod-like λ-DNA [464]). As a convenient solution, a fractionation at low flow velocities was suggested at which no marked orientation of separated particles in the flow gradient should occur. Nevertheless, the entropic contributions are still likely to influence retention under these conditions as they are based on limited rotational freedom degrees near the accumulation wall [463].

Provided that the particle dimensions are known from other sources (microscopy etc.), equations were derived to correct the retention ratios for these entropic effects [463]. Nevertheless, the distortion of the elution of non-spherical

particles due to entropic contributions was also found for the normal mode in A-Fl-FFF [128]. Here, well-characterized proteins and polysaccharides of defined shapes ranging from spherical to highly elongated structures were examined by A-Fl-FFF and AUC. Whereas the shape was correctly obtained by AUC, A-Fl-FFF yielded significantly too high diffusion coefficients in the case of the elongated structures. The effect was found to increase with increasing elongation of the solute. These results confirmed the theoretical predictions of Gajdos and Brenner [88].

That no indication of the significant influence of particle shape on FFF elution behavior has been published until recently may be attributed to the fact that the majority of the approximately 500 papers so far published have reported on spherical or nearly spherical samples, and that the studies on the non-spherical samples focused only on sample fractionation rather than on a quantitative assessment of physicochemical quantities. This problem can be solved if fractions from FFF are further characterized, for example, by dynamic light scattering or if an independent detector for diffusion coefficients is available.

4.3 Recent Developments

The last few years have seen significant developments in the Fl-FFF technique with respect to increasing its application range for organic solvents, accessible physicochemical quantities (FFF/MALLS) or instrument design (frit inlet-outlet Fl-FFF). Parallel to these developments, the application of Fl-FFF as an analysis technique has increased, possibly catalyzed by the commercial availability of S-Fl-FFF as well as A-Fl-FFF channels of different designs. For other FFF techniques, instrumentation has been more or less unmodified with the exception of El-FFF so that, in the next section, only improvements to Fl-FFF are discussed. The development of the other FFF techniques is discussed in Sect. 2.

4.3.1 *Fl-FFF for Organic Solvents*

Fl-FFF is the most flexible of the FFF techniques as it is based only on the sample diffusion coefficient. Hence it was conclusive to optimize the materials used for the construction of Fl-FFF channels so that non-aqueous solvents could be applied as well. Here, the selection of a suitable membrane is the biggest problem. Brimhall et al. were the first to apply Fl-FFF for the separation of polymers in non-aqueous solvents [365]. They separated polystyrenes ($M=2.0\times10^4$–1.8×10^6 g/mol) in ethylbenzene using a cellulose nitrate membrane. Other papers on Fl-FFF using organic solvents followed from the Giddings group [121,465].

An A-Fl-FFF channel was described by Kirkland and Dilks [367] where the glass plate as the upper wall, in principle also suitable for organic solvents, was replaced by a stainless steel metal plate compatible with HPLC stainless steel connections/fittings which are better suited for organic solvents. Standard po-

ly(ethylene oxide) mixtures were fractionated in methanol with salt addition using regenerated cellulose membranes whereas polystyrenes and poly(methyl methacrylate) standards adhered to this membrane when non-protic solvents, such as toluene, were used. Hydrophobization of the membrane by silanes enabled the investigation of these samples in THF. However, the modified membranes were not optimal as the membrane dissolved in the mobile phase after three weeks of continuous use. Nonetheless, using published Mark–Houwink coefficients, molar mass distributions of the poly(ethylene oxide) samples were calculated.

In 1996, a paper was published which was dedicated to selecting suitable membranes for separations in organic solvents [466]. Membranes tested in an asymmetrical channel included polysulfone MWCO 20,000 g/mol, regenerated cellulose MWCO 20,000 g/mol, PTFE pore size 0.02 mm, polyaramide MWCO 50,000 g/mol, poly(vinylidene fluoride) MWCO 50,000 g/mol, poly(phenylene oxide) MWCO 20,000 g/mol and a DDS fluoro polymer MWCO 30,000 g/mol. The first membrane was tested with water, the others with THF or a THF/acetonitrile mixture. Numerous problems occurred with the different membranes. The best membrane for THF was found to be the DDS fluoro polymer membrane.

Recently, a "universal separator" has been developed which can be applied for aqueous and organic solvents at temperatures up to 140 °C [368]. This instrument is a specially designed Fl-FFF channel operating in an oven. Here, a PET ultrafiltration membrane with a high molar weight cut off of 30000 g/mol was applied. Solvents which were reported to be applicable were water, toluene, xylene, heptane, cyclohexane and THF.

4.3.2 *FFF Coupled with MALLS Detection*

By combining a mass-sensitive detector with multiangle laser light scattering (MALLS), both the size and molecular weight can be determined. MALLS has been used in several applications of SEC [467,468], but only recently been combined with FFF [140]. As in SEC, the FFF channel is used as a fractionating device producing almost monodisperse sample slices which are subsequently characterized by light scattering. The combination of Th-FFF with MALLS is particularly effective for ultrahigh molecular weight polymers, where high resolution and multiangle capability are critical factors. Although low molar masses are a problem for light scattering detection, molar mass distributions can still be obtained on an absolute basis by applying electrospray mass spectrometry, as has recently been suggested [152].

Lee compared the accuracy of SEC and Th-FFF with and without the use of a MALLS detector for such samples [140]. Without the MALLS detector, SEC consistently underestimated the molecular weight (M). But even with MALLS, the accuracy was limited by the resolution of SEC to achieve monodispersity in each data slice. In conclusion, Th-FFF was found to be better than SEC.

The FFF-MALLS hybrid proved to be a powerful analysis technique on an absolute basis [139,254,461]. In analogy to SEC-MALLS, the molar mass distribution as well as the radius of gyration r_G of the sample can be determined permitting the setting up of a double logarithmic plot of M vs. r_G. The slopes of these linear dependencies then provide information about the architecture and conformation of the sample. Further information about the sample can, in principle, also be derived by the determination of the hydrodynamic radius r_H via the D determination using the standard FFF evaluation from UV or RI detector responses. Then, the ratio r_G/r_H can be determined which also gives information about the particle shape, as was demonstrated and discussed in detail for different pullulan standards by Adolphi and Kulicke [469] and for bovine serum albumin (spherical) and tobacco mosaic virus (rod) by Thielking and Kulicke [470].

With respect to the virtually very low sample loads, one could argue that the determined diffusion coefficient is at infinite dilution. However, there is no possibility in FFF techniques to perform a safe extrapolation to infinite dilution as in analytical ultracentrifugation or dynamic light scattering. In addition there is a severe problem for all particles deviating from the spherical shape (see Sect. 4.2.3 for a detailed discussion), as the evaluation of D from the FFF experiments using the conventional theory is inappropriate.

In principle, every FFF technique is suitable for MALLS coupling. The first papers on an S-FFF-MALLS hybrid appeared as early as 1991 [53]. The coupling of Th-FFF to MALLS proved to be especially advantageous, as demonstrated for polystyrene polymers and microgels and poly(styrene sulfonates) [109,471] or, more recently, for polybutadienes or natural rubbers [374]. S-FFF-MALLS was applied for the characterization of starch polymers, a type of sample which is very sensitive to shear [137]. Many more applications have been reported for Fl-FFF-MALLS. S-Fl-FFF-MALLS was successfully used for the molar mass characterization of polystyrene latexes and dextran [135], size characterization of polystyrene standards 50–300 nm [136] and 50–500 nm [139], sulfonated poly(styrene sulfonate) standards (18×10^3–3×10^6 g/mol) [138], bovine serum albumin and size differences between different polystyrene standard latex batches of only 3% [374] (see also Fig. 31), and to characterize poly(diallyldimethylammonium chloride) (poly-DADMAC, a polycation) and pectin (complex system with aggregates) [470]. Recently, the advantages of the MALLS coupling to Fl-FFF for the measurement of particle size distributions of shear sensitive vesicles [472] or the molar mass distributions of shear sensitive commercial ultrahigh molar mass polyacrylamides in the range 0.35–9×10^6 g/mol [166,364] have been elucidated.

A-Fl-FFF/MALLS has been used for the determination of the molar mass and size distribution of dextrans and pullulans of various molar masses [473], hydroxypropylmethylcelluloses [474] and κ-carrageenan in different conformations and aggregation states [475].

Recently, the advantages of coupling FFF to MALLS with respect to the traditional evaluation of an identical FFF experiment with a UV or an RI detector have been pointed out by Wyatt, who demonstrated the tiny differences between

the apparent particle sizes derived from both evaluations for different PS latex standards [461]. In this paper, experimentally determined particle size distributions of polystyrene latex mixtures, emulsions and liposomes were presented, using S-Fl-FFF and El-FFF coupled with MALLS [461].

For more complex solute mixtures, it is obvious that the change of the light scattering regime from Rayleigh to Mie scattering is a problem if the particle size approaches the wavelength of the light.

4.3.3
Other Fl-FFF Improvements

Zahoransky et al. described an improved Fl-FFF channel which assures a uniform cross-flow in the whole channel [476]. This is achieved by a division of the hollow compartment under the membrane supporting frit into three separate chambers with an independent pressure control. By means of special spring-loaded clamping devices, the spacer and membrane change is reported to be simple, thus making the whole experimental handling with this new channel convenient.

Beside the frit inlets for Fl-FFF (see Fig. 12) which help to enhance the sample relaxation, Moon et al. have recently suggested a frit inlet which applies a small permeable frit near the injection point in the A-Fl-FFF channel [51,401]. As sample materials injected into the flow streams are hydrodynamically relaxed by the compressing action of high speed frit flow, the usual focusing relaxation procedure can be avoided which makes the experiment more reliable and faster.

Frit outlets which work in reverse to the frit inlets (see Fig. 12) have been constructed allowing a sample concentration due to the fact that the sample is compressed near the accumulation wall so that the majority of the solvent containing no sample can leave through the frit thus concentrating the sample at the outlet [52].

Such sample concentration procedures are very important, since one must often cope with a very poor detector response if the sample is not concentrated at the outlet. For very diluted analytes, a new on-line sample concentration method called "opposed flow sample concentration" (OFSC) has recently been proposed and tested for Fl-FFF [477]. This method applies two opposing flowstreams to focus sample into a narrow band near the inlet of the Fl-FFF channel which enables concentration factors up to 10^5 to be achieved. Such a concentration procedure appears particularly interesting for environmental samples. An example for the concentration of river water colloids was given.

4.4
Outlook to the Future

Looking at recent FFF developments, one can try to predict some future trends. One is certainly the on-line coupling of absolute techniques like MALLS to the fractionating FFF channel which can yield very fast determinations of the distribution of molar mass and other molecular properties. In this respect, the poten-

tial of other detection techniques like electrospray mass spectroscopy (molar mass) or ICP-MS (for chemical composition) is also promising. The better and smoother separation characteristics of an FFF channel compared to SEC or other chromatographic techniques with a stationary phase, combined with the very large application range, make FFF particularly well suited for such coupling.

Another important trend is focused on faster and more efficient analyses, requiring thinner channels and stronger, more uniform fields. Thinner channels enhance the separation speed of FFF dramatically due to the square dependence of the retention time on the channel thickness [118,478,479]. Applying stronger and more uniform fields definitely has its physical and/or experimental limits. For example, in Th-FFF, the field is limited by the cooling capacity at the cold wall. Regarding the uniformity of the field, Th-FFF separations have benefited greatly from improvements in the path of water flow through the cold wall.

In A-Fl-FFF, field-strength limitations are governed by the channel pressure required to drive carrier liquid through the small pore membrane, necessary to retain the analyte. The back pressure caused by the accumulation wall membrane keeps the field fairly uniform throughout the channel, so long as the pressures at the axial- and cross-flow outlets are equalized through the adjustment of the back-pressure valve. Future work may focus on a more automated method for controlling the back pressure, so that the field strength can be varied without operator assistance. Automated control of the back pressure will also make field programming more attractive for A-Fl-FFF.

Another development with much potential benefit is the design of new channels and membranes for Fl-FFF in order to make this technique truly universally applicable. However, at the moment, the design of these novel membranes which will fulfill all of the numerous requirements of Fl-FFF is proceeding only very slowly and may even be impossible.

A further interesting development is multidimensional FFF where several FFF separation mechanisms are coupled, like helical Fl-FFF. Such techniques certainly have much future potential as they combine the merits of two or maybe even more FFF methods with all the possible information of each of the combined FFF techniques. However, the effective practical realization is a current problem which deserves attention.

Applying FFF techniques for preparative separations in the form of SPLITT channels also seems to be very promising. Here, future developments must concentrate not only on the application of other physical fields for the separation in SPLITT but also on the coupling of various SPLITT channels with different cut off limits to design a preparative fractionator for broadly distributed samples.

Other future FFF developments may address the highly desired continuous preparative FFF fractionation apart from SPLITT channels. This requires the following experimental conditions:

– Very fast hydrodynamic relaxation as can be achieved by stream splitters or frit inlets (see Fig. 12) so that there is no need for a stop-flow or focusing period. It is important that the injection time can serve as a triggering pulse for an automated fractionator coupled to the FFF outlet.

- Sample concentration after the sample fractionation as can be achieved by stream splitters or frit outlets.
- Automated, computer-controlled fractionation from the FFF outlet coupled to the injection time.
- Automated repetition of the sample injection after one fractionation cycle which is indicated by a signal decrease of a concentration detector to the baseline signal. If samples with multimodal distributions are to be fractionated, the threshold logic for sample reinjection needs to be modified accordingly.
- Highly stable flow and field strength conditions.

Even then the fractionation of gram quantities will be tedious and time-consuming work if one considers that the typical amount per injection into an FFF channel is in the μg range. Nevertheless, the fractionation of mg amounts of samples is especially interesting for modern biopolymer samples, such as DNS fragments, or molecular factors which are produced in such amounts.

5 Conclusions

It is clear that FFF comprises a family of flexible analytical techniques which can supply a tremendous amount of physicochemical information when complimentary FFF methods are used. Also, the application range (1 nm–100 μm for colloids or 1000 g/mol up to more than 10^{18} g/mol for polymers) is larger than with any other analytical technique for particle size or molar mass measurement coupled with usually short measurement times.

There are, however, also some drawbacks to these techniques: The inversion of elution from the normal to the steric mode complicates measurements in the particle size range around 1 μm and, although this transition region can be shifted by experimental conditions, serious interpretation errors can occur if the particle size distribution spans this transition region.

In addition, quantitative evaluation of FFF experiments shows that the idealized FFF theory can only rarely be applied. Numerous corrections taking account of the various deviations from the idealized behavior may become necessary. On the other hand, qualitative information on a separation and the number of resolved components is often already sufficient. If an independent absolute detector like MALLS is coupled to the FFF channel, FFF can be operated as a relative separation device. Even in this restricted mode, FFF offers numerous advantages for polymer analysis over the dominant SEC (see Sect. 1.5.1).

FFF is therefore regarded as an extremely promising, but still underdeveloped, technique and many other experimental problems remain to be overcome, like sample adsorption to the walls and solute–solute interactions, etc., which keep FFF from being a "black box" universal laboratory analytical technique. The experimental conditions have to be optimized for the specific sample of interest. Nevertheless, in the hands of an expert, FFF shows a superb resolution

and is thus well suited for a large variety of problems in fundamental research, industrial production control, biotechnology or environmental analysis.

FFF is an analytical technique well deserving of a more widespread application at least in its most developed variants: Fl-FFF, Th-FFF and S-FFF. Especially for complex colloidal or particulate matter, emulsion and dispersion technology, there are many advantages of FFF which certainly justify the implementation and research in most analytical laboratories dealing with such problems.

6 FFF on the Internet

Currently, there are two Internet web sites which are devoted to FFF methods. The first is based at the University of Ferrara, Italy: http://dns.unife.it/~rsk/ and gives an introduction to various FFF techniques as well as a short literature review on Gr-FFF. Furthermore, a "Who is Who in the FFF World" library is found there which lists the expertises and experimental equipment of various workers in the FFF field.

The other server is an FFF literature database at Rohm & Haas: http://www.rohmhaas.com/fff/ which is updated frequently. It is possible to get e-mail notice on database updates. Furthermore, it is planned to install an FFF user discussion forum on this web site.

Acknowledgements. The authors thank A. Pape for substantial help with manuscript typing and U. Ziehut for large parts of the artwork. Dr. R. Hecker is acknowledged for careful proofreading of the manuscript and several useful suggestions towards the quality of the manuscript.

References

1. Giddings JC (1966) Sep Sci 1:123
2. Gunderson JJ, Giddings JC (1989) Field-flow fractionation. In: Booth C, Price C (eds) Polymer characterization. Pergamon, Oxford, pp 279–291
3. Caldwell KD (1988) Anal Chem 60:959A
4. Giddings JC (1981) Anal Chem 53:1170A
5. Lightfoot EN, Chiang AS, Noble PT (1981) Annu Rev Fluid Mech 13:351
6. Kirkland JJ, Rementer SW, Yau WW (1981) Anal Chem 53:1730
7. Giddings JC, Graff KA, Caldwell KD, Myers MN (1983) Adv Chem Ser 203:257
8. Janca J, Kleparnik K, Jahnova V, Chmelik J (1984) J Liq Chrom 7:1
9. Giddings JC, Caldwell KD, Jones HK (1987) Measuring particle size distribution of simple and complex colloids by sedimentation field-flow fractionation. In: Provder T (ed) Particle size distribution: assessment and characterization. American Chemical Society, Washington, DC, pp 215–230
10. Janca J (1987) Chem Listy 81:1034
11. Beckett R, Bigelow JC, Jue Z, Giddings JC (1989) Analysis of humic substances using flow field-flow fractionation. In: MacCarthy P, Suffet IH (eds) Influences of aquatic humic substances on fate and treatment of pollutants. American Chemical Society, Washington, DC, pp 65–80

12. Giddings JC, Barman BN, Liu MK (1991) Separation of cells by field-flow fractionation and related methods. In: Kompala DS, Todd P (eds) Cell separation science and technology. American Chemical Society, Washington, DC, pp 128–144
13. Levin S (1991) Biomed Chromatogr 5:133
14. Giddings JC (1993) Science 260:1456
15. Myers MN, Chen P, Giddings JC (1993) Polymer separation and molecular-weight distribution by thermal field-flow fractionation. In: Provder T (ed) Chromatography of polymers: characterization by SEC and FFF. American Chemical Society, Washington, DC, pp 47–62
16. Barman BN, Giddings JC (1993) Separation and characterization of polymer latex beads and aggregates by sedimentation field-flow fractionation. In: Provder T (ed) Chromatography of polymers: characterization by SEC and FFF. American Chemical Society, Washington, DC, pp 30–46
17. Ratanathanawongs SK, Giddings JC (1993) Particle size analysis using field-flow fractionation. In: Provder T (ed) Chromatography of polymers: characterization by SEC and FFF. American Chemical Society, Washington, DC, pp 13–29
18. Janca J (1993) Mikrochim Acta 111:135
19. Mori Y (1994) Adv Colloid Interf Sci 53:129
20. Giddings JC, Ratanathanawongs SK, Barman BN, Moon MH, Liu GY, Tjelta BL, Hansen ME (1994) Adv Chem Ser 234:309
21. Schimpf ME (1996) Trends Polym Sci 4:114
22. Myers MN (1997) J Microcolum Sep 9:151
23. Moon MH, Lee SH (1997) J Microcolum Sep 9:565
24. Janca J (1997) J Liq Chromatogr Rel Technol 20:2555
25. Martin M (1998) Theory of field-flow fractionation. In: Brown PR, Grushka E (eds) Advances in chromatography. Marcel Dekker, New York, pp 1–138
26. Janca J (1998) Chem Listy 92:449
27. Janca J (1988) Field-flow fractionation: analysis of macromolecules and particles. Marcel Dekker, New York
28. Giddings JC (1991) Unified separation science. John Wiley & Sons, New York
29. Thompson GH, Myers MN, Giddings JC (1967) Sep Sci 2:797
30. Berg HC, Purcell EM (1967) Proc Natl Acad Sci USA 58:862
31. Berg HC, Purcell EM (1967) Proc Natl Acad Sci USA 58:821
32. Berg HC, Purcell EM (1967) Proc Natl Acad Sci USA 58:1286
33. Giddings JC (1968) J Chem Phys 49:81
34. Hovingh ME, Thompson GH, Giddings JC (1970) Anal Chem 42:195
35. Caldwell KD, Kesner LF, Myers MN, Giddings JC (1972) Science 176:296
36. Kesner LF, Caldwell KD, Myers MN, Giddings JC (1976) Anal Chem 48:1834
37. Lee HL, Reis JFG, Dohner J, Lightfoot EN (1974) AIChE J 20:776
38. Yang FJF, Myers MN, Giddings JC (1974) Anal Chem 46:1924
39. Giddings JC, Smith LK, Myers MN (1976) Anal Chem 48:1587
40. Giddings JC, Caldwell KD, Moellmer JF, Dickinson TH, Myers MN, Martin M (1979) Anal Chem 48:30
41. Giddings JC, Yang FJF, Myers MN (1976) Anal Chem 48:1126
42. Giddings JC, Yang FJF, Myers MN (1977) Sep Sci Technol 12:381
43. Giddings JC, Martin M, Myers MN (1979) Sep Sci Technol 14:611
44. Doshi MR, Gill WN (1979) Chem Eng Sci 34:725
45. Vickrey TM, Garcia-Ramirez JA (1980) Sep Sci Technol 15:1297
46. Giddings JC, Brantley SL (1984) Sep Sci Technol 19:631
47. Wahlund KG, Giddings JC (1987) Anal Chem 59:1332
48. Liu M-K, Williams PS, Myers MN, Giddings JC (1991) Anal Chem 63:2115
49. Liu MK, Li P, Giddings JC (1993) Protein Sci 2:1520
50. Dean GA, Cardile CM, Stead RJ, Alecu ID (1994) J Mater Sci Lett 13:872
51. Moon MH, Kwon H, Park I (1997) J Liq Chrom Related Tech 20:2803

52. Li P, Hansen M, Giddings JC (1998) J Microcol Sep 10:7
53. Wyatt PJ (1991) Polym Mat Sci Eng 65:198
54. Giddings JC, Kumar V, Williams PS, Myers MN (1990) Polymer separation by thermal field-flow fractionation: high speed power programming. In: Craver CD, Provder T (eds) Polymer characterization: physical properties, spectroscopic, and chromatographic methods. American Chemical Society, Washington, DC, pp 1–21
55. Gunderson JJ, Giddings JC (1986) Macromolecules 19:2618
56. Mori Y, Scarlett B, Merkus HG (1990) J Chromatogr 515:27
57. Hansen ME, Giddings JC, Beckett R (1989) J Coll Interf Sci 132:300
58. Sisson R, Giddings JC (1994) Anal Chem 66:4043
59. Benincasa MA, Giddings JC (1992) Anal Chem 64:790
60. Giddings JC, Benincasa MA, Liu M-K, Li P (1992) J Liq Chromatogr 15:1729
61. Williams PS, Moon MH, Xu Y, Giddings JC (1996) Chem Eng Sci 51:4477
62. Williams PS, Moon MH, Giddings JC (1996) Colloids Surf A 113:215
63. Small H (1974) J Colloid Interface Sci 48:147
64. Husain A, Hamielec AE, Vlachopoulos J (1981) J Liq Chromatogr 4(S-2):295
65. Penlidis A, Hamielec AE, MacGregor JF (1983) J Liq Chromatogr 6:179
66. Jahnová V, Janca J (1984) Chem Listy 78:346
67. Giddings JC (1978) Sep Sci Technol 13:241
68. Myers MN, Giddings JC (1982) Anal Chem 54:2284
69. Moon MH, Giddings JC (1992) Anal Chem 64:3029
70. Schauer T (1995) Part Syst Charact 12:284
71. Giddings JC (1983) Sep Sci Technol 18:765
72. Janca J (1982) Makromol Chem Rapid Commun 3:887
73. Janca J (1983) Makromol Chem Rapid Commun 4:267
74. Janca J, Chmelik J (1984) Anal Chem 56:2481
75. Caldwell KD, Li J (1989) J Colloid Interface Sci 132:256
76. Kirkland JJ, Rementer SW, Yau WW (1989) J Appl Polym Sci 38:1383
77. Giddings JC (1988) Chem Eng News 66:34
78. Chase MW, Davies CA, Downey JR, Frurip DJ, McDonald RA, Syverud AN (1985) Janaf thermochemical tables, 3rd edn. 1. AL-CO. J Phys Chem Ref Data 14 (Suppl 1):1–926
79. Williams PS, Koch T, Giddings JC (1992) Chem Eng Comm 111:121
80. Giddings JC, Yang FJF, Myers MN (1975) Sep Sci 10:133
81. Giddings JC, G. Karaiskakis, Caldwell KD, Myers MN (1983) J Colloid Interface Sci 92:66
82. Giddings JC, Karaiskakis K, Caldwell KD (1981) Sep Sci Technol 16:607
83. Janca J, Jahnova V (1983) J Liq Chrom 6:1559
84. Schimpf ME, Giddings JC (1989) J Polym Sci Polym Phys Ed 27:1317
85. Giddings JC (1973) J Chem Educ 50:667
86. Giddings JC (1973) Sep Sci 8:567
87. Krishnamurthy S, Subramanian RS (1977) Sep Sci 12:347
88. Gajdos LJ, Brenner H (1978) Sep Sci Technol 13:215
89. Giddings JC, Schure MR, Myers MN, Velez GR (1984) Anal Chem 56:2099
90. Davis JM, Giddings JC (1985) J Phys Chem 89:3398
91. Giddings JC (1986) Anal Chem 58:735
92. Berthod A, Armstrong DW (1987) Anal Chem 59:2410
93. Andreev VP, Semenov SN, Kustensov AA, Reifman LS (1987) Zh Fiz Khim 61:1
94. Giddings JC, Schure MR (1987) Chem Eng Sci 42:1471
95. Ugrozov VV (1989) Zh Fiz Khim 62:89
96. Davis JM (1989) Sep Sci Technol 24:219
97. Martin M, Williams PS (1992) Theoretical basis of field-flow fractionation. In: Dondi F, Guichon G (eds) Theoretical advancement in chromatography and related separation techniques. Kluver, Dordrecht, pp 513–580
98. Andreev VP, Stefanovich LA (1993) Chromatographia 37:325

99. Giddings JC (1993) J Microcol Sep 5:497
100. Williams PS, Giddings JC (1994) Anal Chem 66:4215
101. Buffham BA (1996) J Colloid Interface Sci 181:490
102. Semenov SN (1996) Zh Fiz Khim 70:1674
103. Zolotarev PP, Ugrozov VV, Skornyakov EP (1988) Zh Fiz Khim 62:1896
104. Davis JM, Giddings JC (1986) Sep Sci Technol 21:969
105. Davis JM (1986) Anal Chem 58:161
106. Hoyos M, Martin M (1994) Anal Chem 66:1718
107. Schure MR, Caldwell KD, Giddings JC (1986) Anal Chem 58:1509
108. Janca J, Chmelik J, Jahnove V, Novekove N, Urbenkov E (1991) Chem Anal 36:657–666
109. Tank C (1995) Trennung und Charakterisierung komplexer Polymere und Kolloide durch Feld-Fluß Fraktionierung. PhD Thesis, Technische Universität Berlin, Germany
110. Schimpf ME, Giddings JC (1987) Macromolecules 20:1561
111. Schimpf ME, Giddings JC (1990) J Polym Sci Part B Polym Phys 28:2673
112. Ko G-H, Richards R, Schimpf ME (1996) Sep Sci Technol 31:1035
113. Giddings JC (1994) Anal Chem 66:2783
114. Schimpf ME (1990) J Chromatogr 517:405
115. Gunderson JJ, Giddings JC (1986) Anal Chim Acta 189:1
116. Stegemann G, van Asten AC, Kraak JC, Poppe H, Tijssen R (1994) Anal Chem 66:1147
117. van Asten AC, Stegemann G, Kok WT, Tjissen R, Poppe H (1994) Anal Chem 66:3073
118. Giddings JC, Martin M, Myers MN (1978) J Chromatogr 158:419
119. Schimpf ME (1993) Ind J Technol 31:443
120. Hellmann MY (1977) In: Cazes J (ed) Liquid chromatography of polymers and related materials. Marcel Dekker, New York, pp 29–39
121. Caldwell KD, Brimhall SL, Gao Y, Giddings JC (1988) J Appl Polym Sci 36:703
122. Schimpf ME, Williams PS, Giddings JC (1989) J Appl Polym Sci 37:2059
123. Schimpf ME, Myers MN, Giddings JC (1987) J Appl Polym Sci 33:117
124. Freifelder D (1982) Applications to biochemistry and molecular biology. In: Physical biochemistry. WH Freeman and Co., San Francisco, chap 13
125. Bird RB, Armstrong RC, Hassager O (1977) In: Dynamics of polymeric liquids. John Wiley, New York, pp 169–253
126. Gao YS, Caldwell KD, Myers MN, Giddings JC (1985) Macromolecules 18:1272
127. Li J, Caldwell KD, Mächtle W (1990) J Chromatogr 517:361
128. Pauck T, Cölfen H (1998) Anal Chem 70:3886
129. Yau WW, Kirkland JJ (1981) J Chromatogr 218:217
130. Yang FS, Caldwell KD, Giddings JC (1983) J Colloid Interface Sci 92:81
131. Janca J, Pribylova D, Bouchal K, Tyrackova V, Zurkova E (1986) J Liq Chromatogr 9:2059
132. Vickrey TM (1983) Liquid chromatography detectors. Chromatogr Sci Ser. Marcel Dekker, New York, chap 23, p 434
133. Ouano AC, Kaye W (1974) J Polym Sci Polym Chem Ed 12:1151
134. Martin M, Hes J (1984) Sep Sci Technol 19:685
135. Roessner D, Kulicke W-M (1994) J Chromatogr A 687:249
136. Thielking H, Roessner D, Kulicke WM (1995) Anal Chem 67:3229
137. Hanselmann R, Ehrat M, Widmer HM (1995) Starch/Stärke 46:345
138. Thielking H, Kulicke WM (1996) Anal Chem 68:1169
139. Shortt DW, Roessner D, Wyatt PJ (1996) Am Lab 28:21
140. Lee S, Kwon O-S (1995) Determination of molecular weight and size of ultrahigh molecular weight polymers using thermal field-flow fractionation and light scattering. In: Provder T, Barth HG, Urban MW (eds) Chromatographic characterization of polymers: hyphenated and multidimensional techniques. Amercian Chemical Society, Washington, DC, pp 93–107
141. Oppenheimer LE, Mourey TH (1984) J Chromatogr 298:217

142. Schimpf ME (1995) Determination of molecular weight and composition in copolymers using thermal field-flow fractionation combined with viscometry. In: Provder T, Barth HG, Urban MW (eds) Chromatographic characterization of polymers: hyphenated and multidimensional techniques. American Chemical Society, Washington, DC, pp 183–196
143. Caldwell KD, Jones HK, Giddings JC (1986) Colloids Surf 18:123
144. Kirkland JJ, Rementer SW (1992) Anal Chem 64:904
145. Kirkland JJ, Rementer SW, Yau WW (1991) J Appl Polym Sci Appl Polym Symp 48:39
146. Stabinger H, Leopold H, Kratky O (1967) Monatsh Chem 98:436
147. Trathnigg B, Jorde C (1984) J Liq Chromatogr 7:1789
148. Kirkland JJ, Yau WW (1991) J Chromatogr 550:799
149. Beckett R (1991) At Spectrosc 12 (special issue):228
150. Taylor HE, Garbarino JR, Murphy DM, Beckett R (1992) Anal Chem 64:2036
151. Murphy DM, Garbarino JR, Taylor HW, Hart BT, Beckett R (1993) J Chromatogr 642:459
152. Hassellöv M, Hulthe G, Lyven B, Stenhagen G (1997) J Liq Chromatgr Rel Technol 20:2843
153. Wyatt PJ (1993) Anal Chim Acta 272:1
154. Barth HG, Boyes BE, Jackson C (1996) Anal Chem 68:445R
155. Lee S, Rao SP, Moon MH, Giddings JC (1996) Anal Chem 68:1545
156. Blo G, Contado C, Fagioli F, Rodriguez MHB, Dondi F (1995) Chromatographia 41:715
157. Dondi F, Blo G, Martin M (1997) Annali di Chimica 87:113
158. Giddings JC (1985) Anal Chem 57:945
159. Lee S, Myers MN, Giddings JC (1989) Anal Chem 61:2439
160. Giddings JC (1990) Anal Chem 62:2306
161. Williams PS, Giddings JC, Beckett R (1987) J Liq Chromatogr 10:1961
162. Grushka E, Caldwell KD, Myers MN, Giddings JC (1973) Field-flow fractionation. In: Perry ES, Oss CJV, Grushka E (eds) Separation and purification methods. Marcel Dekker, New York, pp 127–151
163. Giddings JC, Caldwell KD (1984) Anal Chem 56:2093
164. Kirkland JJ, Yau WW (1985) Macromolecules 18:2305
165. Wahlund K-G, Winegarner HS, Caldwell KD, Giddings JC (1986) Anal Chem 58:573
166. Hecker R (1998) The characterization of polyacrylamide flocculants. PhD Thesis, Curtin University of Technology, Perth, Australia
167. Yau WW, Kirkland JJ (1981) Sep Sci Technol 16:577
168. Kirkland JJ, Rementer SW, Yau WW (1988) Anal Chem 60:610
169. Williams PS, Giddings JC (1987) Anal Chem 59:2038
170. Kirkland JJ, Yau WW (1990) J Chromatogr 499:655
171. Kirkland JJ, Yau WW, Doerner WA, Grant JW (1980) Anal Chem 52:1944
172. Yang FJ, Myers MN, Giddings JC (1977) J Colloid Interface Sci 60:574
173. Wyatt PJ, Villalpando D (1997) Langmuir 13:3913
174. Giddings JC, Yang FJF, Myers MN (1974) Anal Chem 46:1917
175. Giddings JC, Myers MN, Caldwell KD, Fisher SR (1980) Analysis of biological macromolecules and particles by field-flow fractionation. In: Glick D (ed) Methods of biochemical analysis. John Wiley, New York, pp 79–136
176. Kirkland JJ, Dilks CH Jr, Yau WW (1983) J Chromatogr 255:255
177. Mächtle W (1992) Analysis of polymer dispersions with an eight cell AUC-multiplexer: High resolution particle size distribution and density gradient techniques. In: Harding SE, Rowe AJR, Horton JC (eds) Analytical ultracentrifugation in biochemistry and polymer science. The Royal Society of Chemistry, Cambridge, pp 147–175
178. Cölfen H (1998) unpublished results
179. Kirkland JJ, Yau WW (1982) Science 218:121
180. Mächtle W (1984) Makromol Chem Macromol Chem Phys 185:1025
181. Müller HG, Herrmann F (1995) Progr Colloid Polym Sci 99:114

182. Yonker CR, Caldwell KD, Giddings JC, van Etten JL (1985) J Virol Methods 11:145
183. Caldwell KD, Karaiskakis G, Myers MN, Giddings JC (1981) J Pharm Sci 70:1350
184. Moon MH, Giddings JC (1993) J Pharm Biomed Anal 11:911
185. Li JT, Caldwell KD (1991) Langmuir 7:2034
186. Beckett R, Ho J, Jiang Y, Giddings JC (1991) Langmuir 7:2040
187. Langwost B, Caldwell KD (1992) Chromatographia 34:317
188. Caldwell KD, Li J, Li J-T, Dalgleish DG (1992) J Chromatogr 604:63
189. Giddings JC, Karaiskakis G, Caldwell KD (1981) Sep Sci Technol 16:725
190. Giddings JC, Yang FS (1985) J Colloid Interface Sci 105:55
191. Karaiskakis G, Myers MN, Caldwell KD, Giddings JC (1981) Anal Chem 53:1314
192. Giddings JC (1986) Anal Chem 58:2052
193. Thompson GH, Myers MN, Giddings JC (1969) Anal Chem 41:1219
194. Myers MN, Caldwell KD, Giddings JC (1974) J Sep Sci 9:47
195. Sanyal SK, Adhikari M (1981) J Indian Chem Soc 58:1055
196. Giddings JC, Myers MN, Janca J (1979) J Chromatogr 186:37
197. Martin M, Reynaud P (1980) Anal Chem 52:2293
198. Giddings JC, Martin M, Myers MN (1981) J Polym Sci Polym Phys Ed 19:815
199. Janca J, Klepárník K (1981) Sep Sci Technol 16:657
200. Giddings JC, Smith LK, Myers MN (1975) Anal Chem 47:2389
201. Emery AH, Drickamer HG (1955) J Chem Phys 23:2252
202. Bonner FJ (1967) Ark Kemi 27:19
203. Grew KE (1969) Transport phenomena in fluids. Marcel Dekker, New York
204. Giddings JC, Caldwell KD, Myers MN (1976) Macromolecules 9:106
205. Gunderson JJ, Caldwell KD, Giddings JC (1984) Sep Sci Technol 19:667
206. Giddings JC (1976) J Chromatogr 125:3
207. Brochard F, Martin M (1982) Bull Soc Fr Phys 46:17
208. Brochard-Wyart F (1983) Macromolecules 16:149
209. Giddings JC, Hovingh ME, Thompson GH (1970) J Phys Chem 74:4291
210. Ngyuen M, Beckett R (1993) Polym Int 30:337
211. Nguyen M, Beckett R (1996) Sep Sci Technol 31:291
212. Nguyen M, Beckett R (1996) Sep Sci Technol 31:453
213. Köhler W (1993) J Chem Phys 98:660
214. Schimpf ME, Wheeler LM, Romeo PF (1993) Copolymer retention in thermal field-flow fractionation: dependence on composition and conformation. In: Provder T (ed) Chromatography of polymers: characterization by SEC and FFF. American Chemical Society, Washington, DC, pp 63–76
215. Liu G, Giddings JC (1992) Chromatographia 34:483
216. Pauck T, Cölfen H, unpublished results
217. van Asten AC, Boelens HFM, Kok WT, Poppe H, Williams PS, Giddings JC (1994) Sep Sci Technol 29:513
218. Westerman-Clark G (1978) Sep Sci Technol 13:819
219. Belgaied JE, Hoyos M, Martin M (1994) J Chromatogr A 678:85
220. Giddings JC (1979) Pure Appl Chem 51:1459
221. Brimhall SL, Myers MN, Caldwell KD, Giddings JC (1981) Sep Sci Technol 16:671
222. Kirkland JJ, Yau WW (1986) J Chromatogr 353:95
223. Smith LK, Myers MN, Giddings JC (1977) Anal Chem 49:1750
224. Martin M, Myers MN, Giddings JC (1979) J Liq Chromatogr 2:147
225. Giddings JC, Myers MN, Moellmer JF (1978) J Chromatog 149:501
226. Ratanathanawongs SK, Lee I, Giddings JC (1991) Separation and characterization of 0.01–50 μm particles using flow field-flow fractionation. In: Provder T (ed) Particle size distribution II. American Chemical Society, Washington, DC, pp 229–246
227. Beckett R, Jue Z, Giddings JC (1987) Environ Sci Technol 21:289
228. Giddings JC, Yang FJ, Myers MN (1976) Science 193:1244
229. Lee HL, Lightfoot EN (1976) Sep Sci Technol 11:417

230. Davis JM (1991) Anal Chim Acta 246:161
231. Wahlund KG, Litzén A (1989) J Chromatogr 461:73
232. Litzén A, Wahlund KG (1989) J Chromatogr 476:413
233. Kirkland JJ, Dilks Jr CH, Rementer SW, Yau WW (1992) J Chromatogr 593:339
234. Joensson JA, Carlshaf A (1989) Anal Chem 61:11
235. Carlshaf A, Jönsson A (1989) J Chromatogr 461:89
236. Carlshaf A, Jonsson JA (1991) J Microcol Sep 3:411
237. Granger J, Dodds J (1992) Sep Sci Technol 27:1691
238. Carlshaf A, Jonsson JA (1993) Sep Sci Technol 28:1031
239. Wijnhoven JEGJ, Koorn JP, Poppe H, Kok WT (1995) J Chromatogr 699:119
240. Giddings JC, Yang FJ, Myers MN (1977) Anal Biochem 81:395
241. Giddings JC, Yang FJ, Myers MN (1977) J Virol 21:131
242. Giddings JC, Lin GC, Myers MN (1978) J Colloid Interface Sci 65:67
243. Giddings JC, Lin GC, Myers MN (1978) J Liq Chromatogr 1:1
244. Giddings JC (1984) Sep Sci Technol 19:831
245. Yang FJ, Myers MN, Giddings JC (1977) Anal Chem 49:659
246. Giddings JC, Lin HC, Caldwell KD, Myers MN (1983) Sep Sci Technol 18:293
247. Giddings JC, Yang FJ, Myers MN (1977) Sep Sci Technol 12:499
248. Granger J, Dodds J, Leclerc D, Midoux N (1986) Chem Eng Sci 41:3119
249. Litzén A, Wahlund KG (1991) Anal Chem 63:1001
250. Williams PS (1997) J Microcolumn Sep 9:459
251. Wittgren B, Wahlund KG, Dérand H, Wesslén B (1996) Macromolecules 29:268
252. Wittgren B, Wahlund KG, Dérand H, Wesslén B (1996) Langmuir 12:5999
253. Litzén A (1992) Asymmetrical flow field-flow fractionation. PhD Thesis, University of Uppsala, Sweden
254. Wittgren B (1997) Size characterization of water-soluble polymers using asymmetrical flow field-flow fractionation. PhD Thesis, Lund University, Sweden
255. Giddings JC (1989) J Chromatogr 480:21
256. Giddings JC, Lin GC, Myers MN (1976) Sep Sci Technol 11:553
257. Caldwell KD, Gao YS (1993) Anal Chem 65:1764
258. Schimpf ME, Russell DD, Lewis JK (1994) J Liq Chromatogr 17:3221
259. Schimpf ME, Caldwell KC (1995) Am Lab 27:64
260. Reis JFG, Lightfoot EN (1976) AIChE J 22:779
261. Reis JFG, Ramkrishna D, Lightfoot EN (1978) AIChE J 24:679
262. Davis JM, Fan FRF, Bard J (1987) Anal Chem 59:1339
263. Subramanian RS, Jayaraj K, Krishnamurthy S (1978) Sep Sci Technol 13:273
264. Hunter RJ (1993) Introduction to modern colloid science. Oxford University Press, Oxford
265. O'Brien RW, White LR (1978) J Chem Soc Faraday Trans 2 74:1607
266. Chiang AS, Kmiotek EH, Langan SM, Noble PT, Reis JFG, Lightfoot EN (1979) Sep Sci Technol 14:453
267. Shah AB, Reis JFG, Lightfoot EN, Moore RE (1979) Sep Sci Technol 14:475
268. Lightfoot EN, Noble PT, Chiang AS, Ugulini TA (1981) Sep Sci Technol 16:619
269. Palkar SA, Schure MR (1997) Anal Chem 69:3223
270. Palkar SA, Schure MR (1997) Anal Chem 69:3230
271. Semenov SN, Kuznetsov AA (1984) Zh Fiz Khim 60:424
272. Semenov SN (1986) Zh Fiz Khim 60:1231
273. Schunk TC, Gorse J, Burke MF (1984) Sep Sci Technol 19:653
274. Gorse J, Schunk TC, Burke MF (1984) Sep Sci Technol 19:1073
275. Pohl HA (1978) Dielectroporesis. Cambridge University Press, Cambridge
276. Pethig R (1991) Application of AC electrical fields to the manipulation and characterization of cells. In: Karube I (ed) Automation in biotechnology. Elsevier, Amsterdam, pp 159–185
277. Becker FF, Wang XB, Huang Y, Pethig R, Vykoukal J, Gascoyne PRC (1995) Proc Natl Acad Sci USA 92:860

278. Gascoyne PRC, Huang Y, Pethig R, Vykoukal J, Becker FF (1992) Meas Sci Technol 3:439
279. Talary MS, Mills KI, Hoy T, Burnett AK, Pethig R (1995) Med Biol Eng Comp 33:235
280. Markx GH, Talary MS, Pethig R (1994) J Biotechnol 32:29
281. Markx GH, Pethig R (1995) Biotechnol Bioeng 45:337
282. Wang XB, Huang Y, Burg JPH, Markx GH, Pethig R (1993) J Phys D: Appl Phys 26:1278
283. Doshi MR, Gill WN, Subramanian RS (1975) Chem Eng Sci 30:1467
284. Pearlstein J, Shiue MP (1995) Sep Sci Technol 30:2251
285. Shiue MP, Pearlstein AJ (1995) J Chromatogr A 707:87
286. Semyonov SN, Maslow KI (1988) J Chromatogr 446:151
287. Kononenko VL, Giddings JC, Myers MN (1997) J Microcolumn Sep 9:321
288. Kononenko VL, Shimkus JK, Giddings JC, Myers MN (1997) Feasibility studies on photophoretic effects in field-flow fractionation of particles. J Liq Chrom Rel Technol 20:2907
289. Cox RG, Brenner H (1968) Chem Eng Sci 23:147
290. Ho BP, Leal LG (1974) J Fluid Mech 65:365
291. Cox RG, Hsu SK (1977) Int J Multiphase Flow 3:201
292. Chen K, Wahlund KG, Giddings JC (1988) Anal Chem 60:362
293. Giddings JC, Moon MH, Williams PS, Myers MN (1991) Anal Chem 63:1366
294. Giddings JC, Myers MN, Moon MH, Barman BN (1991) Particle separation and size characterization by sedimentation field-flow fractionation. In: Provder T (ed) Particle size distribution. American Chemical Society, Washington, DC, pp 198–216
295. Compton BJ, Myers MN, Giddings JC (1983) Chem Biomed Environ Instrum 12:299
296. Caldwell KD, Cheng ZQ, Hradecky P, Giddings JC (1984) Cell Biophys 6:233
297. Caldwell KD, Nguyen TT, Myers MN, Giddings JC (1979) Sep Sci Technol 14:935
298. Giddings JC, Chen X, Wahlund KG, Myers MN (1987) Anal Chem 59:1957
299. Peterson RE, Myers MN, Giddings JC (1984) Sep Sci Technol 19:307
300. Koch T, Giddings JC (1986) Anal Chem 58:994
301. Williams PS, Lee S, Giddings JC (1994) Chem Eng Commun 130:143
302. Williams PS, Moon MH, Giddings JC (1992) Fast separation and characterization of micron size particles by sedimentation/steric field-flow fractionation: role of lift forces. In: Stanley-Wood NG, Lines RW (eds) Particle size analysis. Royal Society of Chemistry, Cambridge, pp 280–289
303. Ratanathanawongs SK, Giddings JC (1992) Anal Chem 64:6
304. DiMarzio EA, Guttman CM (1970) Macromolecules 3:131
305. Mori S, Porter RS, Johnson JF (1974) Anal Chem 46:1599
306. DosRamos JG, Silebi CA (1990) J Colloid Interface Sci 135:165
307. Meselson M, Stahl FW, Vinograd J (1957) Proc Natl Acad Sci USA 43:581
308. Janca J (1992) Am Lab 24:15
309. Chmelik J, Janca J (1986) J Liq Chromatogr 9:55
310. Janca J (1987) Makromol Chem Rapid Comm 8:233
311. Janca J, Novakova N (1987) J Liq Chromatogr 10:2869
312. Janca J, Novakova N (1988) J Chromatogr 452:549
313. Janca J (1991) J Liq Chromatogr 14:3317
314. Chmelik J, Thormann W (1992) J Chromatogr 600:305
315. Chmelik J, Deml M, Janca J (1989) Anal Chem 61:912
316. Giddings JC (1992) Am Lab 24:20D-M
317. Chmelik J (1991) J Chromatogr 539:111
318. Chmelik J, Janca J (1989) Chem Listy 83:321
319. Chmelik J (1991) J Chromatogr 545:349
320. Chmelik J, Thormann W (1992) J Chromatogr 600:297
321. Chmelik J, Thormann W (1993) J Chromatogr 632:229
322. Karaiskakis G, Koliadima A (1989) Chromatographia 28:31
323. Koliadima A, Karaiskakis G (1990) J Chromatogr 517:345
324. Koliadima A, Karaiskakis G (1994) Chromatographia 39:74

325. Athanasopoulou A, Karaiskakis G (1995) Chromatographia 40:734
326. Hansen ME, Giddings JC (1989) Anal Chem 61:811
327. Athanasopoulou A, Koliadima A, Karaiskakis G (1996) Instrum Sci Technol 24:79
328. Karaiskakis G, Athanasopoulou A, Koliadima A (1997) J Microcolumn Sep 9:275
329. Kataoka K, Okano T, Sakurai Y, Nishimura T, Maeda M, Inoue S, Watanabe T, Tsuruta T (1982) Makromol Chem Rapid Comm 3:275
330. Kataoka K, Okano T, Sakurai Y, Nishimura T, Inoue S, Watanabe T, Maruyama M, Tsuruta T (1983) Eur Polym J 19:979
331. Maruyama A, Tsuruta T, Kataoka K, Sakurai Y (1987) Makromol Chem Rapid Comm 8:27
332. Bigelow JC, Nabeshima Y, Kataoka K, Giddings JC (1991) Separation of cells and measurement of surface adhesion forces. In: Compala DS, Todd P (eds) ACS Symp Ser. American Chemical Society, Washington, DC, p 146
333. Janca J, Pribylova D, Konak C, Sedlacek B (1987) Anal Sci 3:297
334. Myers MN, Giddings JC (1979) Powder Technol 23:15
335. Schure MR, Myers MN, Caldwell KD, Byron C, Chan KP, Giddings JC (1985) Environ Sci Technol 19:686
336. Giddings JC (1985) Sep Sci Technol 20:749
337. Levin S, Giddings JC (1991) J Chem Tech Biotechnol 50:43
338. Giddings JC (1992) Sep Sci Technol 27:1489
339. Fuh CB, Trujillo EM, Giddings JC (1995) Sep Sci Technol 30:3861
340. Giddings JC (1988) Sep Sci Technol 23:119
341. Giddings JC (1985) Sep Sci Technol 20:749
342. Fuh CB, Chen SY (1998) J Chromatogr 813:313
343. Williams PS, Levin S, Lenczycki T, Giddings JC (1992) Ind Eng Chem Res 31:2172
344. Fuh CB, Levin S, Giddings JC (1993) Anal Biochem 208:80
345. Reid RC, Prausnitz JM, Sherwood TK (1977) The properties of gases and liquids; 3rd edn. MacGraw-Hill chemical engineering series. McGraw-Hill Book, New York, p 688
346. Morawetz H (1975) Macromolecules in solution. Wiley-Interscience, New York
347. Giddings JC, Yoon YH, Caldwell KD, Myers MN, Hovingh ME (1975) Sep Sci Technol 10:447
348. Giddings JC, Myers MN, Yang FJF, Smith LK (1976) Mass analysis of particles and macromolecules by field-flow fractionation. In: Kerker M (ed) Colloid and interface science. Academic Press, New York, pp 381–398
349. van Asten AC, Venema E, Kok WT, Poppe H (1993) J Chromatogr 644:83
350. van Asten AC, Kok WT, Tijssen R, Poppe H (1994) J Chromatogr A 676:361
351. Pasti L, Roccasalvo S, Dondi F, Reschiglian P (1995) J Polym Sci Part B: Polym Phys 33:1225
352. Martin M, Ignatiadis I, Reynaud R (1987) Fuel 66:1436
353. Janca J, Martin M (1992) Chromatographia 34:125
354. Giddings JC, Li S, Williams PS, Schimpf ME (1988) Makromol Chem Rapid Commun 9:817
355. Lee S (1993) Gel-content determination of polymers using thermal field-flow fractionation. In: Provder T (ed) Chromatography of polymers: characterization by SEC and FFF. American Chemical Society, Washington, DC, pp 77–88
356. Lee S, Molnar A (1995) Macromolecules 28:6354
357. Shiundu PM, Remsen EE, Giddings JC (1996) Appl Polym Sci 60:1695
358. van Asten AC, van Dam RJ, Kok WT, Tijssen R, Poppe H (1995) J Chromatogr A 703:245
359. Kirkland JJ, Boone LS, Yau WW (1990) J Chromatogr 517:377
360. Rue CA, Schimpf ME (1994) Anal Chem 66:4054
361. Kirkland JJ, Dilks CH Jr., Rementer SW (1992) Anal Chem 64:1295
362. Tank C, Antonietti M (1996) Macromol Chem Phys 197:2943
363. Derand H, Wesslen B, Wittgren B, Wahlund K-G (1996) Macromolecules 29:8770
364. Hecker R, Fawell PD, Jefferson A, Farrow JB (1999) J Chromatogr A 837:139

365. Brimhall SL, Myers MN, Caldwell KD, Giddings JC (1984) J Polym Sci Polym Lett Ed 22:339
366. Brimhall SL, Myers MN, Caldwell KD, Giddings JC (1984) Polym Mater Sci Eng 50:48
367. Kirkland JJ, Dilks CH (1992) Anal Chem 64:2836
368. Miller ME, Giddings JC (1998) J Microcolumn Sep 10:75
369. Schallinger LE, Yau WW, Kirkland JJ (1984) Science 225:434
370. Arner EC, Kirkland JJ (1989) Biochim Biophys Acta 993:100
371. Schallinger E, Arner EC, Kirkland JJ (1988) Biochim Biophys Acta 966:231
372. Schallinger LE, Gray JE, Wagner LW, Knowlton S, Kirkland JJ (1985) J Chromatogr 342:67
373. Lou J, Myers MN, Giddings JC (1994) J Liq Chromatogr 17:3239
374. White RJ (1997) Polym Int 43:373
375. Liu M-K, Giddings JC (1993) Macromolecules 26:3576
376. Dycus PJM, Healy KD, Stearman GK, Wells MJM (1995) Sep Sci Technol 30:1435
377. Beckett R (1987) Environ Technol Lett 9:339
378. Schimpf ME, Wahlund KG (1997) J Microcolumn Sep 9:535
379. van den Hoop MAGT, van Leeuwen HP(1997) Coll Surf A: Physicochem, Eng Aspects 120:235
380. Dixon DR, Wood FJ, Beckett R (1992) Environ Technol 13:1117
381. Beckett R, Wood FJ, Dixon DR (1992) Environ Technol 13:1129
382. Washizu M, Suzuki S, Nishizaka T, Shinohara T (1992) 1992 IEEE Ind Appl Soc Annu Meetings 1 and 2, pp 1446–1452
383. Yang FS, Caldwell KD, Myers MN, Giddings JC (1983) J Colloid Interface Sci 93:115
384. Kirkland JJ, Yau WW (1983) Anal Chem 55:2165
385. Oppenheimer LE, Smith GA (1988) Langmuir 4:144
386. Barman BN, Giddings JC (1992) Langmuir 8:51
387. Jones HK, Barman BH, Giddings JC (1988) J Chromatogr 455:1
388. Barman BN, Giddings JC (1991) Overview of colloidal aggregation by sedimentation field-flow fractionation. In: Provder T (ed) Particle size distribution II: Assessment and characterization. American Chemical Society, Washington, DC, pp 217–228
389. Barman BN, Giddings JC (1995) Anal Chem 67:3861
390. Arlauskas RA, Burtner DR, Klein DH (1993) Calibration of a photosedimeter using sedimentation field-flow fractionation and gas chromatography. In: Provder T (ed) Chromatography of polymers: characterization by SEC and FFF. American Chemical Society, Washington, DC, pp 2–12
391. Yang F-S, Caldwell KD, Giddings JC, Astle L (1984) Anal Biochem 138:488
392. Arlauskas RA, Weers JG (1996) Langmuir 12:1923
393. Hansen ME, Short DC (1990) J Chromatogr 517:333
394. Li J, Caldwell KD, Anderson BD (1993) Pharm Res 10:535
395. Weers JG, Arlauskas RA (1995) Langmuir 11:474
396. Levin S, Klausner E (1995) Pharm Res 12:1218
397. Schimpf ME (1987) Characterization of polymers and their thermal diffusion by thermal field-flow fractionation. PhD Thesis, University of Utah, USA
398. Liu G, Giddings JC (1991) Anal Chem 63:296
399. Shiundu PM, Liu G, Giddings JC (1995) Anal Chem 67:2705
400. Shiundu PM, Giddings JC (1995) J Chromatogr 715:117
401. Moon MH, Kwon H, Park I (1997) Anal Chem 69:1436
402. Ratanathanawongs SK, Giddings JC (1993) Polym Mater Sci Eng 70:26
403. Caldwell KD, Li J, Li J (1993) Polym Mater Sci Eng 69:404
404. Ratanathanawongs SK, Shiundu PM, Giddings JC (1995) Colloids Surf A: Physicochem Eng Aspects 105:243
405. Tan JS, Harrison CA, Li JT, Caldwell KD (1998) J Polym Sci B: Polym Phys 36:537
406. Dunkel M, Tri N, Beckett R, Caldwell KD (1997) J Microcolumn Sep 9:177
407. Karaiskakis G, Graff KA, Caldwell KD, Giddings JC (1982) Int J Environ Anal Chem 12:1

408. Beckett R, Nicholson G, Hart BT, Hansen M, Giddings JC (1988) Water Res 22:1535
409. McCarthy JF, Zachara JM (1989) Environ Sci Technol 23:496
410. Beckett R, Hotchin DM, Hart BT (1990) J Chromatogr 517:435
411. Caldwell KD, Karaiskakis G, Giddings JC (1981) Colloids Surf 3:233
412. Kirkland JJ, Yau WW, Szoka FC (1982) Science 215:296
413. Cardot PJP, Gerota J, Martin M (1991) J Chromatogr 568:93
414. Merino A, Bories C, Gantier J-C, Cardot PJP (1991) J Chromatogr 572:291
415. Merino-Dugay A, Cardot PJP, Czok M, Guernet M, Andreux AP (1992) J Chromatogr 579:73
416. Bories C, Cardot PJP, Abramowski V, Poüs C, Merino-Dugay A, Baron B (1992) J Chromatogr 579:143
417. Urbánková E, Vacek A, Nováková N, Matulík F, Chmelík J (1992) J Chromatogr 583:27
418. Pazourek J, Chmelík J (1993) Chromatographia 35:591
419. Pazourek J, Urbánková E, Chmelík J (1994) J Chromatogr A 660:113
420. Cardot PJP, Elgéa C, Guernet M, Godet D, Andreux JP (1994) J Chromatogr B 654:193
421. Bernard A, Bories C, Loiseau PM, Cardot PJP (1995) J Chromatogr B 664:444
422. Reschiglian P, Torsi G (1995) Chromatographia 40:467
423. Meng H, Caldwell KD, Giddings JC (1984) Fuel ProcessTechnol 8:313
424. Graff KA, Caldwell KD, Myers MN, Giddings JC (1984) Fuel 63:621
425. Giddings JC, Moon MH (1991) Anal Chem 63:2869
426. Giddings JC, Ratanathanawongs SK, Moon MH (1991) KONA: Powder Particle 9:200
427. Beckett R, Jiang Y, Liu G, Moon MH, Giddings JC (1994) Part Sci Technol 12:89
428. Ratanathanawongs SK, Giddings JC (1989) J Chromatogr 467:341
429. Ratanathanawongs SK, Giddings JC (1994) Chromatographia 38:545
430. Fox A, Schallinger LE, Kirkland JJ (1985) J Microbiol Methods 3:273
431. Mozersky SM, Caldwell KD, Jones SB, Maleeff BE, Barford RA (1988) Anal Biochem 172:113
432. Gilbart J, Wells AF, Hoe MH, Fox A (1987) J Chromatogr 387:428
433. Caldwell KD, Nguyen TT, Giddings JC, Mazzone HM (1980) J Virol Methods 1:241
434. Caldwell KD, Compton BJ, Giddings JC, Olson RJ (1984) Invest Ophthalmol Visual Sci 25:153
435. Sklaviadis T, Dreyer R, Manuelidis L (1992) Virus Res 26:241
436. Moon MH, Giddings JC (1993) J Food Sci 58:1166
437. Li P, Giddings JC (1996) J Pharm Sci 85:895
438. Li P, Hansen M, Giddings JC (1997) J Liq Chromatogr Rel Tech 20:2777
439. Barman BN, Myers MN, Giddings JC (1989) Powder Technol 59:53
440. Barman BN, Ashwood ER, Giddings JC (1993) Anal Biochem 212:35
441. Barman BN (1994) J Colloid Interf Sci 167:467
442. Yue V, Kowal R, Neargarder L, Bond L, Muetterties A, Parsons R (1994) Clin Chem 40:1810
443. Tong X, Caldwell KD (1995) J Chromatogr B 674:39
444. Hoffstetter-Kuhn S, Rösler T, Ehrat M, Widmer HM (1992) Anal Biochem 206:300
445. Sharma RV, Edwards RT, Beckett R (1993) Appl Environ Microbiol 1864
446. Fuh CB, Giddings JC (1995) Biotechnol Prog 11:14
447. Caldwell KD, Karaiskakis G, Giddings JC (1981) J Chromatogr 215:323
448. Myers MN, Graff KA, Giddings JC (1980) Nucl Technol 51:147
449. Giddings JC, Graff KA, Myers MN, Caldwell KD (1980) Sep Sci Technol 15:615
450. Martin M, Reynaud R (1984) Collect Colloq Semin Inst Fr Pet 40:263
451. Markx GH, Rousselet J, Pethig R (1997) J Liq Chromatogr Rel Tech 20:2857
452. Keil RG, Tsamakis E, Fuh CB, Giddings JC, Hedges JI (1994) Geochim Cosmochim Acta 58:879
453. Contado C, Dondi F, Beckett R, Giddings JC (1997) Anal Chim Acta 345:99
454. DeGennes PG (1976) Macromolecules 9:594
455. Litzén A, Wahlund K-G (1991) J Chromatogr 548:393

456. Inagaki H, Tanaka T (1980) Anal Chem 52:201
457. Williams PS, Xu Y, Reschiglian P, Giddings JC (1997) Anal Chem 69:349
458. Dilks CH Jr., Yau WW, Kirkland JJ (1984) J Chromatogr 315:45
459. Janca J (1984) Steric exclusion liquid chromatography of polymers. Chromatogr Sci Ser. Marcel Dekker, New York, chap 25, p 329
460. Jahnova V, Matulik F, Janca J (1987) Anal Chem 59:1039
461. Wyatt PJ (1998) J Colloid Interface Sci 197:9
462. Dalas E, Karaiskakis G (1987) Colloids Surf 28:169
463. Beckett R, Giddings JC (1997) J Colloid Interf Sci 186:53
464. Kirkland JJ, Schallinger LE, Yau WW (1985) Anal Chem 57:2271
465. Miller ME, Lee H, Li X, Szentirmay R, Giddings JC (1994) Polym Prepr (ACS Div Polym Chem) 35:764
466. Wijnhoven JEGJ, van Bommel MR, Poppe H, Kok WT (1996) Chromatographia 42:409
467. Johann C, Kilz PJ (1991) J Appl Polym Sci: Appl Polym Symp 48:111
468. Wyatt PJ (1991) J Liq Chromatogr 14:2351
469. Adolphi U, Kulicke WM (1997) Polymer 38:1513
470. Thielking H, Kulicke WM (1998) J Microcolumn Sep 10:51
471. Antonietti M, Briel A, Tank C (1995) Acta Polymer 46:254
472. Korgel BA, Vanzanten JH, Monbouquette HG (1998) Biophys J 74:3264
473. Wittgren B, Wahlund KG (1997) J Chromatogr A 760:205
474. Wittgren B, Wahlund KG (1997) J Chromatogr A 791:135
475. Wittgren B, Borgstrom L, Piculell L, Wahlund KG (1998) Biopolymers 45:85
476. Zahoransky RA, Dummin H, Laile E, Schauer T (1997) Talanta 44:2225
477. Lee H, Kim S, Williams R, Giddings JC (1998) Anal Chem 70:2495
478. Jensen KD, Williams SK, Giddings JC (1996) J Chromatogr 746:137
479. Moon MH, Giddings JC (1996) Ind Eng Chem Res 35:1072

Received: February 1999

Capillary Electrophoresis in Polymer Analysis

H. Engelhardt, O. Grosche

Institute of Instrumental and Environmental Analysis, University of the Saarland,
66123 Saarbrücken, Germany
e-mail: iaua@rz.uni-sb.de

Abstract. Capillary electrophoresis has demonstrated its enormous potential for the separation of biopolymers for several years. For the separation of proteins and carbohydrates, and to an even larger extent in DNA sequencing, new buffer systems and capillary coatings as well as derivatization agents have been developed. Recently, synthetic water-soluble polymers, for example, polyethylene glycols, or polyelectrolytes, such as polystyrenesulfonic acid or polyvinylypyridinium hydrochloride, have been successfully separated. This article introduces the principles of capillary electrophoresis, capillary gel electrophoresis, as well as giving an overview of the recent literature. Finally, it provides a strategy as to how to optimize an individual separation system.

Keywords. Capillary electrophoresis, Gel electrophoresis, Polystyrenesulfonate, Biopolymer, DNA

Advances in Polymer Science, Vol. 150

List of Abbreviations

η	dynamic viscosity
ζ	zeta potential
ε	dielectric constant
ξ_b	blob size for the entangled polymer solution
μ	electrophoretic mobility; mobility in free solution
μ_1	mobility of the closest solute
μ_{EOF}	mobility of the electroosmotic flow
a	Mark-Houwink constant
b	peak width in half height
c	gel or polymer concentration
c^*	entanglement concentration of the polymer solution
D	diffusion coefficient
e	elementary charge
K	Mark Houwink constant
K_0, K_{rep}	constants
K_r	retardation coefficien
L_{eff}	effective length of the capillary
L_{tot}	total length of the capillary
M, M_w	molecular weight
N	number of theoretical plates
N_P	molecular size of the solute
r	radius of the solvated molecule
R	resolution
R_g	radius of gyration
r_s	thickness of the polymer strand of the buffer additive
T	temperature
t, t_m	migration time
U	applied Voltage
u	electrophoretic velocity
z	effective charge of the solute

1 Introduction

Capillary electrophoresis (CE), also designated with the acronym HPCE for High Performance Capillary Electrophoresis, unites the classical separation technique of electrophoresis on plates with the instrumental methods of chromatography with respect to direct detection of the solutes separated in the capillary and their ready identification and quantification [1–3]. As a rapid and reliable separation system it is available for ionic compounds from the smallest cation (the lithium ion) up to polyanions with molecular weights ranging in the millions, such as DNA molecules. The concept of capillary electrophoresis encompasses various separation techniques. In capillary zone electrophoresis (CZE) the capillary is filled only with an appropriate electrolyte, and the separation is based solely on the mobility differences of the solutes. The method resembles elution chromatography in that the zones migrate at different velocities through the separation system and, in the optimum case, are separated from each other by buffer electrolyte. Always superimposed onto the electrophoretic migration is a more or less strong electroosmotic flow (EOF) that contributes passively to the transport of the solutes zones, but not to their separation. This EOF depends strongly on the pH value of the buffer and the surface properties of the capillary.

Due to the dissociation of the surface silanol groups in most buffers, negative charges exist on the surface of the fused silica (FS) capillary. They induce a positive counterion layer in the solution adjacent to the wall. As a result, the EOF

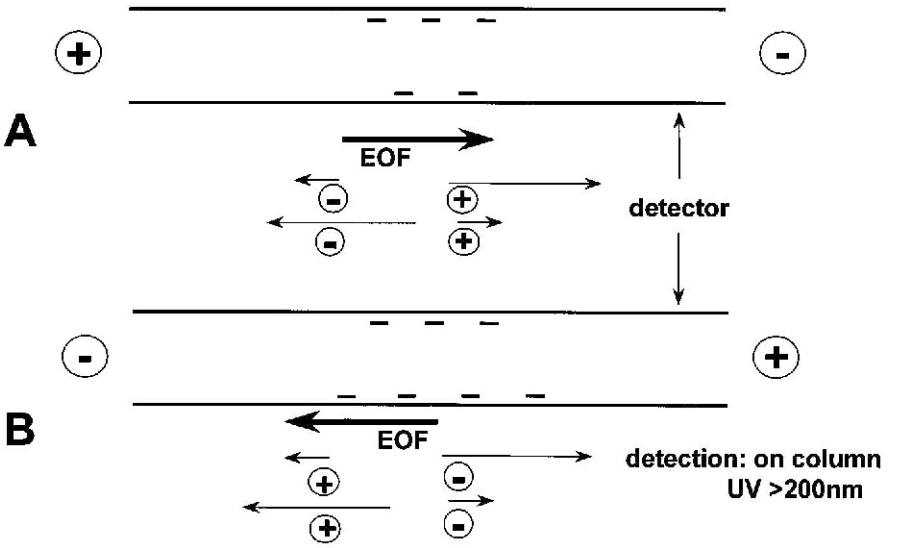

Fig. 1. Separation scheme for capillary electrophoresis

moves in the direction of the cathode. Therefore, the detector is located in the vicinity of the cathode compartment in the usual instrumental configuration. The EOF can be so large that not only neutral molecules, but even negative ions, can be transported to the detector in an opposite direction to their electrophoretic mobility. A schematic presentation of the system with the indication of the EOF direction is given in Fig. 1.

Biopolymers as well as synthetic polymers, as polyanions or polycations, exist with the same surface/charge ratio and migrate with almost identical velocity and cannot be separated in a normal electric field without an auxiliary aid. Since these polymers differ greatly in size, however, a gel can be used to influence the mobility of a large polymer more than that of a smaller one. In capillary gel electrophoresis (CGE), the electrophoretic migration of macromolecules is hindered by the gel matrix. The transport of the solutes through the capillary is based on the charge of the macromolecules, but the separation is dependent on the molecular size. It is easy to understand that with this technique EOF should be eliminated because otherwise the gel is extruded from the capillary.

2
Mobility and Diffusion

2.1
Electrophoretic Migration

In an electrical field ions move at constant velocity. The velocity u increases with the potential U and consequently the field strength E. The electrophoretic mobility μ relates the velocity and the field strength as:

$$u = \mu \cdot E = \frac{L_{eff}}{t} \tag{1}$$

The velocity of the ion is determined by dividing the traversed path length (capillary length from inlet to detector) by the migration time of the zone t. It should be pointed out that the field decreases over the total capillary length L_{tot} between the two buffer vials, whereas the solutes traverse only the effective capillary length L_{eff} during the migration time. The migration mobility can be determined by the following equation:

$$\mu = \frac{L_{eff}}{t \cdot E} = \frac{L_{eff} \cdot L_{tot}}{t \cdot U} \tag{2}$$

The mobility is determined by the equilibrium of the driving electrical force and the frictional force approximated by Stokes' law:

$$\mu = \frac{z \cdot e}{6 \cdot \pi \cdot \eta \cdot r} \tag{3}$$

where z is the effective charge of the solute ion, e the elementary charge, η the dynamic viscosity of the electrolyte, and r the radius of the solvated molecule. The effective charge of a solute ion is the charge of that ion minus the fractional charge of the surrounding oppositely charged ions (in the rigid double layer model). During migration the ion drags this portion of the double layer with it and therefore migrates more slowly than would correspond to its actual charge. This is called the electrophoretic effect and is largest for thin, diffuse double layers surrounding the ion. This characteristic double layer can be calculated from the Debye–Hückel theory and is inversely proportional to the square root of the electrolyte concentration. It can be shown experimentally that the effective charge and therefore the migration velocity decreases with increasing ionic strength.

For large molecules of similar composition and sizes larger than the double layer, the mobilities are independent of the size, which makes their separation by electrophoresis difficult. Thus the migration velocity of polyelectrolytes like DNA molecules and proteins denatured with sodium dodecyl sulfate (SDS) is almost identical in pure electrolytes. Separations are attained only if their migration is modified by exclusion or sieving effects.

2.2 Electroosmotic Flow

In CE, the electroosmotic flow is in most cases superimposed on the electrophoretic migration. The EOF depends on the distribution of charges in the proximity of the capillary surface. Nearly all surfaces carry a charge. These are negative charges from the dissociation of surface silanol groups in the case of FS capillaries. In solution these surface charges are counterbalanced by oppositely charged ions (counterions). If an electrical field is applied parallel to the surface, the field pulls the counterions from the mobile layer along its axis and thus moves the entire liquid in the capillary along with it. In FS capillaries with an enrichment of positive ions in the boundary layer, the EOF is induced to move to the cathode. An extremely flat (piston-shaped) flow profile is produced, which is the reason for the narrower peaks obtained in CE in comparison to the pressure-driven (hydrodynamic) flow in liquid chromatography (LC) where the Hagen–Poiseuille force is the reason for peak broadening.

The migration velocity u of the EOF can be described in simplified form by means of the Helmholtz equation:

$$u = \frac{\varepsilon \cdot E \cdot \zeta}{4\pi \cdot \eta} \tag{4}$$

The EOF is inversely proportional to the viscosity η of the electrolyte, proportional to its dielectric constant ε, the applied field strength E and the ζ-potential (zeta-potential). For FS capillaries, the EOF diminishes with increasing electrolyte concentration, and increases with the degree of dissociation of the surface

silanol groups, i. e. with the pH value. The addition of organic components to the electrolyte also has a significant influence on the magnitude of the EOF. However, no consistency in the behavior of the EOF was found on the addition of organic solvents, and no correlation with the buffer viscosity detected. In general, the addition of methanol leads to a decrease in the EOF, whereas with acetonitrile in the buffer an increase is observed. Tetrahydrofuran has little effect on the EOF, whereas isopropanol produces a drastic reduction of the EOF.

EOF appears in all electrophoretic separation modes because surface charges cannot be completely eliminated. On the one hand, it can lead to convective mixing of the electrophoretic zones but, on the other, it also plays an essential and decisive role in the transport of the zones through the capillary. The detector in CE is usually placed on the cathode side because of the ever present EOF. Cations move with the EOF (comigration), resulting in very short analysis times for this group of components. Even anions that migrate opposite to the direction of the EOF (countermigration) are transported to the detector (on the cathode site) if their migration velocity is lower than the velocity of the EOF. Only the anions that migrate faster than the flow velocity of the EOF migrate into the anode compartment and escape detection.

Through chemical modification of the capillary surface the EOF can be controlled, nullified, or even reversed. When working with gel-filled capillaries, the EOF should be completely suppressed, otherwise the gels will be flushed out of the capillary. By modifying the capillary surface, interactions between the sample components and the wall can be suppressed. Sorption effects of sample components (especially of positively charged solutes) at the walls always degrade the efficiency (resistance to mass transfer) and, in particular in the separation of proteins, lead to a significant reduction in the plate numbers and/or loss of sample through irreversible adsorption.

2.3 Modification of Capillary Surfaces

By adding long-chain cationic detergents, such as cetyltrimethylammonium salts, to the buffer the EOF can be reversed. By adsorption on the surface silanols a double layer is formed, with positive charges directed toward the electrolyte. Polymers like Polybren™, a polyamine with quaternary groups, or lower polyamines like spermine can, in part, be adsorbed so strongly that they are not flushed out during a buffer change. Their application is limited to neutral or medium-acidic pH values. These modifications, as well as the adsorption of surfactants, are termed "dynamic coatings". They reduce or reverse the EOF and the irreversible adsorption of positively charged biopolymers, e. g. proteins.

The EOF can also be controlled by chemical modification of the capillary surface. Various options initially developed for modification of silica in high performance liquid chromatography (HPLC) and for coating capillaries in gas chromatography (GC) are available for the chemical coating of capillaries. The surface silanols at the capillary wall can be reacted with silanes introducing anchor

groups containing olefinic groups such as γ-methacryloxypropyltrimethoxysilane which can be copolymerized in a second step with, for example, acrylamide in aqueous solution [4,5]. These coatings with linear polyacrylamide completely suppress the EOF and are stable in the pH-range 2.5–8. Their instability at high pH values becomes noticeable by a reappearance of the EOF and fluctuations in migration times.

On account of their simple preparation and commercial availability there is a wide variety of applications for linear polyacrylamide coatings. These involve not only the separation of proteins but also include biomolecules such as DNA fragments. They are also used for the preparation of gel-filled capillaries.

Higher hydrolytic stability is exhibited by capillaries based on vinyl coatings as primary anchor group, where, in the second step, vinyl acetate is polymerized and subsequently hydrolyzed with sodium methylate in methanol [6]. Such capillaries are stable up to a pH value of 10. Polyvinyl alcohol has also been thermally immobilized onto the capillary surface [7]. With such stable layers in the acidic and neutral region no measurable EOF is present and the stability of the capillaries is very good.

Many types of adsorptive and permanent coatings have been described in the literature. In this review only well described and/or commercially available coated capillaries have been included. Table 1 summarizes the possibilities of modifying the EOF.

Table 1. Possibilities to modify the EOF

Change in separation system	Effect on EOF	Comments
pH value of buffer	EOF increases with pH	May effect charges of analytes
Buffer concentration	EOF increases with decreasing concentration	High concentrations lead to high currents, low ones to overloading
Temperature	Viscosity changes	Selectivity may be affected
Organic solvents	Affect EOF and buffer viscosity	Complex changes in separation system
Surfactants as buffer additives	Drastic changes of EOF through adsorption on wall	Anionic surfactants increase EOF; cationic reduce or reverse it
Ionic polymers	Adsorption on capillary wall	With positively charged polymers, flow reversal
Neutral polymers	Adsorption on capillary wall	Reduction of EOF and solute adsorption
Covalently bonded coatings	Affect EOF; reduce wall adsorption	Stability problems
Additional radial electric field	Change in EOF	Limited applicability

2.4 Band Broadening

The well-known parameters of chromatography, such as the number of theoretical plates, N, have been adapted to describe the zone dispersion in CE. Analogous to chromatography, the plate numbers are calculated from the migration time t and peak width b in half height:

$$N = 5.54 \cdot \left(\frac{t}{b} \right)^2 \tag{5}$$

If all other causes of band broadening are neglected, the plate number is directly proportional to the electric field E and inversely proportional to the diffusion coefficient D of the solute in the electrolyte. The relationship is given by:

$$N = \frac{\mu U}{2D} \tag{6}$$

Only the longitudinal diffusion term has to be considered. The main contribution to band broadening in chromatography stems from the restricted mass transfer in the mobile phase, which is unimportant in CE due to the plug-like flow profile. In contrast to LC the plate number increases with the decreasing diffusion coefficient of the solute. From this it can be deduced that CE is particularly suited for the separation of polymers because they predominately possess low diffusion coefficients which decrease with increasing molecular weight. It has been shown [8] that at room temperature and over a wide range of molar masses the equation for the plate number can be approximately reduced to:

$$N \cong 20 \cdot z \cdot U \tag{7}$$

where z is the effective charge of the solute in the buffer. With potentials up to 30,000 V and effective charges between 1 and 10, up to 10 million theoretical plates are attainable. These high plate numbers have actually been verified for DNA molecules in gel-filled capillaries. This demonstrates that CE is superior to HPLC in respect to possible separation efficiency. However, DNA molecules represent a special case as because of their large number of negative charges they do not interact with the capillary surface, and as elongated molecules they possess a very low diffusion coefficient in the gel matrix.

Other effects may also contribute to band broadening causing reduced achievable plate counts. Besides the already-mentioned wall adsorption, temperature effects (Joule heating) may reduce plate numbers. Sample application can have a strong influence on plate count, especially when large volumes and/or high sample concentrations are injected. Mobility differences between buffer constituents and analyte ions lead to asymmetric (triangular) peaks caused by electrodispersion, which is extremely noticeable with smaller molecules. Differ-

ences in the liquid levels of the buffer vials may introduce a hydrodynamic flow with the corresponding flow profile also resulting in reduced plate counts.

3 Principles of Optimization in Capillary Electrophoresis

Before discussing the separation of polyions, the principle optimization strategies in CZE will be discussed. During the entire separation the buffer, its pH value, and the field strength remain constant. Only solutes differing in mobility can be separated. The solutes are introduced in a mixture as a concrete zone at the beginning of the capillary and reach the detector as discrete zones. The buffer has the function of holding the pH constant and to assure the passage of the current. The buffer pH selected determines the charge of the analyte molecule and hence its direction of migration. The buffer concentration and its pH affect the EOF. The selectivity is optimized by choosing a suitable pH, and the analysis time depends strongly on the buffer concentration, the capillary length and the applied potential.

The resolution R in CZE can be determined from the following equation:

$$R = \frac{\sqrt{N}}{4} \cdot \frac{\Delta u}{\bar{u}} \tag{8}$$

The equation is similar to that used in chromatography [8] if the relative migration differences are inserted. These are proportional to the relative observed mobilities that include the contribution of the EOF:

$$\frac{\Delta u}{\bar{u}} = \frac{\mu_1 - \mu}{\mu + \mu_{EOF}} \tag{9}$$

It is evident that increasing the mobility simultaneously raises the EOF, and the relative velocity for each pair of zones is reduced along with the resolution. On the other hand, if the analyte migrates in an opposite direction to the EOF, the resolution increases because the residence time in the capillary is prolonged and the effective migration distance is lengthened, so that even components with very small differences in mobility can be separated from each other.

3.1 Influence of pH

The mobility of the ions is determined by their extent of dissociation in the carrier electrolyte and therefore by its pH. The largest migration differences are obtained when the buffer pH lies between the pK values of the sample components. The pH range between 2 and 12 can be exploited. At lower and higher pH values the current transport is overtaken by hydrogen or hydroxide ions, respectively. Due to their very high mobilities, only very low buffer concentrations can be

used in these ranges. The magnitude of the EOF in FS capillaries is, as mentioned above, also influenced by the pH. At pH values below 2, the EOF becomes negligible and may even be reversed due to protonation of the silanol groups.

3.2 Effect of Buffer Concentration

The buffer concentration selected should be high enough to maintain the pH constant during the analysis and to keep overloading effects to a minimum, while still permitting rapid analysis via the EOF but preventing the appearance of band broadening through thermal effects. The conductivity in the system should not be affected by sample introduction, therefore the buffer concentration should be higher than that of the ions in the sample solution. For the most frequently used capillaries with 75 μm internal diameter (i. d.), buffers of 10 to 50 mmol (mM) concentrations are most commonly employed.

Increasing the buffer concentration:

1. increases the current and consequently Joule heating,
2. increases the danger of band broadening by thermal convection,
3. decreases the EOF and, consequently,
4. increases analysis time,
5. decreases the danger of overloading phenomena,
6. decreases the danger of electrodispersion, and
7. decreases the danger of wall adsorption, e. g. with proteins.

3.3 Type of Buffer

As discussed above a certain buffer concentration is required to perform optimal analyses. The minimum ionic strength required determines the current and Joule heating. This effect can be measured as a deviation from Ohm's law. With organic buffers the conductivity is much smaller for a given ionic strength. Consequently organic zwitterionic buffers, or at least buffers with counterions of low mobility, should be preferred especially when long capillaries have to be used.

During the electrophoretic run, electrolysis takes place in the buffer vials, which are usually very small in modern instrumentation. A sufficiently large buffer capacity is required to achieve reproducible analyses because of the generated protons and hydroxide ions in the buffer compartments. The buffer is transported via the EOF into the capillary. Therefore, only high capacity buffers should be used and/or the buffer solutions in the vials should be frequently replenished.

4
Separation of Biopolymers

CE has found wide application in the analysis of proteins and in nucleic acid analysis in combination with the human genome project. DNA-analyzers based on CE have been introduced recently. Many biopolymers have identical electrophoretic mobilities because of the constant charge to size ratio. Consequently they cannot be separated in free solution. Some sort of sieving matrix has to be used. Generally, gels like cross-linked polyacrylamides, common in slab-gel electrophoresis, are also used in CE. One of the main disadvantages of these gels when prepared within the capillary is possible shrinkage during polymerization, air bubble formation (causing current disruption), drying out during injection, and degradation during use. These problems can be prevented when so-called "liquid" gels are used, consisting of more or less concentrated solutions of water-soluble polymers, which can be easily replaced in the capillaries. It was found that these "entangled polymer solutions" are comparable to cross-linked gels.

The theoretical treatment by CE of biopolymers has been established for nucleic acids, consequently in the following the fundamentals are described for this example.

4.1
Properties of Sieving Media

Initially, gels were prepared within the capillary by copolymerization of acrylamide with bisacrylamide [9] as in slab gel electrophoresis. The capillary wall was coated with an acrylate as described above to remove the EOF. Thus the gel could also be chemically fixed on the wall. Agarose which can be thermally mobilized has also been used [10]. With these gels the problem discussed above arose. Therefore liquid gels were introduced [11] after they had already been proposed for classical electrophoresis [12]. Some remarks on the properties of the sieving media will be given as the information found in the literature can be very confusing.

Generally, gels are somewhat intermediate between a solid and a liquid. Under deformation this shows elasticity, but it keeps a permanent memory of its form. Water and dilute solutions do not show any elasticity, they flow under pressure and are purely viscous (Newtonian liquids). In between both viscous-elastic fluids are located. These solutions have the property of a viscous solution and of a solid, depending on the forces applied and on the time scale. Under fast deformation they are elastic, keep a memory of their shape, but under slow deformation they behave like viscous solutions.

In dilute solutions of polymers the chains are hydrodynamically isolated from each other and the solutions behave as a liquid. When the concentration of the polymer in the solution is increased the polymer chains become entangled, forming a transient network of obstacles. This entanglement takes place above

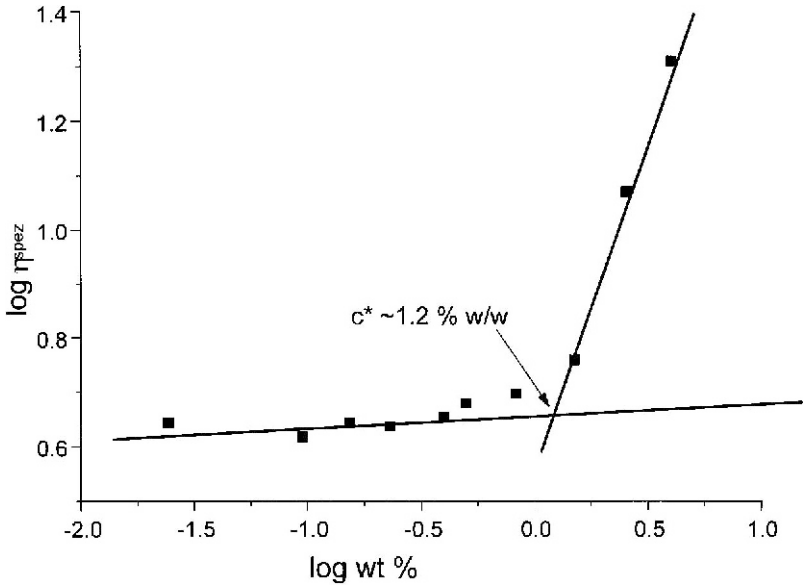

Fig. 2. Determination of the overlap threshold of dextran T 2000 as buffer additive in phosphate 50 mmol/l (pH 2.0) with the CE instrument. Conditions: capillary length 50–60 cm; pressure 1.5 psi

the overlap threshold c^*. It can be determined for each polymer experimentally by measuring the viscosity of the polymer solution at different concentrations. The point of deviation from linearity is defined as the overlap threshold [13]. It can be estimated experimentally in the CE instrument [14], as shown in Fig. 2.

The threshold concentration can also be calculated [15] from the Staudinger index or intrinsic viscosity $[\eta]$ according to Eq. (10):

$$c^* \cong 1.5\left[\eta\right]^{-1} \tag{10}$$

The intrinsic viscosity is a measure of the ability of a polymer to enhance the viscosity of a solution. It is related to the molecular weight of the polymer by the Mark–Houwink equation:

$$\left[\eta\right] \cong KM_w^a \tag{11}$$

where K and a are characteristic constants for a given polymer solvent combination. Characteristic values for some polymers used in CGE are summarized in Table 2 (Data taken from [16]).

For separations in CGE the "pore size" of such a polymer solution is interesting. The chain segment between two points of entanglement can be regarded as an independent subunit which can undergo random walk per se. The volume en-

Table 2. Mark–Houwink constants of some polymers used in CGE

Polymer	K (ml g^{-1})	a
Polyacrylamide	6.31×10^{-3}	0.80
Polydimethylacrylamide	2.32×10^{-2}	0.81
Polyethylene glycol	1.25×10^{-2}	0.78
Hydroxyethyl cellulose	9.53×10^{-3}	0.87
Methyl cellulose	0.316	0.55
Dextran	4.93×10^{-2}	0.60

closed by this chain segment is called a "blob". This "blob size" ξ_b should be used as "pore size" [15]. In DNA analysis, it is calculated by the following equation:

$$\xi_b = 1.43 R_g \left(\frac{c}{c^*} \right)^{-\frac{3}{4}} \tag{12}$$

It can be shown that the "pore size" of an entangled polymer solution does not depend on the degree of polymerization, only on its concentration. This means also that two solutions of the same type of polymer and with the same concentration but different molecular weights may have the same "pore size" as long as they are entangled. However, the viscosity of the two solutions is different because viscosity depends on the molecular weight. This has important consequences for the choice of the appropriate polymer solution. The pressure with CE instrumentation needed to displace the buffer solutions is limited, therefore the viscosity should not exceed a certain value. Explicit descriptions can be found in literature [16] for the selection of appropriate polymers and their concentrations for DNA analysis.

Above concentrations of 10% w/w one speaks of "concentrated solutions" whose properties are still poorly understood. They have little use in CE, partially because of their high viscosity.

4.2 Migration Theories for DNA Molecules in Capillary Gel Electrophoresis

DNA is a stiff polyelectrolyte. The collision of the migrating DNA and the separation media have different quantitative and even qualitative effects on DNAs of different size. Different conformations of the analytes exist during the separation, depending on the pore size of the gel and the length of the biopolymer. These conformations are ultimately responsible for the different mobilities and the apparent irregularities. The different conformations reproduced in Fig. 3 were observed by fluorescence microscopy [17,18].

The observed phenomena and anomalies lead to different migration models [19]. It is obvious that a compact or a relaxed conformation develops a different

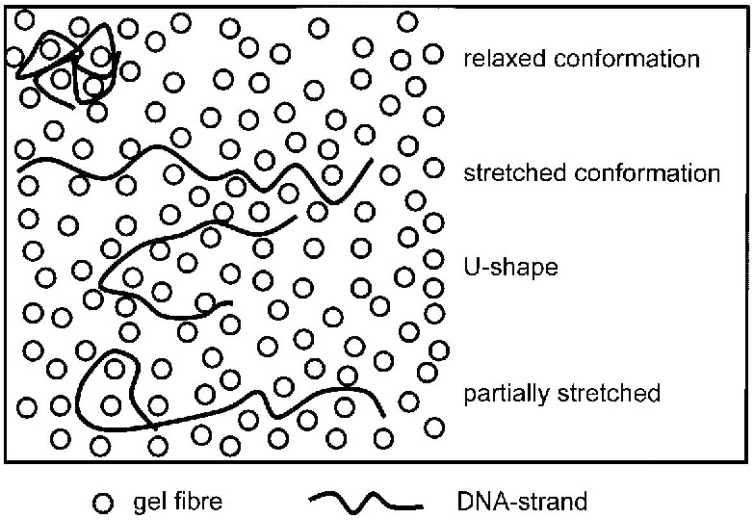

Fig. 3. Dependence of the mobility of a biopolymer on its conformation in a separation gel

mobility than, for example, an extended form. Separation is determined by the interaction of the analytes of increasing molecular weight with the polymer chains and the "pores" formed by them. In general, the mobility of an analyte in an entangled polymer solution is found to vary with respect to its size in the way depicted in Fig. 4. Four different regions can be distinguished in this curve. In the first part of the curve, the mobility changes very little with increasing analyte molecular weight or its length. The separation selectivity of the gel is very low for the smaller fragments. The "pore size" is much larger than the size of the molecule. The molecules can migrate through the gel without great resistance. A theoretical model describing the migration in this region has been developed by Ogston [20].

Using geometrical considerations, the mobility μ of a solute in the polymer solution is related to that in free solution μ_0 and the concentration c of the sieving polymer by:

$$\log\mu = \log\mu_0 - K_O(r_s + R_g)^2 c \tag{13}$$

The retardation coefficient K_r is a constant and depends on the thickness r_s of the polymer strand of the additive and the radius of gyration of the analyte:

$$K_r = K_O(r_s + R_g)^2 \tag{14}$$

It is important that the field intensity is low enough so that the DNA molecule retains a coiled conformation. Gels with narrower "pore size", i.e. larger cross-linking or higher polymer concentrations, must be selected for this separation

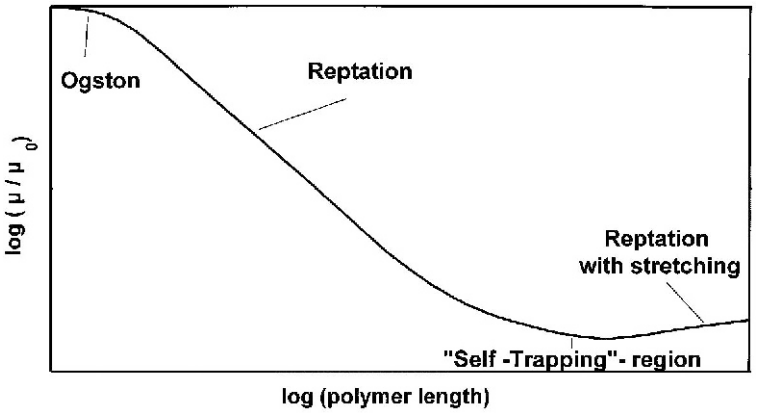

Fig. 4. Simulation of the log(analyte mobility) vs. log(analyte segment length) at a constant pore size of the separation matrix

region to improve the separation selectivity. The plot log μ vs. c, known as the Ferguson plot, should be a straight line with the slope of the retardation coefficient. The linearity of this plot is a necessity but not a condition to infer that the solute follows the Ogston model.

The greatest dependence of the analyte mobility on its chain length and therefore the greatest selectivity is found in the so-called reptation region. The size of the DNA molecule is much larger than the average pore size of the gel. It cannot fit into a single pore and must deform during its migration, especially if the field strength is not negligible. The analytes move through the gel via a snake-like movement (reptation). The largest interactions of the analyte with the gel matrix are possible, reflecting the maximum selectivity for separation according to chain length. The reduced electrophoretic mobility in this region is inversely proportional to the molecular weight.

In the reptation region the electrophoretic mobility depends on the solute's molecular size N_P and on the field strength E according to the biased reptation model [13]:

$$\mu = K_{rep}\left(\frac{1}{N_P} + b\left(\frac{E}{T}\right)\right)^2 \tag{15}$$

where K_{rep} is a constant and b is a function of the solute and the polymeric network.

It is evident from this equation that the mobility is inversely proportional only to the analyte chain length when the second term is negligible. This holds, however, only when relatively low field strengths (less than 200 V cm^{-1}) are used for CE. The relationship between mobility and the reciprocal of the chain length should become clearer at elevated temperatures. This effect can be seen in Eq. (15).

The higher the field strength and the lower the temperature of the separation system, the less dependent is the mobility on the reciprocal of the chain length.

For intermediate size DNA molecules a region can be observed where the mobility reaches a minimum. The mobility no longer depends on molecular weight in this abnormal migration area, where even a reversal ("band inversion") of migration may occur. One explanation for this phenomenon is that both ends of the DNA molecule migrate in the same direction and become strongly entangled with the polymer strands (*self*-trapping). The trapping cannot occur with small molecules as they can free themselves very quickly from this conformation. The probability of extremely large molecules reaching this status is very small. These effects remain the focus of scientific discussions [17] because they can also be explained assuming tertiary structures with DNA molecules. It has also been observed that the field strength, temperature, and gel concentration also exert strong influences on the expected migration sequence and on the mobilities. In the cases of inversion (larger molecules migrate faster than smaller ones) they can generally be eliminated by reducing the applied field strength, raising the temperature, decreasing the gel concentration, incorporating buffer additives such as ethidium bromide as DNA intercalates, and using pulsed electric fields.

Anomalous migration data where the mobility decreases very rapidly with molecular size have been described by an entropic trapping of the molecules within the gel matrix. This effect should be noticeable when the pore size of the polymer matrix corresponds to the radius of gyration of the analyte. However, the electric forces reduce the entropic effect; consequently it should contribute only at extremely low field strength. It does not seem relevant under normal CGE conditions, and cannot improve separations.

4.3 Separation of DNA

A typical separation of DNA restriction fragments is shown in Fig. 5 with a capillary filled with a linear polyacrylamide (LPA). The concentration of the acrylamide was 3% (3%T, 0% C in the standard nomenclature, where C is the crosslinker and T the monomer concentration). Since all fragments in the range between 34 base pairs and 622 base pairs are present in an equimolar ratio, the larger fragments have more absorption units in the molecule. As a result, the peak area increases with chain length. Deviations from this general trend are caused by insufficient separation or by inversion of migration order. The short fragments appear as small peaks and, because of their low resistance in the gel, they are first in the electropherogram. Between 600,000 and 1 million plates/m have been generated with this separation.

In Fig. 6 the dependence of the relative mobility vs. the number of base pairs (chain length) is given. It can be seen that the theoretical model discussed above is able to describe the experimental data. Temperature influence has already been discussed in the previous section.

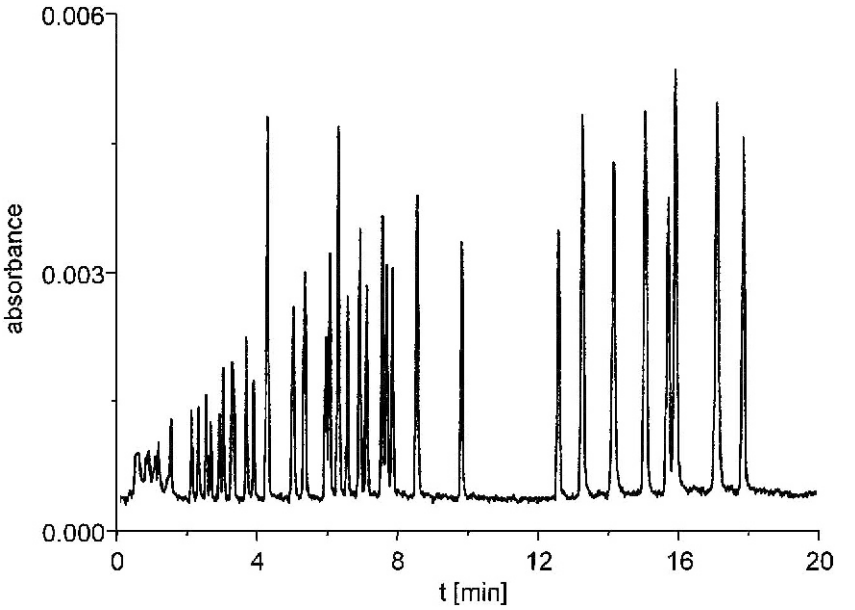

Fig.5. Separation of DNA restriction fragments in a capillary filled with linear polyacrylamide. Separation conditions: L=40–47 cm, E=150 V cm^{-1}, T=50 °C; buffer: 0.1 M TBE, pH 8.3 with 3% T, 0% C LPA; detection: 254 nm; sample: pBR 322 MSP I, pBR322 Hae III (peak assignment right to left: number of base pairs (bp): 622, 582, 540, 527, 504, 458, 434, 404, 309, 267, 242, 238, 234, 217, 213, 201, 192+190, 184, 180, 160+160, 147+147, 123+123+124, 110, 104, 89+90, 80, 76, 67, 64, 57, 51, 34+34)

Separation of DNA molecules is also possible in uncross-linked polymer solutions at concentrations well below the polymer overlap threshold [21]. Working with dilute solutions the molecular weight of the polymer is a very important factor for the efficiency of DNA separations with these systems. Low-molecular-weight hydroxyethyl cellulose (HEC) will provide good separations of small DNA fragments well below the threshold concentration. Increasing the concentration does not result in improved separation of longer fragments. However, a high-molecular-weight HEC in dilute solutions is advantageous for the separation of these molecules.

In contrast, with entangled solutions the molecular weight of the sieving polymer is not an important factor in determining the "pore size" of the polymer network and should, therefore, not strongly influence the DNA separation. Once the overlap threshold has been passed, the pore size of the network should only depend on the total polymer concentration. As the viscosity of the polymer solution depends strongly on the polymer molecular weight, it seems to be advantageous to select a polymer which is large enough to be well entangled at the concentration required for high resolution, but small enough to yield a manageable viscosity.

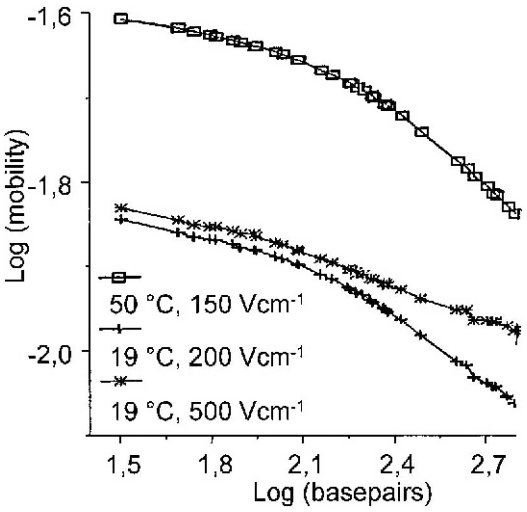

Fig. 6. Plot of log(mobility) of a mixture of DNA restriction fragments against log(number of base pairs). Separation conditions: L=40–47 cm; buffer: 0.1 M TBE, pH 8.3 with 3% T, 0% C LPA; various field strengths and temperatures

Recently, it has been shown [22] that the separation capability in DNA sequencing can be improved by using two different LPAs as sieving matrix. When a 2% solution of a high-molecular-mass LPA (MW 9 mio Da) was used, high efficiency could only be obtained in the 700 base pairs region (14 million plates/m), whereas with smaller fragments (49 base pairs) only low efficiency (3 million plates/m) and reproducibility could be achieved. In adding 0.5% of low-molecular-mass LPA to the electrolyte buffer, the separation efficiency was improved to determine short and long DNA fragments with equal efficiency.

4.4 Separation of Proteins

Proteins are mostly separated by CZE. Strong interactions between the analyte molecules and the capillary wall that are predominately electrostatic in nature have a strong influence on separation efficiency. By the use of buffer additives like amines or the use of dynamically or permanently coated capillaries, highly efficient separation of proteins in CZE is achievable. Here, the native proteins with their tertiary structure are separated. Denatured proteins as SDS complexes can be separated in gels. Advantageous are polysaccharide-based polymers, because they permit UV detection at low wavelength (214 nm), impossible with acrylamide-based gels. A separation of SDS-denatured protein standards in a dextran gel is shown in Fig. 7.

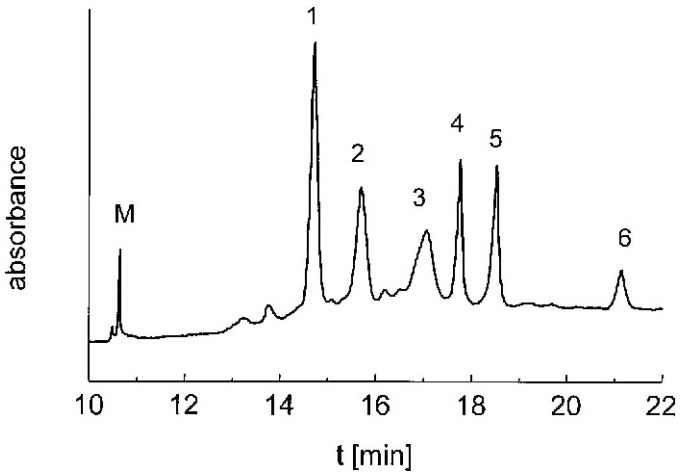

Fig. 7. Separation of SDS protein complexes with an exchangeable dextran polymer solution. Separation conditions: L=30–37 cm, E=300 V cm^{-1}, T=20 °C; (Beckman SDS protein kit); detection: 214 nm; analytes: Orange G (*M*), carboanhydrase (*1*), ovalbumin (*2*), bovine serum albumin (*3*), phosphorylase B (*4*), β-galactosidase (*5*), myosin (*6*)

5
Separation of Synthetic Polyelectrolytes

CE presents a great advantage over conventional chromatographic techniques in characterizing polyelectrolytes by operating in a single aqueous phase system thus excluding any unwanted interaction with a solid stationary phase. It allows investigation of the behavior of ionic polymers under conditions close to their area of application at high speed and high resolving power.

5.1
Polystryrenesulfonates

Polystryrenesulfonates (PSSs) can be analyzed easily by CE in plain silica capillaries, because they do not interact with the surface and are commercially available with low dispersities and different molecular masses. As early as 1992 Poli and Schure [23] showed the advantages of CE separation compared to conventional techniques like SEC. The behavior of PSSs in CE has also been studied by Minárik et al. [24], Cottet et al. [25] and Clos et al. [26].

Polystryrenesulfonates are already fully dissociated even at low pH values, where the EOF in unmodified fused silica capillaries is strongly suppressed. Consequently, it is possible to separate them in a counter electroosmotic way in free solution at pH values around or below 2.5. It is only possible to separate PSSs in free solution up to a molecular mass of 8000. Schure et al. [23] discussed wall adsorption because they could not separate PSSs at a pH value of 5. It seems

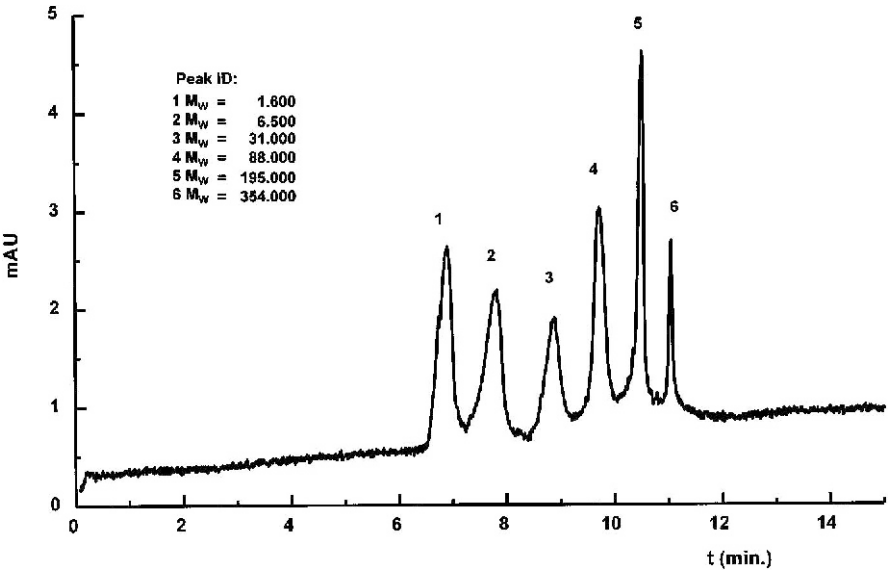

Fig. 8. Separation of polystyrole-4-sulfonates at pH 2.5 with dextran T 2000 as buffer additive. Separation conditions: fused silica L=50–57 cm, i.d.=75 μm; buffer 50 mM phosphate, pH 2.5+2% w/w dextran T 2000; E=–300 V cm^{-1}; injection: t=5 s, p=0.5 psi; detection: UV 254 nm

more likely that at this pH the EOF and the migration were balancing each other. Consequently, the overall mobility of the PSS was zero. Wall adsorption of negative PSS at the negatively charged capillary wall seems unlikely and has not been observed by others for PSS and for DNA molecules. Cottet [25] determined the mobilities of PSS in free solution with uncoated as well as with PEG (polyethylene glycol) coated capillaries and did not observe significant adsorption of the analytes at the wall of uncoated capillaries. Even at non-dissociated silanols (at pH 2.5) no wall adsorption was noticed [26].

When using sieving polymer solutions, it is more favorable to diminish the influence of the sieving media to the EOF (wall adsorption, changes in viscosity) with coated capillaries in order to avoid changes in migration times and, thus, separation efficiencies. Besides PEG coatings [25], polyacrylamide (PAA) coatings [24] and polyvinyl alcohol coatings [26] have been used. However, uncoated capillaries can also be used at low pH values. A separation of PSS standards at low pH values and with uncoated capillaries is shown in Fig. 8. The separation efficiency is highest in the molecular mass range below 100,000. The peak broadening of the higher-molecular-mass standards (e.g. 354,000) is extremely small compared with that of the standards with molecular mass below 100,000. This demonstrates that the sieving efficiency of the dextran used here is limited to the lower-molecular-mass range, where standard polydispersity is causing the broad peak observed.

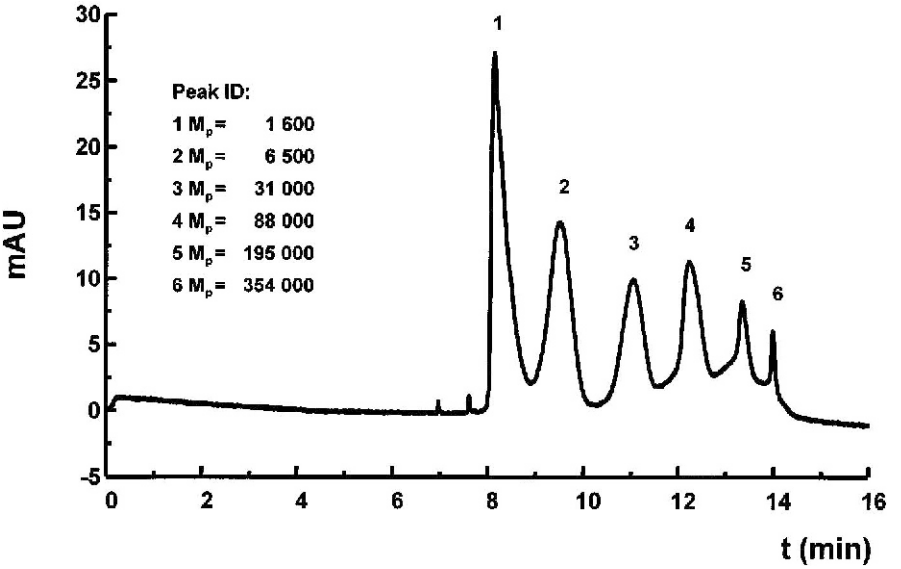

Fig. 9. Separation of polystyrole-4-sulfonates at pH 8.8 in a PVA-coated capillary with dextran T 2000 as buffer additive. Separation conditions: PVA capillary L=50–57 cm, i.d.=75 µm; buffer 60 mM AMPD/phosphoric acid, pH 8.8+2% w/w dextran T 2000; E=–300 V cm^{-1}; injection: t=20 s, p=0.5 psi; detection: UV 254 nm

Hydroxyethyl cellulose (HEC) was initially used as the sieving medium [23]. The differences in migration of PSS in HEC and PEG were studied [25]. The separation potential of PEG was inferior to that of HEC, and the PSS adsorption at the PEG coating increased with increasing PEG concentration in the buffer.

The problem with HEC solutions are their high viscosities. Therefore, dextrans differing in molecular mass have been used as sieving media [26]. These solutions can easily be replenished due to their low viscosities and exhibit good separation properties.

PSSs with molecular masses between 1 and 1000 kDa were studied by various authors. Their experimental results in references 23–25 are comparable to separations in dextran solutions. A separation of PSS standards with dextran (T 2000) in a coated capillary at pH 8.5 is shown in Fig. 9. There is no significant difference to the separation shown in Fig. 8. This demonstrates that uncoated capillaries can also be used if the polymer contains a strongly acidic group.

When plotting the log of the reduced mobility vs. the log of the molecular mass of the analyte the typical sigmoidal curves known from DNA analysis are also obtained. The concentration of the sieving polymer has to be beyond its entanglement threshold concentration c^*. A typical plot is shown in Fig. 10, where different concentrations of dextran T 2000 have been added to the running buffer. Also included are the reduced mobilities of the PSS in the plain buffer. As can be seen, the sieving properties are improved with increasing dextran concentra-

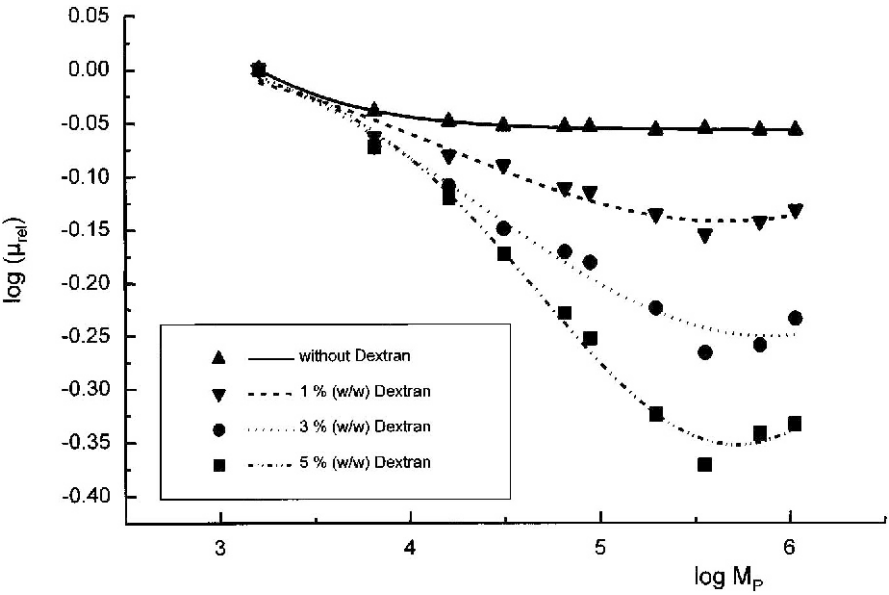

Fig. 10. Influence of the polymer additive concentration. Separation conditions: PVA capillary L=50–57 cm, i.d.=75 µm; buffer 60 mM AMPD/phosphoric acid, pH 8.8+2% w/w dextran T 2000; E=–300 V cm^{-1}; injection: t=20 s, p=0.5 psi; detection: UV 254 nm

tion, because the mesh size of the sieving media is decreased. The mass resolution improves in the reptation region.

The Ogston model can be applied at low molecular masses. According to Poli and Schure [25], this region extends up to molecular masses of 100,000. However, the region where the greatest mobility differences are observed belongs certainly to the reptation region. Here, the average mesh size in the polymer solution is smaller than the radius of gyration of the analyte. According to the discussions for DNA migration, the sigmoidal curve of the slope should be –1 at the point of inflection when a pure reptation mechanism is responsible for the separation. This, however, was not observed for PSS solutions. The slope depends on the sieving polymer concentration and its average weight and is smaller than –1. This deviation has been explained by an overlap of Ogston and reptation mechanisms [25]. The loss of resolution at high PSS molecular masses can be explained by increasing orientation of the sieving polymer and small relaxation times of the matrix pore structure caused by the size of the analytes.

It should always be kept in mind that the analysis time increases with increasing concentration of the sieving media. The regime where a separation is no longer possible seems to drift to lower molecular masses. This has been observed with PEG and dextrans (cf. Fig. 10).

As already discussed for DNA separation, the pore size of the sieving media should only be dependent on its concentration, and not on its molecular mass.

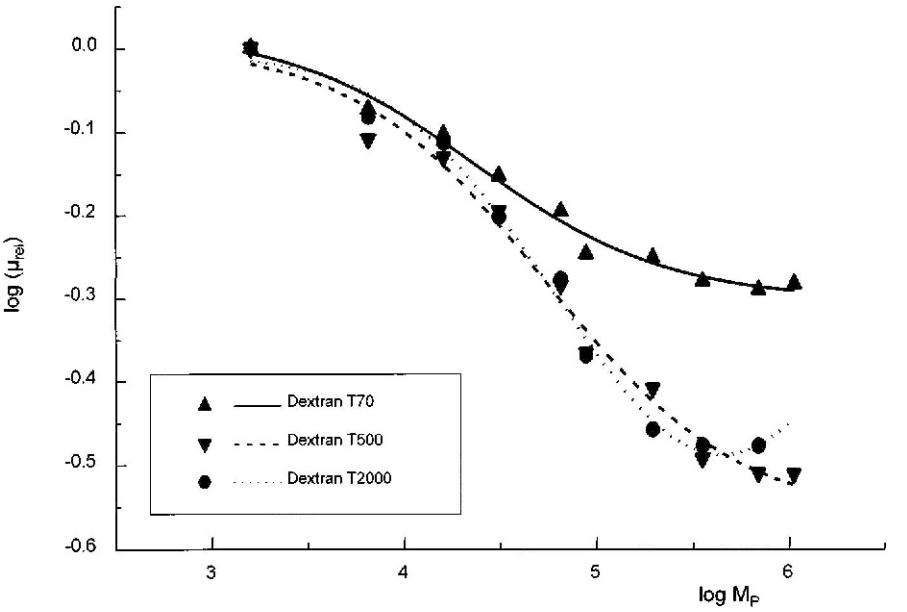

Fig. 11. Influence of the molecular weight of the polymer additive. Separation conditions: PVA capillary L=50–57 cm, i.d.=75 µm; buffer 60 mM AMPD/phosphoric acid, pH 8.8 +10% w/w dextran; E=–300 V cm^{-1}; injection: t=20 s, p=0.5 psi; detection: UV 254 nm

In Fig. 11 the influence of the molecular mass of the sieving medium is demonstrated. There is no difference between dextran T 500 and T 2000 at identical concentration. Less efficient separations are only observed with dextran T 70. The mass concentration here is just around the overlap threshold. For practical reasons it is advisable to use the sieving polymer which gives the lowest viscosity in the buffer solution at the required concentration.

The increasing rigidity of the pore structure with increasing molecular mass of the sieving polymer may be the reason for better separation efficiency in the case of the high-molecular-weight solutes [24]. The mesh structure of the sieving media with higher molecular masses may be deformed by the analyte to a lesser extent.

The selection of the sieving polymer follows to a great extent the rules applied in DNA separations. Studies have revealed [27] that the efficiency of the sieving polymer depends on its chain stiffness and its hydrophobicity. The higher the flexibility of the polymer and the smaller its gyration radius due to hydrophobic interactions, the higher the concentration in the buffer has to be in order to achieve comparable separation efficiencies.

When comparing different sieving polymers, it seems reasonable to keep the mesh size in the solution constant. As shown, beyond the threshold concentration the mesh size seems to be independent of the molecular mass of the polymer. Consequently, it is only important to compare the sieving properties as a

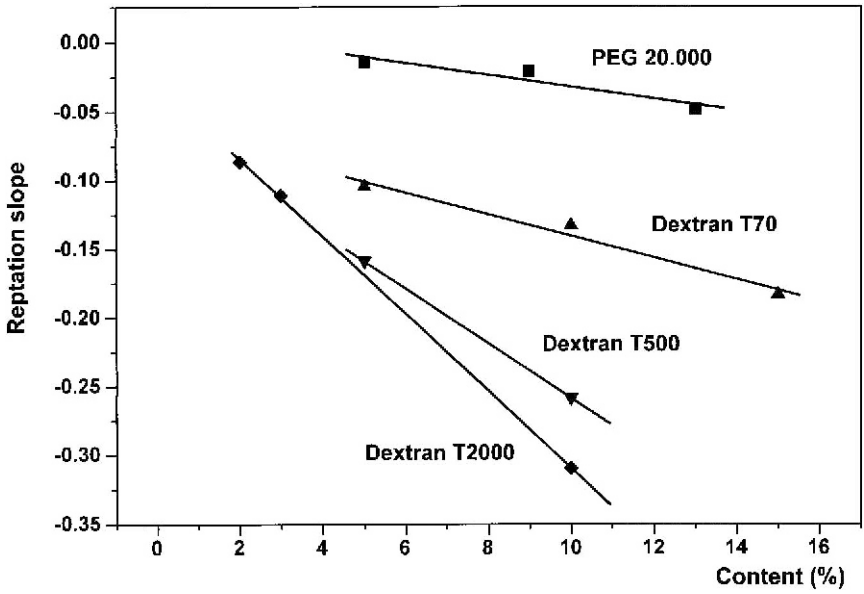

Fig. 12. Quantification of the sieving performance of a polymer solution. The slope at the point of inflection of the log μ/log M_w diagram is plotted vs. the polymer concentration

function of the concentration. This is shown in Fig. 12, where PEG 20,000 is compared with dextrans of different molecular masses. As a measure of efficiency the slope in the reptation region was taken [28]. From this it can be seen that the best sieving polymer in the separation of PSS is dextran T 2000. The comparison of sieving polymer solutions of identical viscosity [24] is only of practical relevance. HEC has good sieving properties in already very dilute solutions. The efficiency of a 0.3% solution corresponds almost to that of a 7% dextran T 2000 solution. However, it takes much longer to fill the separation capillary with this solution. The superiority of HEC over PEG at identical pore structure has been described [25]. It should be mentioned that in this case the PEG concentration was just below the threshold concentration.

Optimization of CE Conditions. As found for DNA separations, the separation efficiency decreases with increasing field strength. The selectivity seems to be optimal [24] at an extremely low field strength of 190 V cm^{-1}. It is feasible that the matrix becomes oriented at higher field strength, resulting in a displacement of the inversion range to lower molecular masses. Low field strength also means higher analysis time. Consequently, for each system, the optimum between analysis time and sufficient selectivity has to be found.

The mobilities of the PSS molecules decrease [25] with increasing ionic strength of the buffer. This can be explained by a shielding effect of the negative charges of the PSS by the higher concentration of the counterions. The reduction

of the intramolecular ionic repulsion forces by the increasing counterion concentration should lead to a reduction of the radius of gyration, resulting in a mobility increase. This effect does not seem to be important here.

The molecular size of the PSS depends on the type of the buffer counterion. The effective charge of the PSS decreases in the series $Li^+/Na^+/K^+/Cs^+$ due to the increasing affinity to the sulfo groups. The decrease in the effective charge leads to a decrease in the radius of gyration of the PSS due to a decrease in ionic repulsion. The consequent increase of the mobility has been observed with PSS with uncoated capillaries in the counter electroosmotic mode [25].

5.2 Separation of Cationic Polyelectrolytes

Cationic polyelectrolytes like Polybren are widely used in CE as buffer additives to reverse the EOF. They are strongly adsorbed at the negatively charged surface silanol groups. Only surface-coated fused silica capillaries can be used for their separation. The problems are similar to those discussed for protein separation.

With PVA-coated capillaries [6], it was possible to separate at pH 2.5 the polyelectrolyte 2-polyvinylpyridinium hydrochloride (2-PVP) in the molecular mass range between 1.5 and 1730 kDa with dextran as sieving matrix [26]. A separation of standards is depicted in Fig. 13. Comparing the efficiencies of the

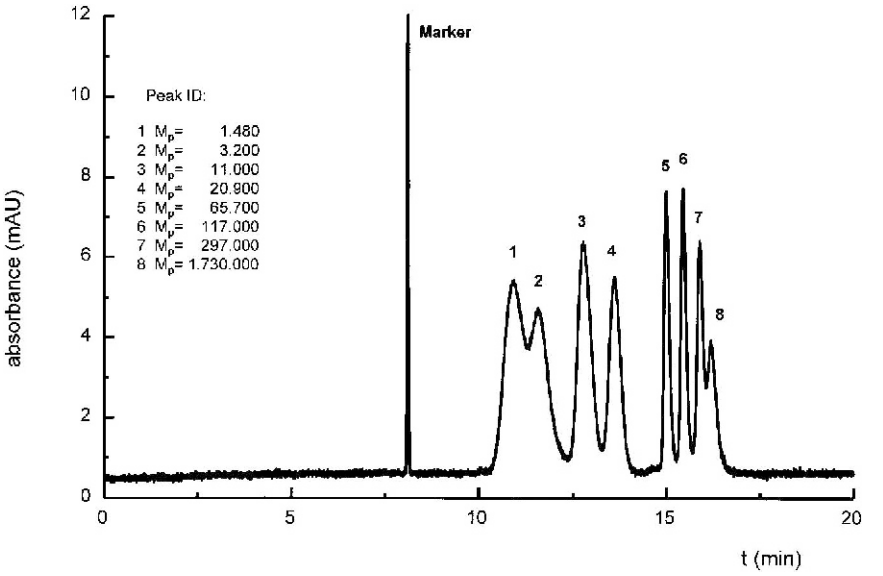

Fig. 13. Separation of polyvinylpyridinium hydrochloride at pH 2.5 in a PVA-coated capillary with dextran T 70 as buffer additive. Separation conditions: PVA capillary L=50–57 cm, i.d.=75 μm; buffer 50 mM phosphate, pH 2.5+5% w/w dextran T 70; E=–300 V cm^{-1}; injection: t=20 s, p=0.5 psi; detection: UV 254 nm

monomolecular marker *p*-aminopyridine with the broad peaks of the standards shows that the polydispersity of the standards is the cause of the observed broad peaks. Reptation dominates ranging from 20 up to 300 kDa. The slope in this range is also smaller than –1, demonstrating also a combined Ogston and reptation separation mechanism.

The hydrophobicity and hence the radius of gyration of PVP derivatives can be changed. Despite their increased molecular masses, the alkylated PVP derivatives migrate faster than the starting PVP. This can be explained by intramolecular hydrophobic interactions in the aqueous buffer resulting in a smaller radius of gyration. Also, the effective ionization can be different. It was possible to separate the ethyl and the benzyl derivative from the underivatized PVP with identical contour length.

5.3 Other Water-Soluble Polymers

Most of the water-soluble natural or synthetic polymers, like oligosaccharides or PEG, have neither a charge nor a chromophore. Because their separation in LC

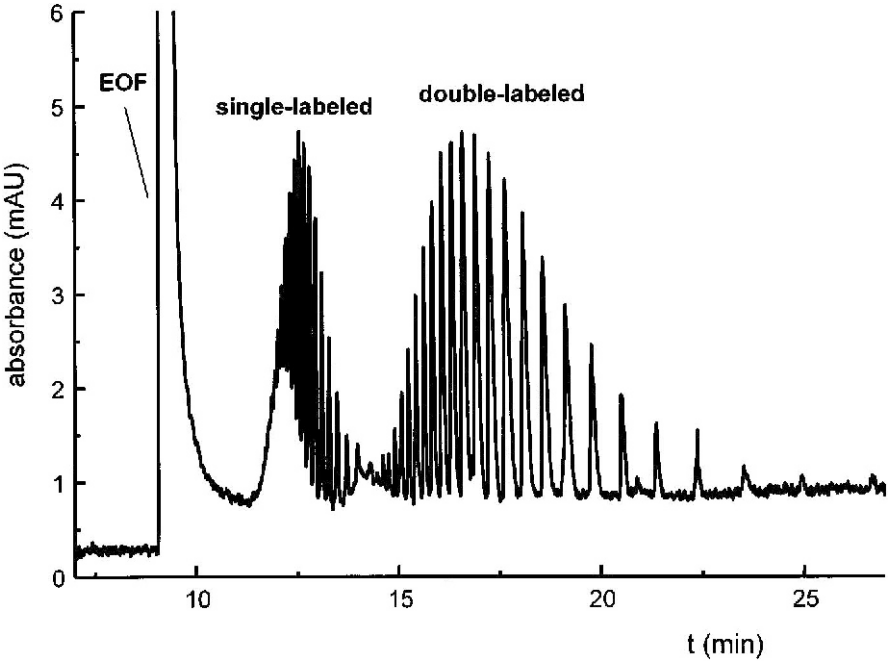

Fig. 14. Oligomeric distribution of PEG 1000 after derivatization with phthalic anhydride. Separation conditions: Fused silica capillary L=50–57 cm, i.d.=75 µm; buffer 110 mM Tris/boric acid, pH 8.3+5% in 20% v/v ethanol; E=526 V cm^{-1}; injection: t=10 s, p=0.5 psi; detection: UV 254 nm

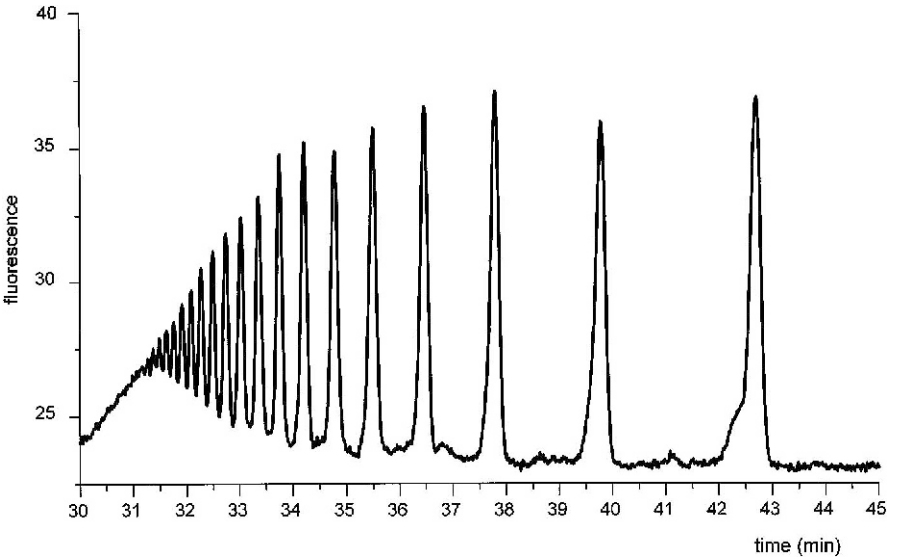

Fig. 15. CGE of a dextran ladder (derivatives with 2-aminoanthracene). Separation conditions: fused silica capillary L=106–120 cm, i.d.=50 μm; buffer 0.3 M borate, pH 10.5+3% w/w dextran T 10; E=250 V cm^{-1}; injection: t=10 s, p=0.5 psi; fluorescence detection: λ_{ex}=263 nm, λ_{em}=496 nm

imposes several problems, the use of CE for their characterization has also been described. Most of the separations in the literature are in the oligomeric range (molecular mass 10,000). For better detection and/or improved mobilities, various derivatization reagents have been applied.

In the separation of oligosaccharides, sulfonic acids (mono-, di- or tri-) of aminonaphthalene have been used [29]. Polyuronic acids like hyaluronic acid have also been characterized by CE [30].

Tensides based on derivatives of PEGs can also be separated by CE [31]. They may already contain charged groups, so that their migration is not problematic, only their detection. Here, indirect detection techniques with creatinine as background electrolyte have also been applied for samples up to molecular masses of 4000.

Phthalic acid anhydride reacts readily with alcoholic end groups of PEG. Besides an appropriate chromophore, charges are introduced simultaneously. Single- and double-labeled molecules are formed when two possible alcoholic end groups are available. The separation of derivatives of low molecular weight, such as PEG 1000, is shown in Fig. 14. Here, no sieving matrix was added. The homologues of the double labeled derivatives were completely separated [32].

Using sieving polymer solutions as buffer additives can enhance resolution [33,34]. However, the mass range of the solutes is far below that necessary for the high resolving reptation regime.

Polysaccharides can be derivatized by reductive amination at the reducing end group. With highly fluorescing labels like 2-aminoanthracene (2-AA), dextrans up to a molecular mass of 20 kDa can be visualized and hence analyzed by CE [35]. The separation of the AA derivative (only one chromophore introduced) of a synthetic dextran (4–6 kDa) is shown in Fig. 15. This opens new possibilities in the characterization of polysaccharides.

6 Conclusions

Synthetic polyelectrolytes can be separated by capillary electrophoresis applying the same rules derived for the electrophoresis of biopolymers. In the reptation regime, determination of the molecular mass and polydispersity of the polyelectrolytes is possible. Introduction of chromophores facilitates the detection of non-UV-absorbing polymers. Indirect detection techniques can probably be applied when analytes and chromophores of similar mobilities are available.

References

1. Li SFY (1992) Capillary electrophoresis. Elsevier, Amsterdam
2. Weinberger R (1993) Practical capillary electrophoresis. Academic Press, New York
3. Engelhardt H, Beck W, Schmitt T (1996) Capillary electrophoresis, methods and potentials. Vieweg, Braunschweig
4. Hjerten S (1985) J Chromatogr 347:191
5. Hjerten S, Ellenbring K, Kilar F, Liao J (1987) J Chromatogr 403:47
6. Engelhardt H, Cunat-Walter MA (1995) J Chromatogr 716:27
7. Gilges M, Kleemiß MH, Schomburg G (1994) Anal Chem 66:20
8. Giddings JC (1991) Unified separation science. Wiley, New York
9. Cohen AS, Karger BL (1987) J Chromatogr 397:409
10. Motsch SR, Kleemiß M, Schomburg GV HRC 14:629
11. Guttman A, Cohen AS, Heiger DN, Karger BL (1990) Anal Chem 62:137
12 Bode HJ (1977) Anal Biochem 83:204
13. Grossman BD, Soane DS (1991) Biopolymers 31:1221
14. Bello MS, Rezzonico R, Righetti PG (1994) J Chromatogr A 659:199
15. Viovy JL, Duke T (1993) Electrophoresis 14:322
16. Heller C (ed.) (1997) Analysis of nucleic acids by capillary electrophoresis. Vieweg, Braunschweig
17. Schwartz D, Koval M (1989) Nature 338:520
18. Carlsson C, Larsson A, Jonsson M (1997) In: Heller C (ed) Analysis of nucleic acids by capillary electrophoresis. Vieweg, Braunschweig
19. Slater GW (1997) In: Heller C (ed.) Analysis of nucleic acids by capillary electrophoresis. Vieweg, Braunschweig
20. Ogston AG (1958) Trans Faraday Soc 54:237
21. Barron AE, Soane DS, Blanch HW (1993) J Chromatogr 652:3
22. Salas-Solana O, Carrilho E, Kotler L, Miller AW, Götzinger W, Sisic Z, Karger BL (1998) Anal Chem 70:3996
23. Poli JB, Schure MR (1992) Anal Chem 64:896
24. Minárik M, Gas B, Kenndler E (1997) Electrophoresis 18:98
25. Cottet H, Gareil P (1997) J Chromatogr A 772:369
26. Clos H, Engelhardt H (1998) J Chromatogr A 802:149

27. Barron A, Sunada WM, Blanch HW (1996) Electrophoresis 17:744
28. Dolník V (1999) Capillary electrophoresis in sieving matrices: what governs the separation?. Poster Presentation at the HPCE'99 conference, Palm Springs, USA
29. Paulus A, Klockow A (1997) J Chromatogr A 772:369
30. Hong M, Sudor J, Stefansson M, Novotny M (1998) Anal Chem 70:568
31. Bullock J (1993) J Chromatogr A 645:169
32. Clos H (1998) Charakterisierung synthetischer ionischer und nichtionischer Polymere mittels Kapillarelektrophorese. PhD Thesis, University of the Saarland, Saarbrücken, Germany
33. Wallingford RA (1996) Anal Chem 68:2541
34. Barry JP, Radtke DR, Carton WJ, Anselmo RT, Evans JV (1998) J Chromatogr A 800:13
35. Grosche O (1998) Kapillarelektrophorese von polymeren Kohlenhydraten nach reduktiver Aminierung. Masters Thesis, University of the Saarland, Saarbrücken, Germany

Received: February 1999

Author Index Volumes 101–150

Author Index Volumes 1–100 see Volume 100

Subject Index